NUREG/CR-2471
EGG-2160

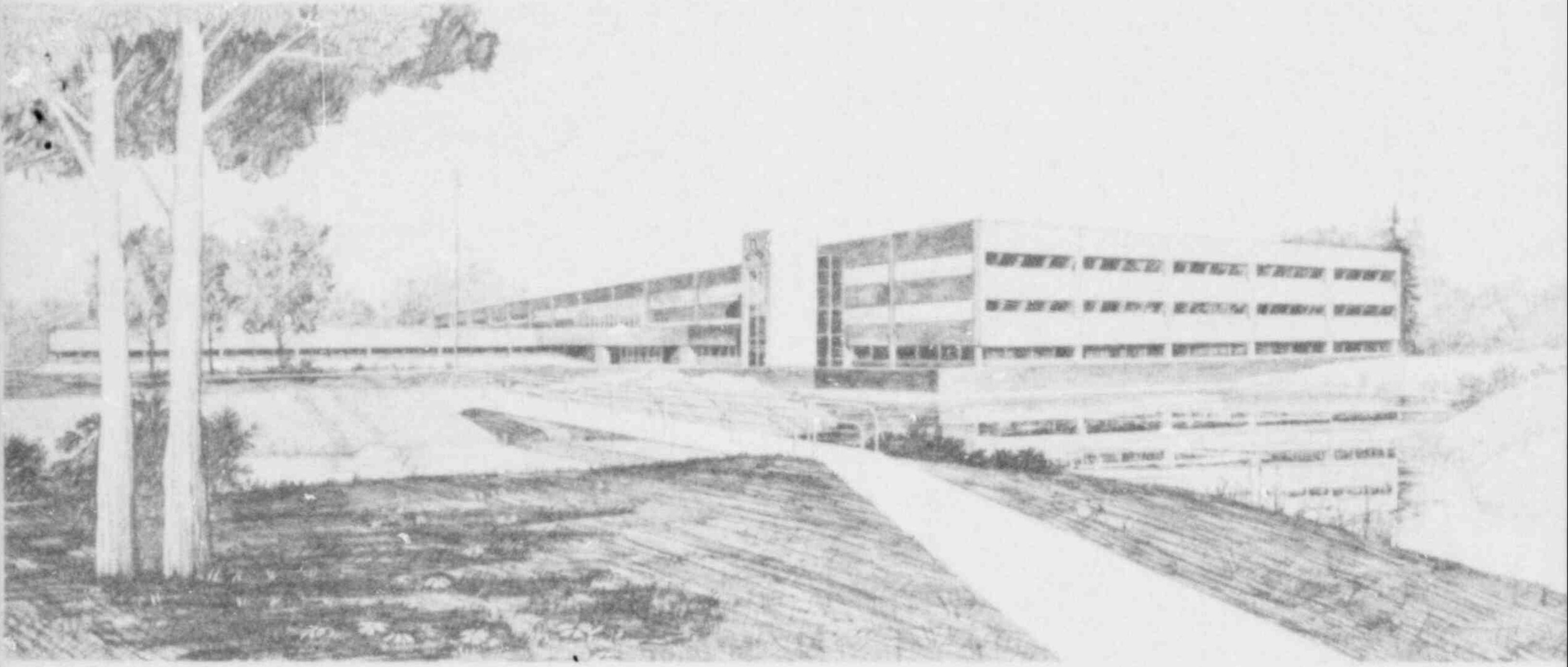

U.S. Department of Energy
Idaho Operations Office • Idaho National Engineering Laboratory

Analysis of the Pulsed Neutron Activation Technique

L. Perez-Griffo
C. Block
T. Lahey

January 1982

Prepared for the
U.S. Nuclear Regulatory Commission
Under DOE Contract No. DE-AC07-76IDO1570

EG&G Idaho

Available from

GPO Sales Program
Division of Technical Information and Document Control
U.S. Nuclear Regulatory Commission
Washington, D.C. 20555

and

National Technical Information Service
Springfield, Virginia 22161

NUREG/CR-2471
EGG-2160
Distribution Category: R2

ANALYSIS OF THE PULSED NEUTRON ACTIVATION TECHNIQUE

L. Perez-Griffo
C. Block
T. Lahey

Published January 1982

EG&G Idaho, Inc.
Idaho Falls, Idaho 83415

Prepared for EG&G Idaho, Inc.
Under Subcontract No. K-6141
and the U.S. Nuclear Regulatory Commission
Under DOE Contract No. DE-AC07-76IDO1570
FIN No. A6048

CONTENTS

Page

LIST OF TABLES

LIST OF FIGURES

Page

Page

Page

ABSTRACT

The Pulsed Neutron Activation (PNA) technique for single- and two-phase water flow is analyzed for small and large diameter pipes.

PNA measurements were performed at the RPI Gaerttner Linac Laboratory using the $^{16}O(n,p)\ ^{16}N$ reaction. Accurate mass-weighted velocities of single- and two-phase flows were obtained by the transit-time method for a vertical 1-in diameter pipe. The potential of ^{16}N tagging techniques for basic single- and two-phase flow measurements is demonstrated.

Analytical techniques were developed to analyze PNA measurements at LOFT. Neutron and gamma transport calculations by Monte Carlo were done at the tagging and detector positions for the 14-in diameter pipes used at LOFT. Flow structure effects on the interpretation of PNA measurements are evaluated. Dispersion models to describe the transport of the irradiated fluid from the source to detector locations were developed in order to interpret the LOFT L3-7 test PNA data.

PART 1

INTRODUCTION AND HISTORICAL REVIEW

There is a crucial need today for better understanding and more accurate prediction of multi-phasic flow phenomena. Applications to chemical, petroleum and nuclear industries require better data and theories than exist today. In reactor safety, measurements of mass flow rates and fluid properties are required to verify the accuracy of the existent methods which assess the safety of nuclear power plants. Proper instrumentation for transient flow measurements is thus extremely important for nuclear safety studies. The object of this work is to demonstrate the applicability of pulsed neutron activation techniques for accurate single- and two-phase flow measurements.

Neutron activation methods for measuring flow are extensions of radioisotope-tracer techniques which are, in turn, improvements on chemical and dye tracer techniques. Tracer methods for measuring flow rates in pipes were used as early as 1923 by Allen and Taylor[1]. Since then, tracer techniques have been in use to determine experimentally fluid flow properties in engineering processes[2-6]. Unfortunately, many of these experiments suffered from intrusive instrumentation, since the tracer typically was injected into the flowing system. In many cases the perturbation caused by the injection was so great as to seriously impair the interpretation of the measurement. Recently, neutron tagging techniques have been developed which are non-intrusive, where the neutrons are introduced from outside the flowing mixture and thus no perturbation takes place in the flow. The neutron activation method used for flow measurements is the Pulsed Neutron Activation (PNA) method, which uses a pulsed high-energy neutron source to induce activity into a flowing fluid. The activated nuclei are then detected at a distance downstream from the activation site by a detector that monitors the passage of the activated fluid as a function of time. Thus, by the analysis of the measured time profile of the irradiated fluid, flow properties can be obtained without introducing any perturbation into the flow.

An essential requirement for successful flow measurements by the PNA technique is that suitable radionuclei with detectable decay product and short half-life are produced in the flowing fluid by neutron interactions[7]. Examples of a number of reactions that might be used for flow measurements by neutron activation are given in Table 1-I, together with the reaction threshold energies, half-lives and characteristic gamma-ray energies of the product nuclides. For water systems, a very useful tagging reaction in Table 1-I is, $^{16}O(n,p)\ ^{16}N$. The combination of the 6.1 MeV high-energy gamma ray (which is easily detected in the presence of lower-energy gamma ray background) and the short half-life of 7.1 s is well suited for measuring single- and two-phase water systems over a large range of flow conditions.

Flow rate measurements of liquid, solids and slurries by neutron activation were first reported by Boswell and Pierce[7]. Some time later, this technique was used to calibrate and measure liquid sodium flows in the secondary system of the Experimental Breeder Reactor II (EBR-II) at Argonne National Laboratory (ANL)[8-13]. Measurements of single- and two-phase water flows with ^{16}N tagging have

TABLE 1-I Suitable Nuclear Reactions to Be Used for Flow Measurements by Neutron Activation Techniques

REACTION	HALF LIFE	E_γ (MEV)	NEUTRON ACTIVATION THRESHOLD (MEV)
$Na^{23}(n,\alpha)F^{20}$	11 s	1.63	4.04
$O^{16}(n,p)N^{16}$	7.14 s	6.13, 7.11	10.24
$Mg^{24}(n,p)Na^{24}$	15 Hr.	1.38, 2.75	4.93
$Al^{27}(n,\alpha)Na^{24}$	15 Hr.	1.28, 2.75	3.24
$Si^{28}(n,p)Al^{28}$	2.3 Min.	1.78	3.99
$Ba^{138}(n,2n)Ba^{137}$	2.6 Min.	0.662	8.67

been reported from ANL[14-19] and the Gaerttner Laboratory here at Rensselaer Polytechnic Institute (RPI)[20-21]. Recently, PNA techniques have been used for mass flow measurements at the Loss-of-Fluid-Test (LOFT) facility located at the Idaho National Engineering Laboratory (INEL).

The work presented in this report has two main objectives. One part is concerned with the description and interpretation of the RPI PNA measurements. These measurements were performed for single- and two-phase conditions flowing in a vertical 1-in diameter pipe. The powerful LINAC neutron source was capable of providing very accurate mass-weighted velocities of the irradiated flows. From these RPI experiments, the potential of ^{16}N tagging techniques for basic single- and two-phase flow measurements[22-23] is demonstrated.

The second part of this work is concerned with the application and analysis of PNA techniques at LOFT. For large diameter pipes, asymmetry effects occur that accentuate the importance of those fluid nuclei moving near the source and detector[12]. To evaluate these effects at LOFT, Monte Carlo neutron and gamma transport calculations were performed at the source and detector locations[24]. Dispersion models were developed to describe the transport of the irradiated fluid from the source to detector positions. The Monte Carlo calculations at the tagging and detector locations were coupled with the fluid transport models in order to interpret the LOFT L3-7 test PNA data.

PART 2

THEORY AND ANALYSIS

2.1 Pulsed Neutron Activation Technique

The Pulsed Neutron Activation (PNA) technique, also known as the transit-time technique[7], uses a pulsed neutron source to induce activity into a flowing fluid. The activated nuclei are then detected at a distance downstream from the activation site by a detector(s) that monitors the passage of the activated fluid as a function of time. By the analysis of the measured time profile of the irradiated fluid, flow properties can be obtained without introducing any perturbation into the flow.

For water systems, a very useful tagging reaction is $^{16}O(n,p)$ ^{16}N, where the 7.1-s half-life ^{16}N emits a gamma ray with greater than 6.1-MeV energy. This reaction is produced only by neutrons with energies greater than 10.2 MeV. The combination of the high energy gamma rays (which are easily detected in the presence of lower-energy gamma ray backgrounds) and the short half-life is well suited for measuring single and two-phase water systems over a large range of flow conditions.

An instrument configuration used for a typical PNA measurement is shown in Fig. 2.1. Briefly, the neutron source is positioned at a selected location on the fluid-bearing pipe and a gamma detector is located a suitable distance downstream. After a pulse of neutrons from the source, the signals from the gamma detector monitoring gamma rays from passage of the activated nuclei are amplified and routed to a multichannel time analyzer, where they are processed to provide a count rate-

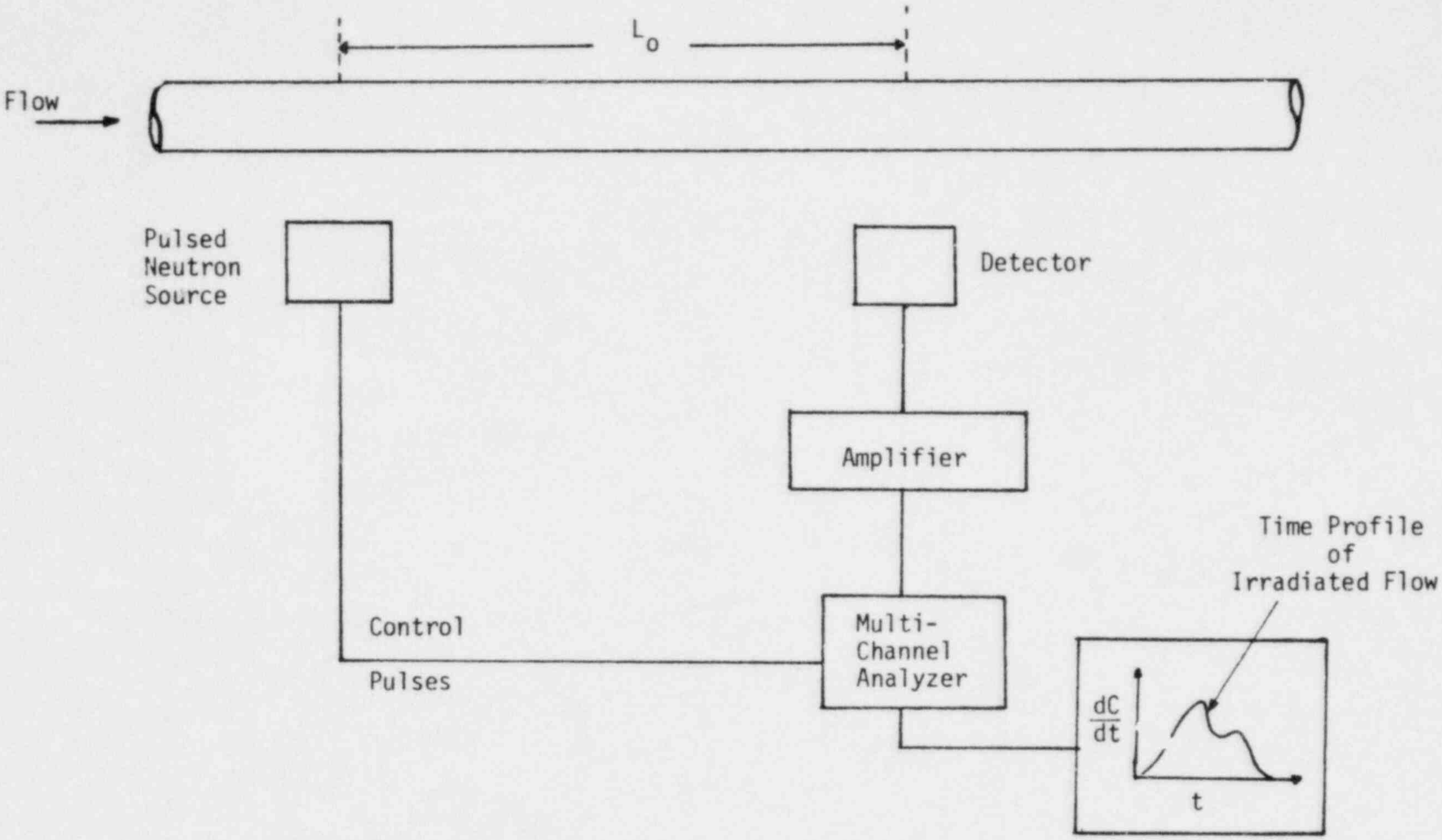

Figure 2-1   Block Diagram of a PNA System

time history. A common control initiating the neutron pulse and simultaneously starting the multichannel time analyzer may be repetitively operated to accumulate counts from several neutron pulses in the multiscaler channels. However, a delay period between neutron-injection pulses must be used to allow the activated fluid to completely pass the detector and the multiscaler to complete its cycle.

PNA techniques are considered to be well suited to obtain accurate mass-weighted velocities of the flowing irradiated fluids. However, some factors have to be taken into consideration in order to correctly interpret a PNA measurement. The flow regime, the non-uniform tagging and non-uniform detector efficiency effects for large diameter pipes, the mixing and dispersion of the irradiated fluid from the tagging to detector positions, etc. affect the interpretation of PNA time profiles. These effects will be discussed later.

2.1.1 Mass-Weighted Velocity. Consider the PNA tagging of a thin slice of fluid with a total activated mass M_A, represented in Figure 2.2. At a distance L_o, dm_A/dt is the activated mass flow rate across L_o. During the time between t and t + dt, dm_A is the activated mass which flows by L_o. The average velocity over the distance L_o of the activated mass dm_A is L_o/t, where t is the time after the irradiation. Thus, the mass-weighted velocity over L_o of the total activated mass, corrected for radioactive decay, is[24],

$$\langle V_{L_o} \rangle_m = \frac{\int_0^\infty \frac{L_o}{t} \, dm_A \, e^{\lambda t}}{\int_0^\infty dm_A \, e^{\lambda t}} \tag{2.1}$$

where λ is the decay constant. From continuity at L_o,

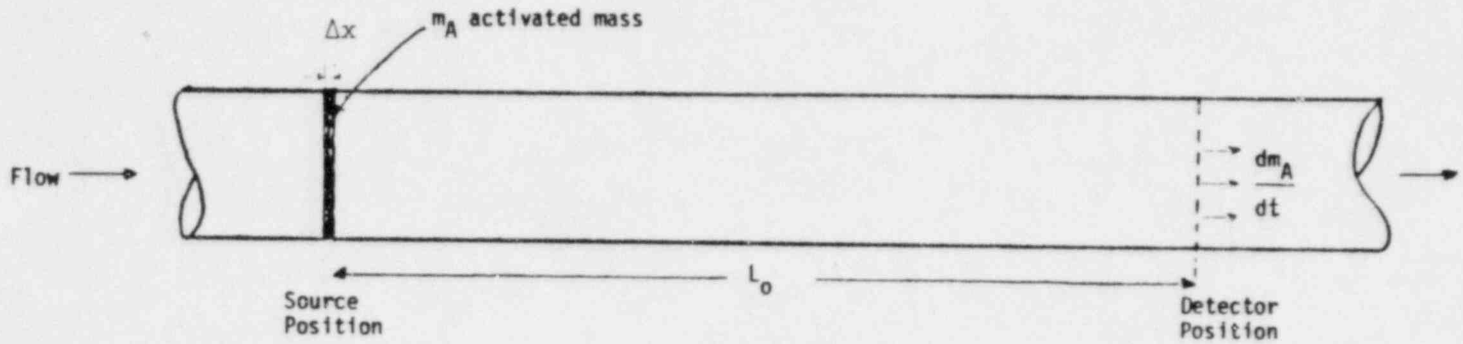

Figure 2-2 PNA Tagging Geometry

$$dm_A = \rho_A \; A_{x-s} \; \langle V_A \rangle \, dt \tag{2.2}$$

where ρ_A is the activated mass density (i.e. the tag concentration), A_{x-s} is the cross sectional flow area, and $\langle V_A \rangle$ is the cross-sectional-averaged velocity of the activated mass dm_A at the position L_o.

Substituting (2.2) into (2.1),

$$\langle V_{L_o} \rangle_m = \frac{\int_0^\infty \left(\frac{L_o}{t}\right) e^{\lambda t} \; A_{x-s} \; \rho_A \; \langle V_A \rangle \, dt}{\int_0^\infty e^{\lambda t} \; A_{x-s} \; \rho_A \; \langle V_A \rangle \; dt} =$$

$$= \frac{\int_0^\infty \frac{L_o}{t} \; e^{\lambda t} \; \rho_A \; \langle V_A \rangle \; dt}{\int_0^\infty e^{\lambda t} \; \rho_A \; \langle V_A \rangle \; dt} \tag{2.3}$$

The counting rate $\frac{dC}{dt}$ is proportional to the activated mass density ρ_A, i.e.

$$\frac{dC}{dt} = k \; \rho_A \tag{2.4}$$

where k is a detection constant.

Therefore, substituting ρ_A from (2.4) into (2.3)

$$\langle V_{L_o} \rangle_m = \frac{\int_0^\infty \frac{L_o}{t} \; e^{\lambda t} \; \frac{1}{k} \left(\frac{dC}{dt}\right) \; \langle V_A \rangle \, dt}{\int_0^\infty e^{\lambda t} \; \frac{1}{k} \left(\frac{dC}{dt}\right) \; \langle V_A \rangle \; dt} =$$

$$\langle V_{L_o} \rangle_m = L_o \frac{\int_o^\infty e^{\lambda t} \left(\frac{dC}{dt}\right) \frac{\langle V_A \rangle}{t} \, dt}{\int_o^\infty e^{\lambda t} \left(\frac{dC}{dt}\right) \langle V_A \rangle \, dt} \quad . \tag{2.5}$$

Since events are counted over time channels of width ζ_1, one can express (2.5) as,

$$\langle V_{L_o} \rangle_m = L_o \frac{\sum_i e^{\lambda t_i} C_i \frac{\langle V_A \rangle}{t_i}}{\sum_i e^{\lambda t_i} C_i \langle V_A \rangle} \tag{2.6}$$

where t_i is the time after irradiation corresponding to the middle of the i^{th} time channel and C_i is the number of counts recorded over the i^{th} channel. That is,

$$C_i = \int_{t_i - \frac{\zeta_1}{2}}^{t_i + \frac{\zeta_1}{2}} \left(\frac{dC}{dt}\right) dt$$

Equation (2.6) is thus the general expression for the mass-weighted velocity. Hence, the mass-weighted velocity strongly depends on the cross-sectional-averaged velocity $\langle V_A \rangle$ of the activated mass at the detector position and thus it is important to use the correct local velocity to interpret PNA experiments.

Consider two fully developed flow cases for $\langle V_A \rangle$:

<u>CASE I:</u> The velocity at the detector is equal to the average velocity over the distance L_o: $\langle V_A \rangle$ [illegible] (i.e.: the particle follows a stream-line). For this condition Equation (2.6) becomes,

$$\langle V_{L_o} \rangle_m = L_o \frac{\sum_i e^{\lambda t_i} C_i \frac{(L_o/t_i)}{t_i}}{\sum_i e^{\lambda t_i} C_i \, (L_o/t_i)} =$$

$$= L_o \frac{\sum_i e^{\lambda t_i} C_i \, / \, t_i^2}{\sum_i e^{\lambda t_i} C_i \, / \, t_i} \qquad (2.7)$$

CASE II: The velocity at the detector position is equal to the average fluid velocity, $\langle V_A \rangle = \bar{u}$ (i.e.: we assume it is uniformly mixed). For this condition Equation (2.6) becomes,

$$\langle V_{L_o} \rangle_m = L_o \frac{\sum_i e^{\lambda t_i} C_i \, \cancel{\bar{u}}/t_i}{\sum_i e^{\lambda t_i} C_i \, \cancel{\bar{u}}} = L_o \frac{\sum_i e^{\lambda t_i} C_i/t_i}{\sum_i e^{\lambda t_i} C_i} \qquad (2.8)$$

It is concluded that the evaluation of the mass-weighted velocity is dependent on the effective velocities of the irradiated masses as they pass in front of the detector. The expression of the mass-weighted velocity for CASE I, given by Equation (2.7) is the one used by Kehler[14]. This case is appropriate for single-phase laminar flow and two-phase flows in which the radial mixing is minimal. On the other hand, CASE II is appropriate for turbulent single-phase and two-phase flows with strong radial mixing.

2.1.2 Void Fraction Evaluation. The area-average void fraction can be obtained from a PNA measurement by the total activity method[14]. This method is based on the fact that the total activity passing by the detector is proportional to the average density of the irradiated two-phase flow. A proportionally constant can be obtained by performing a measurement with a liquid filled pipe where the density is known. A derivation of this method is given in Appendix - A. where it is observed that the average density also depends on the cross-sectional-averaged velocity $\langle V_A \rangle$ of the activated mass at the detector position.

In considering the two cases for $\langle V_A \rangle$ it is shown in Appendix-A. that for flows where there is no radial mixing (CASE I), the appropriate expression is the one proposed by Kehler[14]. On the other hand, for flows with strong radial mixing (CASE II), the averaged fluid velocity past the detector must be known in order to correctly obtain the average density. Thus, we must have an independent measurement of the vapor and liquid flow rates.

An alternative to this method is to interpret the mass-weighted velocity as the oxygen center-of-mass velocity, i.e. the velocity of propagation of the plane through which no net oxygen mass flux passes. Using the same method to obtain the compact form of the conservation equations of a two-phase system[25], i.e. by equating the oxygen mass flux terms in Figure 2.3,

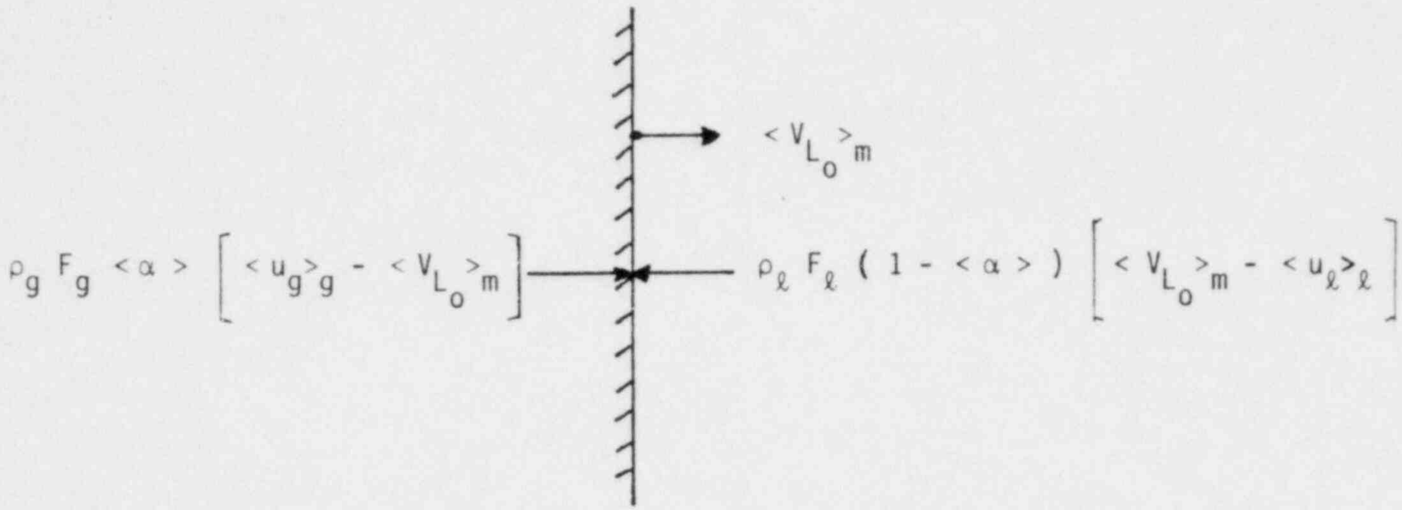

Figure 2-3 Velocity of the Oxygen Center-of-Mass

$$\rho_g \; F_g \; \langle\alpha\rangle \; [\langle u_g\rangle_g - \langle V_{L_o}\rangle_m] \; = \; \rho_\ell \; F_\ell \; (1-\langle\alpha\rangle) \; [\langle V_{L_o}\rangle_m - \langle \mu_\ell\rangle_\ell]$$

which yields

$$\langle V_{L_o}\rangle_m = \frac{\rho_\ell F_\ell (1-\langle\alpha\rangle)\langle u_\ell\rangle_\ell + \rho_g F_g \langle\alpha\rangle\langle u_g\rangle_g}{\rho_\ell F_\ell (1-\langle\alpha\rangle) + \rho_g F_g \langle\alpha\rangle} \tag{2.9}$$

where,

ρ_ℓ and ρ_g are the liquid and gas densities, respectively. $\langle u_\ell\rangle_\ell$ is the cross-sectional average of the liquid velocity across the flow area of the liquid phase, $\langle u_g\rangle_g$ is the cross-sectional average of the gas velocity across the flow area of the gas phase, F_ℓ and F_g are the weight fraction of oxygen in the liquid and gas phase, respectively, and $\langle\alpha\rangle$ is the cross-sectional-averaged void fraction. It can be pointed out that for a steam/water system $F_g/F_\ell = 1.0$ and $\langle V_{L_o}\rangle_m$ given by Equation (2.9) is the well-known one-dimensional center-of-mass velocity[25]. Now, using the definition of the superficial liquid and gas phase velocities,

$$\langle j_\ell\rangle = (1-\langle\alpha\rangle) \langle u_\ell\rangle_\ell$$

$$\langle j_g\rangle = \langle\alpha\rangle \langle u_g\rangle_g$$

Equation (2.9) becomes,

$$\langle V_{L_c}\rangle_m = \frac{\rho_\ell F_\ell \langle j_\ell\rangle + \rho_g F_g \langle j_g\rangle}{\rho_\ell F_\ell (1-\langle\alpha\rangle) + \rho_g F_g \langle\alpha\rangle} \tag{2.10}$$

Therefore, the void fraction will be given by:

$$\langle\alpha\rangle = \frac{\rho_\ell - [\rho_\ell \langle j_\ell\rangle + \rho_g \frac{F_g}{F_\ell} \langle j_g\rangle]/\langle V_{L_o}\rangle_m}{\rho_\ell - \rho_g \frac{F_g}{F_\ell}} \qquad (2.11)$$

That is, just as for CASE II in Appendix A, it is observed that in order to obtain the void fraction of a two-phase flow by PNA tagging techniques, an independent measurement is required. Both $\langle j_\ell\rangle$ and $\langle j_g\rangle$ have to be determined independently.

For water/air two-phase flows at low pressure $\rho_g \ll \rho_\ell$ and $F_g/F_\ell = 0.233/0.888 = 0.262$, thus Equation (2.11) can be approximated by,

$$\langle\alpha\rangle \approx 1 - \frac{\langle j_\ell\rangle}{\langle V_{L_o}\rangle_m} \qquad (2.12)$$

In this case, it is only necessary to measure $\langle j_\ell\rangle$ independently in order to obtain $\langle\alpha\rangle$ from a PNA measurement. For the PNA two-phase flow measurements at RPI, described in Section 3.3.1 the void fraction could be determined by (2.12) since $\langle j_\ell\rangle$ was maintained constant through the measurements and was determined as the mass-weighted velocity when no air was introduced into the two-phase system (single-phase).

2.1.3 Measurement Uncertainty. The uncertainty in the measurement of the mass-weighted velocity is estimated by using the relationship for normally distributed errors. If $\langle V_{L_o}\rangle_m$ is a function of M independent parameter variables q_j:

$$\langle V_{L_o}\rangle_m = f(q_1, q_2, \ldots\ldots, q_M)$$

then, if we assume these errors are uncorrelated, the uncertainty $\delta\langle V_{L_o}\rangle_m$ is given by[26]

$$\delta\langle V_{L_o}\rangle_m = \pm \sqrt{\sum_{j=1}^{M} \left(\frac{\partial \langle V_{L_o}\rangle}{\partial q_j} \delta q_j\right)^2} \qquad (2.13)$$

where δq_j is the uncertainty in the q_j parameter, nominally the standard deviation.

In looking at the expressions for the mass-weighted velocity [Equations (2-7) and (2-8)] it can be observed that the accuracy in $\langle V_{L_o}\rangle_m$ is entirely controlled by count statistics and the precision with which L_o can be measured, i.e. the parameter variables q_j will be the C_i's and L_o.

Up to this point, the C_i data have been assumed to be net counts (i.e. background counts have been removed prior to analysis). When the background is present it must be properly modelled on a channel-by-channel basis, and its statistical error included in the total uncertainty on the mass-weighted velocity.

Another factor affecting the accuracy of the mass-weighted velocity is the geometry of the system. The asymmetry effects at the tagging and detector positions for large diameter pipes are discussed as follows.

2.1.4 Asymmetry Effects in PNA. All the preceding development has been based upon the assumption of equal probablility of activation and detection of activated nuclei from any fluid particle within the pipe. Because fluid nuclei are preferentially activated on the side of the pipe near the neutron source and the activated nuclei are preferentially detected on the side of the pipe near the detector, a bias effect occurs that accentuates the importance of those fluid nuclei moving near the neutron source and detector. For penetrating radiation, the fluid in a small diameter pipe will much more closely approximate the case for uniform activation and detection than a fluid in a pipe of very large diameter. It is then recognized that an ultimate limitation on the PNA method is the pipe size[27].

To a significant degree, these asymmetry effects can be minimized by the experimental geometry employed. The use of two or more neutron sources located symmetrically around the circumference of the pipe will reduce the asymmetry of the activation process. A similar approach using multiple detectors will also benefit the detection process.

Because of the three-dimensional nature of these asymmetries and their introduction of non-linear characteristics, they are not easily handled by using a simple analytical model[12]. Moreover, for large diameter pipes with thick walls the problem becomes too complex to be treated by uncollided neutron and gamma flux approximations. Monte Carlo transport methods are very well suited to quantize the asymmetry effects at the tagging and detector positions.

2.1 Monte Carlo Transport Method

The Monte Carlo method is distinguished from other techniques in numerical analysis by the use of random sampling to construct the solution of a physical or mathematical problem. A stochastic model to the problem is set up and by sampling from appropriate probability distributions, the required numerical answers to the problem are estimated by statistical means. In the treatment of particle-transport problems, the probabilistic methods used may require rather sophisticated mathematical tools to justify them rigorously. However, much of Monte Carlo is intuitive in nature and requires only a knowledge of elementary probability theory[28]. A summary of Monte Carlo techniques is given here. References (28-32) give full treatment and applications of this method.

The principle of a Monte Carlo calculation for a particle transport problem is the simulation of particle paths through matter using input data describing the geometry and nuclear properties of the system. A series of particle life-histories is generated using the input data and a list of random numbers to choose collision points and decide the outcome of a collision. These histories are analyzed in order to derive relevant data, such as flux densities, currents, etc. The final results are statistically averaged values obtained by repeating the same numerical experiment many times and analyzing a large number of particle histories.

2.2.1 "Analog" and "Non Analog" Monte Carlo. Since the Monte Carlo method is based on statistical sampling, any results produced have an associated statistical uncertainty. The magnitude of this uncertainty can be reduced by running more histories or by altering the process of generating histories. There are several techniques which can be used to improve the error of a quantity calculated by "Analog" Monte Carlo.

"Analog" Monte Carlo in the transport sense, means tracking a particle by a realistic simulation. For example, if a particle had a collision, and absorption has been chosen over scattering, then the particle dies. "Analog" Monte Carlo treats each particle with a weight of one or zero, success or failure. This method is inefficient if quantities are needed optically far from the source. If a statistical weight is assigned to a particle and is adjusted for such things as absorption, then more information can be extracted from a history, and the variance will be reduced.

"Non Analog" Monte Carlo assigns a statistical weight to each particle. This weight starts out equal to 1.0 and is adjusted by various techniques in order to reduce the variance. This weight may decrease in a highly absorbing medium or increase in a highly multiplying medium. A particle with high weight may also be split by tracking two particles with one half the weight of the original. Survival weight, splitting, Russian Roulette and importance sampling are the most common "Non-Analog" techniques used to reduce the statistical variance[29].

2.2.2 Statistical Estimators. The results from Monte Carlo calculations of neutron and photon transport problems depend on the kind of problem being treated: reaction rates, particle fluxes and densities, K_{eff} in criticality calculations, etc. To get the desired outcome, the statistical estimators are used. The majority of the currently used estimators in Monte Carlo codes are of four basic types[28]. These are the collision estimator, the last-event estimator, the track-length estimator, and the next-event (point-detector estimator).

The collision estimator scores Σ/Σ_t at each collision event in the region of interest; Σ is the macroscopic cross-section for the reaction of interest and Σ_t is the total macroscopic cross-section. The last-event estimator differs from the collision estimator in that the scoring occurs only when the particle history is terminated by capture, (i.e. it only score Σ/Σ_a where Σ_a is the macroscopic capture cross-section).

Both the collision estimator and last-event estimator tend to suffer statistically in optically thin regions (i.e. regions in where the particle mean free path is large compared with the dimensions of the region) since few collisions occur there. This statistical problem is usually improved with the use of a path-length estimator. The path-length estimator scores $\Sigma \ell$ for each particle flight within the region of interest, where ℓ is the length of the flight. This estimator is in extensive use since it has excellent properties in optically thin regions and tends to perform satisfactorily for optically thick regions as well. Actually, the path-length estimator is a limiting form of the collision estimator[33].

The collision, last-event, and track-length estimator all tend to suffer from increasing statistical errors as the volume of the detector region becomes arbitrarily small. The next-event (point-detector) estimator is a candidate for such problems. For this estimator, the weight of the particle is multiplied by the probability that at a collision the particle scatters with an angle directed towards the detector.

Other estimators are used in Monte Carlo calculations like the modified track-length estimator[34] for particles whose final flights start in the region of interest and end with absorption in that region, or the expectation estimator[34] which scores the probability that a particle flight within a region will end in the reaction of interest. For low density regions or for detection purposes, it is interesting to record the particles crossing regions. This can be done with the surface crossing estimator which scores the number of particles crossing the surface, bounding a region of interest.

Combinations of statistical estimators are widely and satisfactorily used in the Monte Carlo codes for transport calculation.

2.2.3 ANDYRPI Monte Carlo Program. ANDYRPI is a Monte Carlo code which can do source-specified and eigenvalue problems. This code, written in FORTRAN IV, computes the time-space-direction-energy group dependence of particle reaction rates and currents in general geometry. ANDYRPI is a modified version of the ANDYMG3 code written by D. R. Harris[35]. A general outline of its features is given here, and a listing of this code is given in Appendix C.

ANDYRPI is able to solve neutron transport, photon transport, coupled neutron-photon transport and eigenvalues problems. Particle and photon type and energy are identified by multi-energy-group. Multi-group cross-section sets can be used which provide extension of familiar multi-group S_N and diffusion theory methods to complex geometries. Isotropic and anisotropic scattering up to P_3 expansion of angular distribution are treated. Scattering patterns in the simulation can be continuous in scattering angles, but since particle splitting and termination routines permit negative weights, another option to treat the P_3 scattering expansion has been recently introduced: the equiprobable scattering method.

The ANDYRPI geometry routine has been devised to be fast and to simplify problem input for complex geometries. Any complex geometry formed by segments of planes, spheres, cylinders, ellipsoids, and cones can be treated. In ANDYRPI, a region is a spatial domain in which macroscopic cross-sections are uniform, and a surface is a set of points in space which satisfy an algebraic equation. A region is bounded in ANDYRPI, not by surfaces, but by surface segments. A surface segment is defined as a set of points which lie in a specified containing surface and have a proper sense with respect to other surfaces. For closed surfaces, sense is defined as + 1,outside,and - 1,inside. For open surfaces sense is defined + 1 on the side of the surface toward which its normal or axial vector points,and as - 1 on the other side.

When a particle emerges into a region from the source of collision, the distance along the particle trajectory to each surface segment surrounding the region is computed. If the new distance to collision is less than any distance to hit a surface segment, then a collision occurs. The space and time coordinates of the particle or photon are translated to the point of collision, and the tallies are incremented. The actual tallies in ANDYRPI are,(i) the collision tally which scores the particle weights at each collision for each region, (ii) the surface segment crossing tallies which score the particle weights when the particle crosses a surface segment inward or outward from a region, and,(iii) the track-length estimator which scores the product of the particle weight and particle flight within a region. The square of these quantities is also tallied for the purpose of estimating the variance of each of these tallies.

For statistical purposes, this code uses batch processing. In running the desired number of histories in a large number of batches, confidence is gained in the results since the central limit theorem is approached. Other sampling techniques used by ANDYRPI are Russian Roulette, splitting and energy biasing at each collision. The latter was introduced in order to take into consideration the threshold energy for ^{16}N production in the non-uniform tagging calculations and the detector bias in the gamma detection efficiency calculations. Thus, a neutron or photon history is terminated by leakage from the system, energy cutoff, weight cutoff or failure from playing Russian Roulette.

ANDYRPI's structure consists of a main program and two major subroutines. A flow diagram of this code is shown in Appendix C. The main program sets the required storage for the particular problem to be treated depending on the geometry and energy groups. The subroutine PREP reads and handles the multigroup cross-sections, and stores the geometry parameters. The subroutine BUSY handles the random walk and tallies of the neutron or photon histories. Other small subroutines are required: the random number generator subroutine (GGUBS), the source subroutine (SOURCE) for source-specififed problems, the isotropic direction subroutine (IDODIR) and when the equiprobable scattering method is used, the subroutine ACHG which changes the direction of the particle in the laboratory system after a collision.

A very useful cross-section set to be used with ANDYRPI for neutron tagging and detector efficiency calculations at LOFT (described later) is CASK[36]. CASK is a 40-group coupled neutron and gamma cross-section set. Table 2.1 shows CASK neutron and gamma group structure. Since 14-MeV neutron sources are used at LOFT, and taking into account that the threshold energy for ^{16}N production is 10.2 MeV, only the first two neutron groups are necessary: from 14.9 to 12.2 MeV and from 12.2 to 10 MeV. On the other hand, taking into account that the ^{16}N emits 6.1 MeV gamma rays and the detector(s) are biased near 4 MeV, only two gamma groups are required: from 6.5 to 5 MeV and from 5 to 4 MeV.

ANDYRPI has proved to be a suitable, fast, efficient and economic Monte Carlo code for neutron tagging and detector efficiency calculations.

TABLE 2-I Neutron and Gamma Group Structure in Cross-Section Data Set CASK[36]

NEUTRON GROUP	UPPER ENERGY (eV)
1	1.492 E 7*
2	1.220 E 7
3	1.000 E 7
4	8.180 E 6
5	6.360 E 6
6	4.960 E 6
7	4.060 E 6
8	3.010 E 6
9	2.460 E 6
10	2.350 E 6
11	1.830 E 6
12	1.110 E 6
13	5.500 E 5
14	1.110 E 5
15	3.350 E 3
16	5.830 E 2
17	1.010 E 2
18	2.900 E 1
19	1.010 E 1
20	3.060 E 0
21	1.120 E 0
22	4.140 E-1
	1.000 E-2

GAMMA GROUP	UPPER ENERGY (eV)
1	1.000 E 7
2	8.000 E 6
3	6.500 E 6
4	5.000 E 6
5	4.000 E 6
6	3.000 E 6
7	2.500 E 6
8	2.000 E 6
9	1.660 E 6
10	1.330 E 6
11	1.000 E 6
12	8.000 E 5
13	6.000 E 5
14	4.000 E 5
15	3.000 E 5
16	2.000 E 5
17	1.000 E 5
18	5.000 E 4
	1.000 E 4

* Where, 1.492E 7 ev ≡ 14.92 Mev

2.3 Dispersion Theory

The interpretation of PNA measurements strongly depends on how the irradiated fluid is transported along the pipe from the tagging to detection positions. The importance of understanding the details of this transport is accentuated in large conduits, when a degree of nonhomogeneity in the initial ^{16}N concentration and ^{16}N gamma detection can be achieved.

For fluids in pipes, the mixing is caused by molecular diffusion and turbulent diffusion (for turbulent flows) superposed on the velocity-profile effect[6]. For turbulent flows, the intrinsic turbulent fluctuations are rapid and numerous but not independent,(i.e., correlations exist between them). Unfortunately, the inclusion of such correlations into the analysis would greatly complicate it. Moreover, the detailed theories of turbulence are not yet sufficiently developed to justify their use to describe mixing. A thorough treatment of these theories is given by Hinze[37].

As an alternative, a phenomenological description of turbulent mixing gives good results for many situations. An apparent diffusivity is defined so that a diffusion-type equation may be used, and the magnitude of this parameter can be estimated or found from experiment.

This section deals with flow regime dependent mixing models to determine how the ^{16}N profile changes as an irradiated single or two-phase flow mixture is convected through the conduit.

2.3.1 General Dispersion Model. The dispersion equation which describes the local concentration, $C(t,r,X)$ of the radioactive fluid flowing in a straight pipe, as a function of axial distance, X, radial distance, r, and time, t, is given by:[38]

$$\frac{\partial C}{\partial t} + u(r)\frac{\partial C}{\partial X} = \frac{1}{r}\frac{\partial}{\partial r}\left(\varepsilon_1(r)\, r\,\frac{\partial C}{\partial r}\right) + \varepsilon_1(r)\frac{\partial^2 C}{\partial X^2} \tag{2.14}$$

For a non-uniform, but radially symmetric initial concentration, the initial and boundary conditions may be written as,

$$C(o,r,X) = C_o\,\Psi(X)\,\Upsilon(r) \tag{2.15a}$$

$$\frac{\partial C(t,o,X)}{\partial r} = \frac{\partial C(t,R,X)}{\partial r} = 0 \tag{2.15b}$$

$$C(t,r,-\infty) = C(t,r,\infty) = 0 \tag{2.15c}$$

where, $u(r)$ is the flow velocity profile

$\varepsilon_1(r)$ is the dispersion coefficient profile

$\Psi(X)$, $\Upsilon(r)$ are the initial concentration profiles in the axial and radial coordinates, respectively

C_o is the total initial concentration

R is the radius of the pipe.

For laminar flow, the dispersion coefficient $\varepsilon_1(r)$ is just the molecular diffusion coefficient, D. On the other hand, for turbulent flow, the dispersion coefficient is the sum of D and the eddy diffusivity for mass, which will be discussed later.

Equation (2.14) cannot be solved analytically, and approximate methods have to be used to obtain an analytical solution. It can, however, be solved numerically by finite difference methods.

2.3.2 Taylor Dispersion Theory. G. I. Taylor[39,40] developed analytic relationships to describe the transport of a tracer material in a single-phase fluid flowing in a straight pipe. Taylor showed both theoretically and experimentally that, in a pipe, the center of diffusion for a tracer initially on a plane perpendicular to the flow moves at the mean velocity of the flow. He showed that this was the case in round, straight pipes for both laminar flow[39] and turbulent flow[40], at large distances from the tracer injection.

In his analytical work, Taylor developed the transport model for a tracer material that is uniformly injected on a plane across the pipe. He showed that at large distances from the injection, point the dispersion process could be described by a one-dimensional dispersion model. That is Equation (2.14) could be approximate by,

$$\frac{\partial \bar{c}}{\partial t} + \bar{u} \frac{\partial \bar{c}}{\partial x} = \kappa \frac{\partial^2 \bar{c}}{\partial X^2} \tag{2.16}$$

where, $\bar{c}$ is the cross-sectional average tracer concentration at axial distance X and time t, and is given by

$$\bar{c}\,(t,X) = \frac{1}{\pi R^2} \int_0^R 2\pi r \;\; C(t,r,X)\, dr,$$

$\bar{u}$ is the mean velocity of the flow, and κ is the effective axial diffusion or dispersion coefficient. Upon defining a coordinate system which moves with the mean speed of flow as, $X_1 = X - \bar{u}t$, Equation (2.16) becomes,

$$\frac{\partial \bar{c}}{\partial t} = \kappa \frac{\partial^2 \bar{c}}{\partial X_1^{\,2}} \, . \tag{2.17}$$

and therefore, Equation (2.17) is simply the one-dimensional unsteady diffusion equation to which solutions are readily available under a variety of conditions. Some of these solutions are discussed later. This diffusion equation is supposed to be valid for both laminar and turbulent flows with the only difference in the effective coefficient κ.

For laminar flows, in the absence of axial molecular diffusion, κ is given by[39],

$$\kappa = \frac{R^2 \bar{u}^2}{48D} \tag{2.18}$$

Aris[41] later extended the analysis to include axial molecular diffusion and demonstrated that the dispersion coefficient for this case contains Taylor's result with an additive term due to the axial molecular diffusion. That is,

$$\kappa = D + \frac{R^2 \bar{u}^2}{48D} \tag{2.19}$$

This combined result is referred to as the Taylor-Aris Theory[42].

For turbulent water flows, κ is given by[40],

$$\kappa = 10.1 \; R \; u_* \tag{2.20}$$

The parameter u_* is the friction velocity, given by,

$$u_* = \sqrt{\tau_0 / \rho} \tag{2.21}$$

where, τ_0 is the shear stress at the wall and ρ is the fluid density. The shear stress at the wall, τ_0, is normally given by,

$$\tau_0 = \frac{1}{2} \; c_f \; \rho \; \bar{u}^2 \tag{2.22}$$

where c_f is the fanning friction factor.

Taylor's most important finding in regard to flow measurement by PNA is that the center of the concentration distribution moves with the mean fluid velocity. Therefore, this finding does imply that the mean fluid velocity is uniquely determinable from the PNA measurement. However, it is important to note the restriction placed on Taylor's theory with respect to large distances L (or large times) (i.e. $L/D \geq 50$) since, unless this is verified, the mean concentration distribution is not well described by his dispersion model.

On the other hand, for short distances a generalized one-dimensional dispersion model has been developed by W. Gill for single-phase laminar flows[43-46], and turbulent film flows[47]. This model describes the average concentration distribution when the dispersion coefficients are defined properly as functions of time. He discusses the fact that at short distances from the injection point the transverse diffusion inhibits longitudinal dispersion and therefore the effective longitudinal dispersion coefficient is smaller. As the time increases (i.e. larger L/D) this dispersion coefficient approximates Taylor's classical value. For turbulent flows in pipes no generalization of Taylor's dispersion model has been done because of the complexity of the problem. An alternative to solve the dispersion equation for this case is to find a numerical solution.

2.3.2.1 Solutions to Taylor's Dispersion Model. Analytical solutions to Equation (2.17) can be obtained for different initial conditions. Some examples are:

CASE A: Planar injection at X = o. The initial conditions are:

$$\bar{c}\ (x,0) = \bar{C}_o\ , \quad 0<x<X \tag{2.23a}$$

$$\bar{c}\ (x,0) = 0\ , \ \{ \begin{matrix} X<x \\ x<0 \end{matrix} \tag{2.23b}$$

thus,

$$\bar{c}\ (x,t) = \frac{\bar{C}_o\ X}{2\sqrt{\Pi\kappa t}} \ \exp\left[- \frac{(x-\bar{u}t)^2}{4\kappa t} \right] \tag{2.24}$$

where, $\bar{c}_o$ is the initial tracer concentration and X is the width of the planar tracer injection.

CASE B: Continuous injection at X = o. The initial conditions are:

$$\bar{c}\ (x,0) = \bar{C}_o \qquad x<0 \tag{2.25a}$$

$$\bar{c}\ (x,0) = 0 \qquad x>0 \tag{2.25b}$$

thus,

$$\bar{c}\ (x,t) = \frac{\bar{C}_o}{2} \left[1-\text{erf}\left\{ \frac{x - \bar{u}t}{2\sqrt{\kappa t}} \right\} \right] \tag{2.26}$$

where the error function (erf) is defined as

$$\text{erf}(y) = \frac{2}{\sqrt{\Pi}} \int_0^y e^{-y^2}\, dy$$

CASE C: Continuous injection at x=0 during a time T. The initial conditions are:

$$\bar{c}\ (0,t) = \bar{C}_o\ , \quad -T<t<0 \tag{2.27a}$$

$$\bar{c}\ (0,t) = 0\ , \ \{ \begin{matrix} t>o \\ t<-T \end{matrix} \tag{2.27b}$$

The solution will be a superposition of the solutions in Eq. (2.26),

$$\bar{c}\ (x,t,T) = \frac{\bar{C}_o}{2} \left[\text{erf}\left\{ \frac{x-u(t-T)}{2\sqrt{\kappa(t-T)}} \right\} - \text{erf}\left\{ \frac{x - \bar{u}t}{2\sqrt{\kappa t}} \right\} \tag{2.28}$$

This case is the one used to interpret the single-phase flow PNA measurements at RPI.

2.3.3 Numerical Treatment of the Dispersion Equation.

Consider the general dispersion Equation (2.14), initial and boundary conditions (2.15a), (2.15b) and (2.15c). In dimensionless form, these equations may be written as

$$\frac{\partial \Theta}{\partial \tau} + U(y)\ \frac{\partial \Theta}{\partial x} = \frac{1}{y}\ \left[\frac{\partial}{\partial y}\ (\varepsilon(y)\ y\ \frac{\partial \Theta}{\partial y}) \right] + \frac{1}{Pe^2}\ \varepsilon(y)\ \frac{\partial^2 \Theta}{\partial x^2} \qquad (2.29)$$

with the initial and boundary conditions,

$$\Theta\ (o,y,x) = \Psi\ (x)\ \ Y\ (y) \qquad (2.30a)$$

$$\frac{\partial \Theta(\tau,o,x)}{\partial y} = \frac{\partial \Theta(\tau,1,x)}{\partial y} = o \qquad (2.30b)$$

$$\Theta(\tau\ ,\ y,\ -\infty) = \Theta(\tau\ ,y,\infty) = o \qquad (2.30c)$$

where,

$$\Theta = \frac{C}{C_o}\ ,\quad U_{(y)} = \frac{u(r)}{u_o}\ ,\quad x = \frac{\varepsilon_o\ X}{R^2}\ ,\quad Pe = \frac{Ru_o}{\varepsilon_o}$$

$$y = \frac{r}{R}\ ,\quad \tau = \frac{\varepsilon_o\ t}{R^2}\quad \text{and } \varepsilon(y) = \frac{\varepsilon_1\ (r)}{\varepsilon_o}$$

The parameters u_o and ε_o are the reference velocity and dispersion coefficient, respectively.

For a turbulent single-phase flow, the velocity profile can be taken as[48],

$$u(r) = u_o \left(1 - \frac{r}{R}\right)^{1/n} \qquad (2.31)$$

where u_o is the velocity at the center line and the exponent n varies with the Reynolds number. It is noted here for further reference that the expression for the ratio of the mean to the maximum velocity $\bar{u}/u_o$, can be easily derived from Equation (2.31) as,

$$\frac{\bar{u}}{u_o} = \frac{2n^2}{(n+1)\ (2n+1)} \qquad (2.32)$$

On the other hand, for turbulent single-phase flows, the dispersion coefficient, ε (r), is just the eddy diffusivity for mass, ε_m, which using the Reynolds analogy can be expressed as [49],

$$\varepsilon_m = \nu - \frac{u_*^2 Ry}{(\partial u/\partial y)} \qquad (2.33)$$

where the first term, the viscosity ν represents the dispersion on a molecular level and the second term represents the dispersion due to turbulence. The parameter u_* is the friction velocity, given in Equation (2.21). For the LOFT geometry and conditions (discussed later), the Reynolds number is ~ 70,000 and the exponent n can be taken as 7. Therefore in dimensionless form, the velocity and dispersion coefficient profiles can be expressed as,

$$U(y) = (1-y)^{1/7} \tag{2.34}$$

$$\varepsilon(y) = \frac{\nu}{u_\star R} - \frac{u_\star y}{u_o} \left(\frac{\partial U}{\partial y}\right)^{-1} \tag{2.35}$$

where $\varepsilon_o \simeq u_\star R$.

Thus, taking the derivative of Equation (2.34) and substituting into Equation (2.35),

$$\varepsilon(y) = \frac{\nu}{u_\star R} + \frac{1}{7} \frac{u_\star y}{u_o} (1-y)^{6/7} \tag{2.36}$$

For highly turbulent flows the molecular dispersion is approximately three orders of magnitude smaller than the turbulent dispersion and therefore could be neglected.

On the other hand, for laminar flows the parabolic velocity profile is given by,[48]

$$u(r) = u_o \left(1-\left(\frac{r}{R}\right)^2\right) \tag{2.37}$$

where the velocity at the center line $u_o = 2\bar{u}$. The dispersion coefficient $\varepsilon(r)$ is just the molecular diffusivity ν. Therefore in dimensionless form, the velocity profile and dispersion coefficient can be expressed as:

$$u(y) = 1 - y^2 \tag{2.38}$$

$$\varepsilon(y) = 1 \tag{2.39}$$

which ε_o has been taken equal to ν.

2.3.3.1 Finite difference method. In general, Equations (2.29), (2.30a), (2.30b) and (2.30c) can be written as:

$$\Theta_\tau + U(z)\ \Theta_x = \frac{1}{(1-z)}\ [(1-z)\ \varepsilon(z)\ \Theta_z]_z + \frac{1}{Pe^2}\ \varepsilon(z)\ \Theta_{xx} \tag{2.40}$$

where,

$Z \triangleq 1-y$

$\Theta_x = \frac{\partial\Theta}{\partial x}$

$\Theta_{xx} = \frac{\partial^2\Theta}{\partial x^2}$

with the conditions,

$$\Theta\ (o,z,x) = \Psi(x)\ \ Y(z) \tag{2.41a}$$

$$\Theta\ (\tau,o,x) = \Theta_z\ (\tau,1,x) = o \tag{2.41b}$$

$$\Theta\ (\tau,z,-L^*) = \Theta\ (\tau,z,L^*_1) = o \tag{2.41c}$$

and where the interval from $-L^*$ to L^*_1 is sufficiently large to include essentially all of the tagged fluid. Let us define Θ^n_{jk} as:

$$\Theta^n_{jk} = \Theta(n\Delta\tau,\ j\ \Delta z,\ k\Delta x) \qquad \begin{array}{l} n = 0,1\ ....\ N \\ j = 0,1\ ....\ J \\ k = 0,1\ ....\ K \end{array}$$

where $\Delta\tau$, Δz, and Δx are the time, radial and axial increments for a given grid. The terms in Equation (2.40) can be approximated as follows:

$$U(z)\ \Theta_x \simeq U_j\ \frac{(\Theta_{j,k} - \Theta_{j,k-1})}{\Delta x} \tag{2.42}$$

$$\Theta_z \simeq \frac{(\Theta_{j+1/2,k} - \Theta_{j-1/2,k})}{\Delta z} \tag{2.43}$$

$$\frac{1}{P_e^2} \quad \varepsilon(z) \; \Theta_{xx} \approx \frac{1}{P_e^2} \quad \varepsilon_j \left[\frac{\Theta_{j,k+1} - 2\Theta_{j,k} + \Theta_{j,k-1}}{\Delta x^2} \right] \tag{2.44}$$

$$\frac{1}{(1-z)} \left[(1-z) \; \varepsilon(z) \; \Theta_z \right]_z \approx \frac{1}{(1-z_j)} \left[(1-z) \; \varepsilon(z) \; \frac{\left[\Theta_{j+1/2,k} - \Theta_{j-1/2,k}\right]}{\Delta z} \right]_z$$

$$\approx \frac{1}{(1-z_j)\Delta z} \left[(1-z_{j+1/2}) \; \varepsilon_{j+1/2} \; \frac{(\Theta_{j+1,k} - \Theta_{j,k})}{\Delta z} - \right.$$

$$\left. - \; (1-z_{j-1/2}) \; \varepsilon_{j-1/2} \; \frac{(\Theta_{j,k} - \Theta_{j-1,k})}{\Delta z} \right] \tag{2.45}$$

To handle the singularity at the center line (z=1), one can expand in a Taylor series and take the limit for $z \to 1$, obtaining:

$$\left. \frac{1}{1-z} \; [(1-z) \; \varepsilon(z) \; \Theta_z]_z \right|_{z=1} = 2 \; \varepsilon_J \left[\frac{\Theta_{J+1,k} - 2\Theta_{J,k} + \Theta_{J+1,k}}{\Delta z^2} \right]$$

Finally, using the explicit method in time,

$$\Theta_\tau \approx \frac{\Theta^{n+1}_{j,k} - \Theta^{n}_{j,k}}{\Delta \tau} \tag{2.46}$$

Therefore, in compact form, Equation (2.40) can be approximate by an explicit finite difference method as,

$$\frac{\Theta^{n+1}_{j,k} - \Theta^{n}_{j,k}}{\Delta\tau} = - U_j \ (\Theta_x)^n_{j,k} + \frac{1}{Pe^2} \ \varepsilon_j \ (\Theta_{xx})^n_{j,k}$$

$$+ \left. \frac{1}{(1-z)} [(1-z) \ \varepsilon(z) \ \Theta_z]_z \ \right|^{n}_{j,k} \tag{2.47}$$

Substituting Equations (2.42), (2.43), (2.44) and (2.45) into (2.47), one obtains:

$$\Theta^{n+1}_{j,k} = a_j \ \Theta^n_{j,k} + b_j \ \Theta^n_{j,k-1} + c_j \ \Theta^n_{j,k+1} + d_j \ \Theta^n_{j-1,k} + f_j \ \Theta^n_{j+1} \tag{2.48}$$

where,

$$a_j = \Bigg[1 - u_j \frac{\Delta\tau}{\Delta x} - \frac{2\varepsilon_j}{Pe^2} \frac{\Delta\tau}{\Delta x^2}$$

$$- \frac{\Delta\tau}{\Delta z^2 (1-z_j)} \quad (1-z_{j+1/2}) \ \varepsilon_{j+1/2} + (1-z_{j-1/2}) \ \varepsilon_{j-1/2}\Bigg]$$

$$b_j = \left[u_j \frac{\Delta\tau}{\Delta x} + \frac{\varepsilon_j}{Pe^2} \quad \frac{\Delta\tau}{\Delta x^2}\right]$$

$$c_j = \left[\frac{\varepsilon_j}{Pe^2} \quad \frac{\Delta\tau}{\Delta x^2}\right]$$

$$d_j = \frac{\Delta\tau}{\Delta z^2(1-z_j)} \quad (1-z_{j-1/2}) \quad \varepsilon_{j-1/2}$$

$$f_j = \frac{\Delta\tau}{\Delta z^2(1-z_j)} \quad (1-z_{j+1/2}) \quad \varepsilon_{j+1/2}$$

The boundary conditions (2.41a) (2.41b) and (2.41c) become,

$$\Theta^o_{jk} = \gamma_j \quad \Psi_k \tag{2.49a}$$

$$\Theta^n_{1,k} = \Theta^n_{-1,k} \quad , \quad \Theta^n_{J+1,k} = \Theta^n_{J-1,k} \tag{2.49b}$$

$$\Theta^n_{j,o} = 0 \quad , \quad \Theta^n_{j,K} = 0 \tag{2.49c}$$

A listing of this finite difference code is given in Appendix D.

2.3.3.2 Numerical solutions for turbulent flow. This model has been applied to the LOFT geometry (discussed later) for the case in which a turbulent single-phase flow at a mean velocity of $\overline{u}$=37 cm/s is initially tagged with a uniform planar concentration. Eleven uniformly spaced radial positions from the center of the pipe to the pipe wall were considered. The behavior of some numerical solutions after 2, 5 and 8 seconds after irradiation is shown respectively in Figures 2-4, 2-5 and 2-6. These figures show the concentration distribution through the pipe for: (i) four of the eleven radial positions and (ii) the summed average over all eleven radial positions. Radioactive decay was

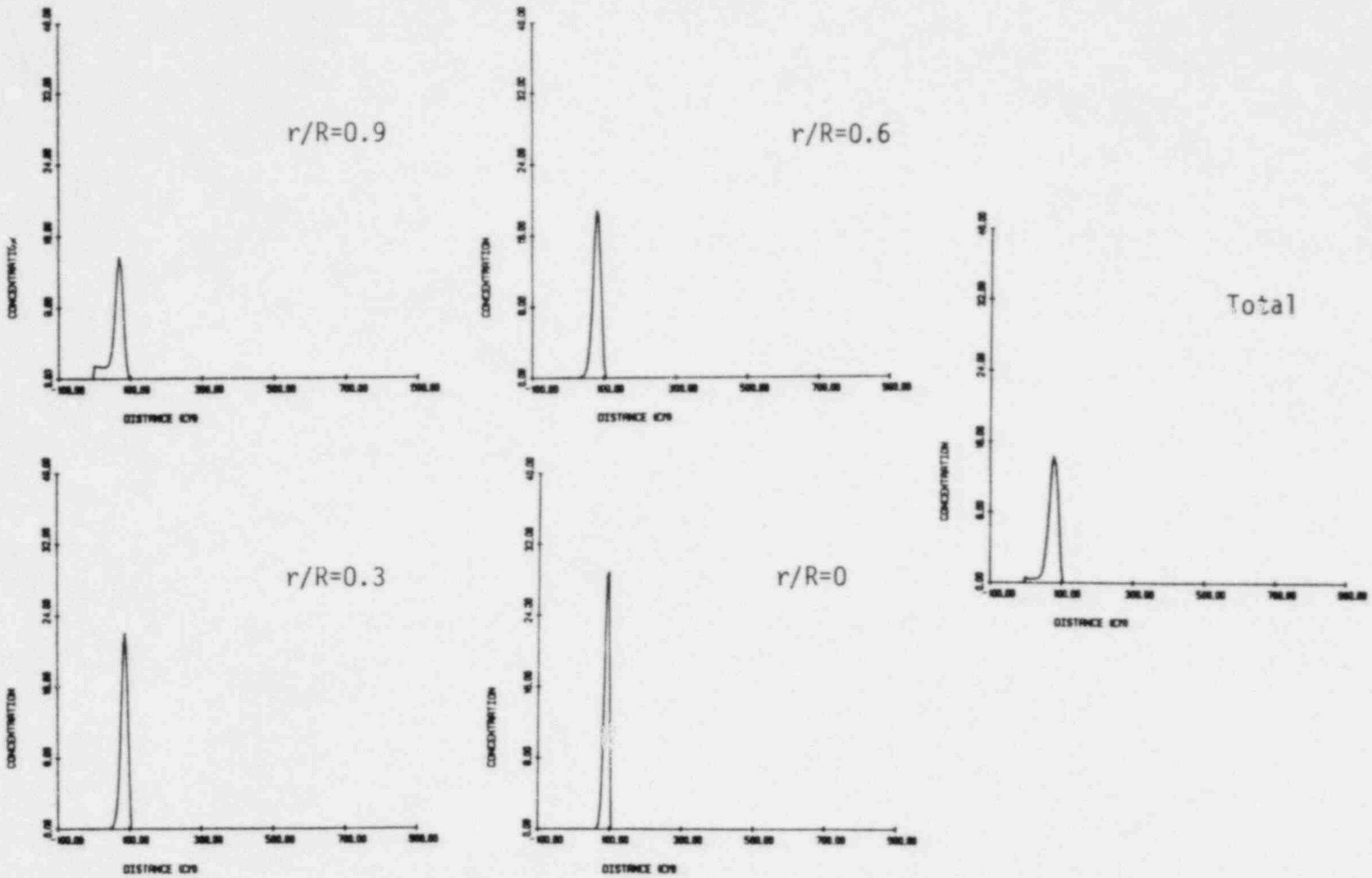

Figure 2-4 Numerical Solutions of the Diffusion Equation after 2 s, for a Mean Flow Velocity of $\bar{u}$=37 cm/s and with the ^{16}N at Time Zero Uniformly Distributed on a Plane at x=0

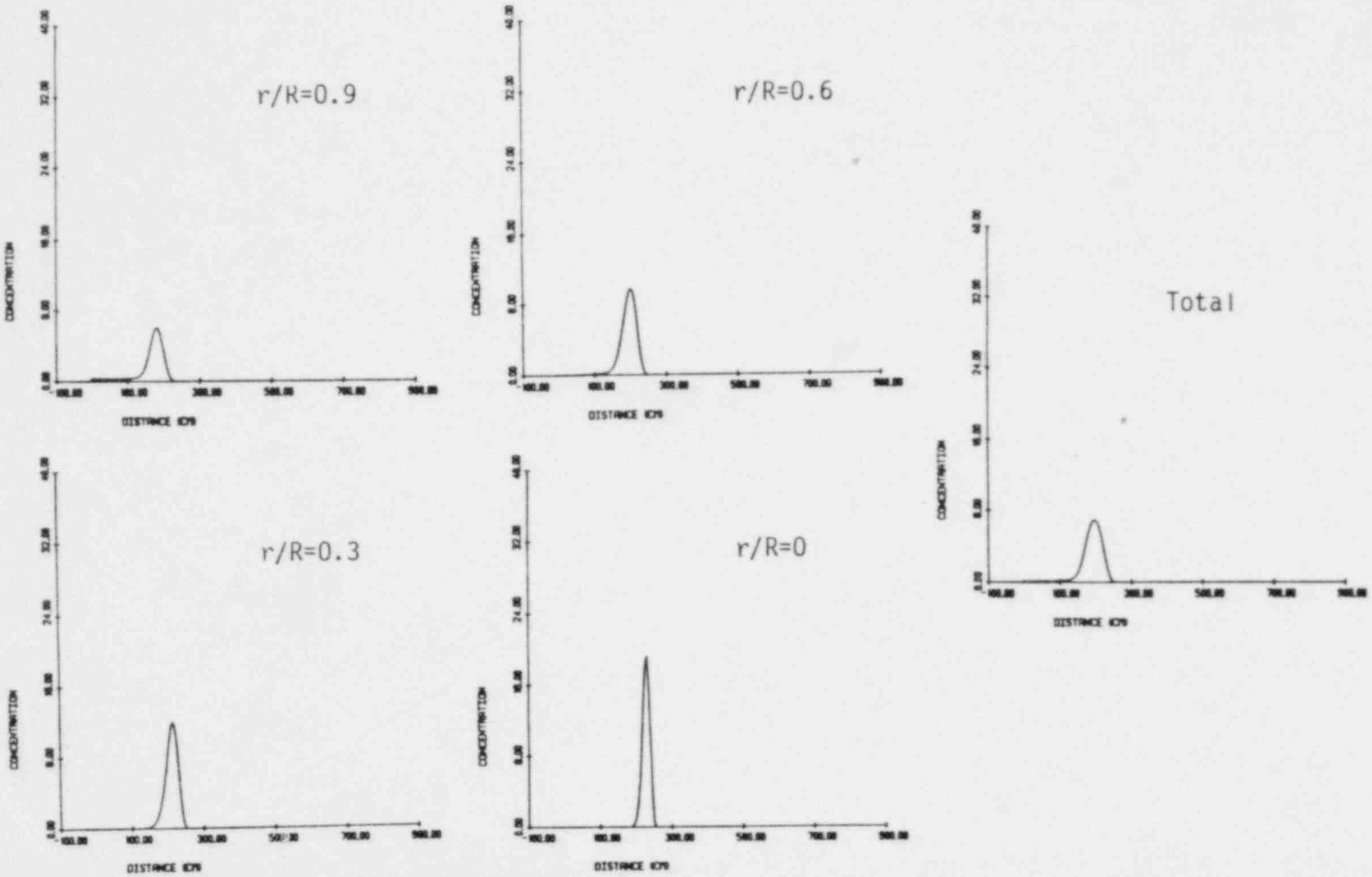

Figure 2-5 Numerical Solutions of the Diffusion Equation after 5 s, for a Mean Flow Velocity of $\bar{u}$=37 cm/s and with the ^{16}N at Time Zero Uniformly Distributed on a Plane at x=0

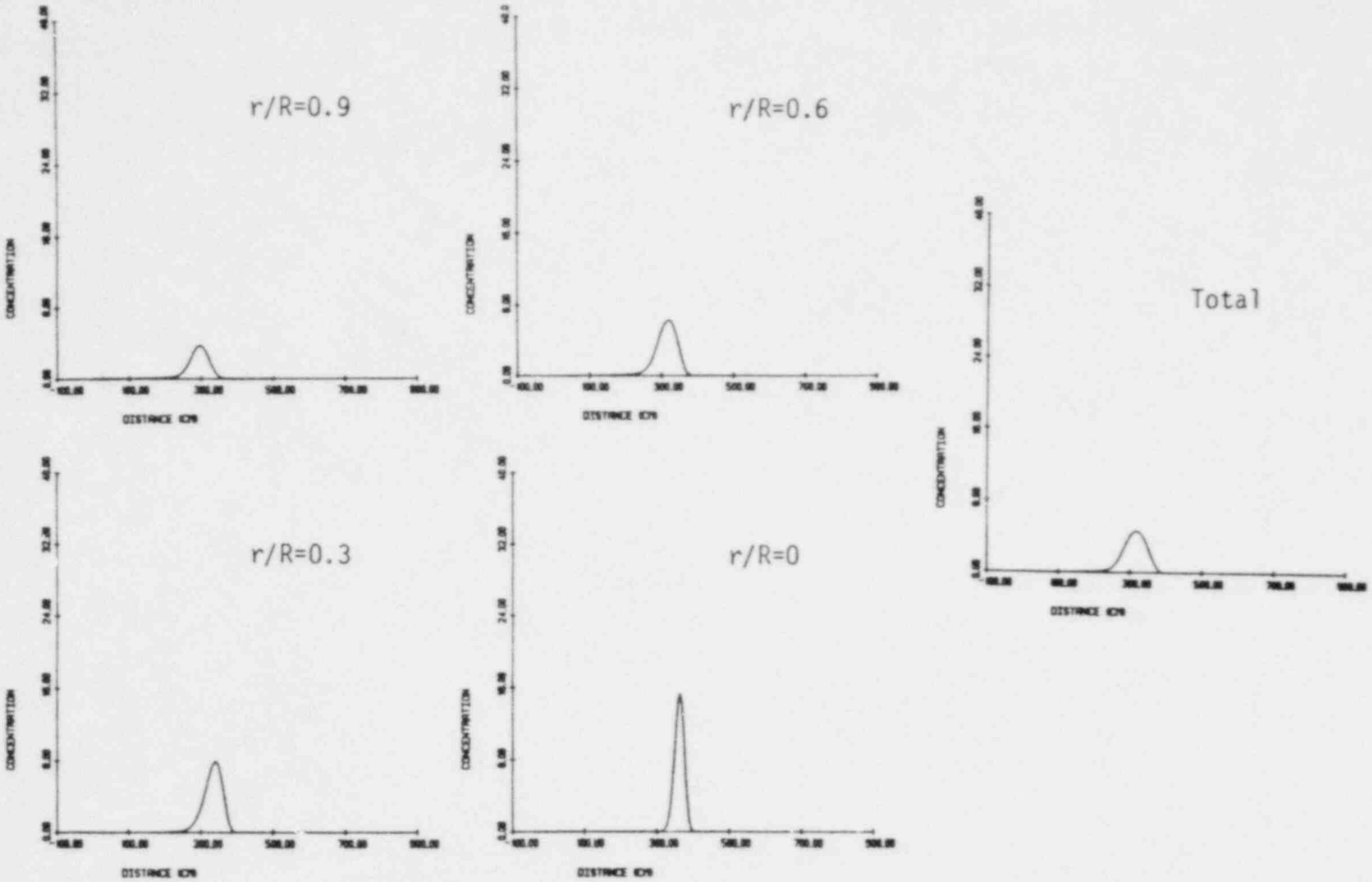

Figure 2-6 Numerical Solutions of the Diffusion Equation after 8 s, for a Mean Flow Velocity of $\bar{u}$=37 cm/s and with the ^{16}N at Time Zero Uniformly Distributed on a Plane at x=0

not considered. It can be observed in Figure 2-4, that at 2s from irradiation the total concentration is very asymmetric. This is due to the asymmetric contribution from the radial regions, over all the regions nearer the pipe walls (e.g.: the one for $r/R=0.9$). At 5s from the irradiirradiation (Figure 2-5), the tag nearer the pipe walls had more time to disperse through the bulk regions, and therefore in the core regions ($r/R=0.3$ through $r/R=0$) the concentration distribution appears to be more symmetrical. Thus, the average concentration does not show the prominent tail as it did at a shorter time. Finally, it is observed in Figure 2-6, that more radial mixing took place through the radial positions at 8s from the injection. This radial transfer is responsible for a more symmetrical total concentration.

From this evaluation it is concluded that the numerical solutions obtained from this finite difference method follow the physical phenomena of radial mass transfer. From Figures 2-4 through 2-6, as the time increases more mixing through the cross-section of the pipe is achieved leading to a more symmetrical total concentration. The validity of this model versus Taylor's classical model for large L/D ratios is discussed in the next section.

2.3.3.3 Comparison between Taylor dispersion and finite difference models. The numerical solutions to the diffusion equation obtained by this finite difference method have been compared with Taylor's analytical solutions[39,40] in order to evaluate the validity of the finite difference model. Three cases have been considered: (i) turbulent single-phase flow for large L/D ratios, (ii) turbulent single-phase flow where Taylor assumptions are included in the finite difference method, and, (iii) laminar single-phase flow without diffusion (pure convection case). For these cases, water was assumed flowing in a 14-in (0.35m) schedule 160 pipe.

Figure 2-7 shows a comparison between the numerical (finite difference) and Taylor analytical solutions for a turbulent single-phase flow with a mean velocity of $\bar{u}$=37 cm/s, and with the ^{16}N at time zero uniformly distributed on a plant at x=0. The concentration time profiles are plotted at 15 meters (Figure 2-7(a)) and 30 meters (Figure 2-7(b)) downstream from the injection position. The corresponding L/D ratios are 52.8 and 105.6, respectively. It can be observed in Figures 2-7(a) and 2-7(b) that the numerical solutions have a broader leading and trailing edges and small peak amplitudes than the Taylor solutions. These discrepancies are due to differences between Taylor's model and the more general numerical model. Also differences result from the coarse axial mesh (Δx=20cm) used to facilitate the computer calculation of the numerical solutions for such long distances. A Δx of 20cm with radial and time increments of 1.4cm and 0.08s followed a stability criteria. The stability criteria for the numerical solutions of the dispersion equation by this finite difference method are [50]:

$[\max u(r)]\ \Delta t/\Delta x \leq 1$ and, $[\max \varepsilon(r)]\ \Delta t/\Delta r^2 \leq 1/2$.

In order to separate out the effect of the axial mesh on the numerical solution for turbulent single-phase flows, Taylor's assumptions were used for the finite difference method; i.e., the 1-D mean velocity was used at each radial position and a constant axial dispersion coefficient was used at all spatial mesh points. Figure 2-8 shows a comparison between Taylor anayltical solutions and two numerical solutions with the same radial increment (Δr=0.7cm) and different axial increments of

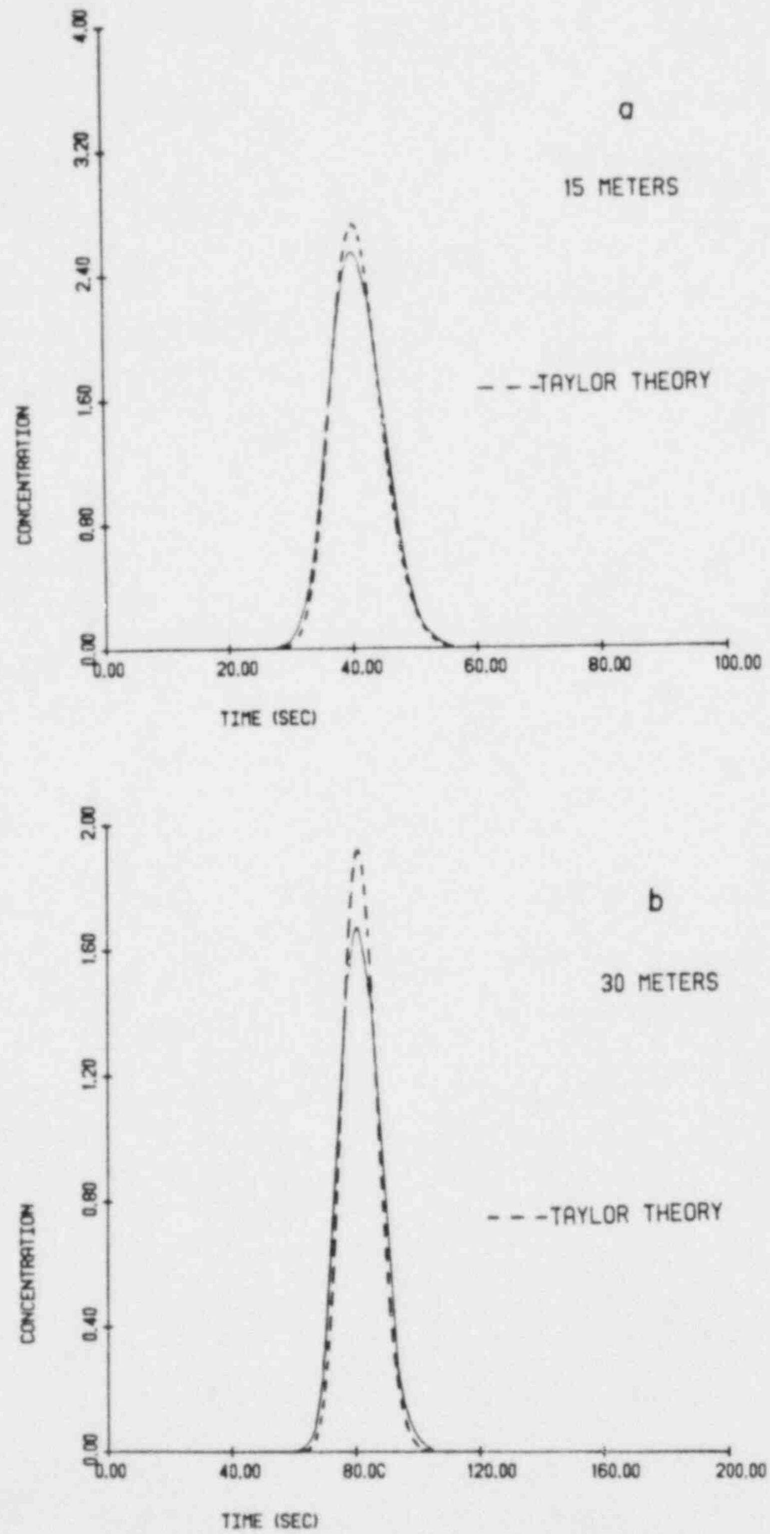

Figure 2-7 Comparison Between Taylor Analytical Solutions and Numerical Finite Difference Solutions Obtained by the Finite Difference Method for a Turbulent Single-Phase Flow at Large L/D Ratios. An Axial Mesh of Δx=20cm Was Used for the Numerical Solutions

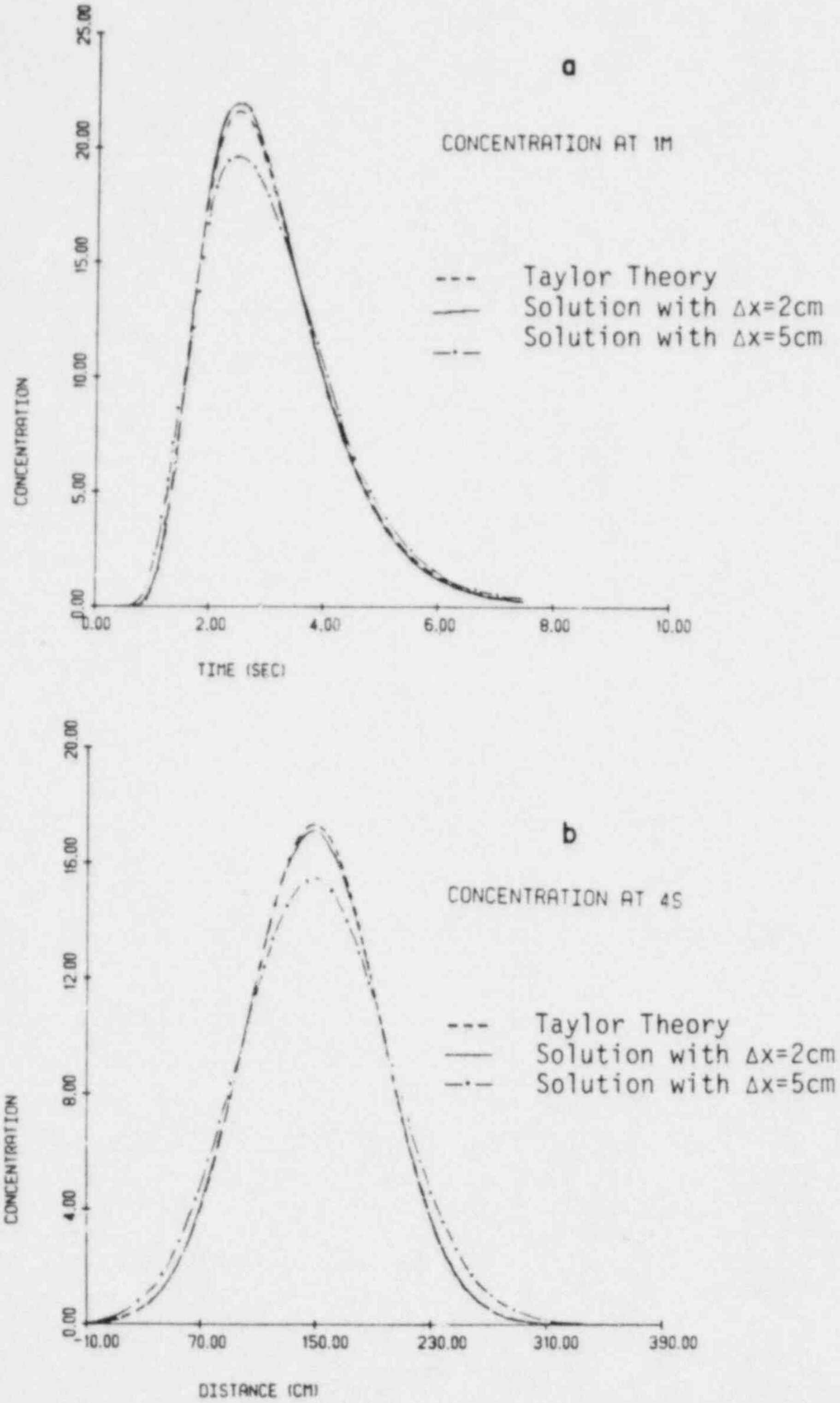

Figure 2-8 Comparison Between Taylor Analytical Solutions and Two Numerical Solutions with Two Different Axial Mesh Increments. Taylor's Assumptions for Turbulent Single-Phase Flow Were Used in the Finite Difference Method

Δx=2cm and Δx-5cm. The turbulent single-phase flow had a mean velocity of $\bar{u}$=37cm/s and the ^{16}N was uniformly distributed, at time zero, on a plane at x=0. Figure 2-8(a) shows the comparison for the concentration time profiles at 1 meter downstream from the tagging position. On the other hand, Figure 2-8(b) shows the comparison for the axial concentration distributions within the pipe at 4 sec after the injection. It is observed in Figures 2-8(a) and 2-8(b) that the numerical solutions with the smaller axial mesh increment (Δx=2cm) give a much better agreement with Taylor solutions with only a small discrepancy on the amplitude of the peak. It is expected that by decreasing the axial mesh this discrepancy would decrease further.

To discuss the validity of this finite difference model for laminar flows, the pure convection case (no diffusion) of irradiated water flowing at a mean velocity of 0.1 cm/s was considered. At time zero, the ^{16}N was assumed to be uniformly distributed within two planes, i.e., 0cm$\leq x \leq$ 10cm. Figure 2-9 shows a comparison of the axial concentration distributions within the pipe obtained from Taylor theory and from the finite difference method with the same radial increment (Δr = 0.28cm) and two axial increments of Δx = 1cm and Δx = 0.1cm. These concentration distributions are given at 50 sec (Figure 2-9 (a)) and 100 sec (Figure 2-9 (b)) after the irradiation. It is observed that the solution with the smaller axial increment gives good agreement with the analytical solution.

From these evaluations, it is concluded that the finite difference method developed here gives a good representation of the transport of irradiated laminar and turbulent single-phase flows, if the spatial

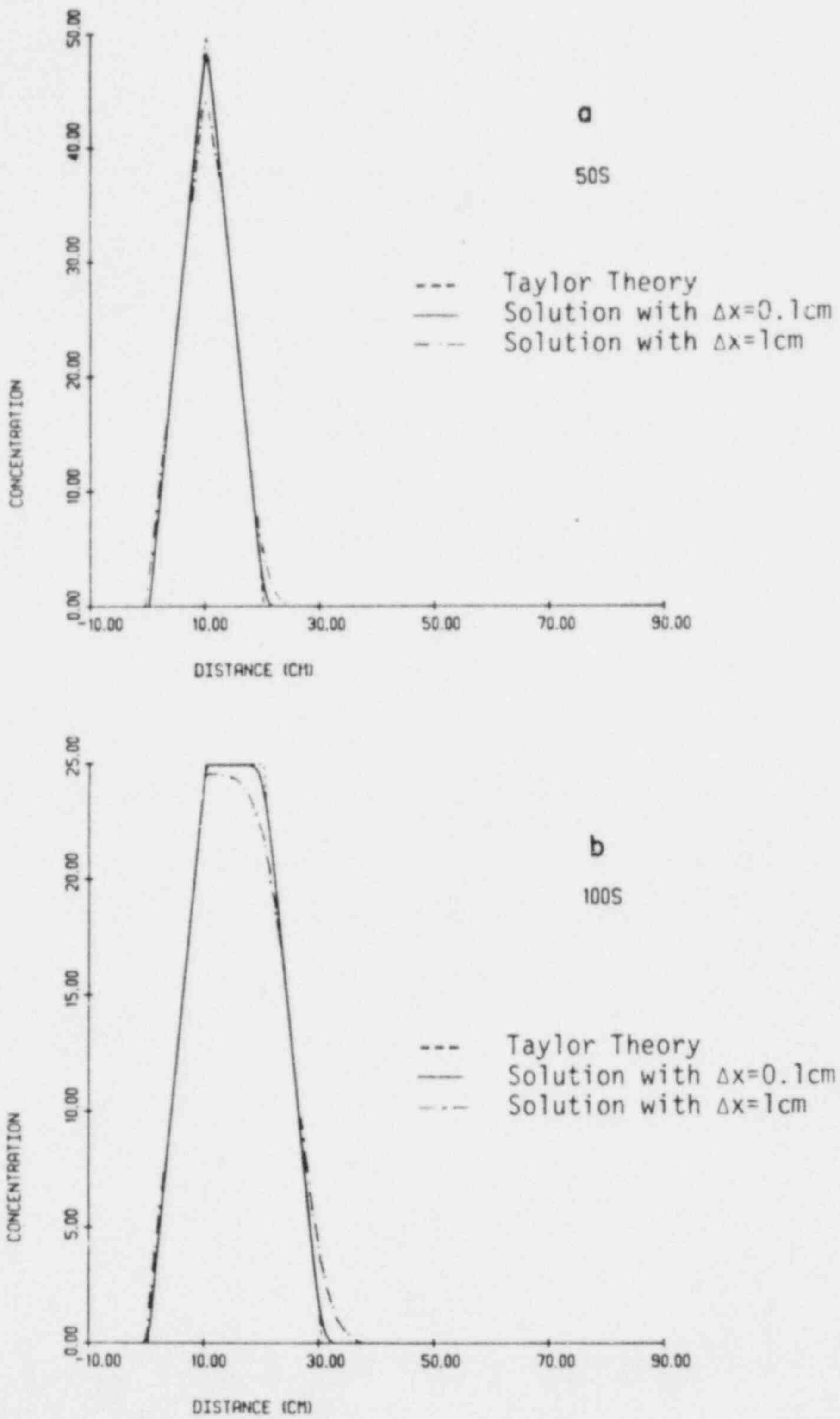

Figure 2-9 Comparison Between Taylor Analytical Solutions and Two Numerical Solutions with Two Different Axial Mesh Increments, for a Single-Phase Laminar Flow Without Diffusion

mesh is adequately chosen. That is, it is not only necessary to select Δr, Δx and Δt which follow the stability criteria for the solutions, but it is also important that they be small enough to give a good representation of the dispersion phenomena. For the LOFT geometry, discussed later, it is estimated that ratios of $\Delta r/\Delta x$ cf $\underset{\sim}{\sim}$ 2.8 for laminar flows and 1.0 for turbulent flows are optimum.

It appears that classical dispersion theory is capable of predicting the fluid transport and mixing phenomena in laminar and turbulent single-phase flows. Indeed, it appears that this technique can be readily extended to two-phase flows once the mixing process has been specified.

Let us next consider the development of an ad hoc mixing model for a particular two-phase flow regime; slug flow.

2.4 Mixing Model for Slug Flow

This mixing model was developed to analyze the fine structure observed in the vertical slug-flow data obtained using ^{16}N tagging techniques at RPI[22,23] (See Section 3.3.2).

Figure 2-10 schematically represents a steady-state, fully developed adiabatic air/water slug flow regime. Consider the control volume "i" which includes all the water in one liquid slug. If one assumes perfect mixing within the liquid slug, the ^{16}N concentration balance equation in control volume "i" can be written as,

$$w_f C_i - w_f C_{i-1} + \frac{d}{dt} [M_i C_i] = 0 \tag{2.50}$$

where,

C_i = ^{16}N concentration in control volume "i" (corrected for ^{16}N decay)

$M_i = M_{i-1} = M_{i+1} \equiv M$, the mass in the control volumes

w_f = Slug-to-slug mass flow rate

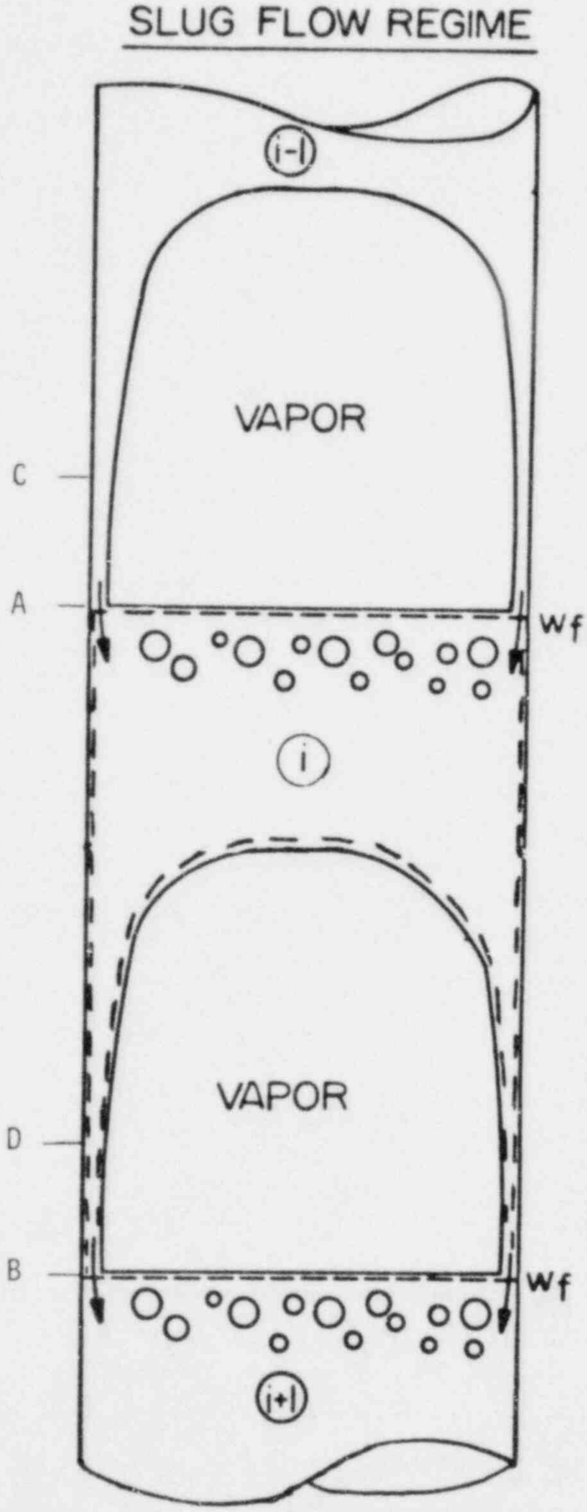

Figure 2-10 Steady-State, Fully Developed Adiabatic Slug Flow Regime

Since we have assumed M is constant,

$$w_f C_i - w_f C_{i-1} + M \frac{dC_i}{dt} = 0 \qquad \text{or,} \tag{2.51}$$

$$\frac{dC_i}{dt} + \tau C_i = \tau C_{i-1} \tag{2.52}$$

where, $\tau = \frac{w_f}{M}$, will be defined as the slug-to-slug exchange rate (i.e., the fraction of slug mass exchanged per unit time).

Equation (2.52) is a Bernoulli equation whose solution is given by,

$$C_i(t) = \tau \int_0^t e^{\tau(t'-t)} C_{i-1}(t')\, dt' + A_i e^{-\tau t} \quad \text{for } i = 1,2,\ldots.. \tag{2.53}$$

where, A_i are determined by the initial conditions.

When the irradiation time corresponds to one slug period (i.e., the period between positions A-B in Figure 2-10), the initial conditions will be given by,

$$C_1(t = 0) = C_0 \tag{2.54a}$$

$$C_i(t = 0) = 0, \text{for } i > 1 \tag{2.54b}$$

where C_0, the initial concentration, is equal to the total ^{16}N mass divided by the mass of one slug. The general solution of Equation (2.53) has been found by recurrence (see Appendix B) to be,

$$\frac{C_i(t)}{C_0} = \frac{(\tau t)^{i-1}}{(i-1)!} e^{-\tau t} \tag{2.55}$$

Therefore, assuming perfect mixing the ^{16}N concentrations in successive slugs divided by the initial concentration, follows a Poisson distribution.

When the irradiation time is split between two adjacent slugs (e.g., between position C-D in Figure 2-10), the initial conditions will be given by:

$$C_1(t=0) = \eta C_0 \tag{2.56a}$$

$C_2(t=0) = (1-\eta)\, C_o$ (2.56b)

$C_i(t=0) = 0 \quad i > 2$ (2.56c)

where, η is the fraction of total ^{16}N activity induced in the first of two adjacent irradiated slugs. Thus, the general solution of Equation (2-53) can be given by the superposition of two Poisson distributions as follows,

$$\frac{C_i(t)}{C_o} = \eta \frac{(\tau\, t)^{i-1}}{(i-1)\,!}\, e^{-\tau t} + (1-\eta) \frac{(\tau\, t)^{i-2}}{(i-2)\,!}\, e^{-\tau t} \qquad (2.57)$$

The NaI detector counting rate is proportional to the ^{16}N activity in the pipe which passes in front of the detector at time "t". Thus, the first activated slug passing in front of the detector is from slug number 1 at time t_o, where t_o is the time of travel of slug 1 from the target to the detector. The next slug, number 2, arrives at time $t + \Delta t$, and the i^{th} slug arrives at $t_o + (i-1)\Delta t$, where Δt is equal to the time period between slugs.

In fitting the experimental data, a gaussian distribution has been chosen to represent the axial dispersion of the tagging liquid within each slug. Figure 2-11 shows six time profiles calculated for an irradiated slug flow mixture. In Figures 2-11a through 2-11c, the first slug has been assumed to be entirely irradiated (η=1.0) and τ has the values of 0.3, 0.5 and 0.7 s^{-1}, respectively. It can be seen that the exchange rate parameter τ determines the exponential-like decay of the trailing edge of the envelope of the time profile. In Figures 2.11d through 2-11f, τ = 0.4 s^{-1} and η has been varied as 0.8,

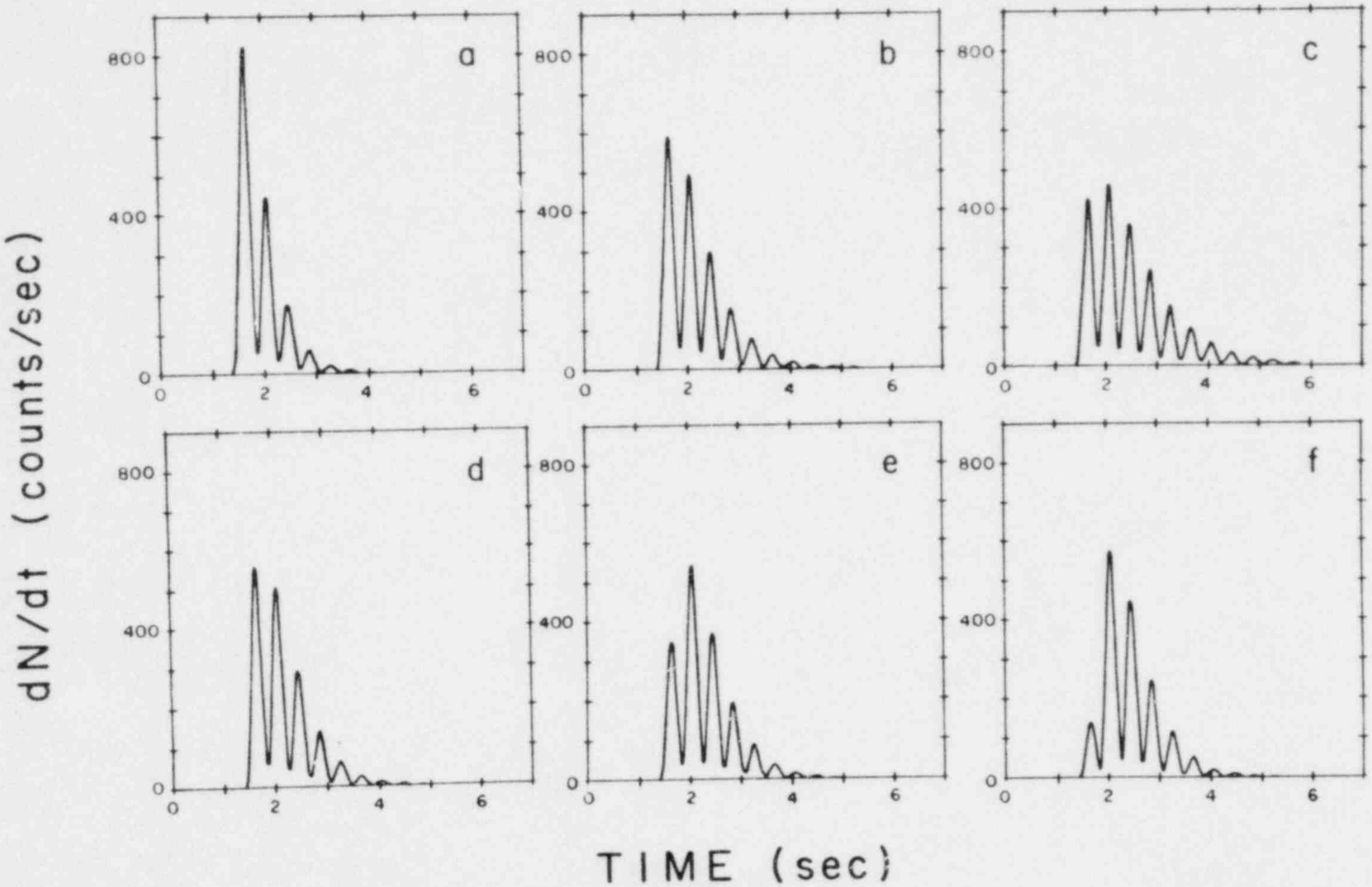

Figure 2-11 Calculated NaI Detector Time Profiles for an Irradiated Slug-Flow Mixture, where the Irradiation Time of 0.4 s Equals the Time Period Between Successive Slugs

0.5 and 0.2, respectively. We observe that η strongly influences the relative amplitudes of the early peaks in the time profiles.

In this ad hoc two-phase mixing model the slug-to-slug mass exchange was considered to be a consequence of the relative velocity between the phases. In addition, uniform mixing within the liquid slug was assumed. As will be discussed later, the experimental slug-to-slug exchange rate obtained with this model differs from the classical value[53] which suggests improvements to this mixing model are necessary.

As discussed previously, a dispersion theory can be generalized to two-phase flows once the mixing process is specified. That is, in principle, an equation similar to equation (2.14) can be derived for the various two-phase flow regimes. This generalization will include the proper modelling of the turbulent structure of the liquid phase. For the case of slug flow, the dispersion will be due not only to the usual single-phase molecular and turbulence effects, but there will also be induced turbulence effect due to the displacement of the liquid by the vapor bubbles. This latter effect could be modeled using classical mixing length arguments.[61]

PART 3

PNA MEASUREMENTS AT RPI

3.1 Experimental Apparatus

The Gaerttner Laboratory electron LINAC at RPI provides an extremely intense source of photoneutrons. Photoneutron targets of tantalum or tungsten-plus-boron carbide are used for neutron production where the latter target is designed for high-energy neutron production. When the LINAC is operated at an electron energy of 65 MeV and average electron current of 100 μA, the total neutron production rate is $\approx 3 \times 10^{13}$ n/s. The epi-threshold neutron production rate for the $^{16}O\ (n,p)^{16}N$ reaction ($E_n > 10.2$ MeV) has been estimated from the evaporation spectra of the boron carbide[51] to be ~10% of the total neutron production rate, thus, the production rate of neutrons capable of tagging is, $\sim 3 \times 10^{12}$ n/s.

A sketch of the apparatus used for two-phase flow measurements is shown in Figure 3-1. The electrons strike a water cooled photoneutron target, and a water/air mixture flowing in a 2.5-cm (1-in) I.D. vertical pipe passes in front of the target. A shielded 7.6-cm-dia. by 5.1-cm-high (3-in by 2-in) NaI crystal is placed downstream from the irradiation position, and this detector is biased to only respond to the 6.1-MeV ^{16}N gamma rays. The detected ^{16}N signals are passed to a 1024-channel multi-channel time analyzer where the ^{16}N activity is recorded as a function of time after the LINAC pulse. The LINAC and multi-channel time analyzer are controlled by an electronic timer to obtain either single or multiple-pulsed irradiations. The sketch and design of this ^{16}N tagging electronic timer are shown in Figure 3-2.

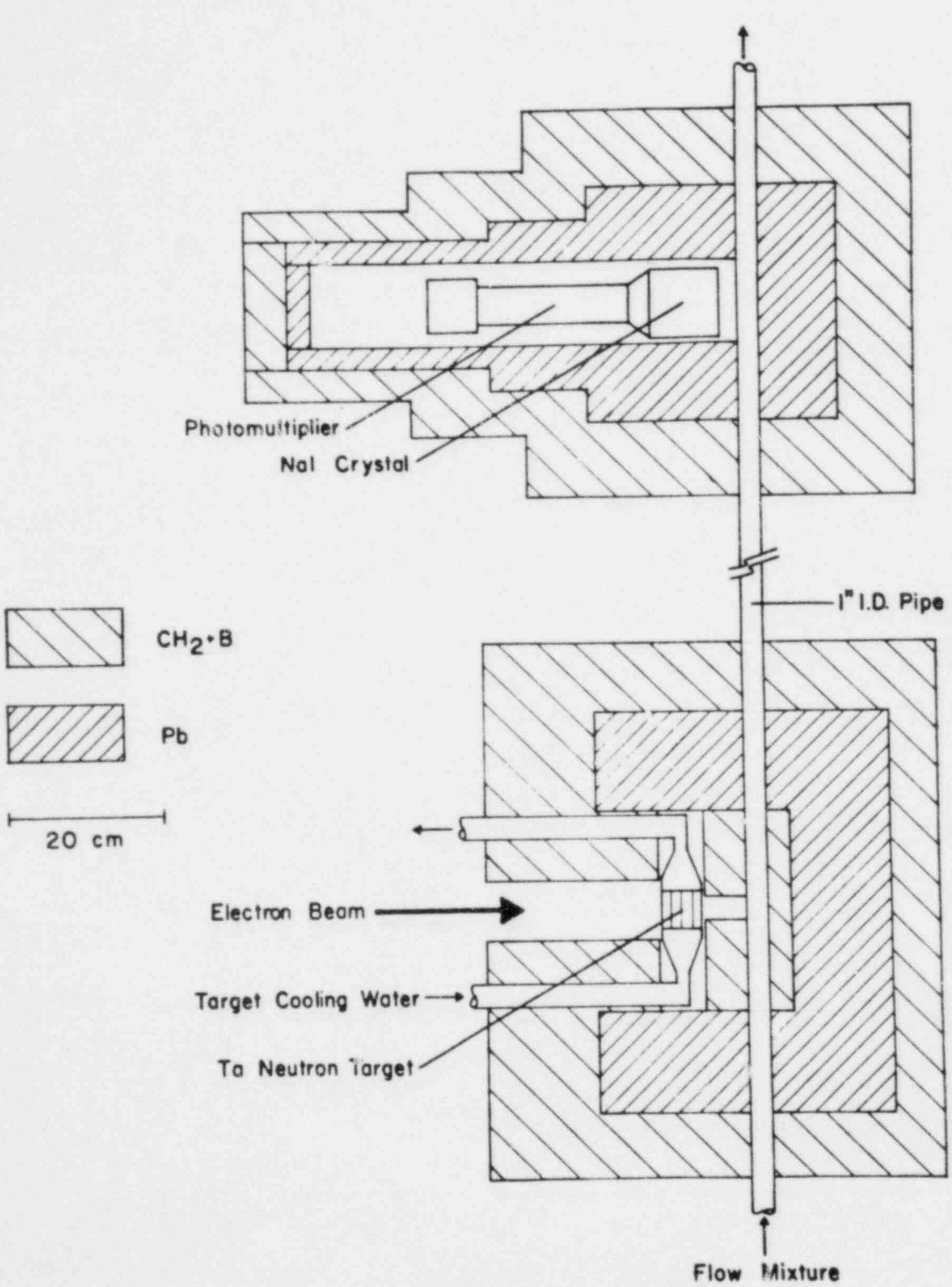

Figure 3-1 Experimental Setup for One-Phase and Two-Phase Flow ^{16}N Tagging Measurements

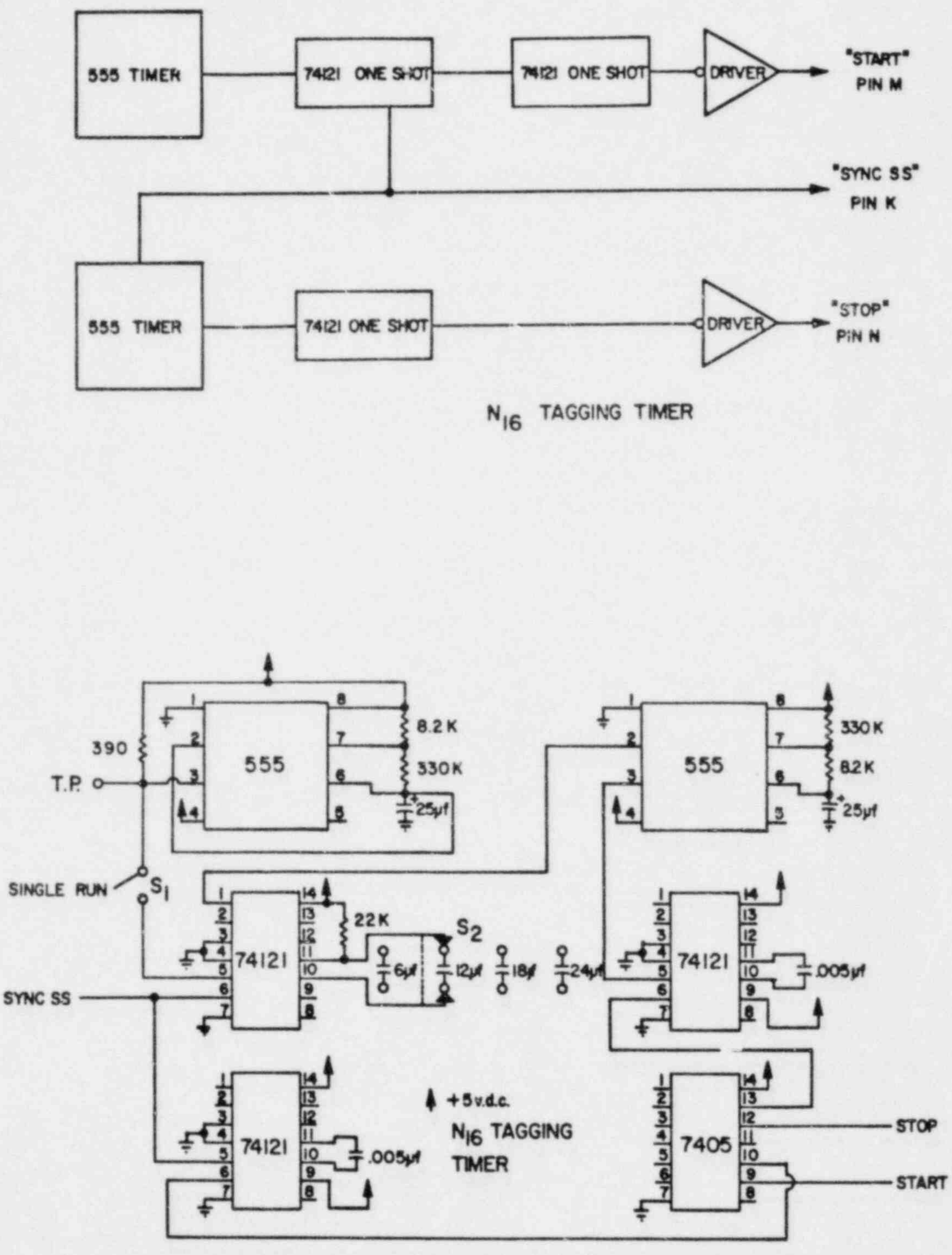

Figure 3-2 ^{16}N Tagging Electronic Timer. Scheme and Circuit Diagram

The air/water loop facility used for these experiments has a water and air flow capability up to 0.5 liter/s (8 gpm) and 6.3 liter/s (800 SCFH), respectively. The air can be introduced into the system through a bubble generator with 0.08-cm-dia. holes or by a porous air stone. This system is capable of simulating a wide range of two-phase flow regimes.

One of the main problems noted with the ^{16}N tagging system was the neutron and gamma activation of the detector. Considerable care was taken to avoid this problem by providing appropriate neutron and photon shielding. As it can be observed in Figure 3-1, the detector as well as the photoneutron target were well shielded from gamma and neutron radiations with lead and borated polyethylene. The shielded detector assembly is shown in Figure 3-3, where it can be seen to be a fairly massive structure.

3.2 Single-Phase Flow Measurements

Single-phase ^{16}N tagging measurements have been carried out both with the arrangement shown in Figure 3-1, and with the target-cooling water passing directly to the NaI detector as shown in Figure 3-4. Some measurements with the target cooling water have been reported.[20] Other of these results are shown in Figure 3-5. The histogram data are the counts per time channel for water irradiated for single pulses of duration 0.3, 0.9, 1.7 and 3.3 s. In this measurement of single irradiated pulses, the signal-to-background ratio is greater than 300:1. The average water velocity of 2.94 m/s (9.64 ft/s) was determined from the data using the transit-time-method (Equation 2.7). The continuous curves are fits to the diffusion theory of G.I. Taylor[40], as explained in

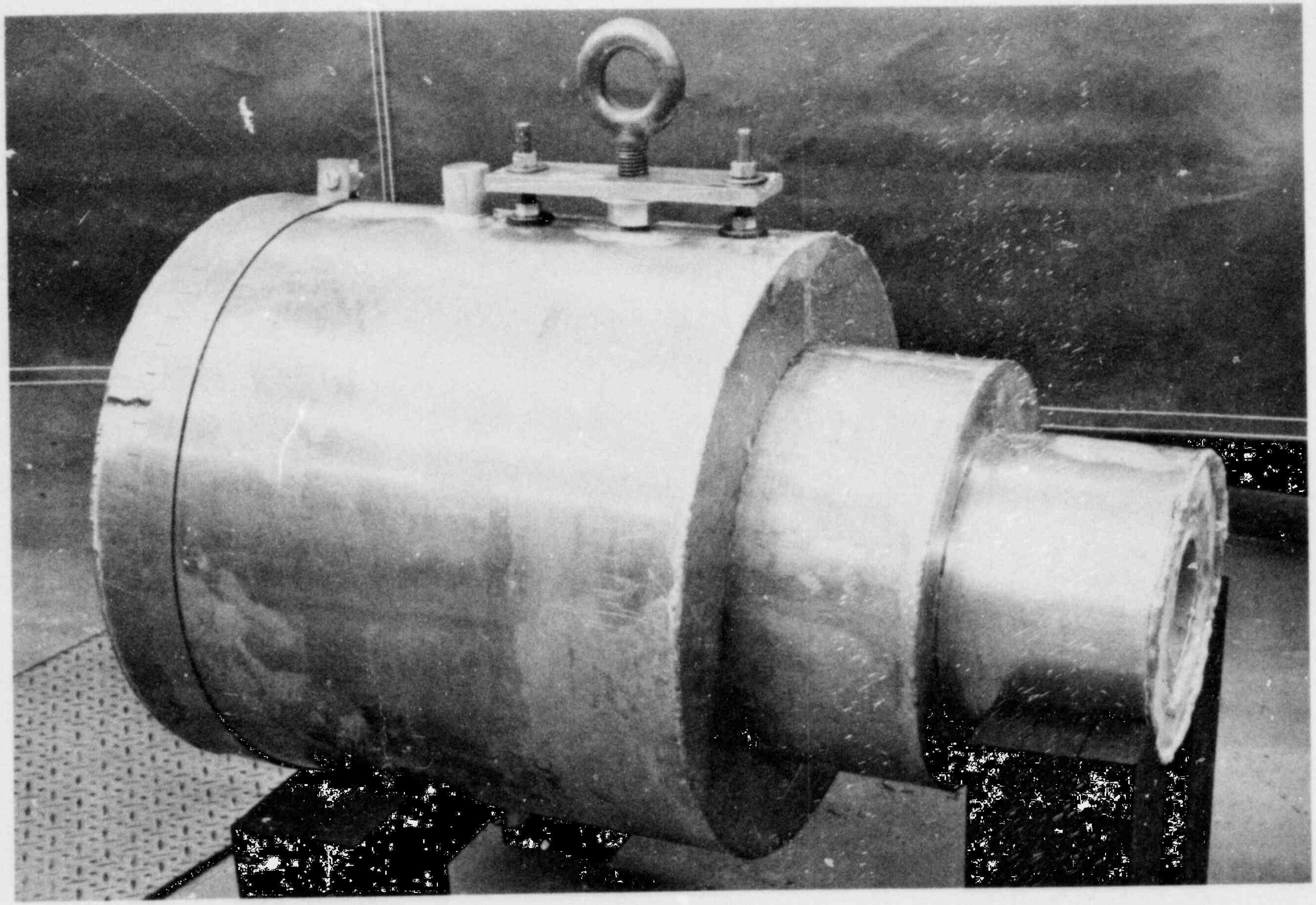

Figure 3-3 Shielded Detector Assembly for ^{16}N Tagging Measurements

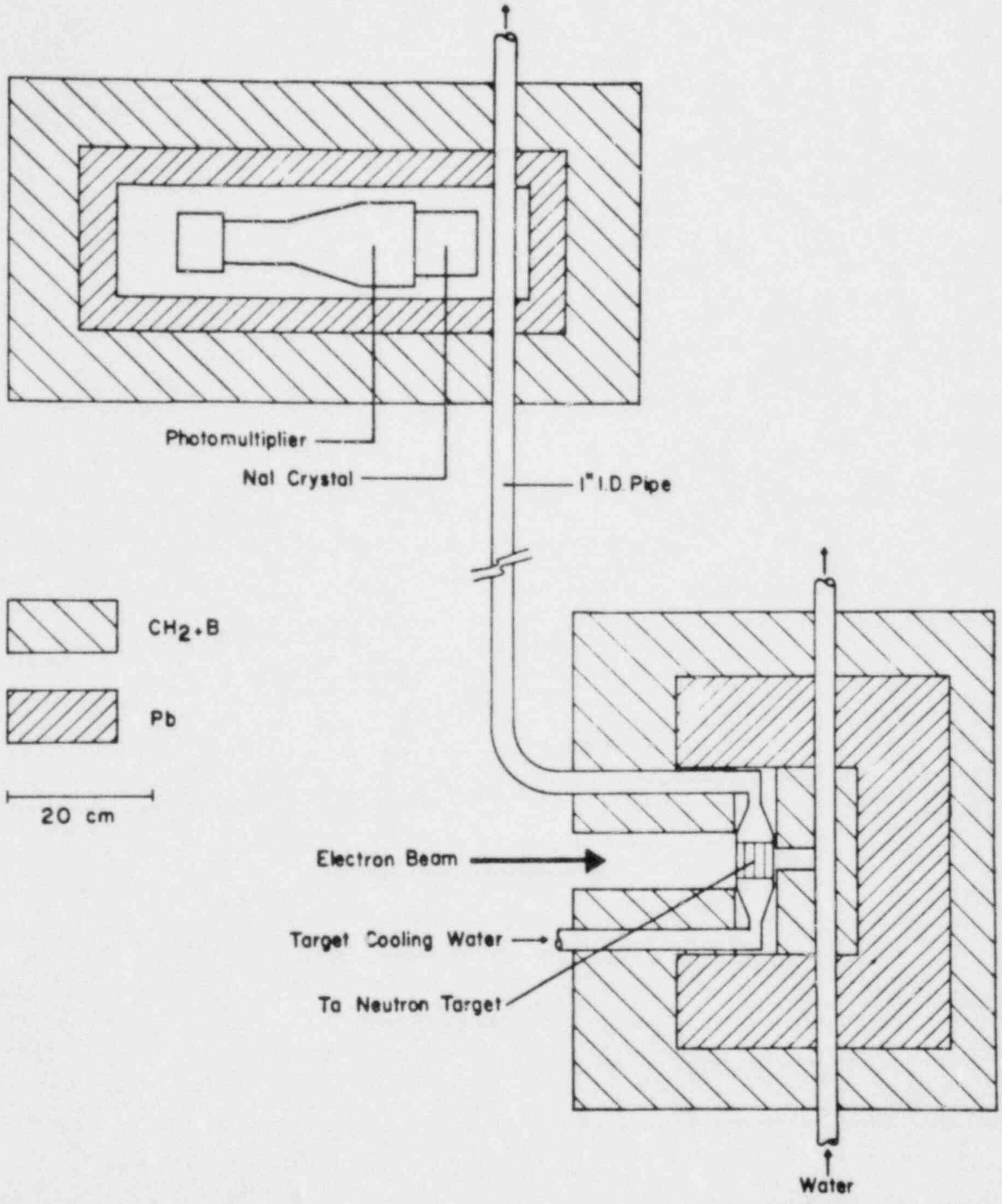

Figure 3-4 Experimental Setup for One-Phase Flow ^{16}N Tagging Measurements when the Target-Cooling Water is used

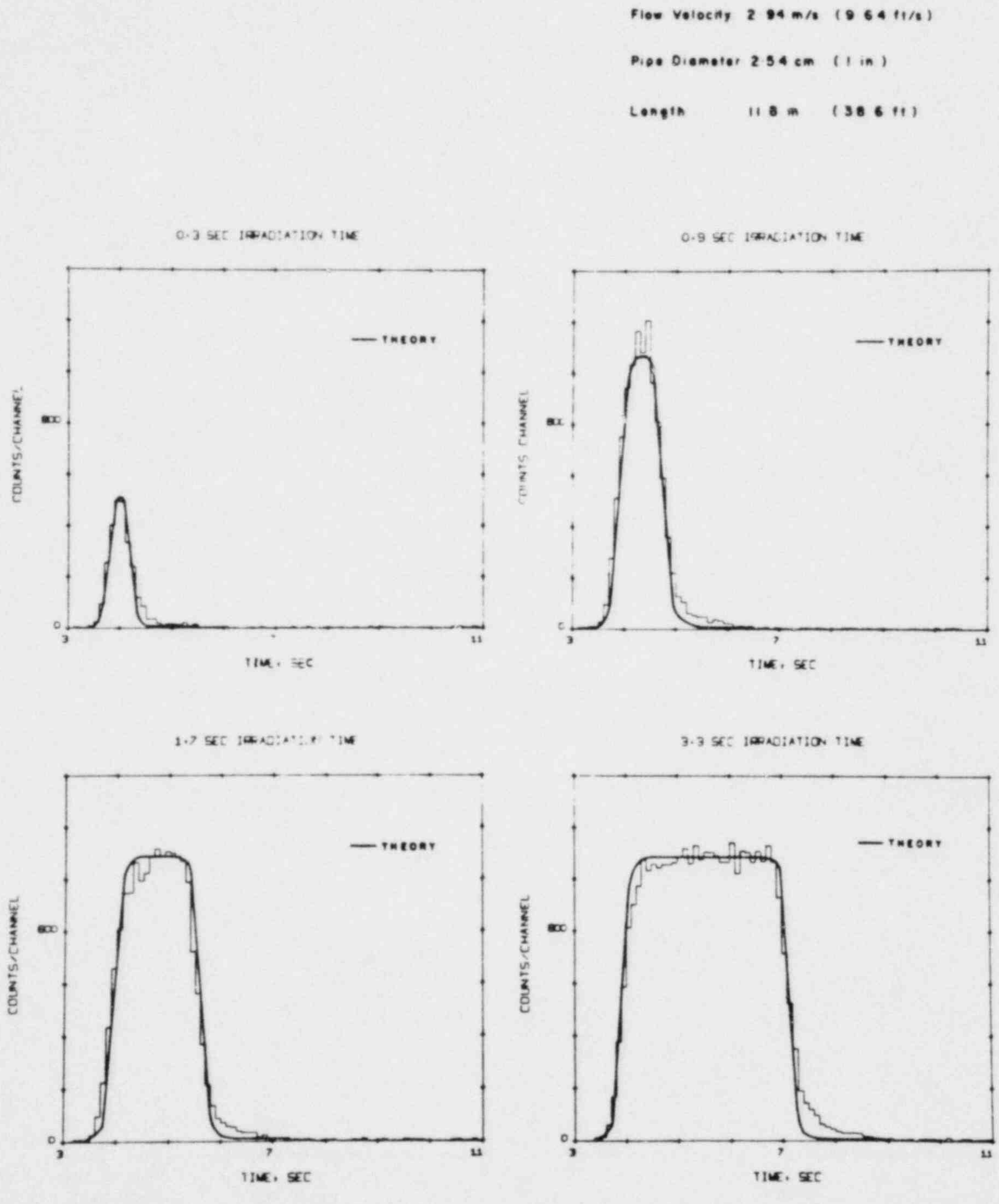

Figure 3-5 Time Profiles of the Gamma-Ray Counting Rate from Single Slugs of Water Irradiated for 0.3, 0.9, 1.7 and 3.3 s

Section 2.3.2. The theoretical fit to the data does reasonably well in predicting the overall mass flow rate profile of tagged water, but there appear to be small departures from this theory near the top of the leading edge and bottom of the trailing edge of each pulse. These deviations were interpreted[20] in terms of some trace of laminar flow near the pipe walls (laminar boundary layer).

3.3 Two-Phase Flow Measurements

Two-phase flow measurements were carried out with the experimental setup shown in Figure 3-1 in which the distance between the target and detector was 1.9 m. The water flow was set at 0.18 liter/s (2.9 gpm), corresponding to a Reynolds number of ≈11,000, to ensure turbulent flow. The air flow was varied to cover the range from bubbly to annular flow. Figures 3-6 and 3-7 show the two-phase flow regimes that were analyzed at the tagging and detector positions, respectively. Measurements were carried out for single pulse, and for an ensemble of pulses of irradiation. The data were corrected for background decay from the 7.11-s half-life of ^{16}N. These results have been already reported.[21]

3.3.1 Ensemble of Pulses of Irradiation. Five time profiles for ensemble of 20 to 25 pulses in the full range from single-phase to annular flow regimes are shown in Figure 3-8. On the ordinate the counting rates are normalized to 100 μCi of electrons onto the target, which implies normalization to the same neutron flux. The mass weighted velocity, $\langle V_{L_o} \rangle_m$, was determined to within 1% by the transit-time method described in Section 2.1.1 (Equation 2-7), where the major error contribution was due to uncertainty in target-detector distance. The results are listed in Table 3-I, where $\langle j_\ell \rangle$ and $\langle j_g \rangle$ are the superficial

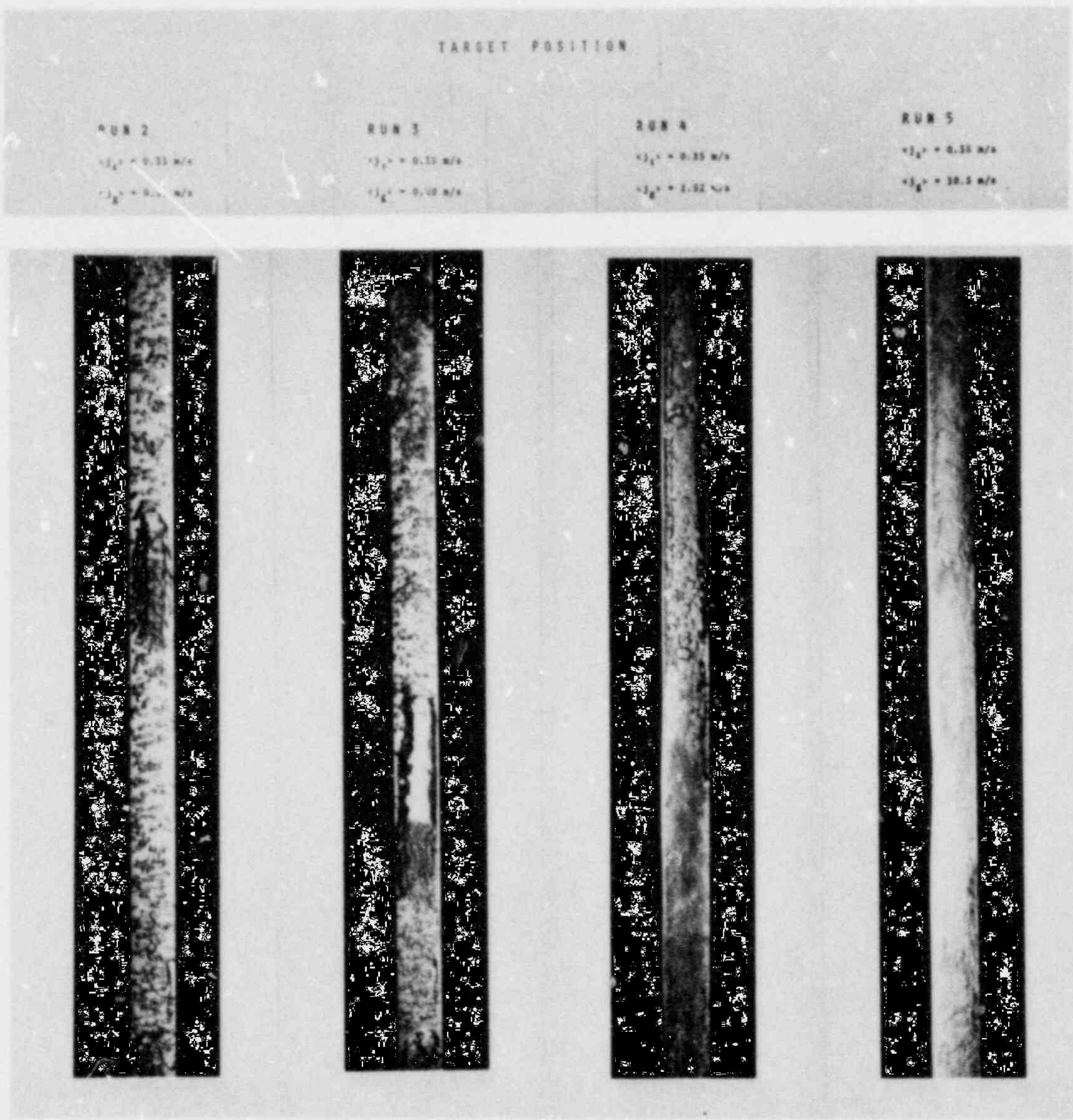

Figure 3-6   Two-Phase Flow Regimes at the Target Position

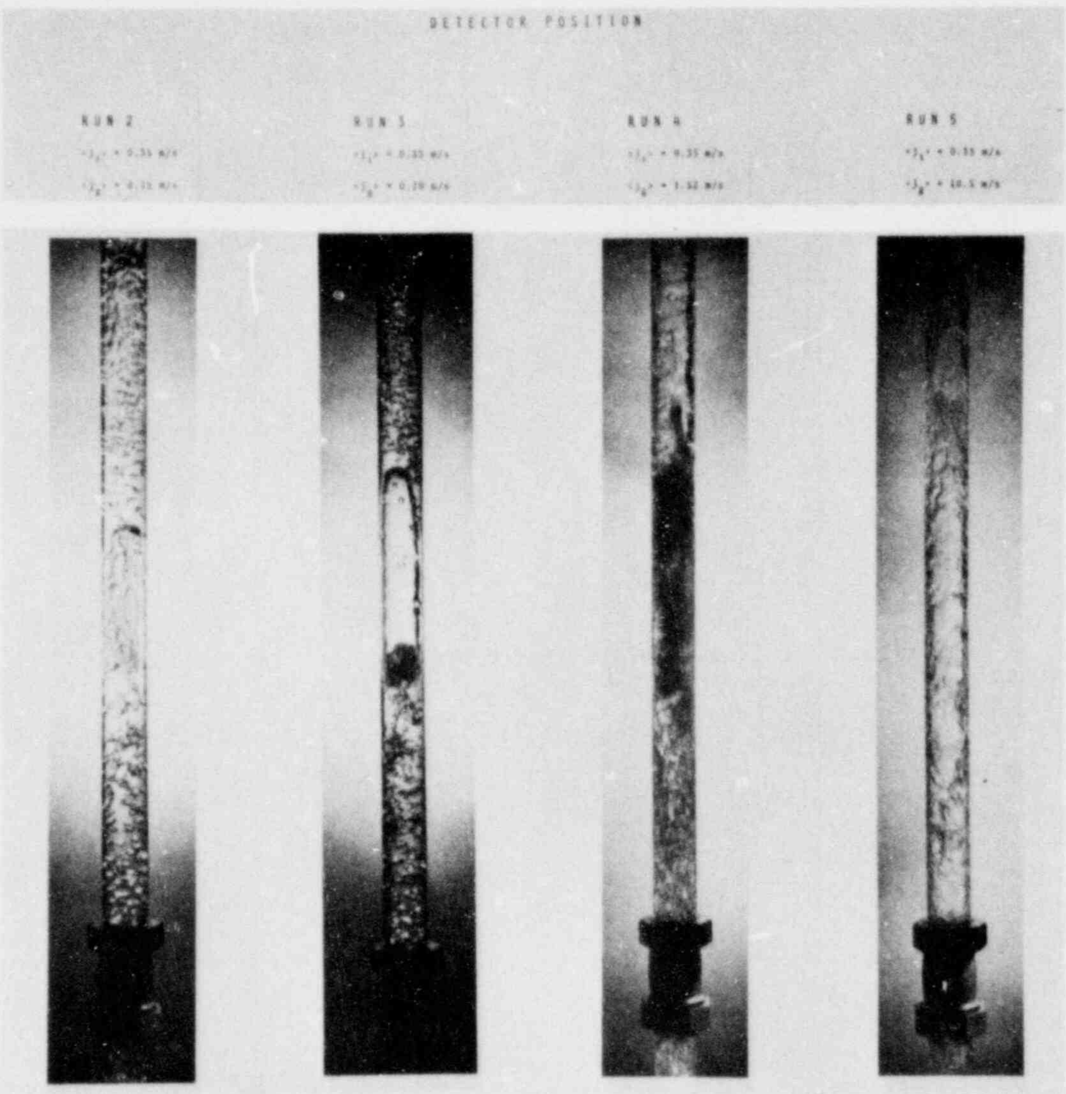

Figure 3-7 Two-Phase Flow Regimes at the Detector Position

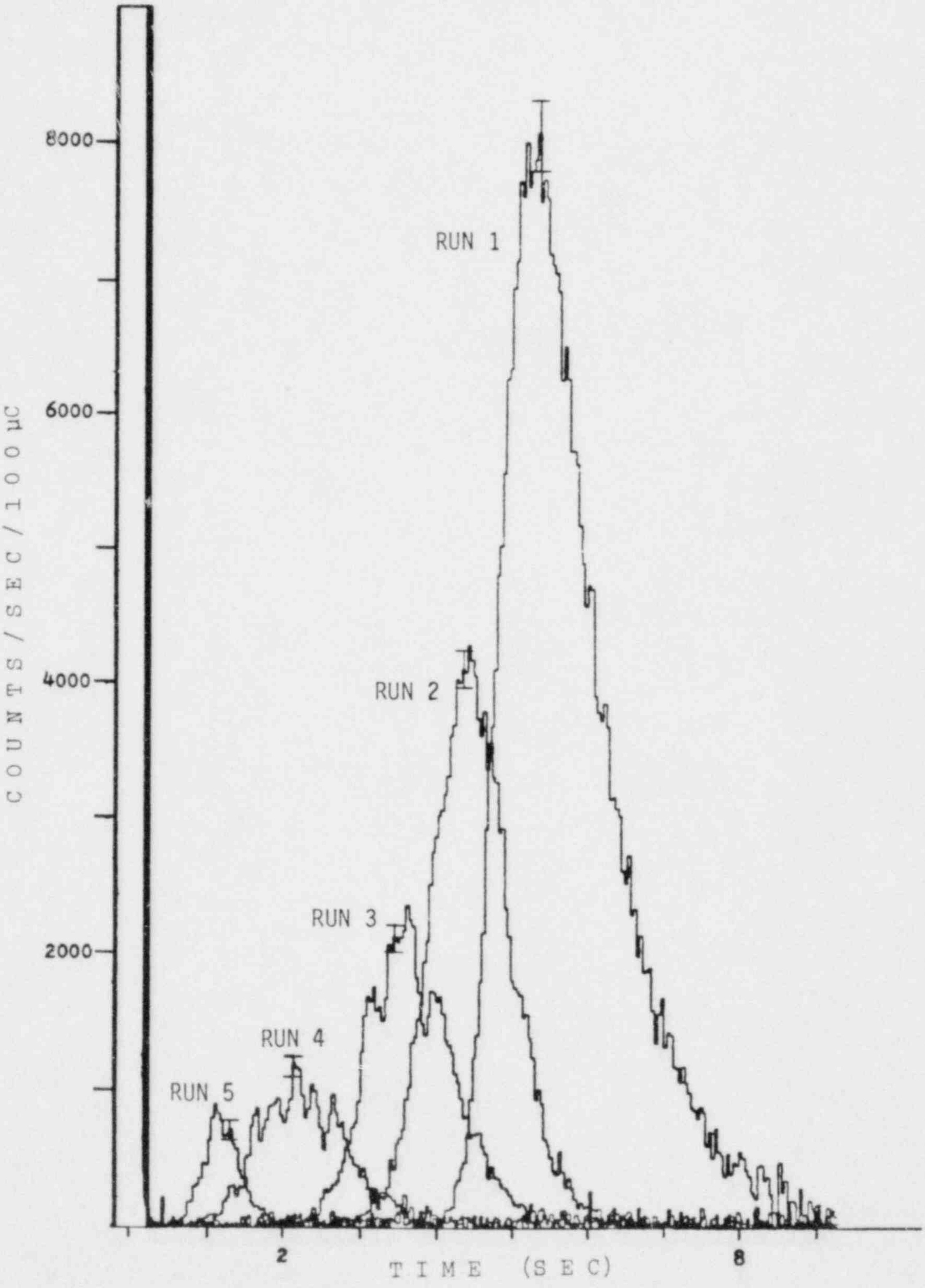

Figure 3-8 Time Profiles for Ensemble of 0.4-s Pulses for Single- and Two-Phase Flow Regimes

TABLE 3-I Superficial Water and Air Velocities $\langle j_\ell \rangle$ and $\langle j_g \rangle$, Measured Mass-Weighted Velocities $\langle V_{L_o} \rangle_m$, Errors $(\delta \langle V_{L_o} \rangle_m)_{L_0}$ and $(\delta \langle V_{L_o} \rangle_m)_s$ and Void Fractions $\langle \alpha \rangle$ for the Time Profiles Shown in Figure 3-8

Run No.	No. Pulses	$\langle j_\ell \rangle$ (m/s)	$\langle j_g \rangle$ (m/s)	$\langle V_{L_o} \rangle_m \pm \delta \langle V_{L_o} \rangle_m$ (m/s)	$(\delta \langle V_{L_o} \rangle_m)_{L_o}$ (m/s)	$(\delta \langle V_{L_o} \rangle_m)_s$ (m/s)	$\langle \alpha \rangle$
1	25	0.346±0.009	0	0.346±0.009	0.008	9×10^{-4}	0
2	25	0.346±0.009	0.15	0.440±0.011	0.011	5×10^{-4}	0.214±0.024
3	25	0.346±0.009	0.29	0.546±0.013	0.013	0.001	0.367±0.019
4	20	0.346±0.009	1.52	0.962±0.026	0.024	0.016	0.640±0.011
5	21	0.346±0.009	10.5	1.79 ±0.05	0.044	0.030	0.806±0.006

$$\delta \langle V_{L_o} \rangle_m = \pm \sqrt{(\delta \langle V_{L_o} \rangle_m)^2_{L_o} + (\delta \langle V_{L_o} \rangle_m)^2_s}$$

water and air velocities, respectively $(\delta\langle V_{L_o}\rangle_m)_s$ and $(\delta\langle V_{L_o}\rangle_m)_{L_o}$ are the counting statistical error and the error in L_o, respectively. The void fraction $\langle\alpha\rangle$ was determined by the method described in Section 2.1.2 (Equation (2-12)).

As can be seen in Figure 3-8, as the air flow increases the mass-weighted velocity increases, which causes displacement of the curves to the left. On the other hand, as the air flow increases the amplitudes of the time profiles decrease because: (i) less water was irradiated, and, (ii) the single-phase water velocity increases and therefore it takes a shorter time to pass by the detector.

3.3.2 Single Pulses of Irradiation. The most striking feature of the two-phase flow data was the fine structure observed in the vertical slug flow regime when the superficial air velocity $\langle j_g\rangle$ was 1.52 m/s (5.0 ft/s). This feature was observed even in the ensemble of pulses of irradiation (see Figure 3-8, Run 4) and more pronounced in the single pulses of irradiation data. Two typical examples are shown in Figure 3-9, where the irradiation time corresponded to one slug and one void passing by the target. These plots can be interpreted as the mass flow profile of the two-phase mixture with the valleys representing the voids and the peaks the liquid slugs.

Calculations were carried out to estimate the spatial variation of the neutral flux along the pipe containing the fluid. Assuming: (a) a point neutron source, (b) the inverse-square-law intensity fall-off, and, (c) any collision in the polyethyelyne shield lowers the neutron to below the threshold energy for ^{16}N production ($E_n \leq 10.2$ MeV), 70% of the total neutron intensity lies within a distance of 7.6 cm along

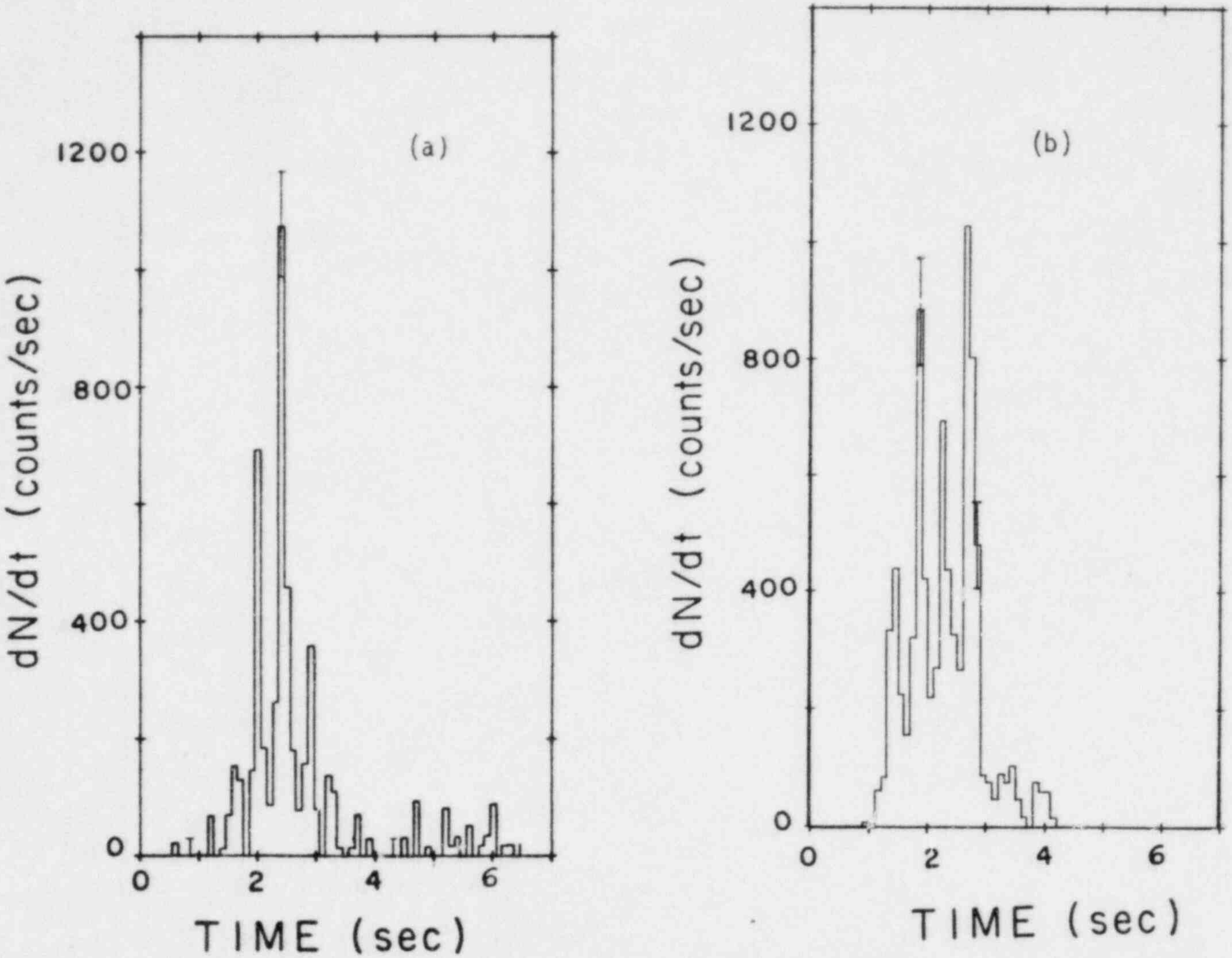

Figure 3-9 Experimental Time Profiles after 0.4-s Single Pulse of Irradiation for a Vertical Slug-Flow Regime

the pipe, as can be seen in Figure 3-10. For the flow condition of this experiment, the distance between slugs[52] is approximately 38 cm. Thus, the ~7.6-cm extent of the neutron intensity is small compared to the 38-cm slug length, and it is concluded that effectively only one slug or at most two adjacent slugs are irradiated at a given time. Thus the dispersion of activity into 5 or 6 slugs, as shown in Figure 3-9 is attributed to slug-to-slug exchange over the 1.9m length, and not to initial irradiation over many slugs.

3.3.2.1 Experimental Slug-to-Slug Exchange Rate. From a mechanistic point of view, it is expected that the observed microstructure should be related to the mixing process. The mixing model described in Section 2.4 was developed to analyze these data.[22,23] As features of this mixing model, it can be recalled that two parameters were characteristic of this model: (a) τ, the slug-to-slug mass exchange rate (i.e. the fraction of slug mass exchange per unit of time), and (b) η, the fraction of total ^{16}N activity induced in the first of two adjacent irradiated slugs.

The measured time profiles shown in Figure 3-9 were fitted with this mixing model (Equation 2.57). The initial ^{16}N concentrations, C_0, were set to the total area underneath the experimental time profiles. The theoretical and experimental time profiles are shown in Figure 3-11. The parameters which appear to best fit these data are τ=0.4 s^{-1} and η=0.2 or η=0.4 for Figures 3-11(a) and 3.11(b), respectively. It is observed that this basic model fits the data reasonably well with the main discrepancy occurring at the third peak near 2.5 s (Figure 3-11(a), and the fourth peak near 2.8 s (Figure 3-11(b)).

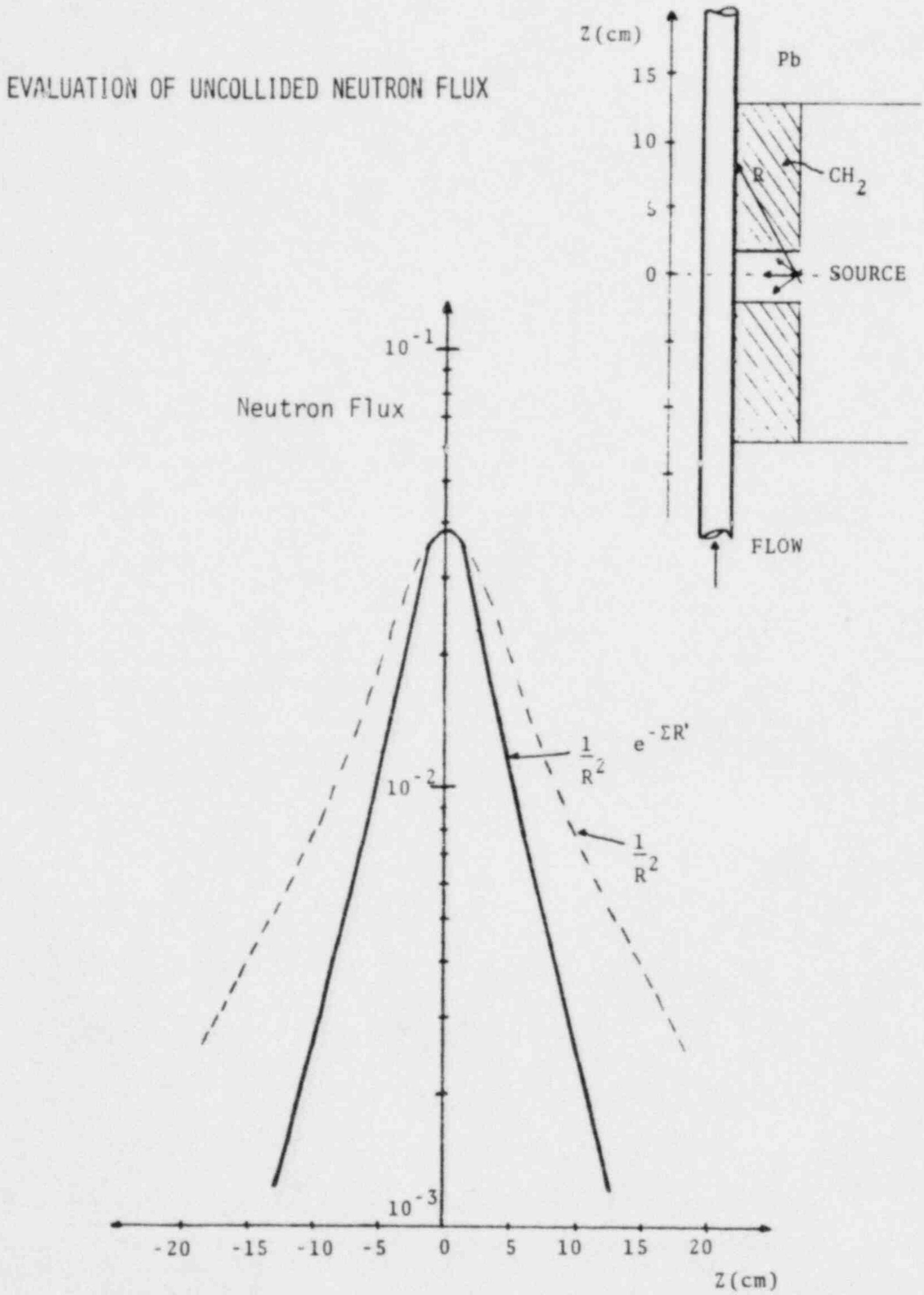

Figure 3-10 Spatial Variation of the Neutron Flux Along the Pipe Containing the Fluid Mixture

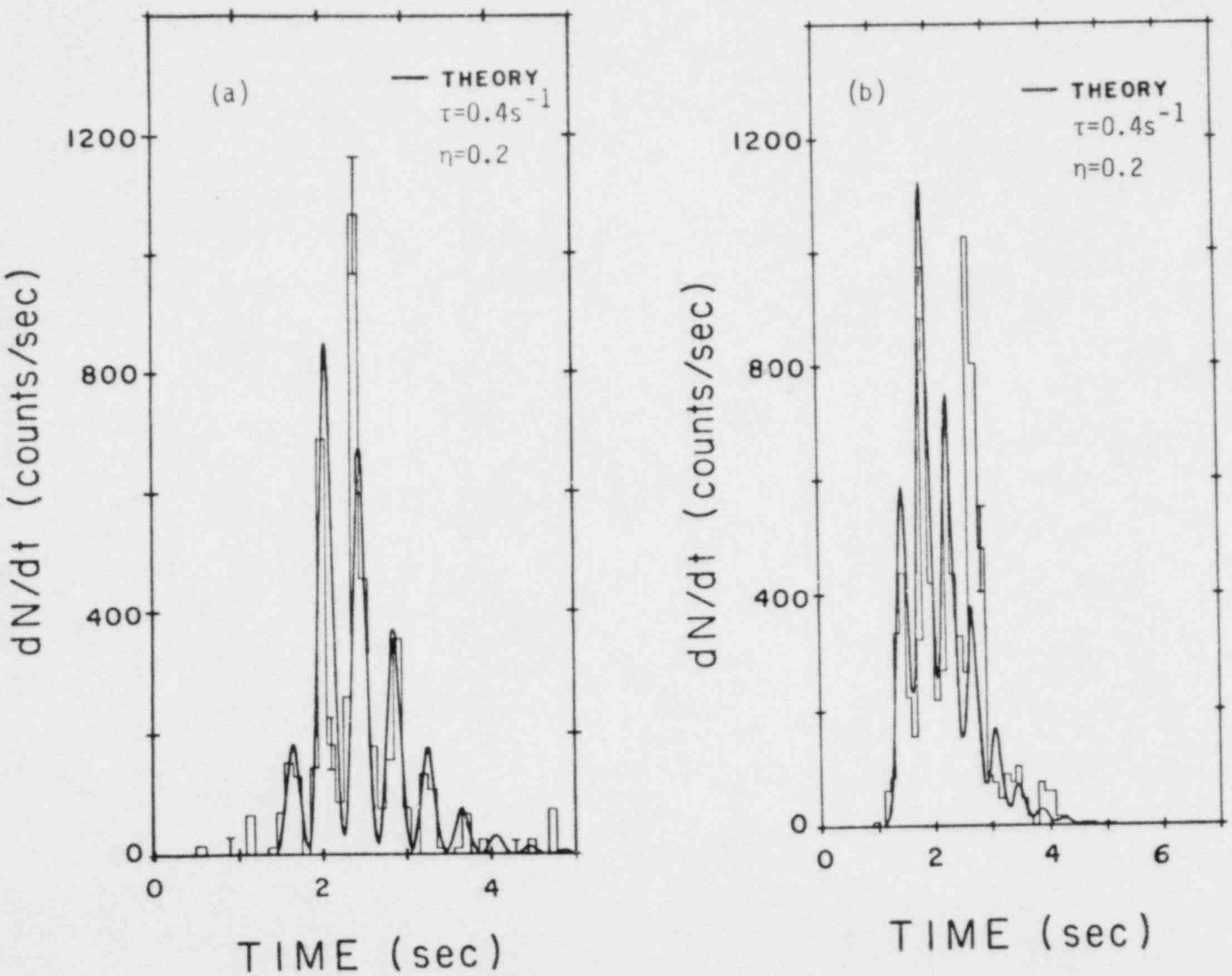

Figure 3-11 Measured NaI Detector Time Profiles for a Vertical Slug-Flow Regime fitted by the Mixing Model

Theoretically, the slug-to-slug exchange rate, τ , can be determined from the Taylor bubble rise velocity[53], and yields a value of 0.8 s^{-1}. The discrepancy between the theoretical and experimental values of τ suggest improvements to this mixing model can be made through the use of more realistic assumptions (such as, for example, mixing gradients or non-uniform mixing).

3.3.3 Liquid Mixing at Very Low Gas Velocities. Another interesting feature of the two-phase flow measurements is shown in Figure 3-12. Here a single-phase flow time profile is compared with a two-phase flow condition having a very small air flow ("champagne" flow). For this two-phase bubbly flow regime the superficial air velocity was only $\langle j_g \rangle = 0.02$ m/s, and it was observed that the air bubbles collected near the pipe walls. These two time profile measurements have the same leading edge and amplitudes but the simgle-phase flow has a long exponential-like tail. The time dependence of these data has been analyzed using the method of Taylor,[40] which assumes that the flowing liquid is single-phase and uniformly activated during the irradiation time. For this experiment the Reynolds number was ≈11,000 so one can assume turbulent flow and, thus, the counting rate at the detector position is given by Equation (2-28), corrected for decay.

This single-phase Equation(2-28) has been fitted to the data by setting $\bar{C}_0$ equal to the experimental amplitudes, and adjusting $\bar{u}$ so the leading edge of the calculated curve goes through the experimental valves. In this work it was assumed that the small air flow does not contribute to the dispersion coefficient and it is observed that the "champagne" flow data fit the Taylor single-phase theory quite

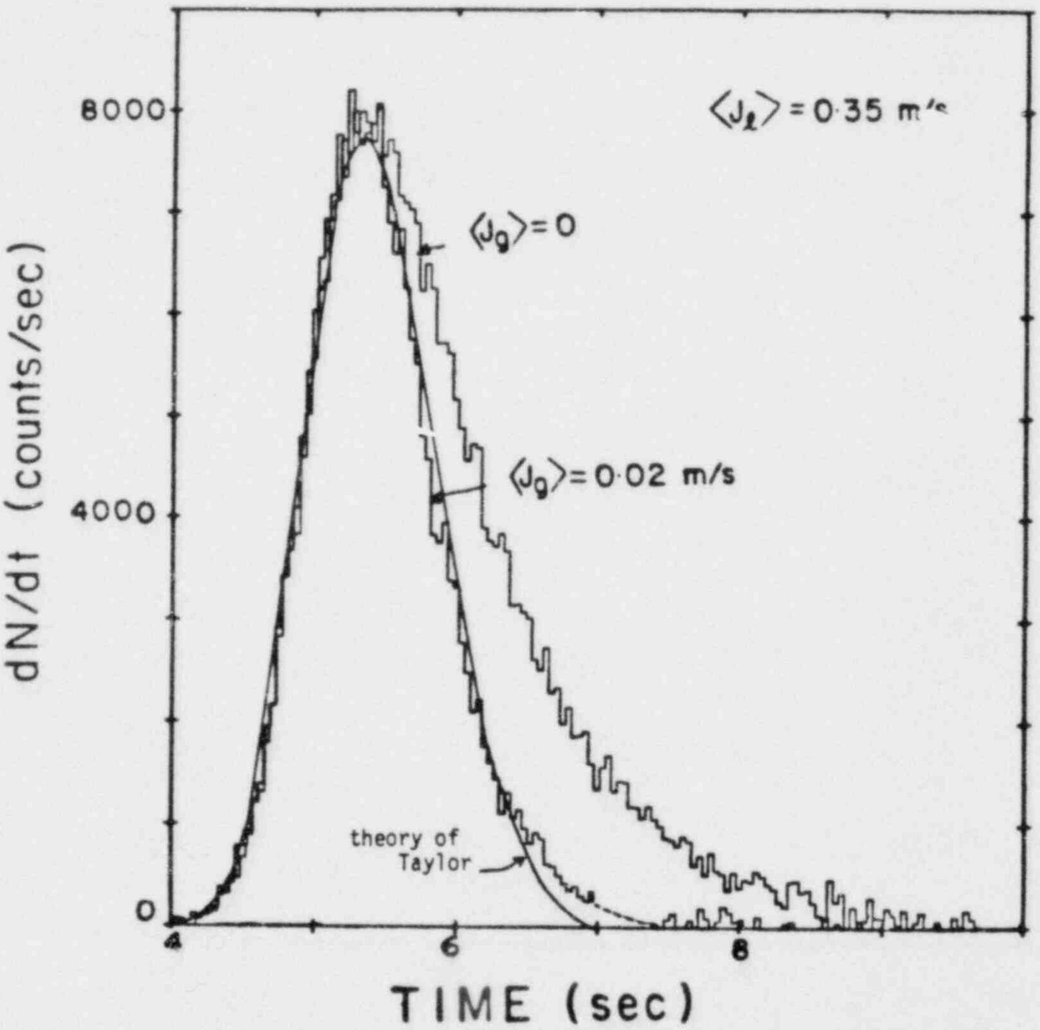

Figure 3-12 Comparison between Single-Phase Flow Time Profile and Two-Phase Vertical Flow Condition with Very Small Air Flow for an Ensemble Average of 25 Pulses

well, whereas the single-phase data has a much longer tail. Apparently the small bubbles present in the two-phase mixture disrupt the laminar sublayer near the pipe wall and lead to more uniform mixing.

PART 4

PNA TECHNIQUES AT LOFT

4.1 Description of LOFT

The Loss-of-Fluid Test (LOFT) program is a series of experiments designed to model the nuclear, thermal, and hydraulic phenomena which would take place in a large Pressurized Water Reactor (PWR) during a hypothetical loss-of-coolant accident (LOCA). These experiments are performed at the LOFT Integral Test Facility located at the Idaho National Engineering Laboratory (INEL).

The LOFT facility can be thought of as a large scale simulation of a PWR. In general, the fluid system volumes and flow areas are scaled to produce a real time response of the LOFT core (55 MW_t) compared to a large PWR core (~ 3000 MW_t). Because of the similarity of designs and the scale size, it is expected that the LOFT experiments will provide a good simulation of PWR LOCA phemomena[54].

A great number of parameters must be determined from the LOFT experiments in order to evaluate and improve the methods used to predict the LOCA response of PWRs. Therefore, a series of experiments have been planned and performed to meet the main LOFT objectives.

This part is concerned with the evaluation and optimization of PNA techniques for the measurement of fluid velocities of the primary coolant in the hot leg of the intact loop in the LOFT reactor during transient tests, particularly for small break LOCA simulations.

4.1.1 PNA Instrumentation at LOFT. Figure 4.1 shows the main components of the LOFT reactor and the location of the PNA test section.

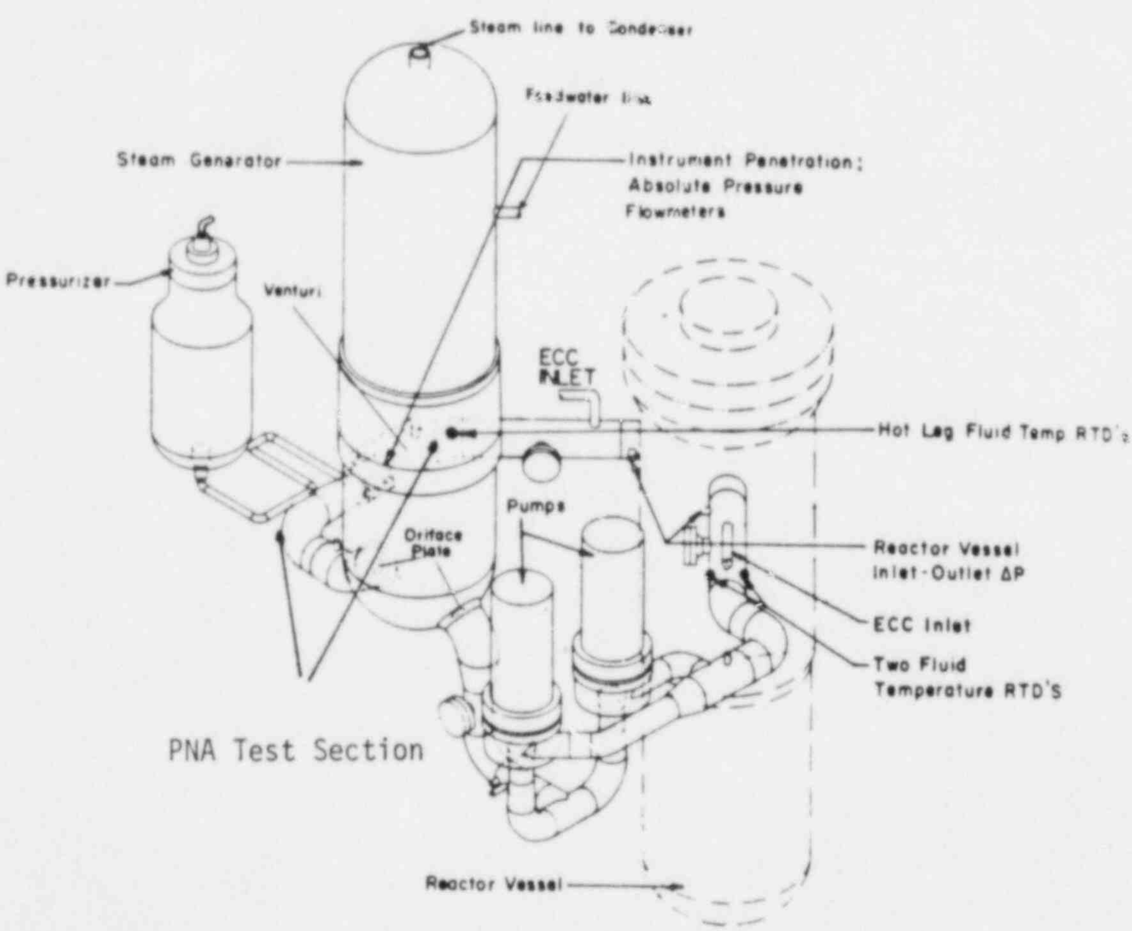

Figure 4-1 LOFT Reactor Main Components and Instrumentation[54]

A more detailed description of the PNA test section at the intact loop is shown in Figure 4.2. At the PNA test section the primary coolant flows in a horizontal 14-in steel pipe schedule 160 (14-in O.D., 11.188-in I.D). At a location A, the flow is tagged by neutron source(s) where it is activated and passes through a venturi. At 60.5 in. (153.7cm) from the tagging position the activated flow is detected by the gamma detector(s) located on a 90^0 pipe bend.

The neutron generators used at LOFT were 14-MeV (Sandia) D-T portable neutron sources.[55] The output of these sources is $\sim 1.3 \times 10^{10}$ neutrons/pulse. The tube-transformer assembly of these sources has a diameter of 30 cm and is 60-cm long. Their 100% tritium-loaded target is a flat circular disk with diameter of 1.4 in (3.6 cm). On the other hand, the gamma detectors are standard 5-in diameter, 3-in-thick NaI crystals located around the pipe.

In order to interpret the PNA LOFT measurements, three main factors have to be considered. Due to the large diameter pipes used at LOFT, the effects of non-uniform tagging and detector efficiency have to be determined. In addition, the transport of the irradiated fluid from the tagging to the detector position has to be suitably modeled for the various flow conditions. These important factors have been discussed previously but are more fully described in the following sections for two principal flow conditions to be used at LOFT: (i) single-phase turbulent flow, and, (ii) a two-phase stratified flow (1/2 liquid, 1/2 vapor).

4.2 Single-Phase Flow PNA Evaluation

A flow condition of single-phase water at 1000 psia, 500^0F (6.9 MPa, 260^0C) flowing in a 14.in steel schedule 160 pipe was analyzed.

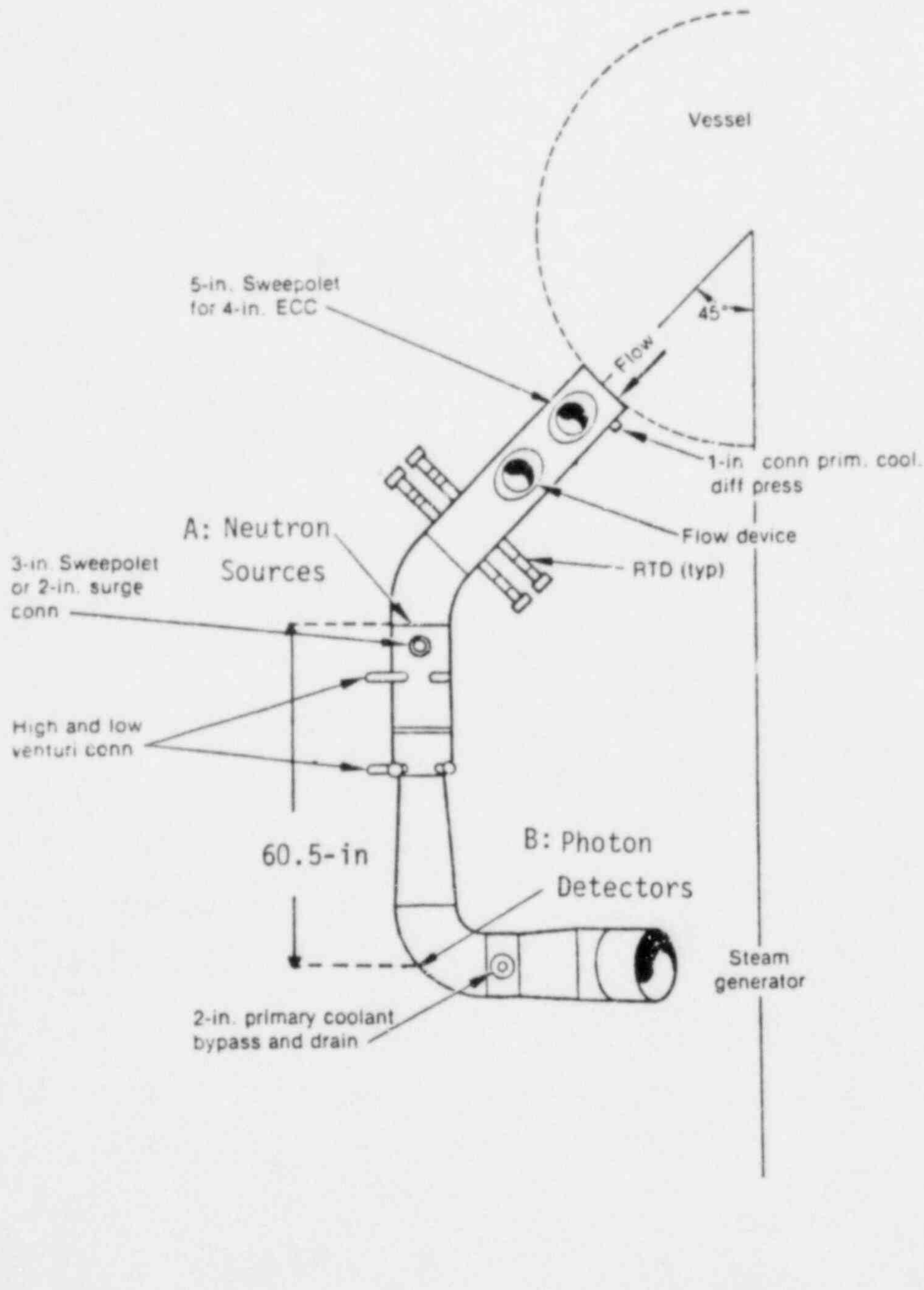

Figure 4-2 PNA Test Section at LOFT

Monte Carlo neutron and gamma transport calculations were performed to determine the magnitude of non-uniform tagging and detector efficiency effects. The dispersion models, discussed in Section 2.3, were used to describe the transport of the irradiated fluid from the tagging to the detector position. A PNA counting rate was then obtained by coupling the Monte Carlo calculations at the tagging and detector positions with the transport calculations to evaluate the effects that the non-uniform tagging and detector efficiency have on the time profile data.

4.2.1 Neutron Transport Calculation at the Tagging Position

4.2.1.1 Geometry description. Detailed neutron transport calculations were performed over 1-m length of pipe. The geometry consisted of 119 regions: 112 water regions, 6 pipe wall regions, and the air region surrounding the source and system. The active neutron source (1.4-in dia. flat circular disk) was located 2-in from the pipe wall. A schematic of this geometry is shown in Figure 4.3.

4.2.1.2 Monte Carlo Results. The Monte Carlo program ANDYRPI[35] and the cross-section data set CASK[36] were used for this simulation. ANDYRPI and CASK have been described previously in Section 2.2.3. To improve the efficiency of the calculation a source emitting neutrons isotropically over the 1-m length of pipe (z-direction) and a pipe diameter (x-direction) was used. The ANDYRPI program was run for a total of 50,000 neutron histories in 50 batches of 1,000 neutrons each. The equiprobable scattering angle technique was used for handling the P_3 Legendre expansion of the cross sections. Two statistical estimates were used: the collision estimator and the track length estimator. The track length estimator was found to be the best scoring

GEOMETRY FOR ^{16}N TAGGING

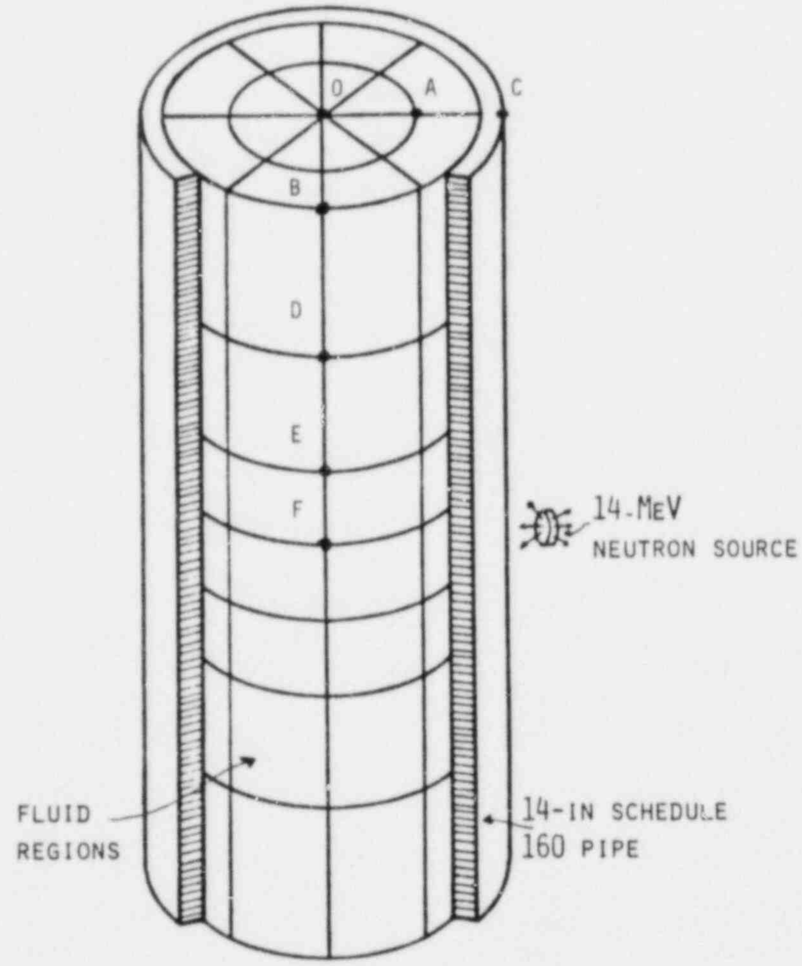

OA = 10.05cm
OB = 14.21cm
OC = 17.78cm
BD = 20. cm
DE = 15. cm
EF = 10. cm

Figure 4-3

technique, giving an average statistical uncertainty of 3%. This was expected because the neutron mean free path in water at the given conditions is $\approx$ 20 cm, and as can be observed in Figure 4-3, this value is comparable to the water region dimensions (optically thin regions).

For each water region, the ^{16}N production per m^3, per pulse was calculated for a source intensity of 1.3 x 10^{10}n/pulse. The ^{16}N specific activities (^{16}N activity per unit volume) were averaged over symmetrical water regions and the relative specific activity in each region was normalized relative to the region of highest activity. The total ^{16}N produced per pulse in the water was (14.77$\pm$0.06) x 10^6 ^{16}N/pulse.

Another tally was introduced in the Monte Carlo program ANDYRPI to take into account the number of secondary collisions and therefore to evaluate the ^{16}N production from non-first- collision neutrons, i.e., multiple scattered neutrons. For this evaluation, 5 batches of 1,000 neutrons each were run, and it was found that 48% of the total ^{16}N production was due to multiple scattering. This high value shows the usefulness of using Monte Carlo methods for this kind of calculation.

4.2.1.3 <u>^{16}N Tagging with one, Two and Four Sources</u>. Figure 4-4(a) through 4-4(h) show the axial profiles of the normalized specific activities for the different inner water regions when the single-phase flow is tagged by only one source. It is observed that for the regions at the axial position of the source, i.e 0.45<Z<0.55m, the activity decreases to 7% in Figure 4-4(d), the region furthest from the source. In the axial direction for the regions nearer the source, Figure 4-4(a), the activity is reduced to $\approx$54% within an axial distance of one radius

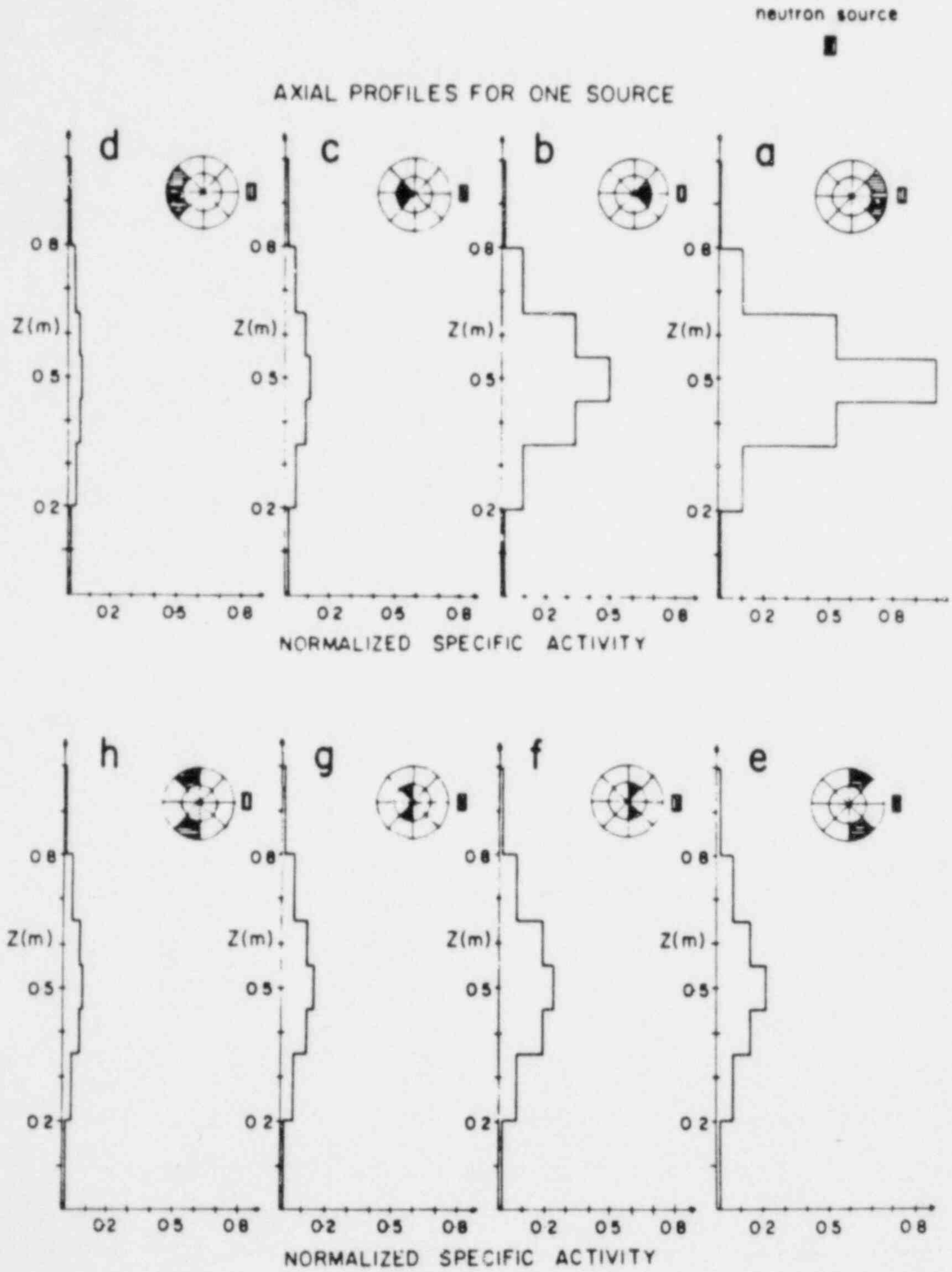

Figure 4-4 Axial Profiles of the ^{16}N Specific Activity when Single-Phase Water at 1000 psia, 500 ^{o}F is Tagged by One Neutron Source

from the midplane and to ≈10% in a distance of two radii. For the inner regions Figure 4-4(b) through 4-4(h), the activity is not as sharply reduced in the axial direction.

A considerable improvement is obtained in the transverse direction when the single-phase flow is tagged by two opposite neutron sources as can be seen in Figures 4-5(a) through (d). At the axial position of the source ($0.45 \leq Z \leq 0.55$m) the activity is reduced to 29% in Figure 4-5(d), the regions furthest from the sources. Little difference is observed in the axial direction in comparison with the flow being tagged by one source.

The case in which single-phase flow is tagged with four symmetric neutron sources is shown in Figure 4-5 (e) and (f). It is observed that at the axial position of the source ($0.45 \leq Z \leq 0.55$m) the activity is only reduced to 76%; the axial dispersion still remains.

In comparing Figure 4-4 with 4-5 it is concluded that at the axial position of the source a considerable improvement is obtained by tagging the flow with two or more sources. The ratio of the lowest to the highest activity at the midplane position ranges from 1:15, 1:3.5, and 1:1.4, for one, two and four sources, respectively. On the other hand, no improvement is observed in the axial direction. If axial dispersion of activities is to be avoided, the sources should be placed further away from the pipe with suitable collimation around them. This will narrow the induced activity in the axial direction although, because of solid angle considerations, the total intensity will be correspondingly decreased.

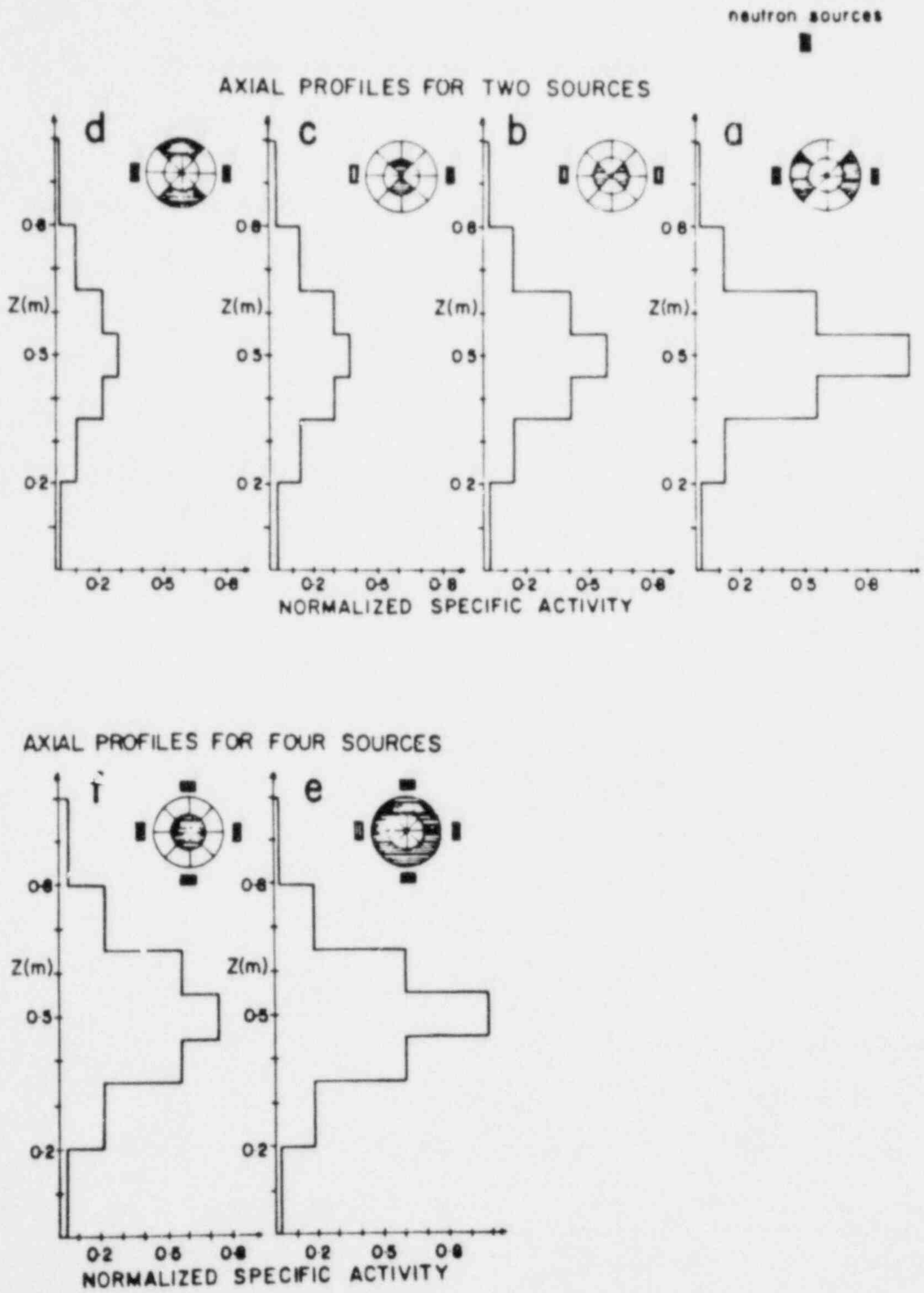

Figure 4-5 Axial Profiles of the ^{16}N Specific Activity when Single-Phase Water at 1000 psia, 500 °F is Tagged by Two and Four Neutron Sources

4.2.2 Gamma Transport Calculation at Detector Position

4.2.2.1 Geometry description. Detailed gamma transport calculations were performed over a 1-m length of pipe. The geometry consisted of 131 regions: 112 water regions, 6 pipe wall regions, 8 detector regions and 5 air regions surrounding the system. The 8 detector regions formed an annulus of NaI 10-cm high by 7.5-cm thick, surrounding the pipe. A schematic of this geometry is shown in Figure 4-6.

4.2.2.2 Monte Carlo Results. The Monte Carlo program ANDYRPI and the cross-section data set CASK were again used for this simulation. The equiprobable scattering angle technique was used for handling the P_3 Legendre expansion of the cross-sections. The ANDYRPI program was run for a total of 400,000 gamma histories in 8 jobs. For each job an isotropic gamma source of 6.5-MeV energy was located at one inner or outer axial water region. For each job 50,000 gamma histories in 50 batches of 1,000 photons each were run.

The detector efficiency per photon for each of the 112 water regions was obtained by the surface crossing estimator into the 8 detector regions. By symmetry the detector efficiency per photon was averaged for symmetrical regions. The values obtained had a statistical uncertainty which varied from ≈ 4% to 15% over the 1-m length of fluid.

4.2.2.3 Detector Efficiency. Figures 4-7 and 4-8 show the axial profiles of the percentage detector efficiency for the different outer and inner water regions. It can be observed that for the regions

GEOMETRY FOR ^{16}N DETECTION

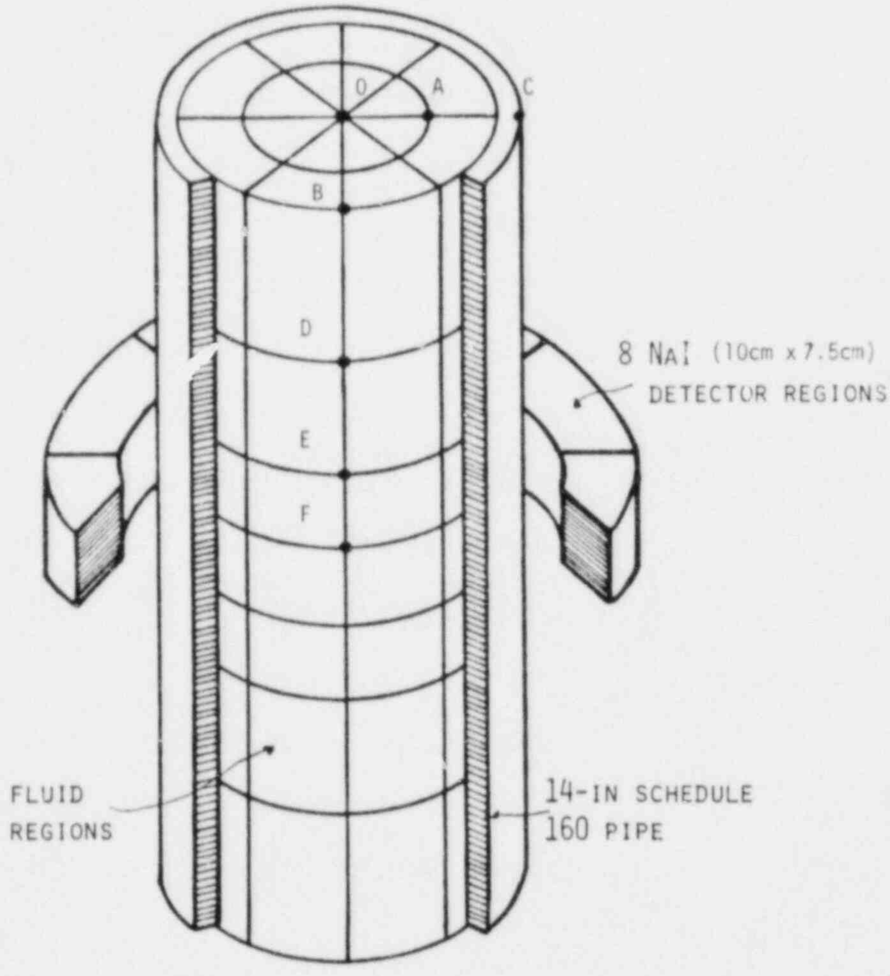

OA = 10.05cm
OB = 14.21cm
OC = 17.78cm
BD = 20. cm
DE = 15. cm
EF = 10. cm

Figure 4-6

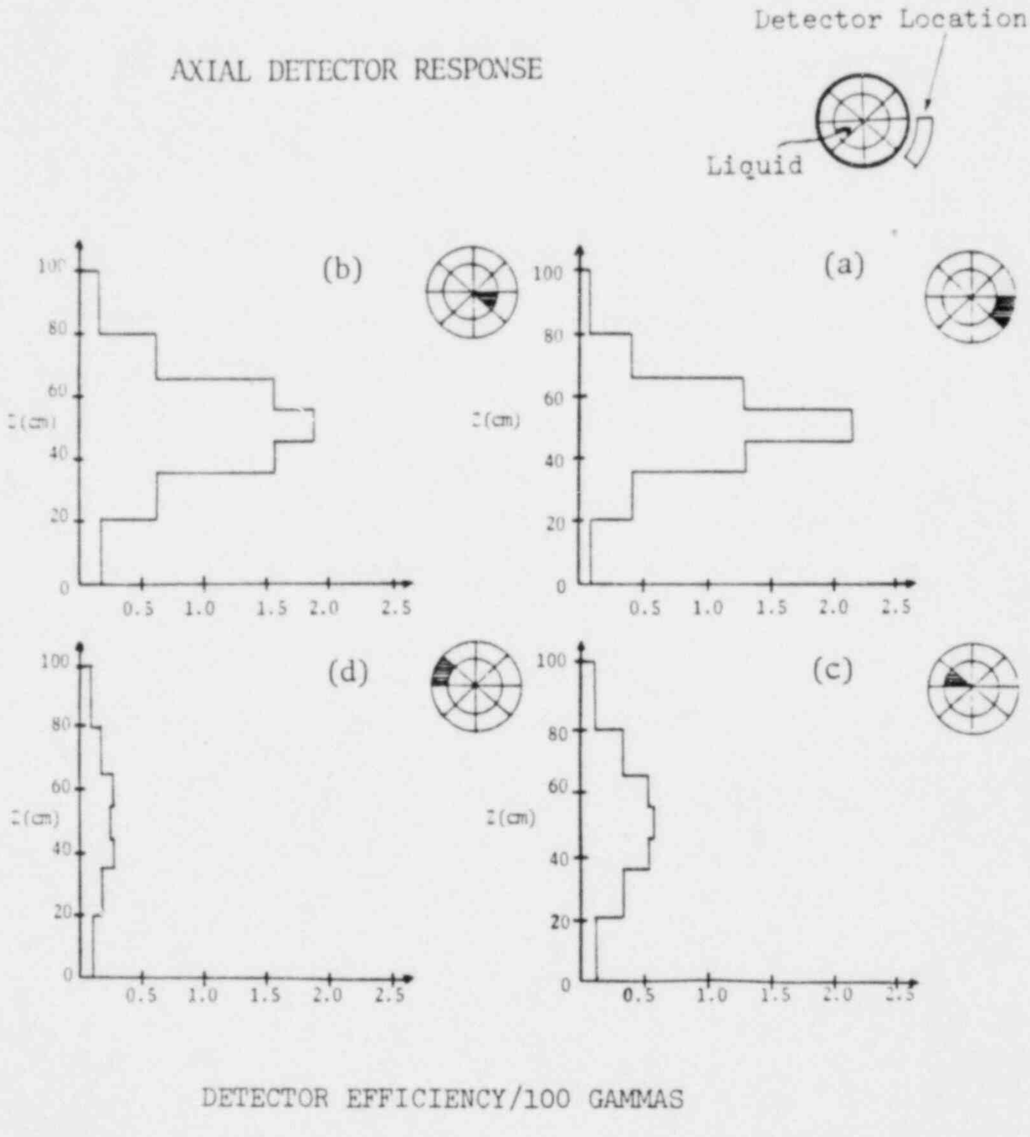

Figure 4-7 Axial Detector Response for ^{16}N Tagged Single-Phase Water at 1000 psia, 500 °F

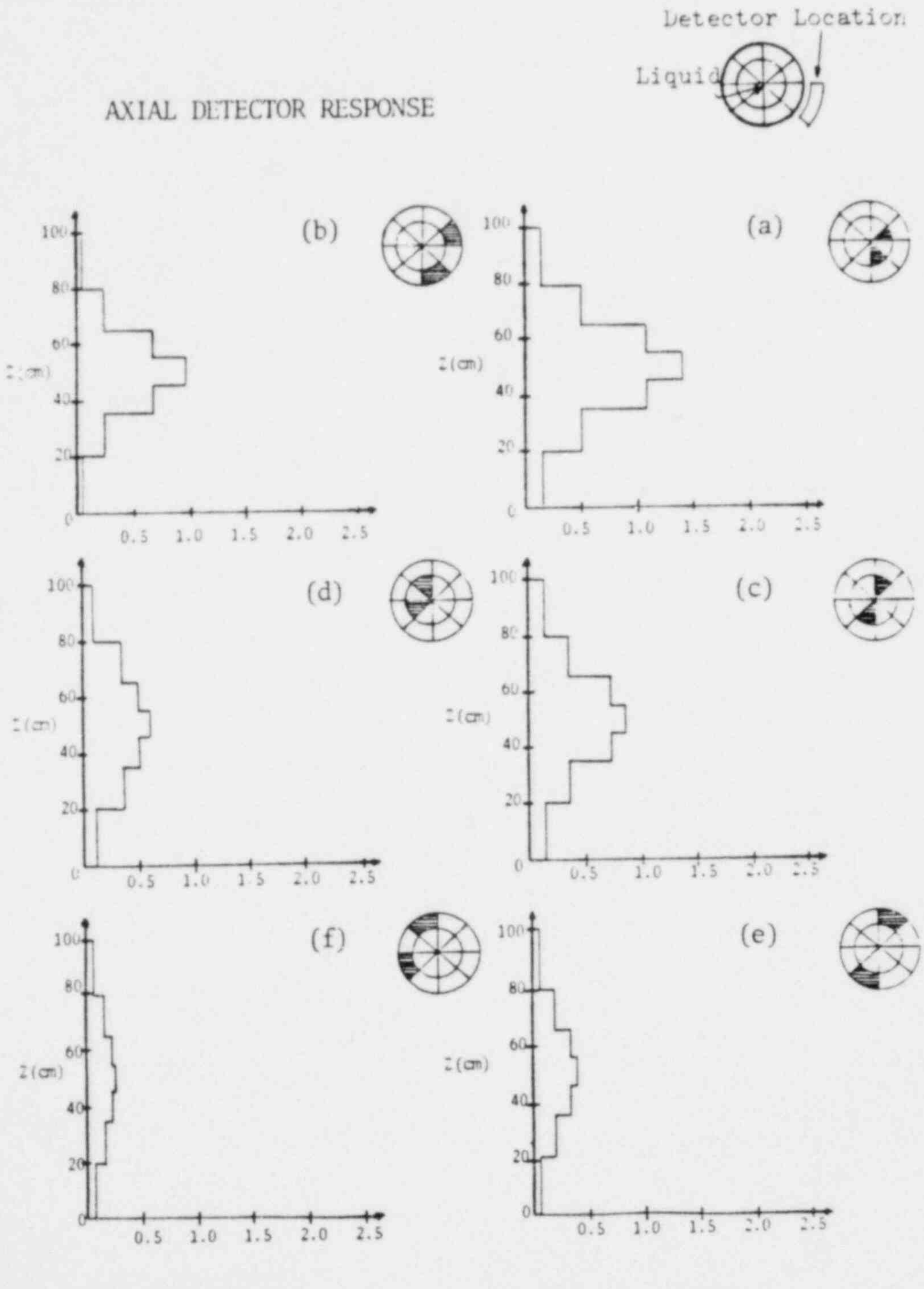

Figure 4-8 Axial Detector Response for ^{16}N Tagged Single-Phase Water at 1000 psia, 500 °F

at the axial position of the detector, i.e., the mid-plane for 45<Z<55 cm, the detector efficiency decreases by a factor of ≈10 in going from the region nearest the detector (Figure 4-7(a)) to the region furthest (Figure 4-7(d)). In the axial direction and for the pie-segment regions nearest the detector, Figure 4-7(a), the detector efficiency decreases by a factor of ≈ 1.7 within a distance of one radius from the midplane and to a factor of ≈ 5.4 in a distance of two radii.

4.2.3 Transport Simulation. The classical dispersion theory of G. I. Taylor[39,40] was used to transport the irradiated single-phase flow from the tagging to the detector location. Two simulations were performed in order to evaluate the error introduced in the mass-weighted velocity by: (i) the flow regime dependence, and, (ii) the non-uniform tagging and detector efficiency, both for LOFT geometry.

4.2.3.1 Flow regime effects on $(\langle V_{L_o} \rangle)_m$. As discussed in Section 2.1.1, in order to evaluate the mass-weighted velocity of irradiated flows from the counting time spectra, two extreme cases can be considered.

Case I: For flows where radial mixing is minimal (e.g. laminar flows) the mass-weighted velocity is obtained by the $1/t^2$ data reduction method given by Equation (2.7).

Case II: For flows with strong radial mixing (e.g. fully-developed turbulent flows) the mass-weighted velocity is obtained by the $1/t$ data reduction method given by Equation (2.8).

The mass-weighted velocity for different single-phase flow regimes was calculated by Equations (2.7) and (2.8) to evaluate the error introduced by using the incorrect mass-weighted velocity expression. The transit-time distributions at the detector position, that is the values of C_i, were simulated from Taylor's dispersion theory.[39,40] The distance between the tagging and detector positions was $L_o = 1.27$ m and the pipe size 14-in (0.35 m) schedule 160. Two cases were considered:

(i) Case A: Single-phase laminar flow in which water was flowing at a mean velocity of 5×10^{-4} m/s. For this case Equation (2.7) gave a mass-weighted velocity of 5.1×10^{-4} m/s, with mean value with 2%, whereas Equation (2.8) gave a mass-weighted velocity of 1.3×10^{-4} m/s, which represents a 74% difference from the mean value. The 2% error given by the correct expression to be used in this case (Equation (2.7)) is mainly attributed to truncation errors resulting from coarse time channel widths and the limited time span included in the simulation.

(ii) Case B: Single-phase turbulent flow in which water was flowing at a mean velocity of 0.5 m/s (to insure turbulence). For this case the mass-weighted velocity obtained by Equation (2.8) was 0.5002 m/s (within 4×10^{-2}% of the mean value) whereas Equation (2.7) gave a mass-weighted velocity of 0.557 m/s, which represents an error of 11.4%.

The main conclusion from these calculations is that the flow structure has to be known a priori in order to apply the correct expression for the mass-weighted velocity to the experimental counting data. For PNA data at LOFT, the error introduced can be as high as ≈70% for laminar flows and ≈11% for turbulent flows.

On the other hand, if the single-phase flow regime was known a priori and therefore the right mass-weighted velocity expression to be applied, the correct answer would still not be obtained for the LOFT PNA data. Equations (2.7) and (2.8) were derived without taking into account the axial dispersion effects of the induced activity and detector efficiency. These axial effects on the 1/t weighting data reduction method for a turbulent single-phase flow are evaluated in the following section.

4.2.3.2 Axial induced activity and detector efficiency effects on $< V_{L_0} >_m$. As described previously in Sections 4.2.1 and 4.2.2, Monte Carlo transport calculations were carried out to determine: (i) the initial ^{16}N tagged concentration in seven axial regions near the PNA source (i) and, (ii) the detector response to ^{16}N in another seven axial regions near the detector position(s) for the LOFT geometry. The next problem is to determine the transport of the ^{16}N from the source regions to the detector regions and to generate the time spectrum of the detector counting rate.

In order to evaluate the axial induced activity and detector efficiency effects on the time-weighting methods, the dispersion theory of G.I. Taylor[40] was applied for each of the seven axial water regions (at the tagging position) to evaluate the ^{16}N concentration at the seven axial water regions (at the detector position). This theory handles the radial mixing within each axial section for large L/D ratios. Although fully developed mixing is never achieved in the short L/D LOFT PNA experiments (as discussed previously), this assumption was made to serve as a reference calculation.

The detector efficiencies were processed to get counting rates from each axial water section at the detector position, per unit of ^{16}N concentration. These values were coupled to the concentrations obtained by Taylor's theory when the single-phase flow is tagged by one source. The initial ^{16}N concentrations were normalized to the highest one and an arbitrary normalization constant (which will depend on the experimental data) was taken equal to 100. Radioactive decay of the ^{16}N was not taken into account, in actual measurements the data will be scaled by $e^{-\lambda t}$, where t is the time from the neutron pulse and λ is the decay constant.

The total detector response for a single-phase fully-developed turbulent flow with a mean velocity of 30cm/s is shown in Figure 4-9. The distance from the midplane of the neutron source to the midplane of the detector was taken to be 127cm. The ^{16}N concentration profile at the midplane of the detector is also shown in Figure 4.9 where the two peaks have been normalized to each other. In comparing both profiles, it is observed that the detector response is somewhat broadened relative to the midplane concentration.

Since complete turbulent mixing was assumed, the mass weighted velocity was calculated for both profiles by the $1/t$-weighting method (Equation (2.8)). With the normalized ^{16}N concentration profile at the midplane of the detector, the mass-weighted velocity evaluated by Equation (2.8) was 30.48 cm/s, 1.6% greater than the mean value. This error is mainly due to the axial dispersion at the tagging position. With the detector response profile, the mass-weighted velocity evaluated

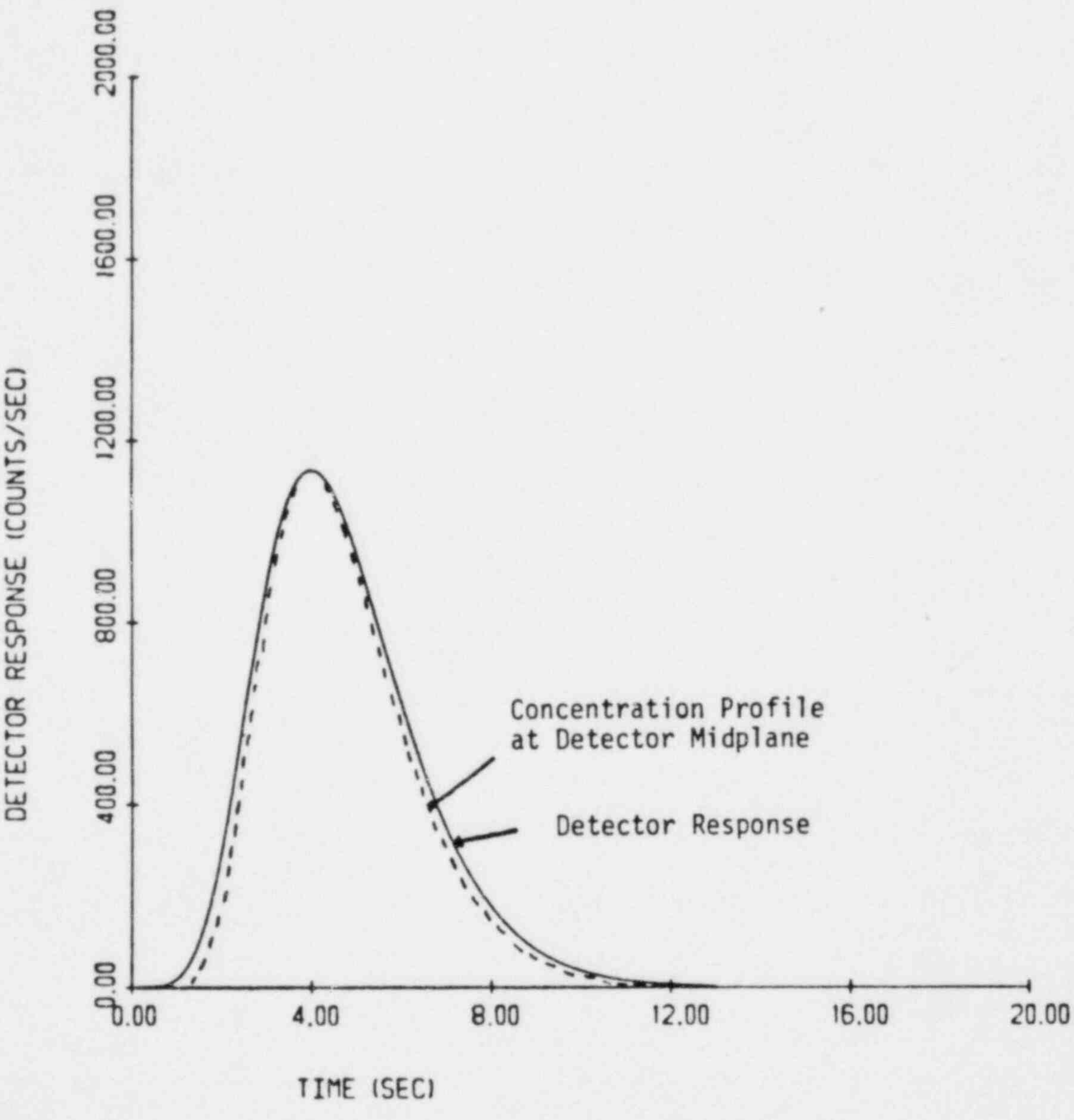

Figure 4-9 Effect of the Axial Detector Response for an Irradiated Single-Phase Flow at 1000 psia, 500 ^{o}F. The Time Profiles where Simulated by Taylor's Dipersion Theory for a Turbulent Flow at $\bar{u}$=30 cm/s

by Equation (2.8)was 31.25 cm/s, 4.2% greater than the mean value. The factor of 2.6 increase in this error is due to the axial dispersion of the detector efficiency.

4.3 1/2-Stratified Flow PNA Evaluation

A saturated two-phase stratified flow (1/2 liquid-1/2 vapor) at 1200psia, flowing in a 14-in steel schedule 160 pipe was analyzed. In the same manner as for the single-phase flow condition, Monte Carlo neutron and gamma transport calculations were performed to determine the magnitude of non-uniform tagging and detector efficiency effects for this two-phase flow condition. Simulated PNA counting rates were obtained by coupling the Monte Carlo calculations at the tagging and detector positions with the transport of the two irradiated fluids by the finite difference method discussed in Section 2.3.3. Unfortunately, no LOFT two-phase 1/2-stratified flow data was available to compare experimental and theoretical PNA results.

4.3.1 Neutron Transport Calculation at the Tagging Position

4.3.1.1 Geometry description. Detailed neutron calculations were performed over a 1-m length of pipe. The geometry consisted of 119 regions: 56 liquid regions, 56 vapor regions, 6 pipe wall regions and the air region surrounding the system. This geometry is equivalent to the one used for ^{16}N tagging of single-phase flow (Figure 4-3), except the pipe was half-filled with liquid and half-filled with vapor. Four source locations, A, B, C and D placed 2-in from the pipe wall were considered, as shown in Figure 4-10.

4.3.1.2 Monte Carlo results. The program ANDYRPI was run for 20,000 neutron histories in 20 batches of 1,000 neutrons each and for three different source locations (A, B and C). For each liquid and

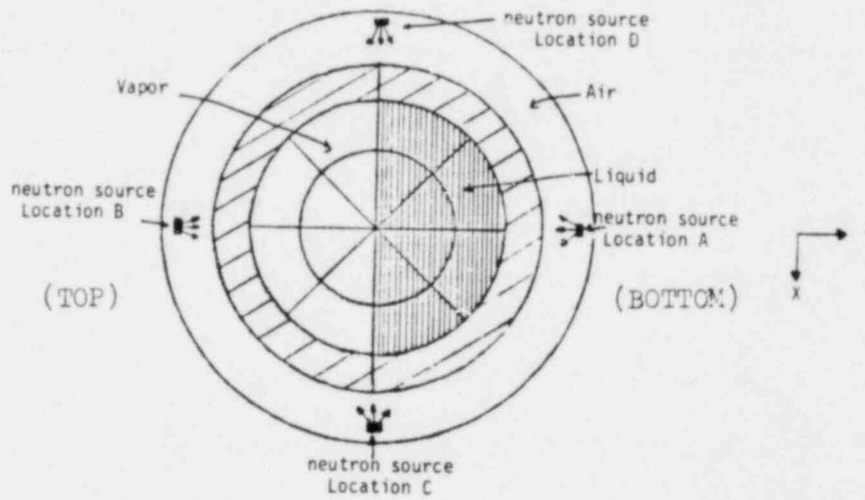

Figure 4-10 Neutron Source Locations for ^{16}N Tagging of 1/2-Stratified Flow

vapor region, the ^{16}N production per cm^3 per pulse was calculated for a 14-MeV source intensity of 1.3×10^{10} n/pulse. The total ^{16}N produced per pulse in the mixture was $(14.0 \pm 0.1) \times 10^6$ ^{16}N/pulse for the source at position A, $(10.1 \pm 0.1) \times 10^6$ ^{16}N/pulse for the source at Position B, and $(10.1 \pm 0.1) \times 10^6$ ^{16}N/pulse for the sources at positions C and D. By symmetry, the $^{16}N/cm^3$-pulse in the 56 19quid and 56 vapor regions were averaged for symmetrical regions and the relative specific activity in each region was obtained by normalization of these values to the region of highest specific activity.

4.3.1.3 <u>^{16}N tagging with one, two and four sources.</u>

Figures (4-11) through (4-17) show the axial profiles of these normalized specific activities for the different liquid and vapor regions when the 1/2-stratified flow is tagged by one source at location A, B or C, two sources at locations A and B, two sources at locations C and D, and four sources at A, B, C and D, respectively. An overall evaluation of these results is summarized in Table 4-I where for each source location(s) is given:

- The ratio of minimum-to-maximum activity at the axial position of the source ($45<Z<55$cm). That is, how much the activity decreases at the axial source position in going from the region nearest the source to the region furthest.
- Axial variation of the activity within one and two pipe radii. That is, how much the activity decreases in going from the midplane position to the axial position of one and two pipe radii for pie-segment regions nearest the source.

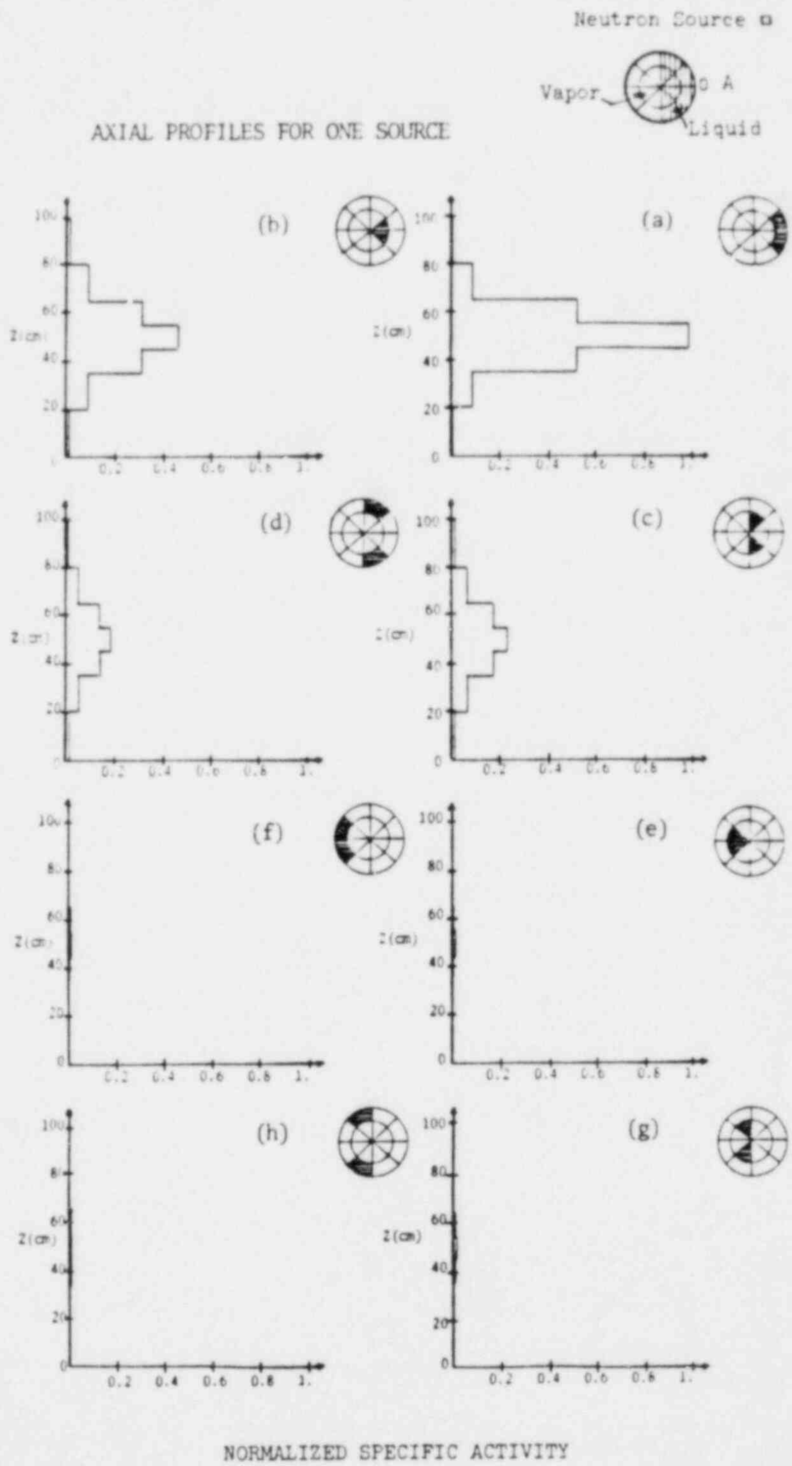

Figure 4-11 Axial Profiles of the ^{16}N Specific Activity when 1/2-Stratified Flow at 1200 psia, Saturation Temperature is Tagged by One Neutron Source (Location A)

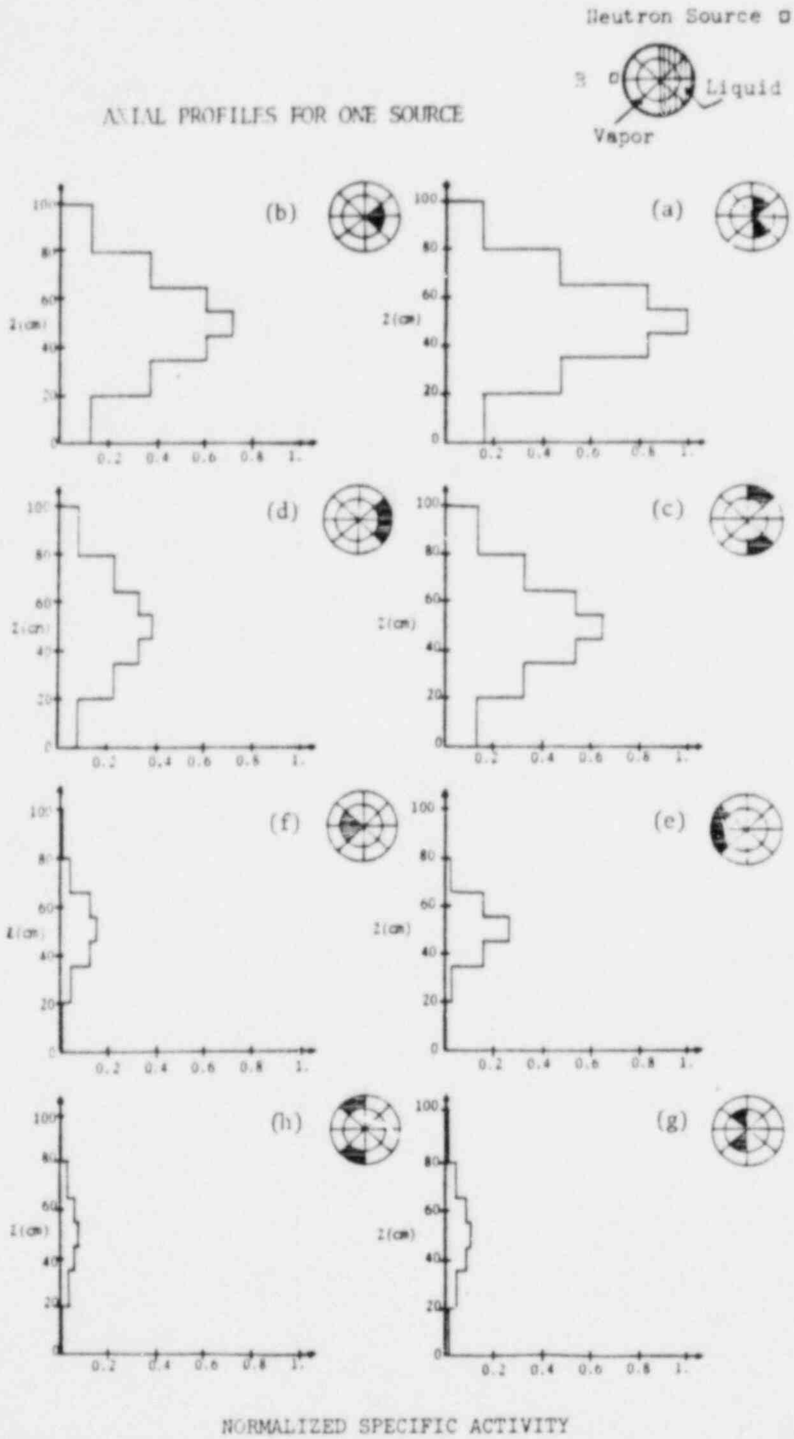

Figure 4-12 Axial Profiles of the ^{16}N Specific Activity when 1/2-Stratified Flow at 1200 psia, Saturation Temperature is Tagged by One Neutron Source (Location B)

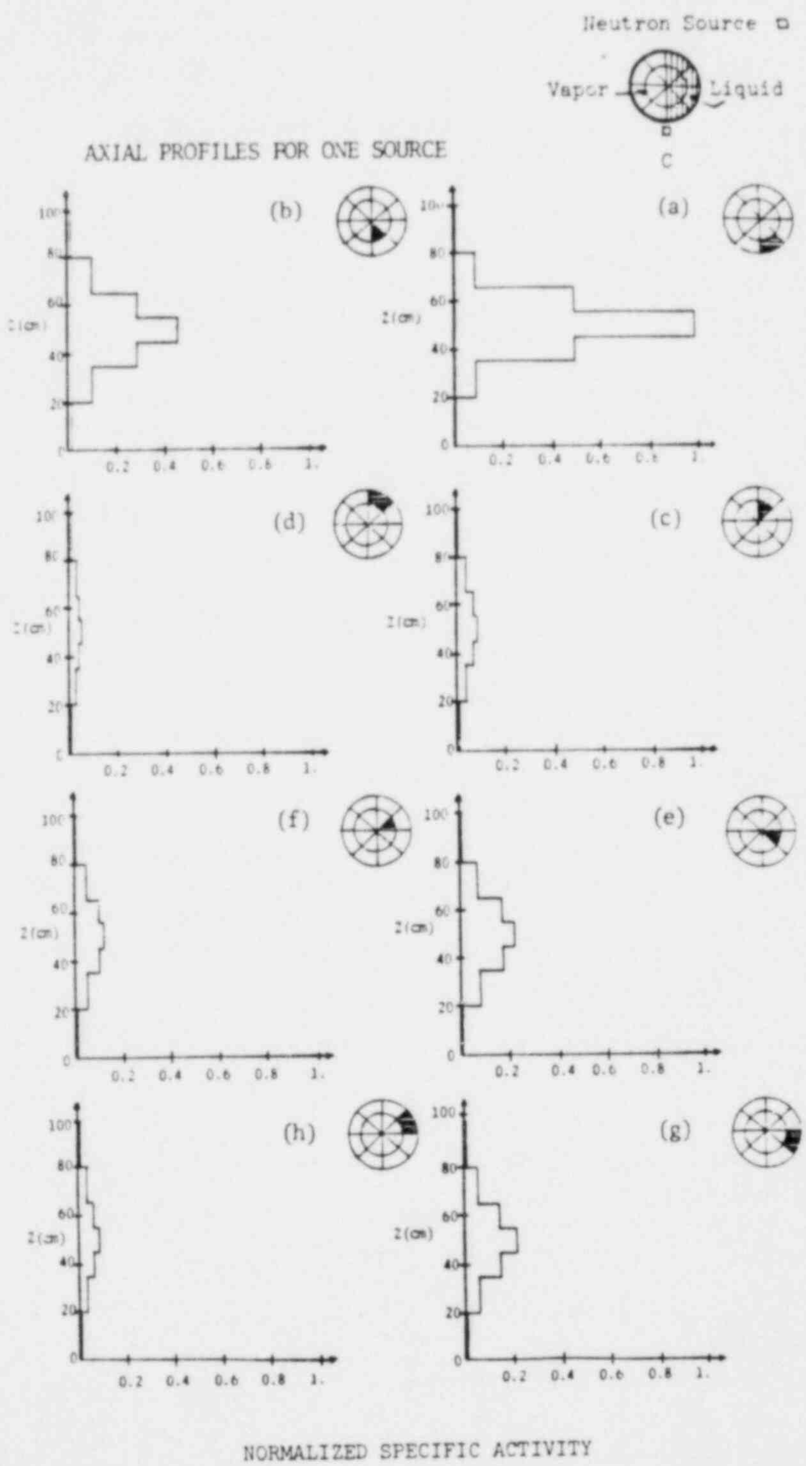

Figure 4-13 Axial Profiles of the ^{16}N Specific Activity when 1/2-Stratified Flow at 1200 psia, Saturation Temperature is Tagged by One Neutron Source (Location C)

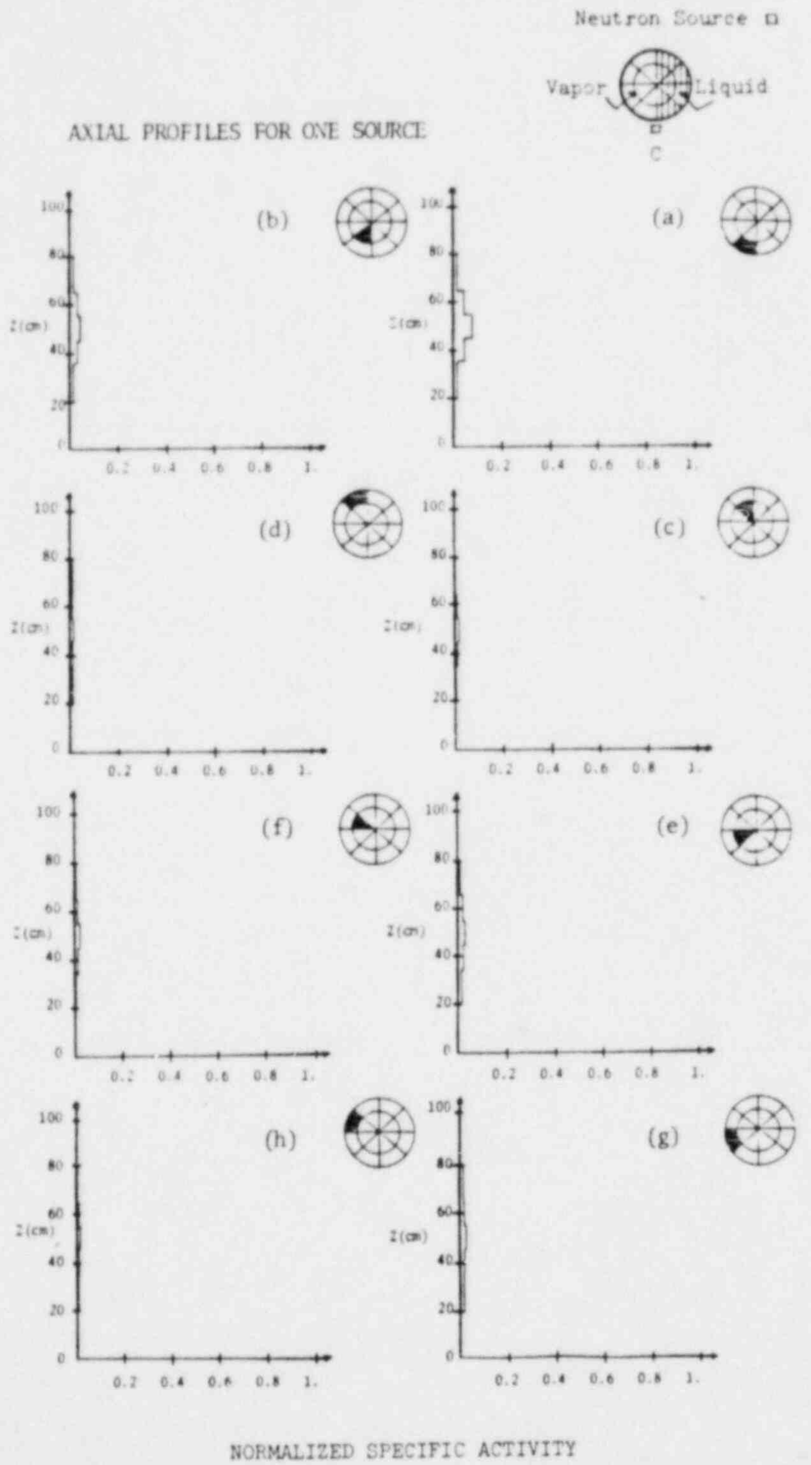

Figure 4-14 Axial Profiles o. the ^{16}N Specific Activity when 1/2-Stratified Flow at 1200 psia, Saturation Temperature is Tagged by One Neutron Source (Location C)

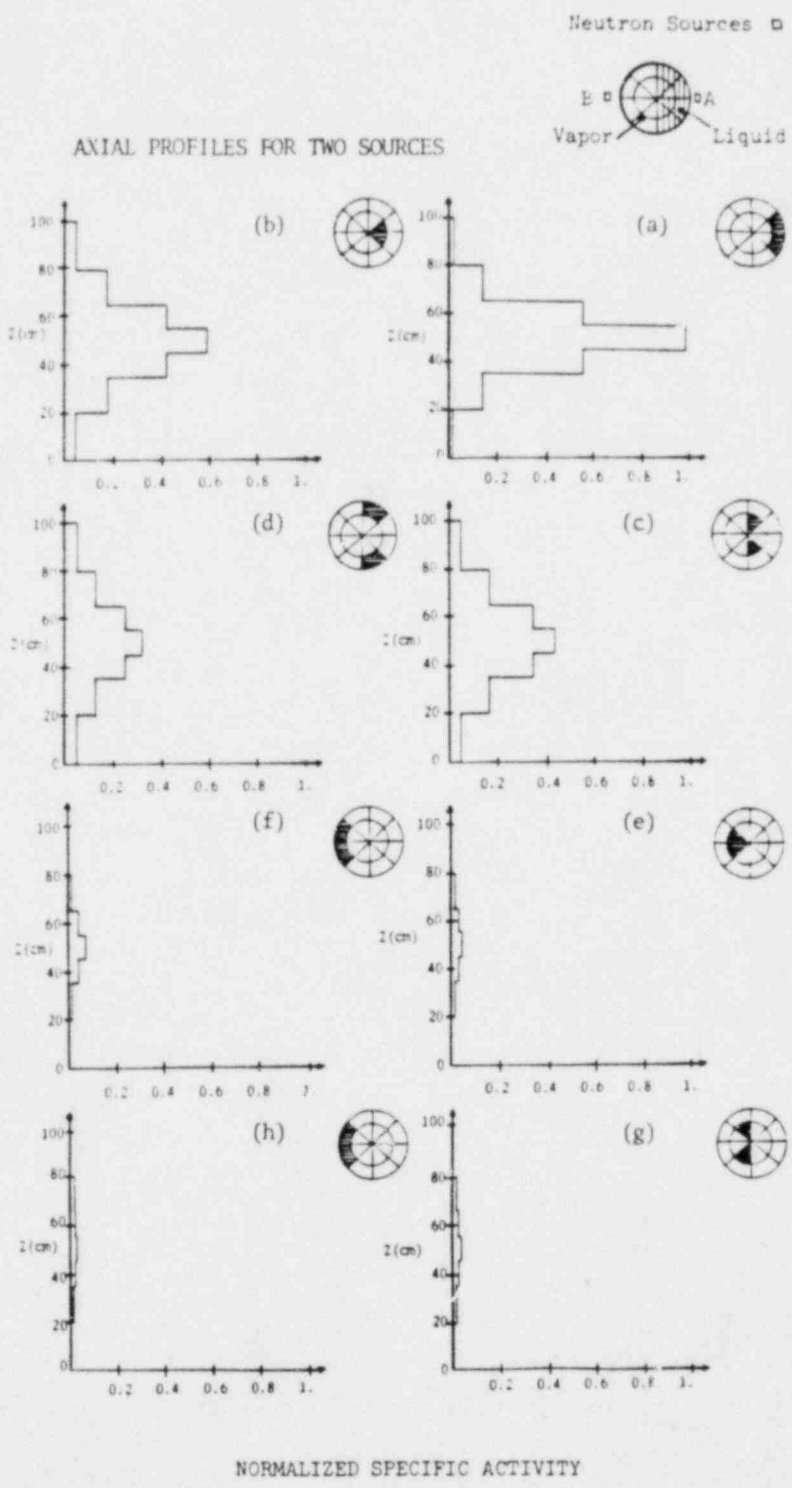

Figure 4-15 Axial Profiles of the ^{16}N Specific Activity when 1/2-Stratified Flow at 1200 psia, Saturation Temperature is Tagged by Two Neutron Sources (Locations A and B)

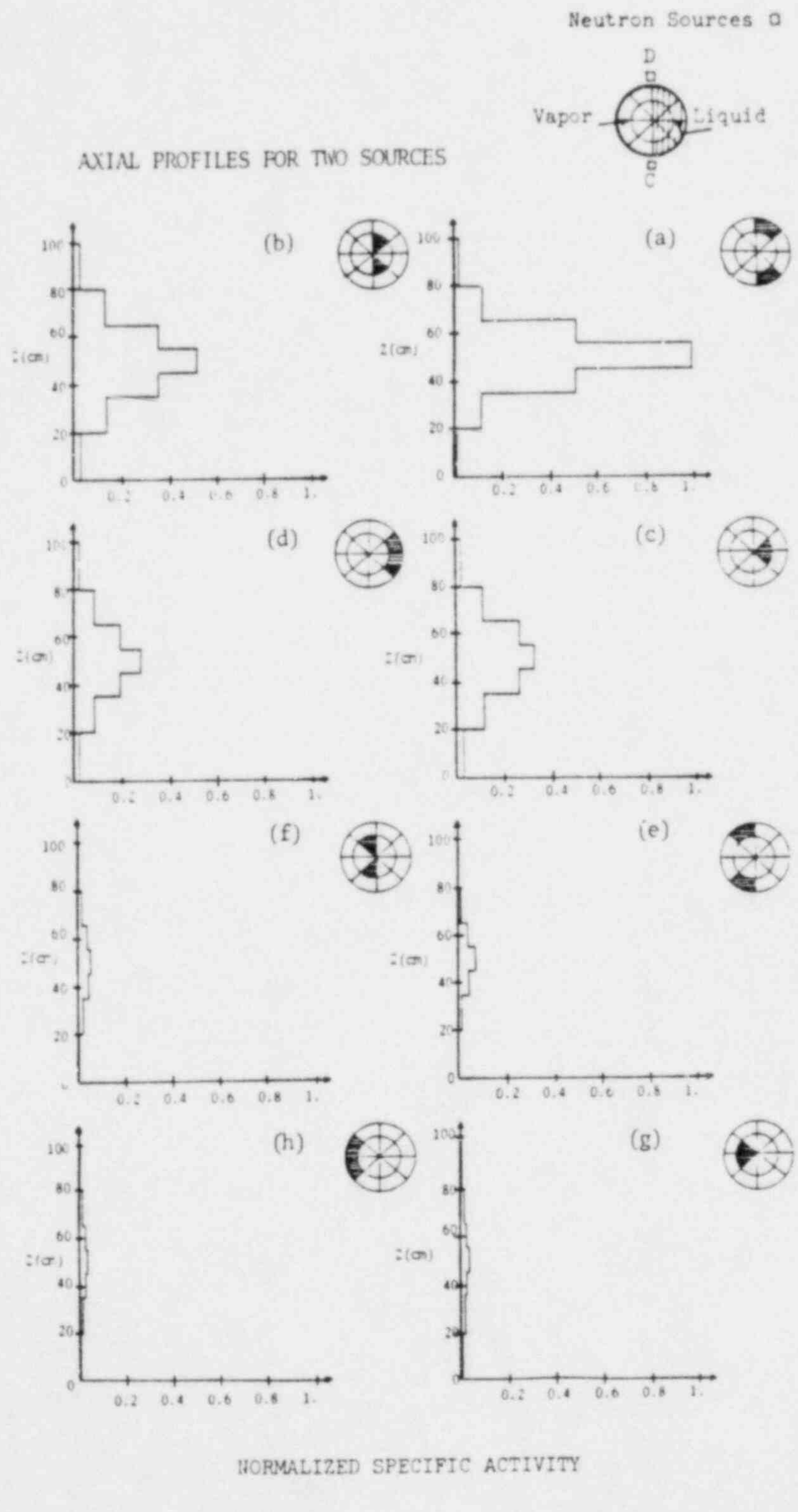

Figure 4-16 Axial Profiles of the ^{16}N Specific Activity when 1/2-Stratified Flow at 1200 psia, Saturation Temperature is Tagged by Two Neutron Sources (Locations C and D)

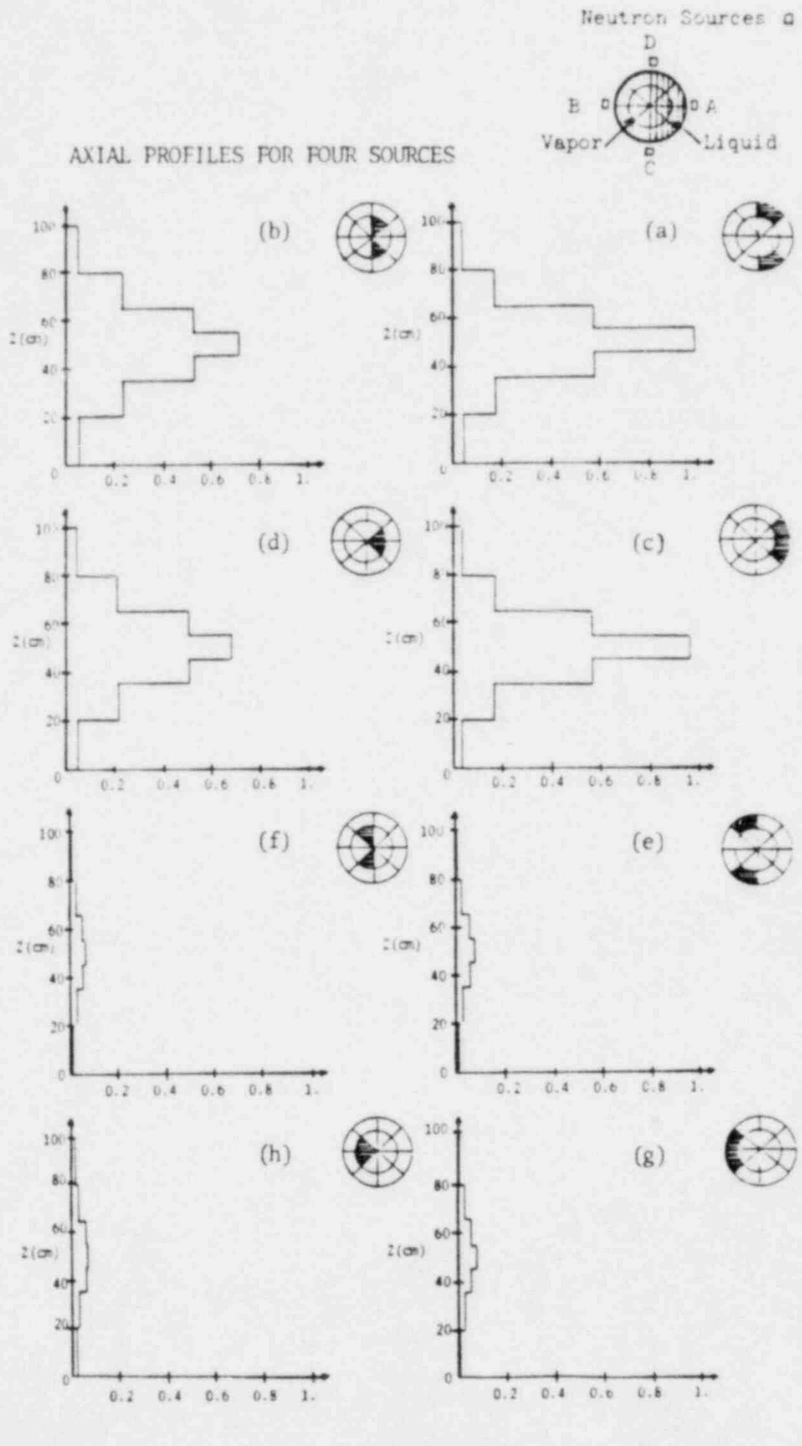

Figure 4-17 Axial Profiles of the ^{16}N Specific Activity when 1/2-Stratified Flow at 1200 psia, Saturation Temperature is Tagged by Four Neutron Sources

TABLE 4-1 Summary of ^{16}N Tagging of 1/2-Stratified Flow by One, Two and Four Neutron Sources

		Liquid Regions			Vapor Regions		
		Ratio of minimum to maximum activity at axial position of source ($45cm \leq Z \leq 55cm$)	Axial activity decrease in regions nearer the source: within 1 radius	Axial activity decrease in regions nearer the source: within 2 radii	Ratio of minimum to maximum activity at axial position of source ($45cm \leq Z \leq 55cm$)	Axial activity decrease in regions nearer the source: within 1 radius	Axial activity decrease in regions nearer the source: within 2 radii
Tagging with One Source	at Location A (Fig. 4-11)	19% (Fig. 4-11d)	53% (Fig. 4-11a)	9%	Negligible Contribution		
	at Location B (Fig. 4-12)	39% (Fig. 4-12d)	83% (Fig. 4-12a)	37%	from 27% (Fig. 4-12e) to 7% (Fig. 4-12h)	from 27% to 16% (Fig. 4-1[illegible]e)	from 27% to 3%
	at Location C (Figs. 4-13,4-14)	5% (Fig. 4-13d)	50% (Fig. 4-13a)	9%	from 7% (Fig. 4-14a) to 1% (Fig. 4-14d)	from 7% to 4% (Fig. 4-14a)	from 7% to 1%
Tagging with Two Sources	at Locations A and B (Fig. 4-15)	32% (Fig. 4-15d)	46% (Fig. 4-15a)	14%	from 7% (Fig. 4-15f) to 2% (Fig. 4-15h)	from 7% to 4% (Fig. 4-15f)	from 7% to 1%
	at Locations C and D (Fig. 4-16)	28% (Fig. 4-16d)	51% (Fig. 4-16a)	11%	from 7% (Fig. 4-16e) to 3% (Fig. 4-16h)	from 7% to 4% (Fig. 4-16e)	from 7% to 1%
Tagging with Four Sources	at Locations A,B,C and D (Fig. 4-17)	69% (Fig. 4-17d)	58% (Fig. 4-17a)	17%	from 7% (Figs. 4-17e,g) to 6% (Figs. 4-17f,h)	from 7% to 5% (Figs. 4-17e,g)	from 7% to 1%

These values are within -3% uncertainty

By comparing these results it was concluded:

(i) When more uniform tagging within the liquid and vapor is desired, the mixture should be tagged by four sources (Figure 4-17).

(ii) If the vapor and the liquid are to both be measured, then the mixture should be tagged by one source at Position B (Figure 4-12). For this case a measurable peak will be observed in the counting spectrum from the vapor in addition to the peak from the liquid.

(iii) When one is only interested in the liquid contribution, the mixture should be tagged by one source at position A (Figure 4-11). For this case the vapor activity is negligible.

4.3.2 Gamma Transport Calculations at Detector Position

4.3.2.1 Geometry description. Detailed gamma transport calculations were performed over a 1-m length of pipe. The geometry consisted of 131 regions: 56 liquid regions, 56 vapor regions, 6 pipe wall regions, 8 detector regions and 5 air regions surrounding the system. The detector regions formed an annulus of NaI 10-cm high by 7.5-cm thick surrounding the pipe. This geometry is equivalent to the one used for single-phase flow (Figure 4-6) except the pipe was half-filled with liquid and half-filled with vapor.

4.3.2.2 Monte Carlo results. As a result of the symmetry of the liquid regions, vapor regions and the annular detector, only 32 Monte Carlo calculations were required to determine the detector efficiency for all 56 liquid and 56 vapor regions. The ANDYRPI Monte Carlo program was run for a total of 320,000 gamma histories in 32 jobs. For each job 10,000 gamma histories in 20 batches of 500 gammas were run. A uniform isotropic 6.5-MeV gamma-ray volume source was placed in one of the 16 liquid or 16 vapor regions for each calculation.

4.3.2.3 Detector efficiency. Figures (4-18) through (4-25) show the axial profiles of the percentage detector efficiency for the different liquid and vapor regions and for four different detector locations, A, B, C and D. An overall evaluation of these results is summarized in Table 4-II where for each detector location is given:

- The ratio of maximum-to-minimum detector efficiency at the axial position of the detector ($45 \leq Z \leq 55$cm). That is, how much the efficiency decreases at the axial detector position in going from the region nearest the detector to the region furthest away.
- Axial variation of the detector efficiency within one and two pipe radii. That is, the ratios of the efficiency at the midplane position to the efficiency at the axial position of one and two pipe radii for pie-segment regions nearest the detector.

4.3.3 Transport Simulation. As described previously, Monte Carlo calculations were carried out to determine: (i) the initial ^{16}N tagged concentration in 56 liquid and 56 vapor regions near the PNA source(s), and,(ii) the detector response to ^{16}N in another 56 liquid and 56 vapor regions near the detector(s). The finite difference model described in Section 2.3.3,with spatial and time mesh increments of Δr= 1 cm, Δx=1 cm and Δt= 0.02 s,was used to transport the irradiated liquid and vapor from the tagging to detector positions. The case in which 1/2-stratified flow at mean liquid and vapor velocities of 10 cm/s and 30 cm/s, respectively,is tagged by four neutron sources and detected by four detectors, was chosen for this simulation. For these flow conditions one can expect 1/2-stratified flow with a smooth interface.[60]

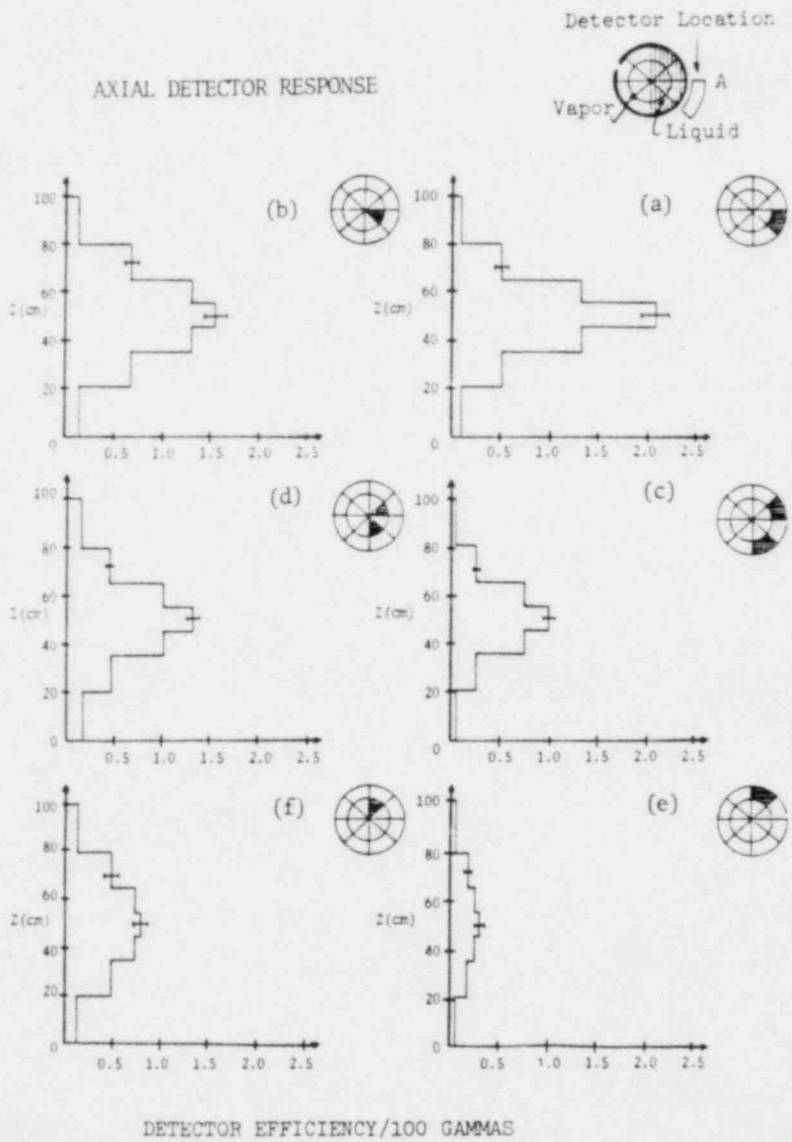

Figure 4-18 Axial Detector Response from Liquid Regions of ^{16}N Tagged 1/2-Stratified Flow at 1200 psia, Saturation Temperature (Detector Location A)

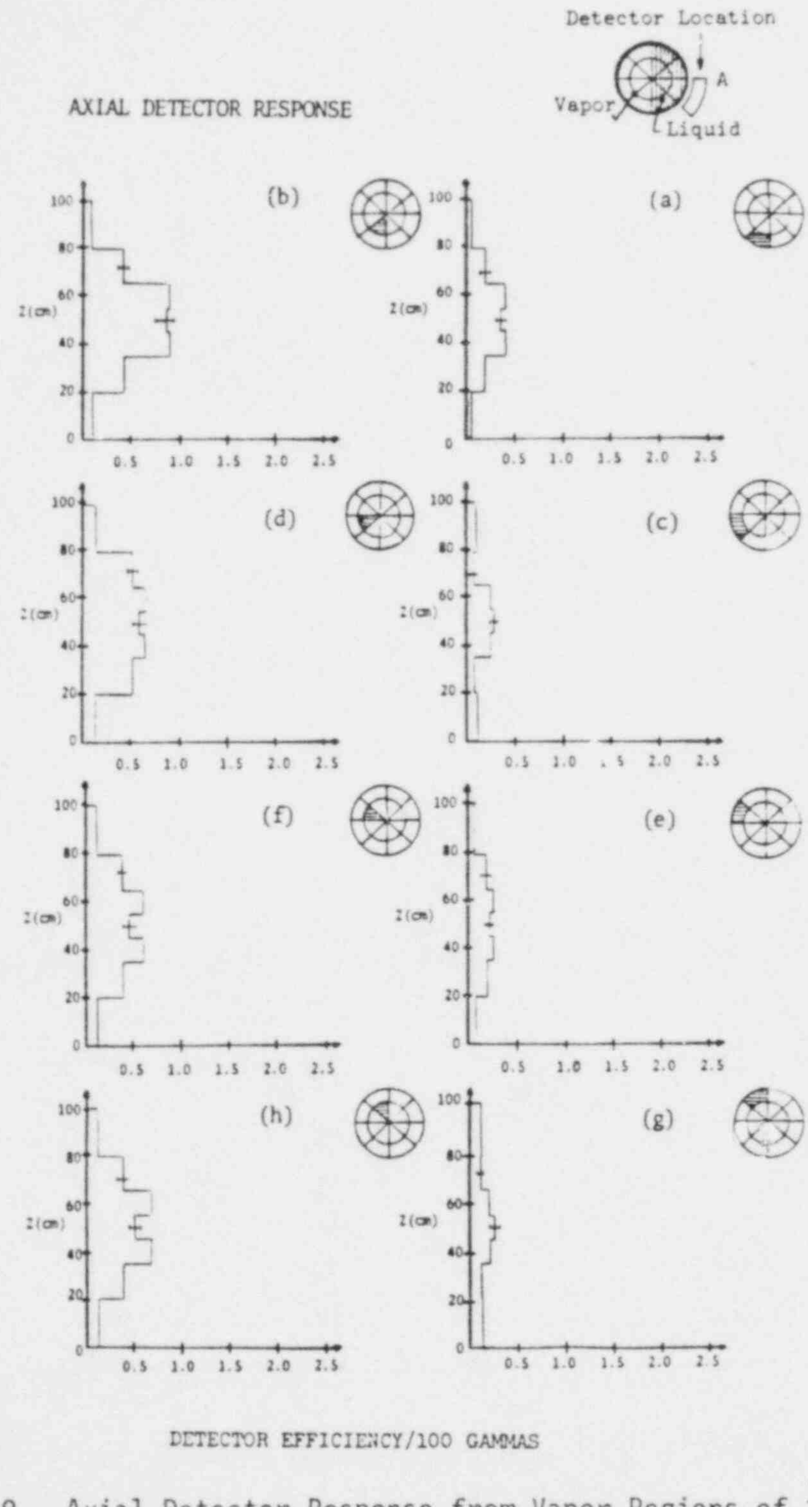

Figure 4-19 Axial Detector Response from Vapor Regions of ^{16}N Tagged 1/2-Stratified Flow at 1200 psia, Saturation Temperature (Detector Location A)

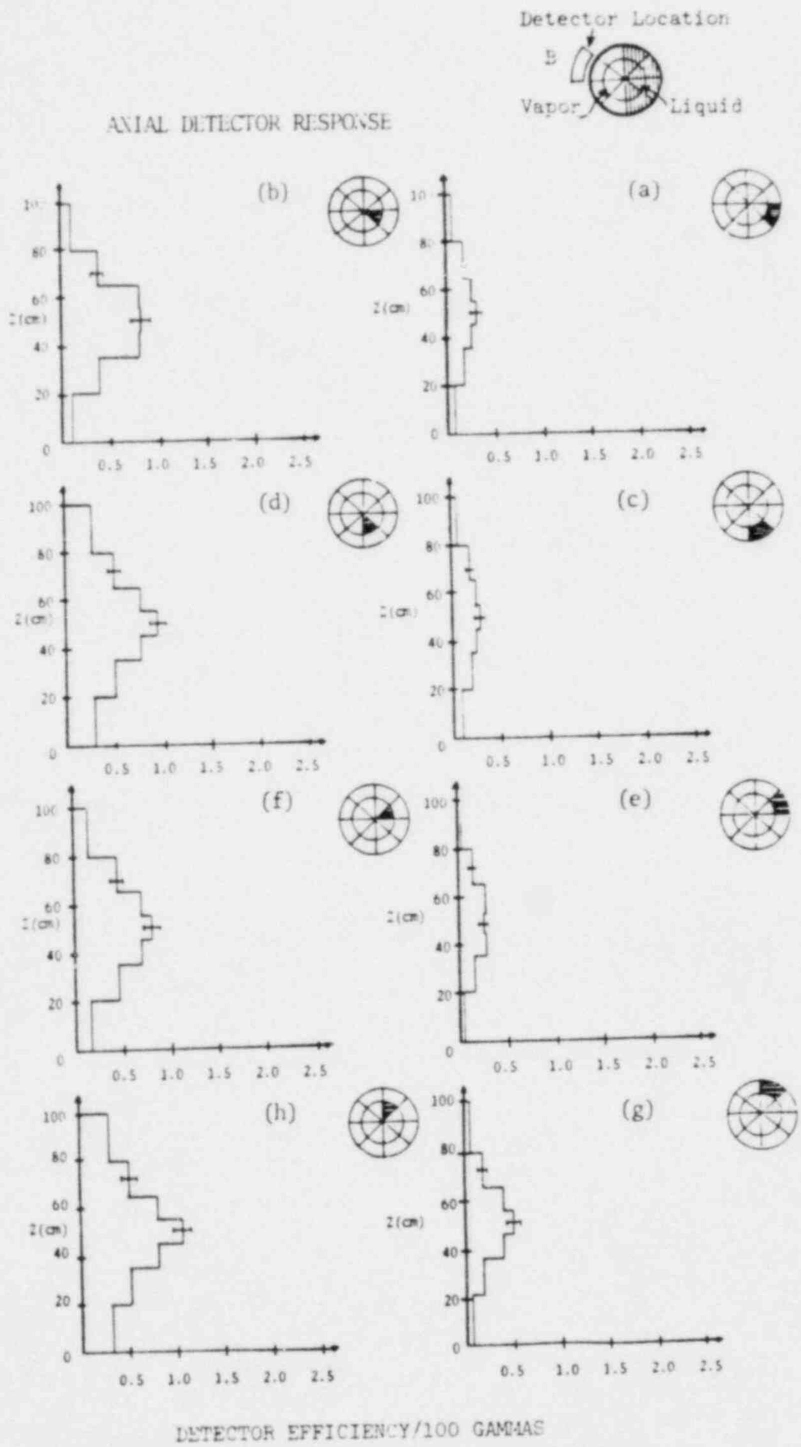

Figure 4-20 Axial Detector Response from Liquid Regions of ^{16}N Tagged 1/2-Stratified Flow at 1200 psia, Saturation Temperature (Detector Location B)

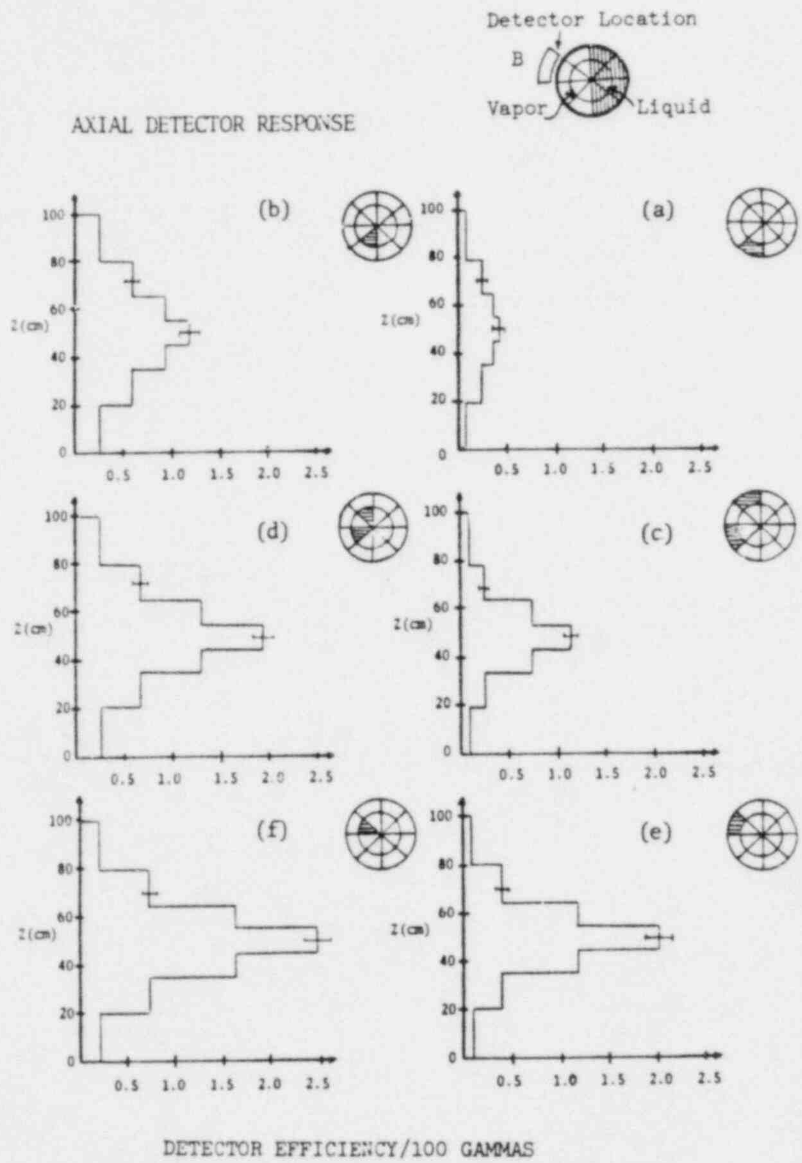

Figure 4-21 Axial Detector Response from Vapor Regions of ^{16}N Tagged 1/2-Stratified Flow at 1200 psia, Saturation Temperature (Detector Location B)

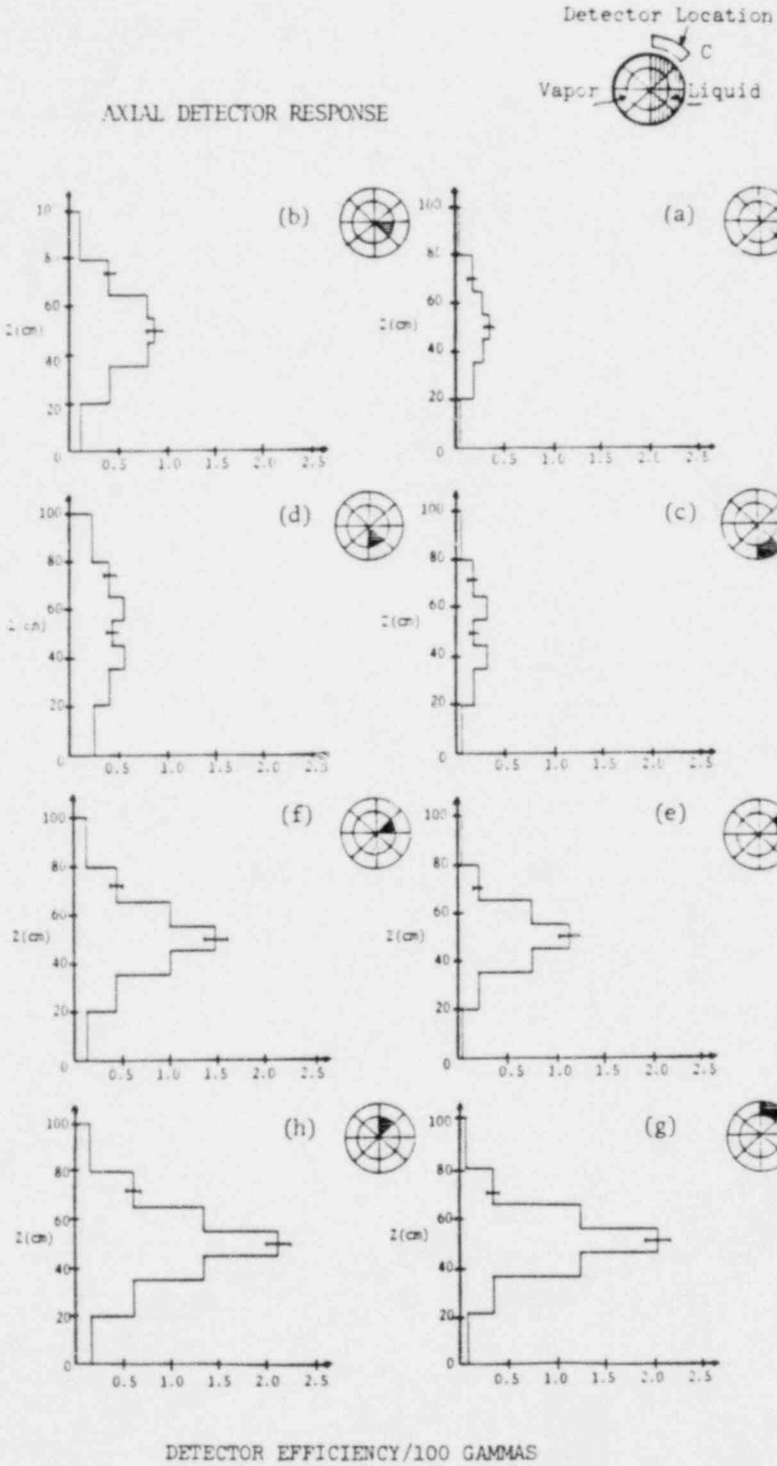

Figure 4-22 Axial Detector Response from Liquid Regions of ^{16}N Tagged 1/2-Stratified Flow at 1200 psia, Saturation Temperature (Detector Location C)

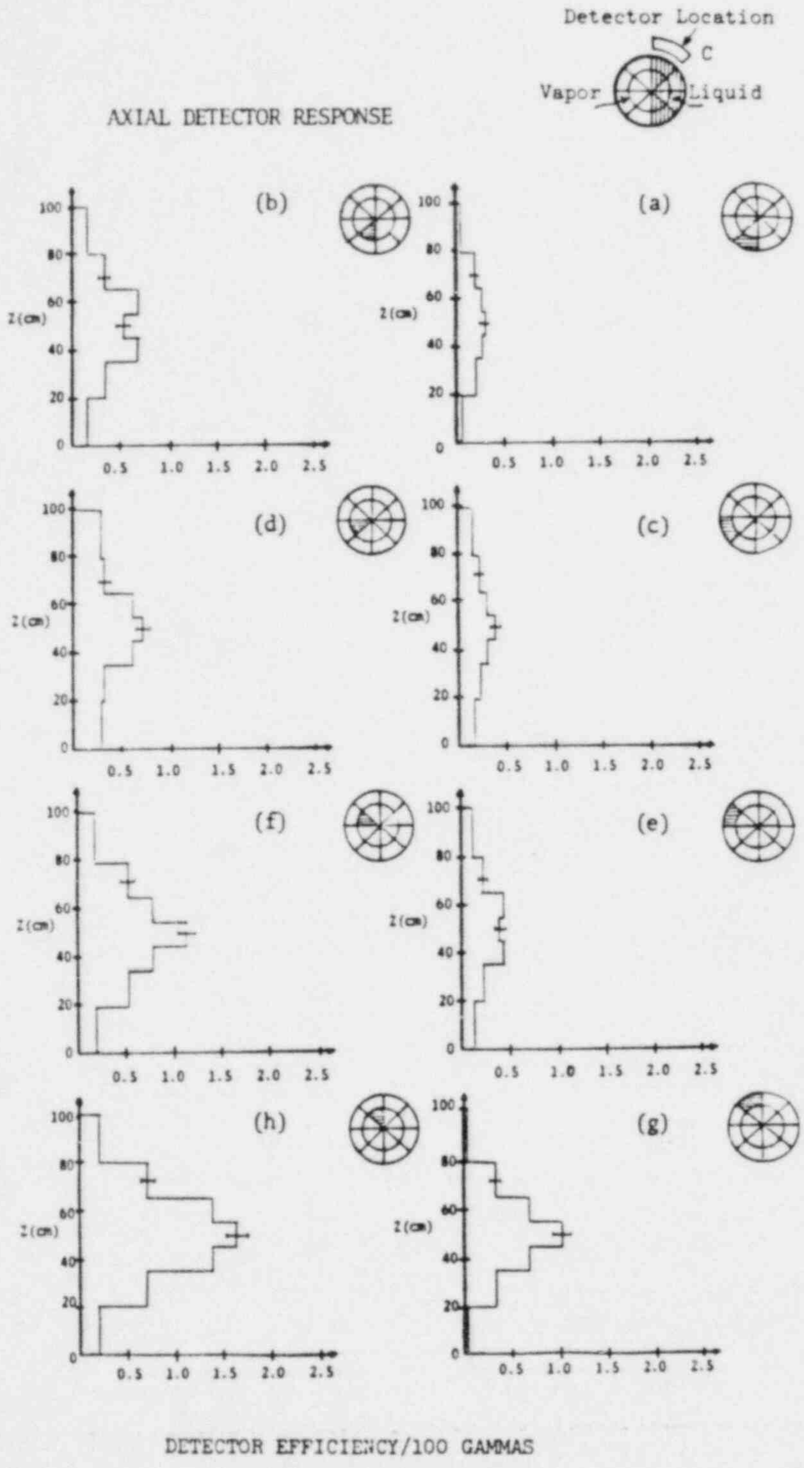

Figure 4-23 Axial Detector Response from Vapor Regions of ^{16}N Tagged 1/2-Stratified Flow at 1200 psia, Saturation Temperature (Detector Location C)

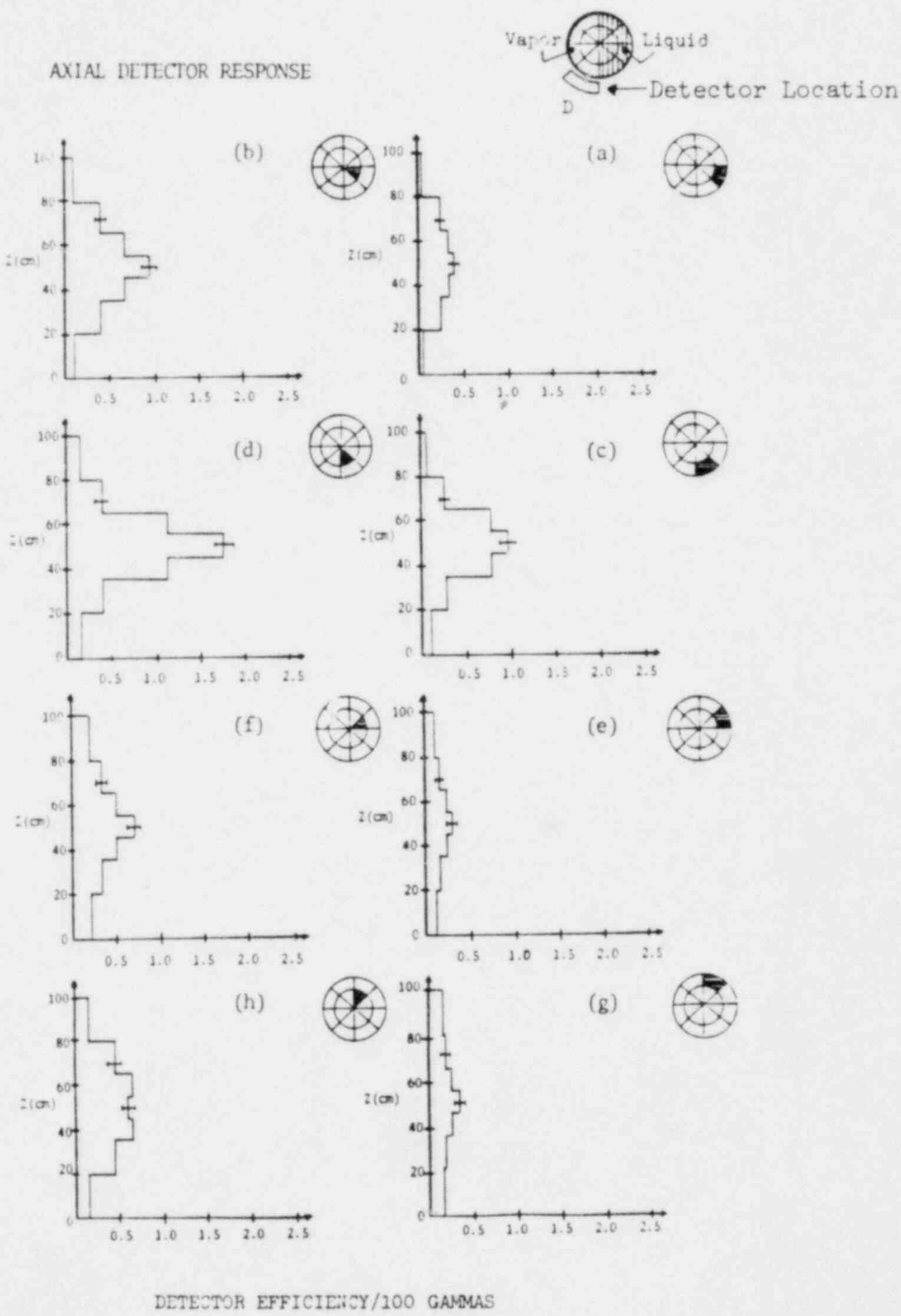

Figure 4-24 Axial Detector Response from Liquid Regions of ^{16}N Tagged 1/2-Stratified Flow at 1200 psia, Saturation Temperature (Detector Location D)

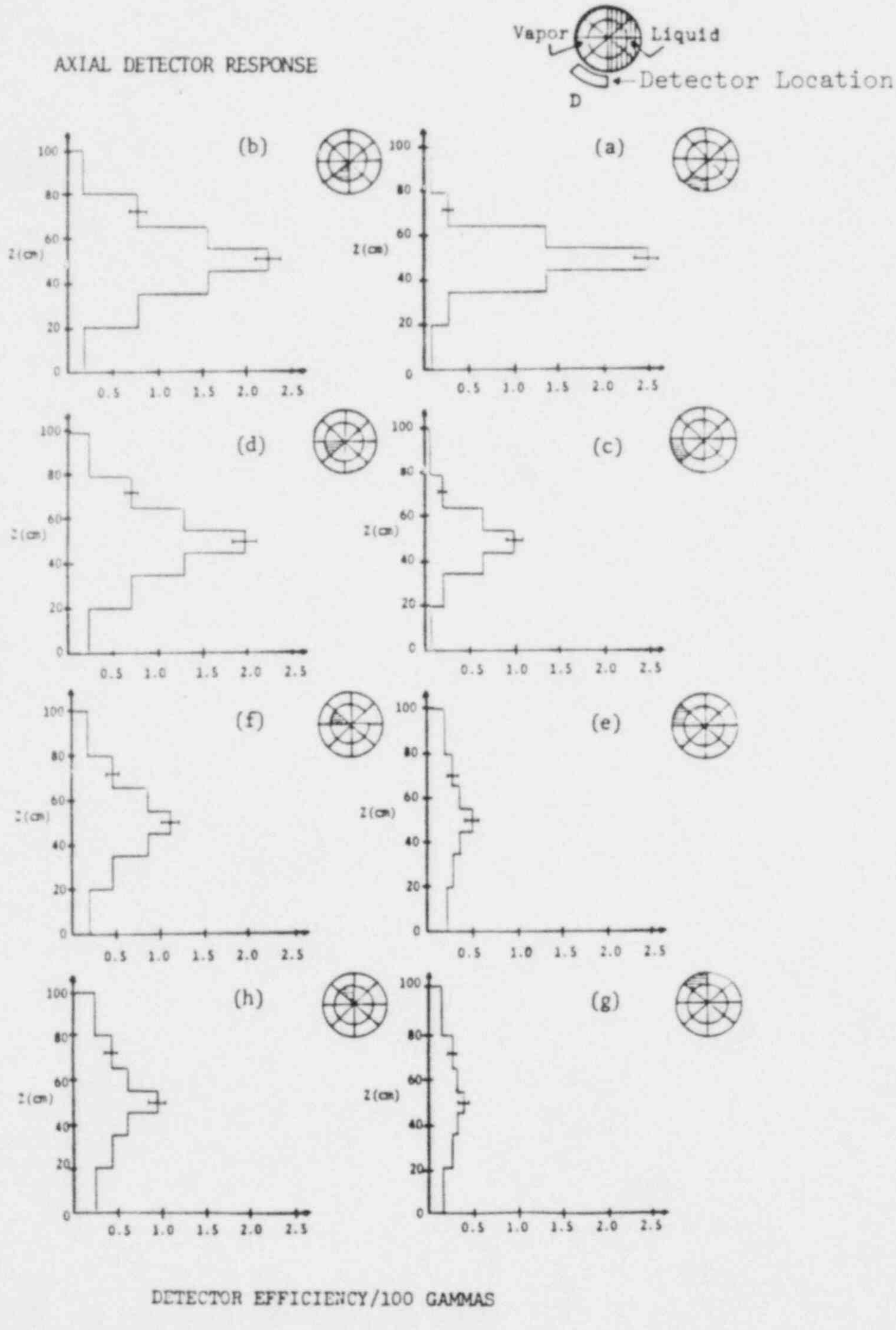

Figure 4-25 Axial Detector Response from Vapor Regions of ^{16}N Tagged 1/2-Stratified Flow at 1200 psia, Saturation Temperature (Detector Location D)

TABLE 4-II Summary of Detector Efficiency/Gamma from ^{16}N Tagged 1/2-Stratified Flow

	Liquid Regions			Vapor Regions		
	Ratio of maximum-to minimum detector efficiency at axial detector position (45cm < Z < 55cm)	Ratios of efficiency at midplane detector position to the efficiency at		Ratio of maximum-to-minimum detector efficiency at axial detector position (45cm < Z < 55cm)	Ratios of efficiency at midplane detector position to the efficiency at	
		1 radius	2 radii		1 radius	2 radii
Detector at Location A	7.1 ± 0.8 (from Figs. 4-18a,e)	1.6 ± 0.2 (Fig. 4-18a)	4.2 ± 0.6	3.1 ± 0.3 (from Figs. 4-19b,g)	0.9 ± 0.1 (Fig. 4-19b)	2.0 ± 0.3
Detector at Location B	4.2 ± 0.4 (from Figs. 4-20h,e)	1.3 ± 0.1 (Fig. 4-20h)	2.1 ± 0.3	6.0 ± 0.6 (from Figs. 4-21f,a)	1.5 ± 0.2 (Fig. 4-21f)	3.4 ± 0.5
Detector at Location C	11.6 ± 1.3 (from Figs. 4-22h,c)	1.6 ± 0.2 (Fig. 4-22h)	3.6 ± 0.5	4.8 ± 0.5 (from Figs. 4-23h,a)	1.1 ± 0.1 (Fig. 4-23h)	2.2 ± 0.3
Detector at Location D	4.5 ± 0.4 (from Figs. 4-24d,e)	1.4 ± 0.1 (Fig. 4-22d)	3.7 ± 0.5	6.9 ± 0.7 (from Figs. 4-25a,g)	1.8 ± 0.2 (Fig. 4-25a)	9.4 ± 1.3

As a result of the symmetry at the tagging position (Figure 4-17) only two finite difference calculations were required; one concerned with the transport of the liquid and other with the transport of the vapor. That is, the finite difference code was used to transport both phases separately. For each phase: (i) the $1/7^{th}$ power law velocity profile was assumed, and, (ii) the Monte Carlo results for the initial ^{16}N tagging concentration and detector efficiency corresponded to the values for that particular phase. A counting spectrum was then simulated by: (i) coupling the results from both phases, (ii) normalizing these values to get the total ^{16}N produced under the area of the theoretical time profile, and (iii) scaling these theoretical values by the radioactive decay of the ^{16}N (i.e. multiplying by $e^{-\lambda t}$).

The total velocity profile for this simulated 1/2-stratified flow is shown in Figure 4-26 and the counting spectrum obtained for a source-detector configuration with $L_o \approx 154$ cm is shown in Figure 4-27.

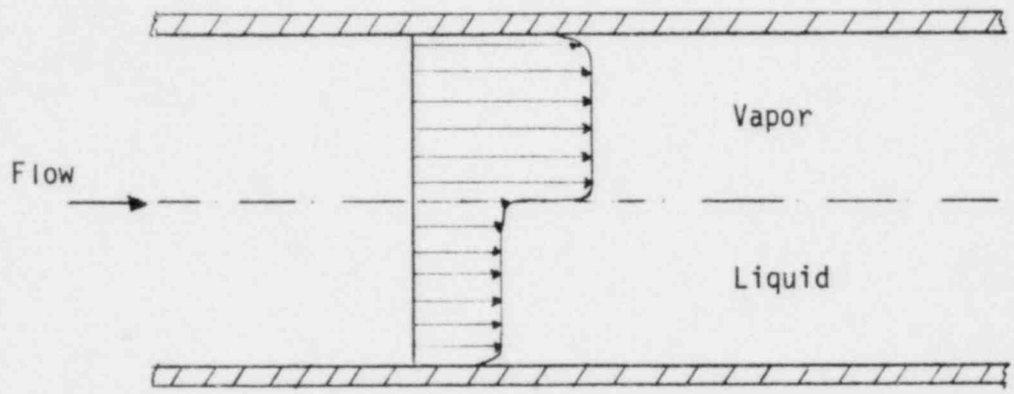

Figure 4-26 Schematic of the Velocity Profile for a Simulated 1/2-Stratified Flow When the Mean Liquid and Vapor Velocities are 10 cm/s and 30 cm/s, Respectively

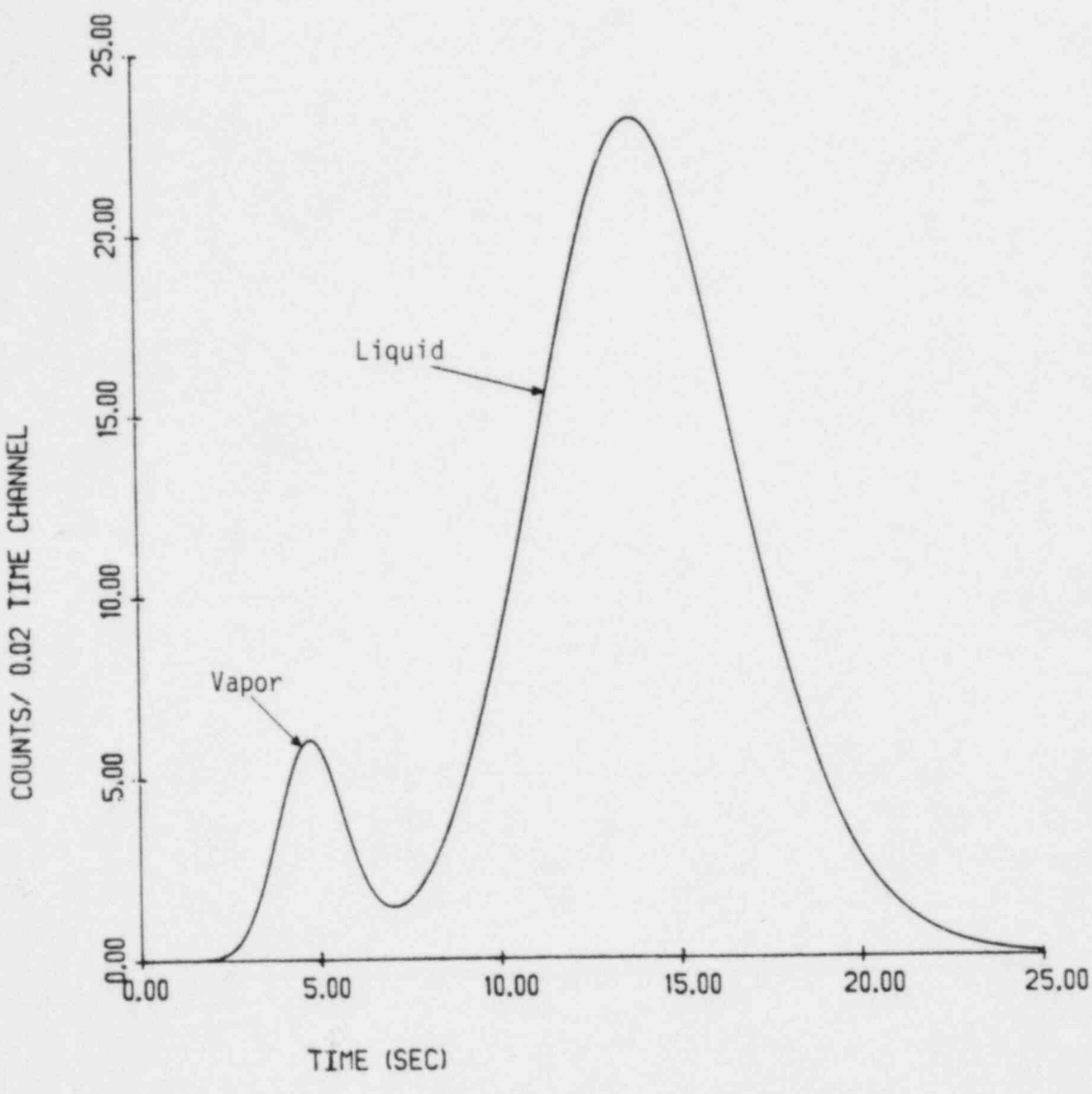

Figure 4-27 Simulated Time Profile for 1/2-Stratified Flow at a Mean Liquid and Vapor Velocities of 10cm/s and 30cm/s, Respectively. The Finite Difference Method Was Used to Couple the Monte Carlo Calculations at the Tagging and Detector Positions

PART 5

INTERPRETATION OF LOFT L3 7 TEST PNA DATA

5.1 PNA Measurements at LOFT

PNA data were recently taken at LOFT during the small break transient L3-7 test, for a single-phase flow condition. The fluid was tagged by four neutron generators fired simultaneously and the induced radiation was detected by four NaI detectors. The experimental time profiles of the irradiated fluid were recorded on a 1024-channel time analyzer with 2 ms time intervals. The number of counts in each of these small time channels was very low, so it was convenient to sum up the counts recorded in ten successive channels and then analyze these summed data. This was done for two sets of LOFT data from the L3-7 test, blocks 24 and 26. Blocks 24 and 26 are measurements in which the PNA neutron generators were pulsed respectively at 80 and 100 minutes after the start of the blowdown transient. A linear background was fitted by least squares to the PNA data in the regions away from the leading and trailing edges of the PNA peak. The experimental time profiles (corrected for background) of these two data sets are shown in Figures 5-1 and 5-2.

5.2 Analysis of the LOFT PNA Data

Several methods can be used in order to analyze the LOFT PNA data. The understanding and applicability of these methods strongly influences the LOFT PNA single-phase data interpretation. A full description of these methods follows.

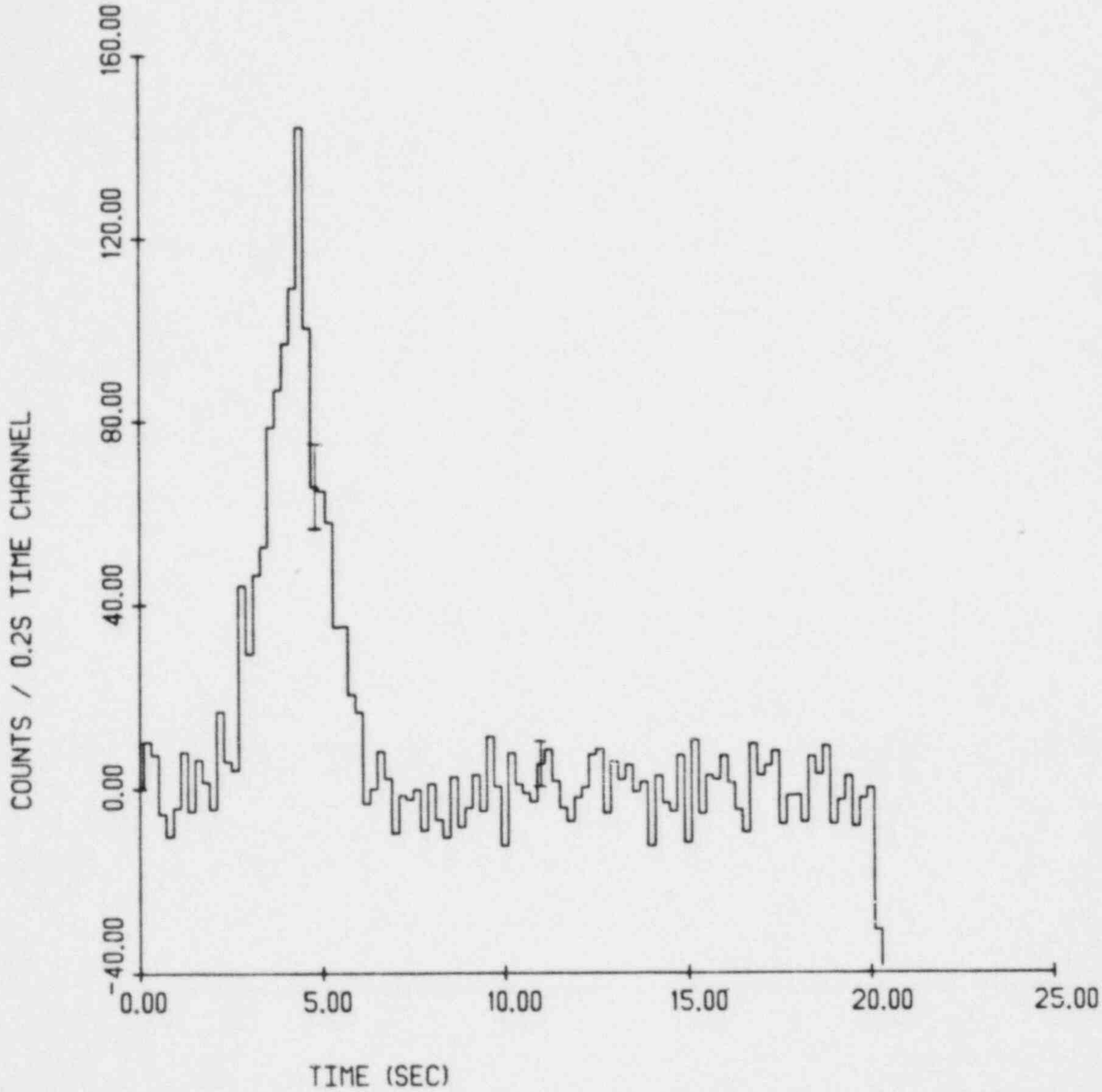

Figure 5-1   Background Corrected L3-7 Test PNA Data, Block 24

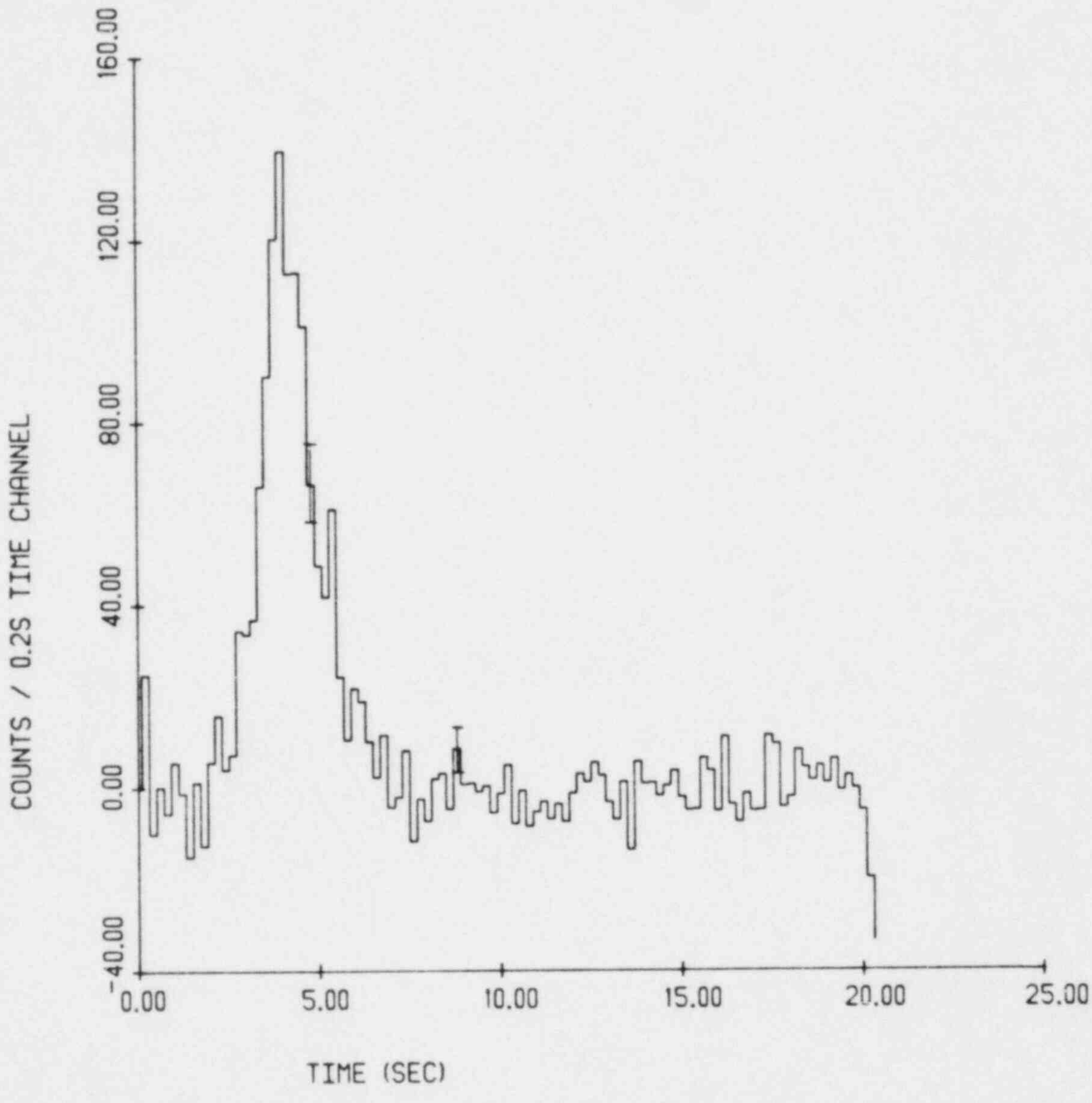

Figure 5-2 Background Corrected L3-7 Test PNA Data, Block 26

5.2.1 Distance-to-Time-Peak Ratio. The simplest, but least accurate method to interpret LOFT PNA data is to merely divide the distance L_o between the source(s) and the detector(s) by the time corresponding to the peak in the time spectrum. This method can lead to large errors since the position of the peak is affected by the counting statistics of only a few datum points. For the LOFT L3-7 test PNA data, shown in Figures 5-1 and 5-2, this method gives mass-averaged velocities of about 35 and 38 cm/s, respectively. Since these data were already grouped into 10-channel sums, this method gives velocities with errors probably no better than $\pm$10%.

5.2.1 The $1/t^2$ and $1/t$ Data Reduction Methods. The mass-weighted velocity for the two L3-7 LOFT tests (blocks 24 and 26) were obtained by the $1/t^2$ and $1/t$ data reduction methods. Equations (2.7) and (2.8) were applied between the 10th and 36th 0.2-s time channels, a region surrounding the PNA peak where the data appears to be above the background. For a source-detector distance of 153.7 cm, the $1/t^2$-weighting gives mass-weighted velocities of (39.8$\pm$1.2) cm/s and (40.2$\pm$1.1) cm/s for blocks 24 and 26, respectively. On the other hand, the $1/t$-weighting method gives a mass-weighted velocity of (38.1$\pm$0.6) cm/s for both sets of data. The given uncertainties on the mass-weighted velocities are based only on counting statistics. As expected, the $1/t^2$-weighting gives a larger mean velocity than the $1/t$-weighting, which for the L3-7 data results in a velocity difference of about 6%.

In Section 2.1.1, the flow regime effect in the mass-weighted velocity was theoretically discussed. On the other hand, in Section 4.2.3, the possible errors introduced by the $1/t$ and $1/t^2$

data reduction methods for LOFT geometry were analyzed. Therefore, neither of the two time-weighted methods is expected to give the correct result. The actual mass-weighted velocity should be expected to differ from these two cases.[24]

5.2.3 Mechanistic Analysis of LOFT PNA Data. A mechanistic analysis was developed to interpret the LOFT single-phase data.[56] This analysis includes the axial dispersion of the induced activity at the tagging position and the axial response of the detector. In a similar way, as described in Section 4.2.3.2, the turbulent single-phase dispersion theory of G. I. Taylor[40] was used to couple the Monte Carlo calculations at the tagging and detector positions, i.e., to transport the irradiated fluid from the seven axial water regions at the source(s) position (Figure 4-3) to the seven axial water regions at the detector(s) position (Figure 4-6). The time spectrum of the detector counting rate was then generated assuming: (i) uniform initial ^{16}N concentration within each axial source region, and, (ii) constant mean liquid velocity. The decay of the ^{16}N was corrected for, in these figures.

The width of the calculated time spectrum depends on the Taylor dispersion coefficient κ, discussed in Section 2.3.2. This coefficient is given by [40]: $\kappa = K\, R\sqrt{\tau_{o/p}}$, where R is the radius of the pipe, τ_o is the shear stress at the wall which depends on the mean flow velocity $\bar{u}$, ρ is the fluid density and K is an empirical constant which Taylor found to be equal to 10.1. By varying the empirical constant K and the mean velocity $\bar{u}$, a good fit can be obtained to the LOFT data.

Figure 5-3 shows the LOFT 13-7, block 26 experimental PNA data and three calculated spectra with $\bar{u}$ = 37 cm/s, for K equal to 10.1

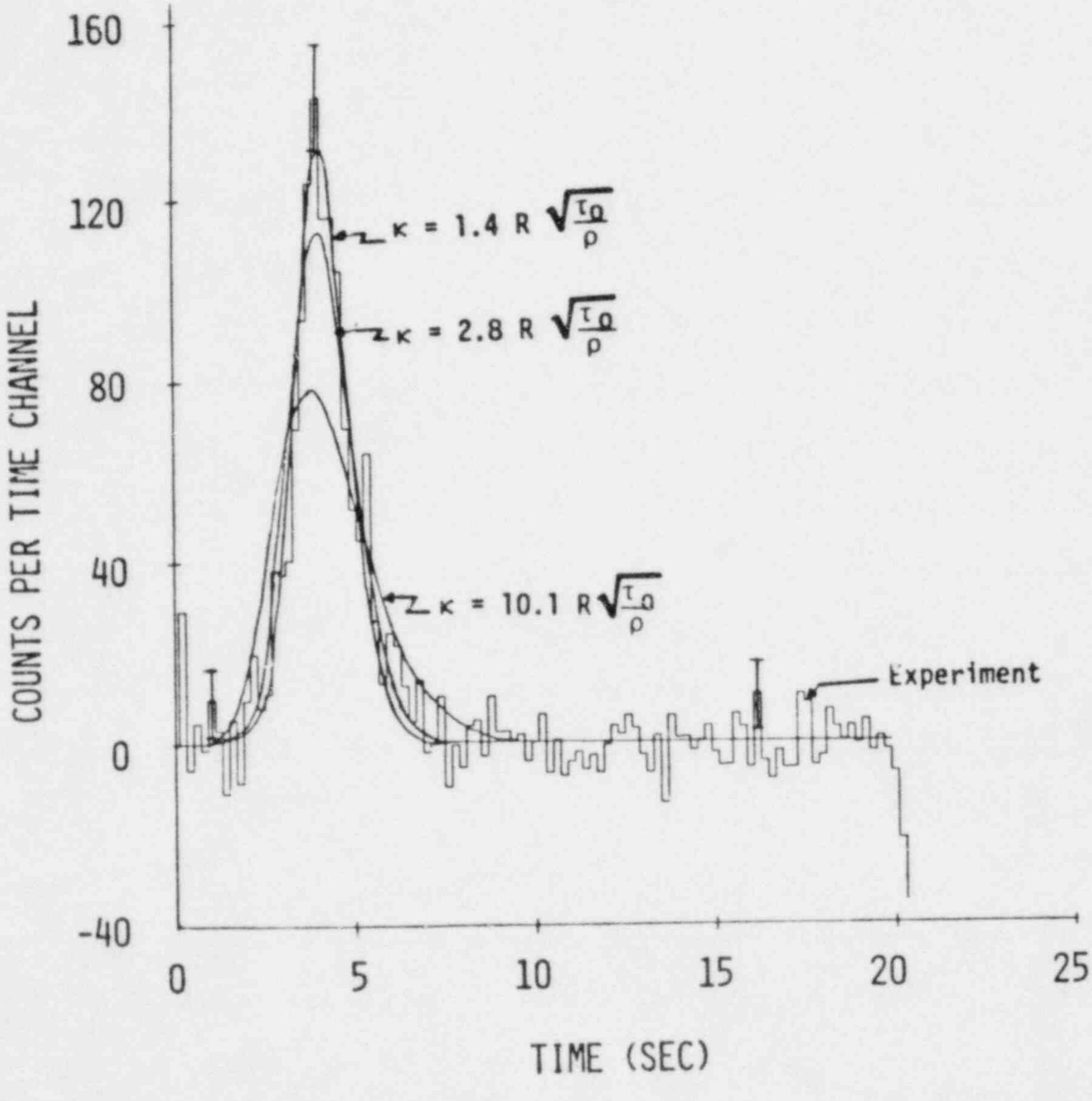

Figure 5-3 Comparison of LOFT L3-7 Block 26 PNA Time Spectrum Data (Histograms) with Time Spectra Calculated with a Mean Flow Velocity of $\bar{u}$=37 cm/s and Three Different Dispersion Coefficients

(the "classical" Taylor value), 2.8 and 1.4. The area under each calculated spectrum was normalized to the area under the experimental peak. A value of K between 1.4 and 2.8 appears to fit the experimental data.

A goodness-of-fit criterion was applied in order to obtain the best statistical fit to the LOFT PNA data by this mechanistic model. The reduced chi-square statistical criterion[57] was applied to blocks 24 and 26 of the L3-7 test. For block 24, the minimum of the chi-square distribution occurs for an average flow velocity of $\overline{u} = 36.5 \pm 0.8$ cm/s and an empirical constant in the dispersion coefficient of $K=1.4\pm0.6$. On the other hand, for block 26, the minimum occurs for $\overline{u} = 37 \pm 0.4$ cm/s and $K = 2.1 \pm 0.2$. The given uncertainties for $\overline{u}$ and K are based on the 95% probability that chi-square lies between these limits.[58] The L3-7 LOFT data, along with their best estimate fits for blocks 24 and 26, are shown in Figures 5-4 and 5-5, respectively.

It is not surprising that the LOFT PNA data can be fitted with a small dispersion coefficient. As discussed in Section 2.3.2, the classical Taylor theory assumes fully-developed radial mixing within each axial section for L/D ratios ≥ 50; whereas, the PNA geometry at LOFT has an L/D ratio of $\simeq 5.4$. W. Gill and co-workers have shown that for short L/D ratios, smaller dispersion coefficients are obtained in single-phase laminar flows[43-46] and in turbulent film flows.[47] They discuss the fact that at short distances from the injection point, the traverse eddy diffusion innibits longitudinal dispersion.

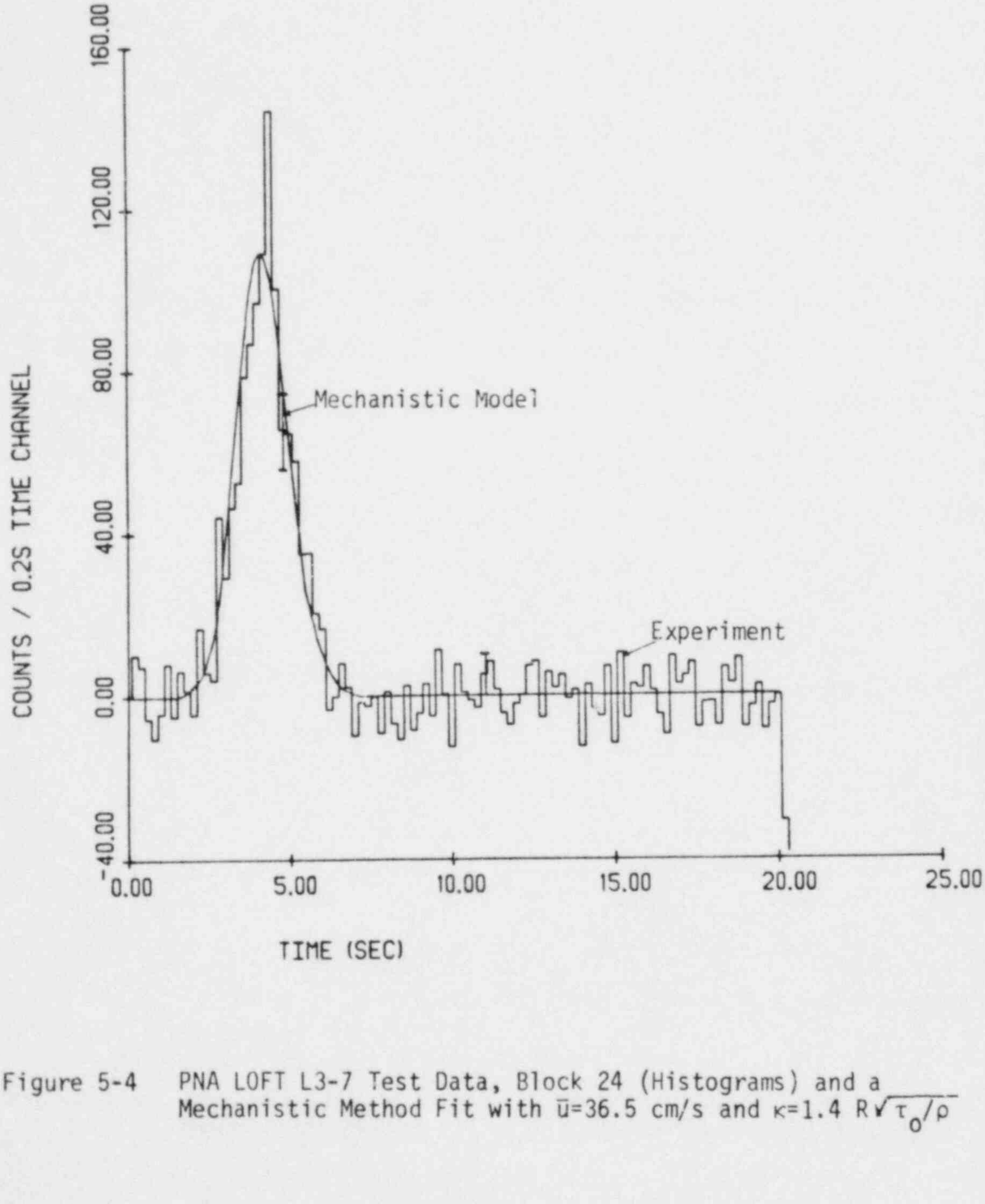

Figure 5-4 PNA LOFT L3-7 Test Data, Block 24 (Histograms) and a Mechanistic Method Fit with $\bar{u}$=36.5 cm/s and $\kappa=1.4\ R\sqrt{\tau_0/\rho}$

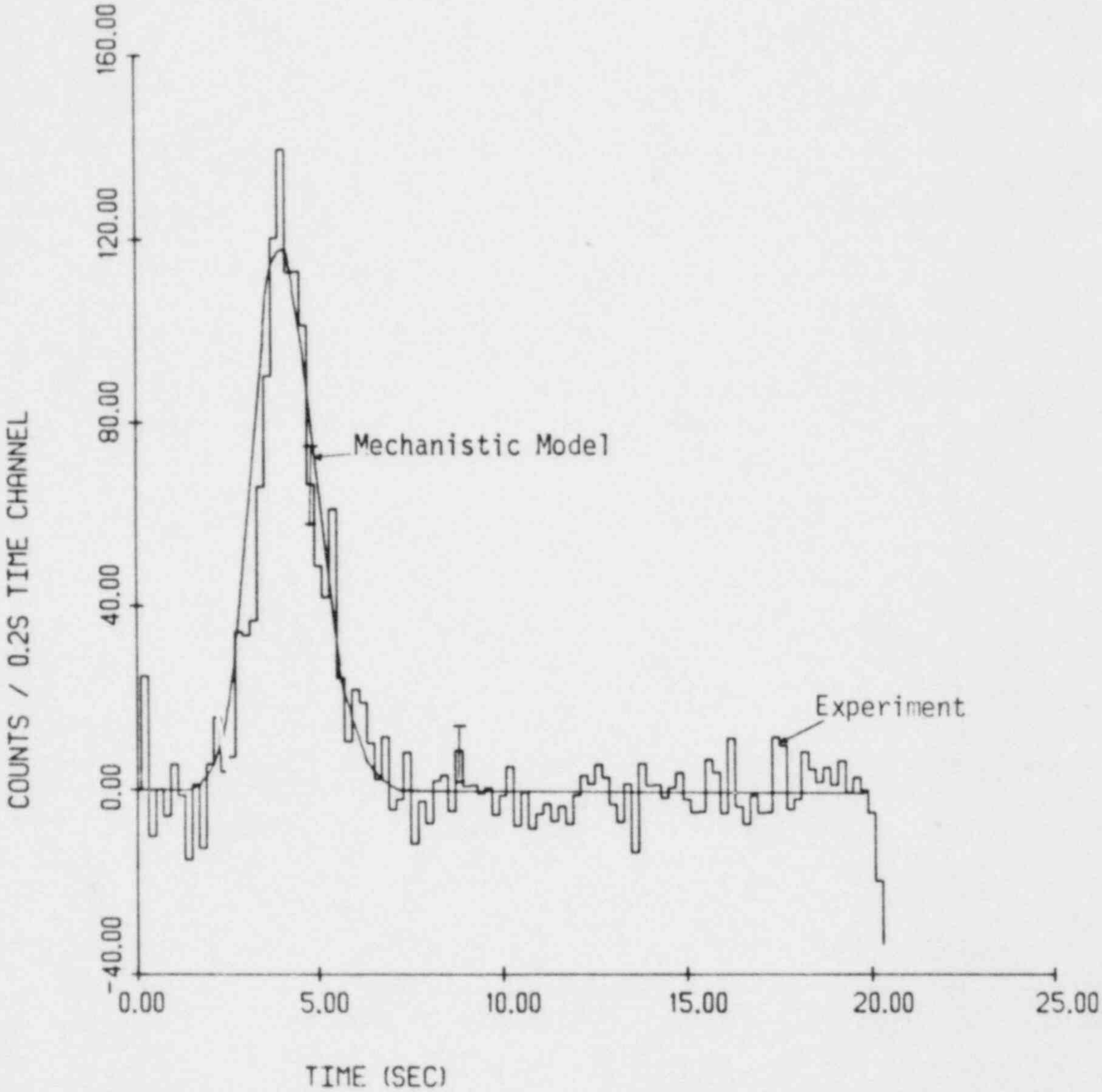

Figure 5-5 PNA LOFT L3-7 Test Data, Block 26 (Histograms) and a Mechanistic Method Fit with $\bar{u}$=37 cm/s and $\kappa=2.1\ R\ \sqrt{\tau_0/\rho}$

We have shown that the L3-7 single-phase LOFT PNA measurements can be fitted with the mechanistic method which includes axial dispersion of the induced ^{16}N activity, axial response of the detector and a turbulent single-phase Taylor theory with an empirical dispersion coefficient. This method has two significant advantages: (i) all the data can be utilized in determining the "best fit", rather than just the data near the peak, and, (ii) the model to which the data are being fit can readily be tested by either "eyeball" comparison between calculated and experimental data, or by goodness-of-fit statistical criteria. A good fit to all counting data lends confidence to the accuracy of the deduced mass-weighted velocity, as well as giving some information on the flow regime during the LOFT test.

5.2.4 Theoretical Fit to the LOFT Data by the Finite Difference Method. As described previously in Sections 4.2.1 and 4.2.2, Monte Carlo calculations were carried out to determine: (i) the initial ^{16}N tagged concentration in 112 liquid regions near the PNA source(s), and, (ii) the detector response to ^{16}N in another 112 liquid regions near the detector(s), for a single-phase flow condition at 1000 psia, 500°F. The finite difference model described in Section 2.3.3, with spatial and time mesh increments of Δr = 1cm, Δx = 1cm and Δt = 0.02s, was used to transport the irradiated water from the tagging to detector positions. A counting spectrum was then simulated by scaling these theoretical values by the radioactive decay of the ^{16}N (i.e., multiplying by $e^{-\lambda t}$) and normalizing them to get the same areas as under the experimental peak. Figures 5-6 and 5-7 show the experimental LOFT L3-7, blocks 24 and 26 PNA data (histo-

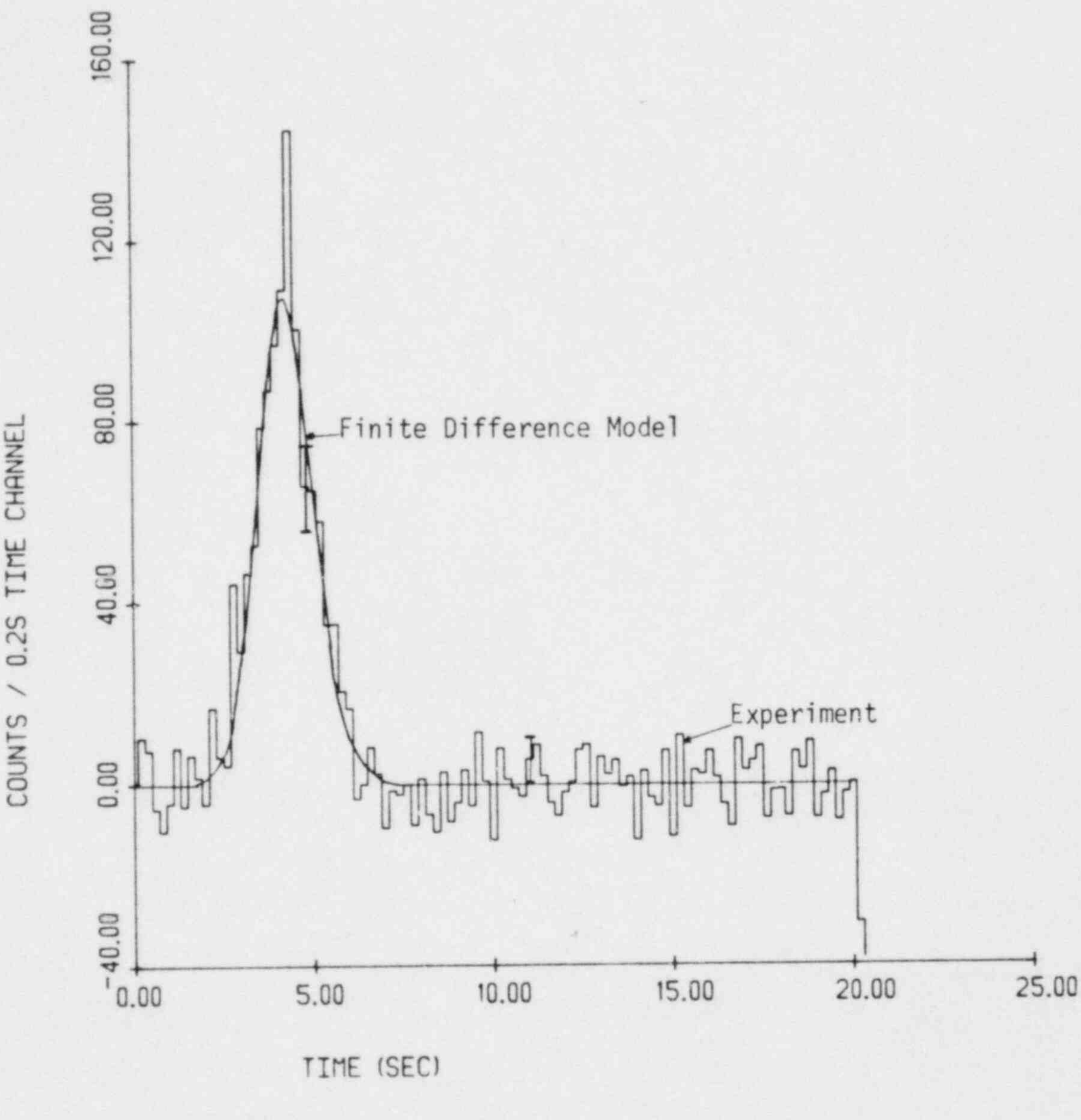

Figure 5-6 PNA LOFT L3-7 Test Data, Block 24 (Histograms) and a Finite Difference Method Fit with $\bar{u}$=34.5 cm/s

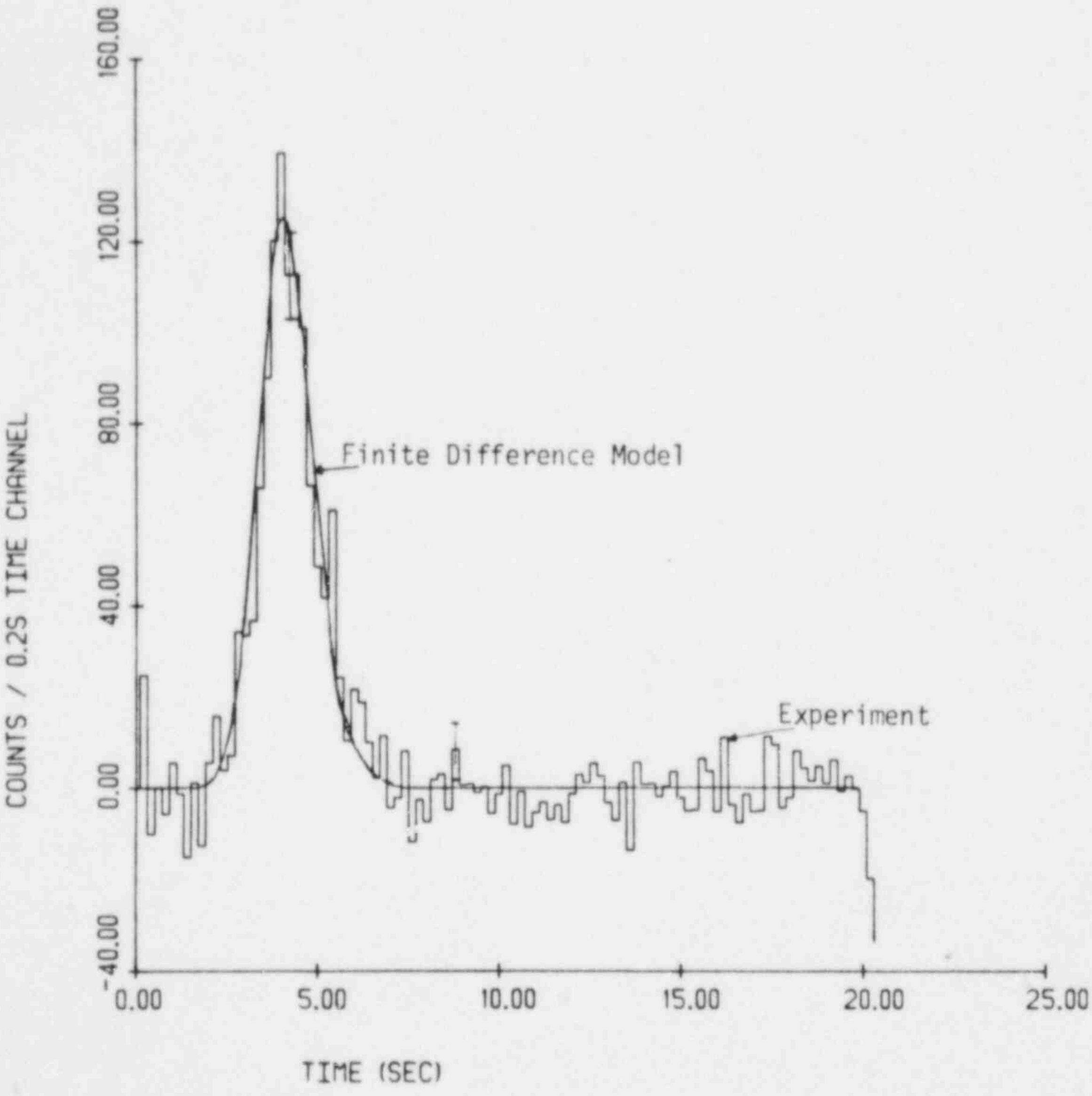

Figure 5-7 PNA LOFT L3-7 Test Data, Block 26 (Histograms) and a Finite Difference Method Fit with $\bar{u}$=35 cm/s

grams (fitted by the finite difference model. The mean flow velocity which appears best to fit the experimental data for a source-detector distance of 154 cm is $\overline{u} \simeq 34.5$ cm/s for block 24 and $\overline{u} = 35$ cm/s for block 26.

A goodness-of-fit criterion was not applied to obtain the best statistical fit to the LOFT data by this finite difference method but it is estimated that a reduced chi-square statistical criterion will give the mass-weighted velocity within 2% undertainty, similar to the results for the mechanistic model. This method tends to underestimate the contribution of the irradiated fluid near the wall, since the 1/7-power law is not a good representation of the velocity profile in this region. It is estimated that the effect of this wall region contributes to the uncertainty of the obtained mass-weighted velocity by $\simeq$ 2%. This method can be improved by using another velocity profile in this wall region with smaller and non-uniformly distributed radial mesh increments.

The L3-7 single-phase LOFT PNA measurements can be fitted by this finite difference method which includes axial and radial dispersion of the induced ^{16}N activity, axial and radial response of the detector, and a physical dispersion transport modeled by finite difference equations. This method has significant advantages: (i) the dispersion phenomena is considered from basic physical principles, and, (ii) all the data can be utilized in determining the mean flow velocity.

5.3 LOFT PNA Data Interpretation

Various methods to analyze the LOFT PNA data were discussed in the previous sections. Up to this point, a source-detector configuration with a straight, horizontal 14-in schedule 160 pipe, 60.5 in ($\simeq$154 cm) long was considered. The effect of the venturi contraction and the 90^0 pipe bend at the LOFT PNA test section (see Figure 4-2) were not taken into account. The venturi effect can be approximated by using an effective source-detector distance of L_{eff}=137 cm.[59] Although a shorter distance will inhibit further the axial dispersion of the irradiated flow, the mass-weighted velocity obtained can be scaled by the ratio L_{eff}/L_o, as a first approximation.

Table 5-I shows a comparison among the mass-weighted velocities obtained for the LOFT L3-7 blocks 24 and 26 data by these different methods, and for the actual and effective distances. The given uncertainties for the distance-to-time-peak ratio and for the time-weighted data reduction methods are based on the counting statistics, and for the mechanistic method on the reduced chi-square statistical criterion. On the other hand, the uncertainties for the finite difference method are based on an estimated reduced chi-square statistical criterion by similarity with the mechanistic model fit.

It can be observed in Table 5-I that differences as high as 14% are obtained in the mass-weighted velocity by these methods. The distance-to-time-peak ratio method is the simplest, but least accurate. Neither of the $1/t^2$ — nor $1/t$ — weighting methods is expected to give the correct result,[24] not only because of the flow regime for which each of these two methods applies, but because the axial dispersion effects at the tagging and detector positions are not

TABLE 5-I Mass-Weighted Velocities for L3-7 LOFT Tests Using Various Methods and the Real or the Effective Source-Detector Distance

$< V_{L_o} >_m \pm \delta < V_{L_o} >_m^*$ (cm/s)

Source-Detector Distance	LOFT L3-7 Test	Distance-to-Time Peak Ratio	$1/t^2$ Data Reduction Method	1/t Data Reduction Method	Mechanistic Method	Finite Difference Method
L_o=153.7 cm	Block 24	35.0±3.5	39.8±1.2	38.1±0.6	36.5±0.8	34.5±0.7
	Block 26	38.0±3.8	40.2±1.1	38.1±0.6	37.0±0.4	35.0±0.7
L_o=137.0 cm	Block 24	31.0±3.1	35.5±1.1	34.0±0.5	32.5±0.7	30.8±0.6
	Block 26	34.0±3.4	35.8±1.0	34.0±0.5	33.0±0.4	31.2±0.6

*Count Statistics Only

included (as discussed in Section 4.2.3.2). These axial dispersion effects are considered in the mechanistic and finite difference methods, but the latter gives the best representation of the dispersion phenomena since it is based on basic, not empirical, principles.

On the other hand, as pointed out in Section 2.1.3, the precision on the source-detector distance contributes to the accuracy of the mass-weighted velocity. For the LOFT PNA case, the uncertainty introduced by the use of either the actual or effective distance is unknown, since it is difficult to estimate accurately the effect of the venturi contraction. This effect could be suitably modeled in the finite difference scheme to obtain an accurate mass-weighted velocity based on physical principles with specific geometrical considerations.

PART 6

DISCUSSION AND CONCLUSIONS

It is convenient to divide the discussion of the results into two parts, the RPI PNA experimental measurements and the LOFT PNA analysis and interpretation.

6.1 RPI PNA Measurements

The ^{16}N tagging technique provided accurate mass-weighted velocities of single- and two-phase flows, for a vertical 1-in diameter pipe.

The turbulent single-phase data in Figure 3-5 were fitted by the dispersion theory of G. I. Taylor[40] which assumes that the flowing liquid is uniformly activated during the irradiation time. This theory does reasonably well in predicting the overall mass flow rate profile of tagged water. The small departures from this theory near the top of the leading edge and bottom of the trailing edge are interpreted in terms of some trace of laminar flow near the pipe walls (laminar boundary layer).

Five time profiles for ensembles of 20 to 25 pulses in the full range from single-phase to annular flow regimes are shown in Figure 3-8. The superficial water and air velocities, mass-weighted velocities, void fractions and uncertainties obtained by the transit-time method are summarized in Table 3-I. It is observed in Table 3-I that the $\simeq$ 1% total uncertainty in these measurements was mainly due to the uncertainty in the source-detector distance.

A simple mixing model was developed to analyze the fine structure observed in the slug-flow data (Figure 3-9). This model assumes perfect mixing within the liquid slug for a steady-state, fully developed, adiabatic air/water slug-flow. It is shown in Section 2.4 that the normalized ^{16}N concentrations in successive slugs follow a Poisson distribution. Slug-flow data fitted with this model are shown in Figure 3-11. The discrepancy between the experimental slug-to-slug-exchange rate of $\tau=0.4\ s^{-1}$ and the theoretical value[53] of $\tau=1.8\ s^{-1}$, suggests improvements of this mixing model through the use of more realistic assumptions.

Experimental evidence for the disappearance of the laminar boundary layer near the pipe wall for a two-phase condition having a very small air flow is presented in Figure 3-12. It is observed that the "champagne" flow data fit the Taylor turbulent single-phase theory[40] quite well; whereas, the single-phase data has a much longer tail. Apparently, the small air bubbles present in the two-phase mixture disrupt the laminar sublayer near the pipe wall and lead to more uniform mixing.

It is concluded that the powerful RPI LINAC neutron source was capable of providing not only very accurate mass-weighted velocities but also basic parameter data such as slug-to-slug exchange rates, for single- and two-phase flow regimes.

6.2 LOFT PNA Analysis and Interpretation

Analytical techniques were developed to analyze PNA measurements at LOFT. Due to the axymmetry effects at the tagging and detector position encountered with large diameter pipes[27], Monte Carlo neutron and gamma transport calculations were done for 14-in schedule 160 pipes. Two conditions were evaluated: single phase water flow at 1000 psia, 500°F, and a saturated two-phase stratified flow (1/2 liquid-1/2 vapor) at 1200 psia. The Monte Carlo program ANDYRPI[34] and the cross-section data set CASK[36] were used in these simulations. The non-uniform ^{16}N tagging and response of the detector were evaluated with the geometrical arrangements shown in Figures 4-3 and 4-6, respectively.

The axial profiles of the normalized ^{16}N specific activities for the different fluid regions obtained from Monte Carlo evaluations at the tagging position are shown in Figures 4-4 and 4-5 for the single-phase flow and in Figures 4-11 through 4-17 for the 1/2-stratified flow. These figures clearly show differences in the induced activity when these flows are tagged by one, two and four neutron sources. From the Monte Carlo calculations at the detector position, the axial profiles for the activated single-phase flow regions are shown in Figures 4-7 and 4-8, and for the activated 1/2-stratified flow regions, in Figures 4-18 through 4-26. From these evaluations, it is concluded that more uniform tagging and detector efficiency are achieved by the by the use of multiple neutron sources and NaI detectors.

The flow structure effects on the interpretation of PNA measurements was evaluated. As discussed in Section 2.1.1, the mass-weighted velocity of the activated flow strongly depends on the effective velocities of the irradiated masses as they pass in front of the detector. The mass-weighted velocity was obtained from the measured time profile by the $1/t^2$ data reduction method (Equation (2.7)) for flows where radial mixing is minimal, and by the $1/t$ data reduction method (Equation (2.8)) for flows with strong radial mixing. For PNA single-phase measurements at LOFT, the error introduced by using the incorrect time-weighted data reduction method can be as high as $\simeq$70% for laminar flows and $\simeq$ 11% for turbulent flows. Even if the single-phase flow regime at LOFT was known a priori, the correct answer would still not be obtained from these time-weighted methods, since the flows measured were not fully developed. As discussed in Section 4.2.3.2, an uncertainty of $\simeq$ 4% can be expected due to the axial induced activity and detector efficiency effects.

A mechanistic and a finite difference models were developed in order to interpret the LOFT L3-7 small break transient single-phase PNA measurements. Experimental PNA data for blocks 24 and 26 are shown in Figures 5-1 and 5-2. As discussed in Section 5.2.3, these measurements can be fitted with the mechanistic method which includes axial dispersion of the induced ^{16}N activity, axial response of the detector and a turbulent single-phase theory due to Taylor[40], which has an empirical dispersion coefficient. The L3-7 test PNA data fitted with this mechanistic model are shown in Figures 5-4 and 5-5. As described in Section 5.2.4, the L3-7 PNA data was also analyzed with a finite difference method which includes axial and radial dispersion of the induced ^{16}N activity, axial and radial response of the detector and a physical dispersion transport. The L3-7 PNA data analyzed with this finite difference model are shown in Figures 5-6 and 5-7. The agreement is seen to be good.

Table 5-I shows a comparison among the mass-weighted velocities obtained for the LOFT L3-7 blocks 24 and 26 data by different methods, and for the actual and effective[59] source-detector distances. It is observed in Table 5-I that differences as high as 14% are obtained in the mass-weighted velocity by these methods. The distance-to-time-peak ratio method is the least accurate. Neither of the time-weighting methods is expected to give the correct result. The axial dispersion effects at the tagging and detector positions are included in the mechanistic and finite difference methods, but the latter gives the best representation of the dispersion phenomena since it is based on physical, not empirical, principles.

It is concluded that a finite difference method should be used to interpret accurately single-phase LOFT PNA measurements. This suggested technique can be based on the finite difference method developed herein.

PART 7

LITERATURE CITED

1. C. M. Allen and E. A. Taylor, "The Salt Velocity Method of Water Measurements", Trans. Am. Soc. Mech. Engrs., 45, 285 (1923).

2. R. P. Gardner and R. L. Ely, Jr., Radioisotope Measurements Applications in Engineering, Reinhold Publishing Corporation, New York (1967).

3. C. G. Clayton, R. Spackman and A. M. Ball, "The Accuracy and Presision of Liquid Flow Measurement by Radioactive Isotopes", Proc. Symp. Radioisotope Traces in Industry and Geophysics, I.A.E.A., Prague (1966).

4. K. Ljunggren, "Review of the Use of Radioactive Traces for Evaluating Parameters Pertaining to the Flow of Material in Plant and Natural Systems", Proc. Symp. Radioisotope Tracers in Industry and Geophysics, I.A.E.A., Prague (1966).

5. R. B. Dowdell, Ed., Flow, Its Measurements and Control in Science and Industry, Flow Measuring Devices, 1, Part 2, Instrument Society of America (1974).

6. O. Levenspiel and K. B. Bischoff, "Patterns of Flow in Chemical Process Vessels", Adv. in Chem. Eng., v. 4, p 95, Academic Press Inc., New York (1963).

7. C. R. Boswell and T. B. Pierce, "Flowrate Determination by Neutron Activation Analysis", Modern Development in Flow Measurements, PPL Conf. Publ.10, 264 (1971).

8. C. C. Price, T. I. Sackett, R. N. Curran and C. L. Livengood, "Flow Measurements in the EBR-II Secondary System Using the Pulsed-Neutron Technique", ANL-RDP 48 (1976).

9. C. C. Price, P. Kehler and J. I. Sackett, "Fluid Flow Measurements at EBR-II Using Pulsed Neutron Activation", Trans. Am. Nucl. Soc., 23, 117 (1976).

10. P. Kehler, "Feasibility of Calibration of Liquid Sodium Flowmeters by Neutron Activation Techniques", ANL-CT-76-17 (1976).

11. P. Kehler, C. C. Price, G. A. Forster, J. I. Sackett and R. N. Curran, "Measurement of Liquid Sodium Flow in the Secondary System of the EBR-II by a Pulsed Neutron Activation Technique", ANL-CT-77-25 (1977).

12. C. C. Price, T. I. Sackett, P. Kehler, R. N. Curran, G. A. Forster and C. L. Livengood, "Application of the Pulsed-Neutron-Activation Technique for Flow Measurements at EBR-II", ANL-77-52 (1977).

13. G. A. Forster and P. Kehler, "Sodium Flow Calibration Using a Pulsed Neutron Activation Technique on a 400 mm (16 inch) pipe at LMEC", ANL-CT-78-9 (1977).

14. P. Kehler, "Two-Phase Flow Measurement by Pulsed Neutron Activation Techniques", ANL-NUREG-CT-78-17 (1978).

15. P. Kehler, "Two-Phase Flow Measurement by Pulsed Neutron Activation Techniques", ASME Publication H00121, Measurements in Polyphase Flows (1978).

16. P. Kehler, "Pulsed Neutron Measurement of Single- and Two-Phase Liquid Flow", IEEE Trans. on Nuclear Science, Vol. NS-26, No. 1, 1627 (1979).

17. P. Kehler, "Pulsed Neutron Activation Techniques for the Measurment of Two-Phase Flow", Proc. of the USNRC Review Group Conference on Advanced Instrumentation for Reactor Safety Research, NUREG/CP-0007 (1979).

18. P. Kehler, "Accuracy of Two-Phase Flow Measurement by Pulsed Neutron Activation Techniques", Multiphase Trans. Fund., Reactor Safety Application, 5, 2483, Hemisphere Publishing Corporation, Washington, D. C. (1980).

19. P. Kehler, "Measurement of Slow Flow Velocities by the Pulsed Neutron Activation Technique", Proc. of the USNRC Review Group Conference on Advanced Instrumentation for Reactor Safety Research, NUREG/CP-0015 (1980).

20. R. C. Block, M. L. Perez-Griffo, U. N. Singh and R. T. Lahey, Jr., "^{16}N Tagging of Water for Transient Flow Measurements", Trans. Am. Nucl. Soc., 27, 682 (1977).

21. M. L. Perez-Griffo, R. C. Block and R. T. Lahey, Jr., "^{16}N Tagging for Two-Phase Mass Flow Measurements", Trans. Am. Nucl. Soc., 30, 500 (1978).

22. M. L. Perez-Griffo, R. C. Block and R. T. Lahey, Jr., "Determination of Mass Exchange Rates in ^{16}N-Tagged Slug Flow", Trans. Am. Nucl. Soc., 32, 984 (1979).

23. M. L. Perez-Griffo, R. C. Block and R. T. Lahey, Jr., "Basic Two-Phase Flow Measurements Using ^{16}N Tagging Techniques", Proc. of the ANS/ASME/NRC International Topical Meeting on Nuclear Reactor Thermal-Hydraulics, NUREG-CP-0014, 2, 923 (1980).

24. M. L. Perez-Griffo, R. C. Block and R. T. Lahey, Jr., "Non-Uniform Tagging and Flow Structure Effects in PNA Measurements", Trans. Am. Nucl. Soc., 35, 637 (1980).

25. R. T. Lahey, Jr., and F. J. Moody, The Thermal-Hydraulics of a Boiling Water Nuclear Reactor, American Nuclear Society (1977).

26. Y. Beers, Introduction to the Theory of Error, Addison Wesley Publishing Company, New York (1957).

27. G. Santee, Jr., C. Price and A. Wilson, "Asymmetry Effects in Fluid Flow Measurements Using Pulsed Neutron Activation", Trans. Am. Nucl. Soc. 27, 216 (1977).

28. L. L. Carter and E. D. Cashwell, Particle-Transport Simulation with the Monte Carlo Method, TID-26607, USERDA Technical Information Center, Oak Ridge, Tennessee (1975).

29. G. Spanier and E. M. Gelbard, Monte Carlo Principles and Neutron Transport Problems, Addison-Wesley Publishing Company (1969).

30. Y. A. Schreider, Ed., The Monte Carlo Method, Pergamon Press, Inc., New York (1966).

31. Y. M. Hammersley and D. C. Handscomb, Monte Carlo Methods, John Wiley and Sons, Inc., New York (1964).

32. E. D. Cashwell and C. J. Everett, A Practical Manual on the Monte Carlo Method for Random Walk Problems, Pergamon Press, Inc., New York (1959).

33. E. M. Gelbard, L. A. Ondis II and J. Spanier, "A New Class of Monte Carlo Estimators", J. SIAM Appl. Math. 14, No. 4, 697 (1966).

34. D. B. MacMillian, "Comparison of Statistical Estimators for Neutron Monte Carlo Calculations", Nuc. Sci. Eng., 26, 366 (1966).

35. D. R. Harris, "ANDYMG3, the Basic Program of a Series of Monte Carlo Programs for Time-Dependent Transport of Particles and Photons", LA-4539 (1970).

36. CASK: 40 Group Coupled Neutron and Gamma-Ray Cross-Section Data, RSIC Data Library Collection, ORNL, Oak Ridge, Tennessee (1974).

37. J. O. Hinze, Turbulence, McGraw-Hill Book Company, Inc., New York (1959).

38. V. I. Maron, "Longitudinal Diffusion in a Flow Through a Tube", J. Multiphase Flow, 4, 339 (1978).

39. G. I. Taylor, "Dispersion of Soluble Matter in Solvent Flowing Slowly Through a Tube", Proc. Roy. Soc. London, Ser. A 219, 186 (1953).

40. G. I. Taylor, "The Dispersion of Matter in Turbulent Flow Through a Pipe", Proc. Roy. Soc. London, Ser. A 233, 446 (1954).

41. R. Aris, "On the Dispression of a Solute in a Fluid Flowing Through a Tube", Proc. Roy. Soc. London, Ser. a 235, 67 (1969).

42. R. J. Nunge and W. N. Gill, "Mechanisms Affecting Dispersion and Miscible Displacement", I and EC, 61, No. 9, 33 (1969).

43. W. N. Gill, "A Note on the Solution of Transient Dispersion Problems", Proc. Roy. Soc. London, Ser. A 298, 335 (1966).

44. W. N. Gill, "Analysis of Axial Dispersion with Time Variable Flow", Engineering Science, Vol. 22, 1013 (1967).

45. W. N. Gill and R. Sankarasubramanian, "Exact Analysis of Unsteady Convective Diffusion", Proc. Roy. Soc. London, Ser. A 316, 341 (1970).

46. W. N. Gill and R. Sankarasubramanian, "Dispersion of a Non-Uniform Slug in Time-Dependent Flow", Proc. Roy. Soc. London, Ser. A 322, 101 (1971).

47. G. Y. Lee and W. N. Gill, "Dispersion in Turbulent Film Flow", Chem. Eng. Commun., Vol. 4, 607 (1980).

48. H. Schlichting, Boundary Layer Theory, McGraw-Hill Book Company, New York (1968).

49. W. M. Kays, Convective Heat and Mass Transfer, McGraw-Hill Book Company, New York (1966).

50. J. Flaherty, Private Communication (1981).

51. N. N. Kaushal, E. J. Winhold, R. H. Augustson, P. F. Yergin and H. A. Medicus, "Absolute Neutron Yields and Energy Spectra from 18 Targets Bombarded by 55 and 85 MeV Bremsstrahlung", J. of Nuclear Energy, 25, 91 (1971).

52. P. Griffith and G. B. Wallis, "Two-Phase Slug Flow", J. of Heat Transfer, Trans. ASME, Series C, 83, 307 (1961).

53. R. R. Davis and G. I. Taylor, "The Mechanics of Large Bubbles Rising Through Extended Liquids in Tubes", Proc. Roy. Soc., London, Ser. A 200, 375 (1950).

54. H. C. Robinson, "LOFT System and Test Description Loss-of-Coolant Experiments Using a Core Simulator", LOFT Technical Report 20-57, USERDA (1976).

55. G. E. Rochau, "A Pulsed Neutron Generator for Use with Pulsed Neutron Activation Techniques", Sandia Laboratories, New Mexico (1979).

56. M. L. Perez-Griffo, R. C. Block and R. T. Lahey, Jr., "A Mechanistic Analysis of LOFT Pulsed Neutron Activation Data", to be presented at the ANS meeting, Miami Beach, Florida, June 1981.

57. P. R. Bevington, Data Reduction and Error Analysis for the Physical Sciences, McGraw-Hill Book Company, New York (1969).

58. H. Cramer, Mathematical Methods of Statistics, Princeton University Press (1958).

59. G. Lassahn, Private Communication (1980).

60. G. M. Govier and K. Aziz, The Flow of Complex Mixtures in Pipes, Van Nostrand Reinhold Company, New York (1972).

61. D. A. Drew and R. T. Lahey, Jr., "A Mixing Length Model for Fully-Developed Turbulent Two-Phase Flow", Trans. Am. Nucl. Soc., 35, 627 (1980).

APPENDIX A

DENSITY BY TOTAL ACTIVITY METHOD

Consider the PNA tagging of a thin slice, Δx, of fluid with a total activated mass M_A, represented in Figure 2.2. M_A is given by,

$$M_A = \langle \rho \rangle A_{x-s} \Delta x \tag{A-1}$$

where $\langle \rho \rangle$ is the total activated mass density over the cross section A_{x-s} at the tagging position. At a distance L_o, dm_A is the activated mass which flows by L_o. Thus the total activated mass M_A passing by L_o, corrected for radioactive decay, is,

$$M_A = \int dm_A \, e^{\lambda t} \tag{A-2}$$

where λ is the decay constant. From continuity at L_o, $dm_A = \rho_A A_{x-s} \langle V_A \rangle dt$ (Equation (2.2)) where ρ_A is the activated mass density passing by L_o and $\langle V_A \rangle$ is the cross-sectional-averaged velocity of the activated mass dm_A at the position L_o. Substituting Equation (2.2) into (A-2) and equating it to (A-1),

$$\langle \rho \rangle A_{x-s} \Delta x = \int P_A A_{x-s} \langle V_A \rangle e^{\lambda t} \, dt \tag{A-3}$$

The counting rate $\frac{dC}{dt}$ is proportional to the activated mass density ρ_A. Thus substituting Equation (2.4) into (A-3),

$$\langle \rho \rangle = \frac{1}{k\Delta x} \int \left(\frac{dC}{dt}\right) \langle V_A \rangle e^{\lambda t} \, dt \tag{A-4}$$

Since events are counted over time channels, one can express (A-4) as,

$$\langle \rho \rangle = \frac{1}{K} \sum_i e^{\lambda t_i} C_i \langle V_A \rangle \tag{A-5}$$

where $K = k \Delta x$ is a proportionality constant which can be obtained with a liquid filled pipe measurement ($\langle \rho \rangle = \rho_\ell$).

Equation (A-5) is the general expression for the total activated mass density. Hence, the total activated mass density strongly depends on the cross-sectional-averaged velocity $\langle V_A \rangle$ of the activated mass at the detector location.

Consider the two fully developed flow cases for $\langle V_A \rangle$:

CASE I: The velocity at the detector is equal to the average velocity over the distance L_o : $\langle V_A \rangle = \frac{L_o}{t}$ (i.e.: the particle follows a streamline). For this condition Equation (A-5) becomes,

$$\langle \rho \rangle = \frac{L_o}{K} \sum_i e^{\lambda t_i} C_i / t_i \tag{A-6}$$

CASE II: The velocity at the detector position is equal to the average fluid velocity, $\langle V_A \rangle = \bar{u}$ (i.e.: we assume it is uniformly mixed). For this condition Equation (A-5) becomes,

$$\langle \rho \rangle = \frac{1}{K} \sum_i e^{\lambda t_i} C_i \bar{u} \tag{A-7}$$

It is concluded that the evaluation of the total activated mass density is also dependent on the effective velocities of the irradiated masses as they pass in front of the detector. The expression for the total activated mass density for CASE I, given by Equation (A-6) is the one suggested by Kehler[14]. On the other hand, for CASE II it is necessary to measure $\bar{u}$ independently in order to obtain $\langle \rho \rangle$ from a PNA measurement.

APPENDIX B

SOLUTIONS OF THE ^{16}N CONCENTRATION BALANCE EQUATION FOR SLUG FLOW

The ^{16}N concentration balance equation in control volume "i" is,

$$\frac{d\,C_i}{dt} + \tau\,C_i = \tau\,C_{i-1}\ . \tag{2.52}$$

This equation is a Bernoulli equation which can be solved using an integrating factor given by exp $[\tau t]$, yielding,

$$\frac{d}{dt}\,[C_i\;e^{\tau t}] = e^{\tau t}\;\;\tau C_{i-1}$$

which after integration becomes

$$C_i(t) = \tau \int_0^t e^{\tau(t'-t)}\;C_{i-1}\;(t')\;dt' + A_i\;e^{-\tau t}\;,\;\;\text{for } i=1,2... \tag{2.53}$$

The general solution of Equation (2.53) with the initial conditions (2.54a) and (2.54b), can be found by recurrence in the following way:

For i = 1: $C_1(t) = A_1\;e^{-\tau t}$

Applying the inital condition,,Equation (2.54a), it is found that $A_1 = C_o$; thus,

$C_1(t) = C_o\;e^{-\tau t}$

For i=2: $C_2(t) = \tau \int_0^t e^{\tau(t'-t)}\;C_1\;(t')\;dt' + A_2\;e^{-\tau t}$

$$C_2(t) = \tau \int_0^t e^{\tau(t'-t)}\;C_o\;e^{-\tau t'}\;dt' + A_2\;e^{-\tau t}$$

$$C_2(t) = C_o\;\tau t\;e^{-\tau t} + A_2\;e^{-\tau t}\quad .$$

Applying the initial condition, Equation (2.54b), $A_2 = 0$; thus,

$C_2(t) = C_o \tau t e^{-\tau t}$.

Similarly, for i=3: $C_3(t) = \tau \int_o^t e^{\tau(t'-t)} C_2(t)\, dt' + A_3\, e^{-\tau t}$

thus,

$$C_3(t) = \tau \int_o^t e^{\tau(t'-t)} C_o\, \tau t' e^{-\tau t}\, dt' + A_3\, e^{-\tau t}$$

or,

$$C_3(t) = C_o\, \tau^2\, \frac{t^2}{2} e^{-\tau t} + A_3\, e^{-\tau t} \quad .$$

Applying the initial condition, Equation (2.54b) $A_3 = 0$; thus,

$$C_3(t) = C_o\, \tau^2 \frac{t^2}{2}\, e^{-\tau t}$$

By recurrence, for the general case "i",

$$C_i(t) = C_o\, \tau^{i-1} \frac{t^{i-1}}{(i-1)!}\, e^{-\tau t} = C_o \frac{(\tau t)^{i-1}}{(i-1)!} e^{-\tau t} \quad . \tag{2.55}$$

APPENDIX C

ANDYRPI MONTE CARLO PROGRAM

The following pages contain a flow diagram and a listing of the Monte Carlo program ANDYRPI.[35] This program with the cross-section data set CASK[36] was used for neutron and gamma transport calculations at the tagging and detector positions at LOFT.

There is also included:

- The subroutine SOURCE used for ^{16}N tagging
- The program STATISTICS which gets the statistical mean and variance from the ANDYRPI's results, and converts them into ^{16}N specific activities
- Sample input for ^{16}N tagging of single-phase flow
- Sample output from the coupling of ANDYRPI and STATISTICS for the ^{16}N tagging of single-phase flow

Diagram for ANDYRPI

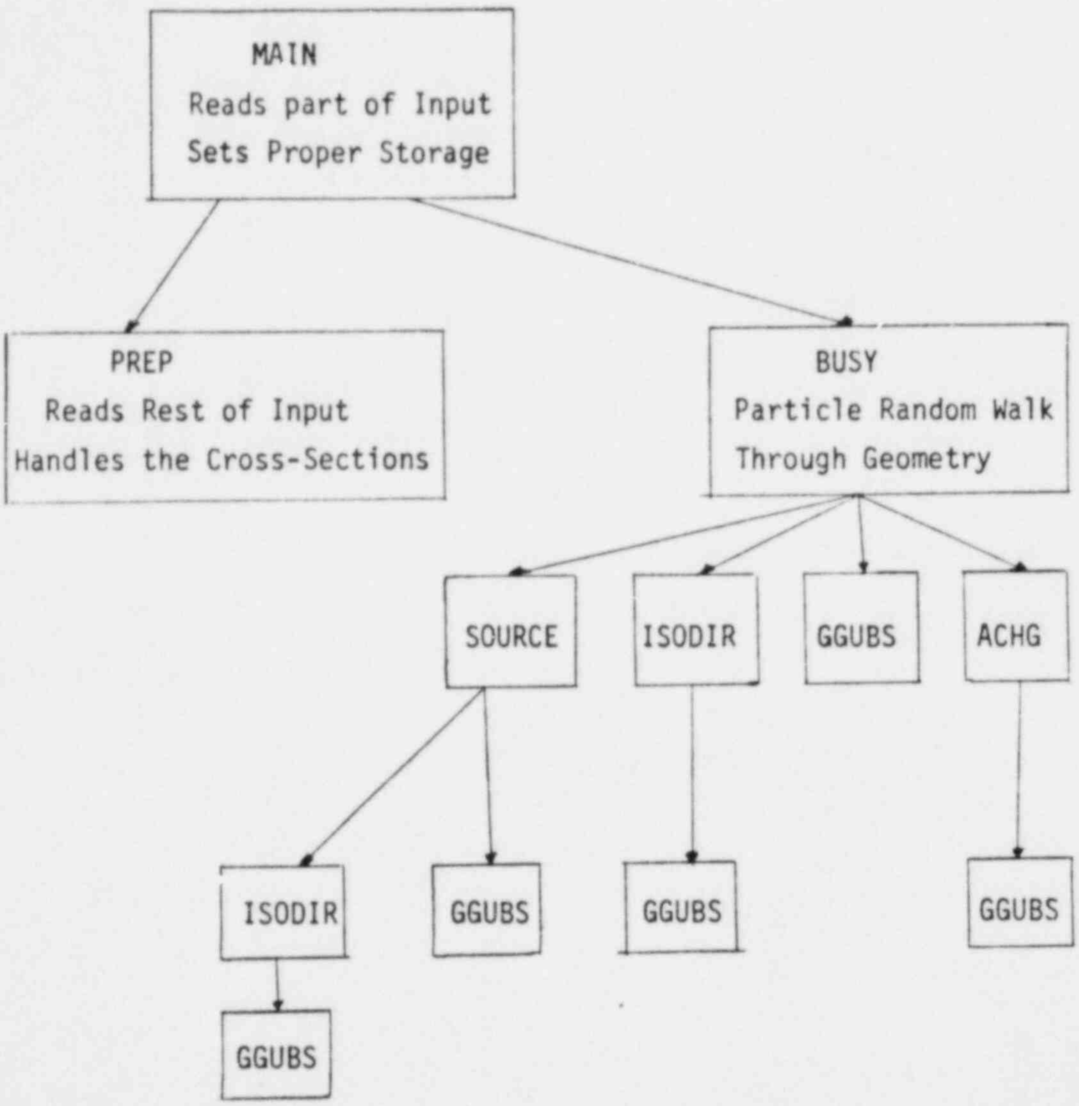

SOURCE: Specifies the source.

ISODIR: Chooses isotropic directions.

GGUBS: Chooses the random number.

ACHG : Changes the direction of the particle after a collision.

Flow Chart of ANDYRPI Geometry Treatment[35]

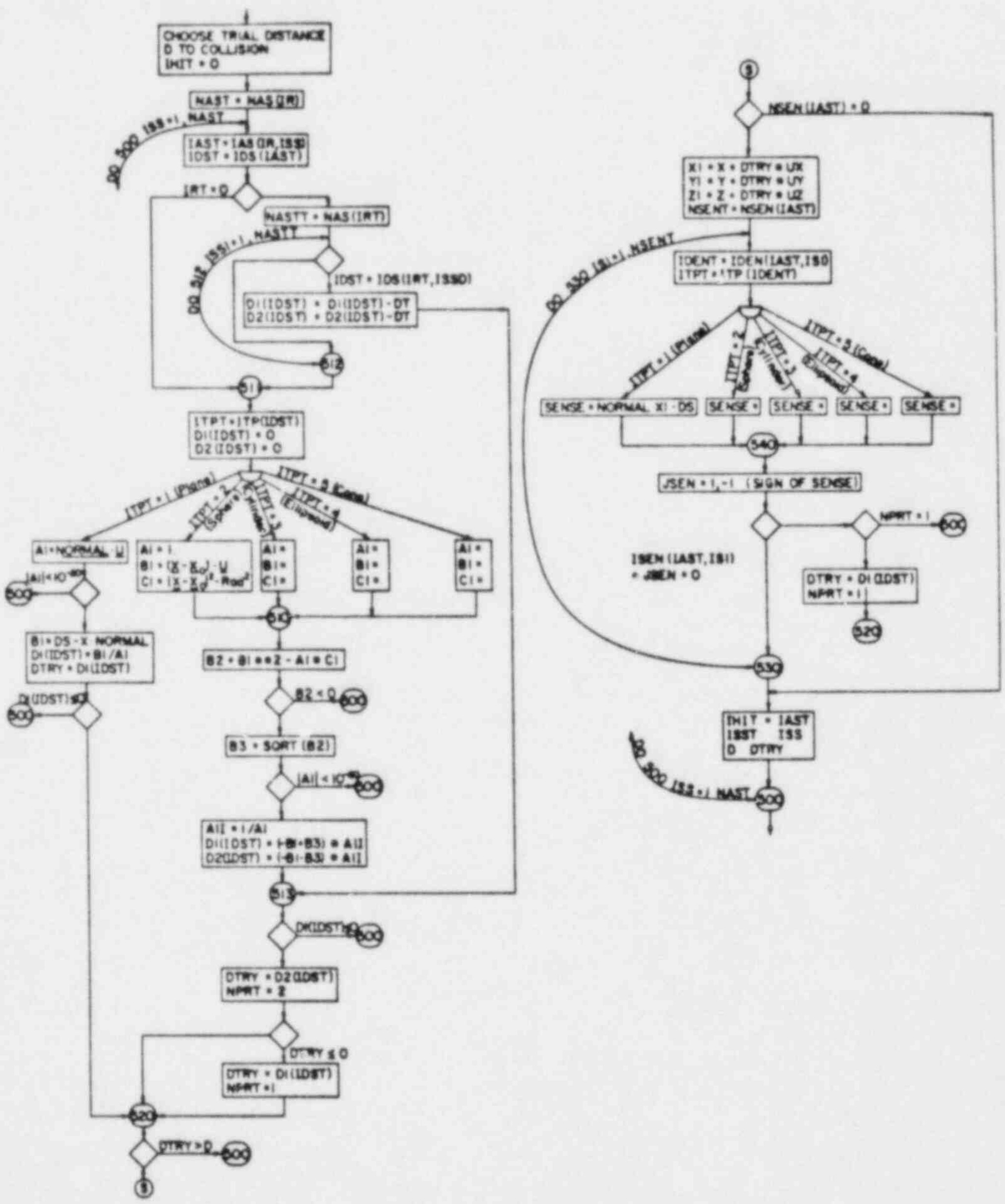

```
C
C
C      THE ANDYRPI PROGRAM (IN FORTRAN IV) COMPUTES THE TIME-SPACE-DIRECTION-
C      ENERGY GROUP DEPENDENCE OF PARTICLE REACTION RATES AND CURRENTS IN
C      GENERAL GEOMETRY
C      SOURCE-SPECIFIED AND CRITICALITY NEUTRON TRANSPORT PROBLEMS
C      CAN BE DONE.
C
C
C VARIABLES
C      AS(IS),BS(IS),.....=PARAMETERS DEFINING SURFACE WITH ID NUMBER IS
C      AKBAR=CRITERIA FOR FISSION SITE SELECTION
C      AEIGEN=AVERAGE KEFF OF ALL GENERATIONS EXCEPT FIRST ISKIP
C      C=PROBABILITY THAT SCATTERED PARTICLE IS EMITTED WITH SCATTERING ANGLE
C           WHOSE COSINE IS COSCAT
C      CHIP(IG)=PROMPT NON-SCATTER PARTICLE YIELD FRACTION PER COLLISION INTO
C           ENERGY GROUPS 1 THROUGH IG
C      CHID(ITPDEL,IG)=TYPE ITPDEL DELAYED PARTICLE YIELD FRACTION PER DECAY
C           INTO ENERGY GROUPS 1 THROUGH IG
C      CL(IP,IG)=MICROSCOPIC CROSS SECTION IN POSITION IP FOR ENERGY GROUP IG AS
C           READ FROM THE LIBRARY
C      CM(IP,IG,IM)=MACROSCOPIC CROSS SECTION OF TYPE IP IN ENERGY GROUP IG IN
C           MIX IM. THEN THESE QUANTITIES ARE PROCESSED TO THE FOLLOWING
C      CM(1,IG,IM)=NUMBER OF PROMPT SECONDARIES PER COLLISION FROM FISSION+SCAT
C      CM(2,IG,IM)=PROBABILITY SECONDARY PARTICLE IS FROM FISSION
C      CM(3,IG,IM)=TRANSPORT MEAN FREE PATH
C      CM (IP,IG,IM),IP=4,NG =PROBABILITY OF SCATTERING FROM ENERGY GROUP IG
C           INTO ENERGY GROUPS IGMIN(IG) THROUGH IP
C      CM1(IP,IG,IM)=MACROSCOPIC P1 COMPONENT FOR SCATTERING IN MIX IM FROM
C           GROUP IG TO GROUP IN POSITION IP
C      CM2(IP,IG,IM)=MACROSCOPIC P2 COMPONENT FOR SCATTERING IN MIX IM FROM
C           GROUP IG TO GROUP IN POSITION IP
C      CM3(IP,IG,IM)=MACROSCOPIC P3 COMPONENT FOR SCATTERING IN MIX IM FROM
C           GROUP IG TO GROUP IN POSITION IP
C      THEN THE CM1, CM2, AND CM3 COMPONENTS ARE CHANGED TO COEFFICIENTS OF
C           POWERS OF COSCAT
C      COSCAT=COSINE OF SCATTERING ANGLE IN LAB COORDINATE SYSTEM
C      CSUM(ISUM,IG)=MACROSCOPIN CROSS SECTION TO BE USED IN GROUPIG FOR SUM ISU
C      D=PARTICLE FLIGHT PATH LENGTH TO SURFACE OR TO COLLISION POINT
C      D1(IAST)=MORE POSITIVE DISTANCE TO SURFACE SEGMENT WITH ID NUMBER IAST
C      D2(IAST)=LESS POSITIVE DISTANCE TO SURFACE SEGMENT WITH ID NUMBER IAST
C      DELPC(ITPDEL,IG,IM)=NUMBER OF DELAYED SECONDARY PARTICLES OF TYPE ITPDEL
C           EMITTED IN ENERGY GROUP IG PER COLLISION IN MIX IM
C      DELT1=WIDTH OF TIME BOX IT (2.LE.IT.LE.ITB1). DELT1I IS INVERSE
C      DELT2=WIDTH OF TIME BOX IT (IT.GT.ITB1.AND.IT.LE.NT). DELT2I IS INVERSE
C      DENS(I,IM)=NUCLEAR OR MOLECULAR DENSITY OF MATERIAL WITH ORDER NUMBER
C           I IN MIX IM
C      DENSM(I,ISUM)=DENSITY OF I-TH DECK TO BE USED IN SUM ISUM
C      DTRY=PARTICLE FLIGHT PATH LENGTH TO CURRENT SURFACE
C      EIGEN=PRESENT GENERATION EIGENVALUE(KEFF)
C      FRN=REAL NUMBER IN (0.,1.) FORMED BY PSEUDORANDOM NUMBER GENERATOR
C      IAR(IR,ISS)=ID NUMBER OF REGION ON OTHER SIDE OF ISS-TH SURFACE SEGMENT
C           FROM REGION IR. IAR(IR,ISS) EXCEEDS NREG IF ISS IS ON SYSTEM BOUNDAR
C      IAS(IR,ISS)=ID NUMBER OF ISS-TH SURFACE SEGMENT ADJACENT TO REGION WITH I
C           NUMBER IR. (IR=1,NREG),(ISS=1,NAS(IR)).
C      IDEN(ISS,IS1)=ID NUMBER OF THE IS1-TH SURFACE BOUNDING SURFACE SEGMENT IS
C      IDS(ISS)=ID NUMBER OF SURFACE CONTAINING SURFACE SEGMENT WITH ID ISS
C      IFIST=TOTAL NUMBER OF FISSION SITES SELECTED
C      IGMAX(IG)=HIGHESTNUMBERED ENERGY GROUP FROM SCATTERING IN ENERGY GROUP IG
C      IGMIN(IG)=LOWEST NUMBERED ENERGY GROUP FROM SCATTERING IN ENERGY GROUP IG
```

```
C       IGSPL(ISPL)=ENERGY GROUP OF ISPL'TH BANKED PARTICLE
C       IHIT=ID NUMBER OF SURFACE SEGMENT HIT BY PARTICLE AND IS ZERO OTHERWISE
C       IMAT(I,IM)=ID NUMBER OF MATERIAL WITH ORDER NUMBER I IN MIX IM
C       IMIX(IR)=CROSS SECTION MIX NUMBER IN REGION IR
C       IRMULT= MULTIPLIER IN PSEUDORANDOM NUMBER GENERATOR
C       INDICES/IT FOR TIME BOX, IS FOR SURFACE, ISS FOR SURFACE SEGMENT,
C            IST FOR STARTER, IR FOR REGION, IG FOR ENERGY-TYPE GROUP, ITPDEL
C            FOR DELAYED PARTICLE TYPE, ISCAT FOR SCATTERING PATTERN COMPONENT,
C            IRT FOR THE REGION JUST LEFT,  IW FOR INTEGRAL TALLY, ISUM FOR SUM
C       IRMULT= MULTIPLIER IN PSEUDORANDOM NUMBER GENERATOR
C       IRORS(ISUM)=1 IF A REGION TALLY IS TO BE USED IN SUM, 0 IF A SURFACE SEG-
C       IRORS(ISUM)=1 IF A REGION TALLY IS TO BE USED IN SUM, 0 IF A SURFACE SEG-
C            MENT TALLY IS TO BE USED IN SUM
C       IRSPL(ISPL)=REGION OF ISPL'TH BANKED PARTICLE
C       ISEN(ISS,IS1)=SENSE OF IS1-TH SURFACE BOUNDING SURFACE SEGMENT ISS
C       ISKIP=NO. OF GENERATIONS SKIPPED IN CRITICALITY CALCULATION.
C       ISPL=NUMBER OF BANKED PARTICLE
C       ISPLC=CUMULATIVE NUMBER OF SECONDARY PARTICLES
C       ISUMTY(ISUM)=ORDER NUMBER OF INTEGRAL TALLY ITALY TO BE USED IN SUM
C       ISPLO=NUMBER OF SECONDARIES OVERFLOWING BANK
C       IST=STORAGE LOCATION OF PRESENT NEUTRON GENERATION PARTICLE
C       ISTR=STORAGE LOCATION OF NEXT NEUTRON GENERATION PARTICLE
C       ITB1=LAST TIME BOX OF WIDTH DELT1 (1.LE.ITB1.LE.NT.LE.100)
C       ITALR(I)=ID NUMBER OF I-TH REGION FOR WHICH WIR IS TO BE TALLIED
C       ITALSS(I)=ID NUMBER OF I-TH SURFACE SEGMENT FOR WHICH WISP AND WISN ARE
C            TO BE TALLIED
C       ITP(IS)=TYPE NUMBER OF SURFACE IS
C            WHETHER PLANE (1), SPHERE (2), CYLINDER (3), ELLIPSOID (4) , CONE (5
C       KMUL=0--SOURCE-SPECIFIED CALC., 1-CRITICALITY CALC.
C       KRN=INTEGER PSEUDORANDOM NUMBER
C       KTRA=1 TO GET DETAILED TRACKING PRINTS B,C,...
C       LENGA=DIMENSION OF STORAGE ARRAY A
C       LENGIA=DIMENSION OF STORAGE ARRAY IA
C       LIBRY=LIBRARY DESCRIPTION
C       LOCINA=NUMBER OF LOCATIONS REQUIRED TO SET UP ARRAYS TO BE STORED IN A
C       LOCINI =NUMBER OF LOCATIONS REQUIRED TO SET UP ARRAYS TO BE STORED IN IA
C       MARI= IF=0 PRINT X-S, COLLISION PARAMETERS...,=1 NO PRINT
C       MATLIB=NUMBER OF MATERIALS IN CROSS SECTION LIBRARY
C       MORE=NUMBER OF CASES IN THIS JOB
C       NAS(IR)=NUMBER OF SURFACE SEGMENTS ADJACENT TO (BOUNDING) REGION IR
C       NBANK=BANK DIMENSION
C       NCOL=NUMBER OF COLLISIONS IN THIS JOB
C       NDEL=NUMBER OF DELAYED PARTICLES FOLLOWED IN JOB
C       NG=NUMBER OF ENERGY GROUPS
C       NGMA= GROUP NUMBER OF IMPORTANCE. (I.E. GROUP 2 FOR N-16 TAG)
C       NING=POSITIONE OF IN-GROUP SCATTERING IN CROSS SECTION TABLE
C       NIT=NUMBER OF INTEGRAL TALLIES
C       NKRN=FACTOR (1,3,5,7,...) FOR STARTING PSEUDORANDOM NUMBER GENERATOR
C       NLIBS(ISCAT)=NUMBER OF MATERIALS IN LIBRARY WITH ANISOTROPIC SCATTERING
C            COMPONENT ISCAT=1,NLIBSC
C       NLIBSC =MAXIMUM NUMBER OF ANISOTROPIC SCATTERING COMPONENTS IN LIBRARY
C       NLIBSM=NUMBER OF DATA SETS IN SUMMING LIBRARY
C       NMAT(IM)=NUMBER OF MATERIALS IN CROSS SECTION MIX IM
C       NMATMA =MAXIMUM NUMBER OF MATERIALS PER CROSS SECTION MIX
C       NMIX=NUMBER OF CROSS SECTION MIXES
C       NP=NUMBER OF POSITIONS PER ENERGY GROUP IN CROSS SECTION TABLE
C       NREG=NUMBER OF REGIONS (1.LE.NREG.LE.20)
C       NS=NUMBER OF SOURCE PARTICLES
C       NSCAT=NUMBER OF ANISOTROPIC SCATTERING COMPONENTS TO BE USED IN PROBLEM
C       NSEG=NUMBER OF SURFACE SEGMENTS (1.LE.NSEG.LE.40)
```

```
C      NSEN(ISS)=NUMBER OF SURFACES BOUNDING SURFACE SEGMENT ISS
C      NSENMA =MAXIMUM NUMBER OF SENSE RELATIONS PER SURFACE SEGMENT
C      NSTAD= IF 1 WRITE WIR,WISN... IN FILE 8
C      NSUM=DESIRED NUMBER OF SUMS
C      NSUR=NUMBER OF SURFACES (1.LE.NSUR.LE.20)
C      NT=NUMBER OF TIME BOXES (1,.LE.ITB1.LE.NT.LE.100)
C      NTALR=NUMBER OF REGIONS FOR WHICH WIR IS TO BE TALLIED GE.1
C      NTALSS=NUMBER OF SURFACE SEGMENTS FOR WHICH WISP AND WISN ARE TALLIED GE.
C      NTPDEL=NUMBER OF TYPES OF DELAYED PARTICLES
C      OFFSET=UPPER LIMIT OF FIRST TIME BOX (0,LE.OFFSET.LT.DELT1).  IF
C           OFFSET=0., TIME BOX IT=1 WILL BE EMPTY, IE, FIRST NON-ZERO TALLY
C           WILL BE IN TIME BOX IT=2
C      ORR=OPTION FOR RUSSIAN ROULETTE, 1-YES, 0-NO
C      RIM(IR)=RELATIVE IMPORTANCE IN REGION IR
C      RMOD=PERIOD OF PSEUDORANDOM NUMBER GENERATOR
C      RNS=NUMBER OF SOURCE PARTICLES IN PROBLEM(RNS=NS*NB)
C      SUM(IT)=A SUM IN TIME BOX IT
C      SUMSCA =TEMPORARY SUM OF MACROSCOPIC OUTSCATERING FROM AN ENERGY GROUP
C      T=CUMULATIVE PARTICLE FLIGHT TIME=REAL TIME AGE OF PARTICLE AT EVENT TIME
C      TB(IT)=UPPER BOUND OF TIME BOX IT=1,2,...NT
C      TD(ITPDEL)=MEAN LIFE FOR DELAYED PARTICLES OF TYPE ITPDEL
C      TITLE=PROBLEM DESCRIPTION
C      TSPL(ISPL)=REAL TIME AGE OF ISPL'TH BANKED PARTICLE
C      TWFIS=TOTAL FISSION WEIGHT OF PRESENT GENERATION
C      TWFISS=TEMPORARY SECOND MOMENT TALLY FOR TWFIS
C      TWFISV=VARIANCE ESTIMATOR FOR TWFIS
C      UX,UY,UZ=DIRECTION COSINES OF PARTICLE
C      UXSPL(ISPL),UYSPL(ISPL),UZSPL(ISPL)=DIRECTION COSINES OF ISPL'TH
C           BANKED PARTICLE
C      V(IG)=PARTICLE SPEED IN ENERGY GROUP IG. INVERSE SPEED AFTER PRECOMPUTE
C      VEIGEN=VARIANCE ESTIMATOR OF AEIGEN
C      WCO=A PARTICLE HISTORY IS TERMINATED IF ITS WEIGHT DROPS BELOW WCO
C      WCOCF=VALUE WHICH IF EXCEEDED BY WCOC PERMITS A LOW WEIGHT (W.LT.WCO)
C           PARTICLE TO CONTINUE WITH WEIGHT WCOC
C      WDEL(ITPDEL)=CUMULATIVE WEIGHT OF DELAYED PARTICLES OF TYPE ITPDEL
C      WDELF=A DELAYED PARTICLE IS FOLLOWED IF WDEL EXCEEDS WDELF
C      WFIS=TEMPORARY FISSION WEIGHT ACCUMULATOR FOR FISSION SITE
C           SELECTION
C      WFIST=TOTAL FISSION WEIGHT OF STORED FISSION SITES
C      WIR(IT,ITALY,IG)=CUMULATIVE WEIGHT OF PARTICLES COLLIDING IN TIME BOX IT
C          IN ENERGY GROUP IG IN REGION ITALR(ITALY)
C      WIRS()=TEMPORARY SECOND MOMENT TALLY FOR WIR
C      WIRV()=VARIANCE ESTIMATOR FOR WIR
C      WIRL(IT,ITALY,IG)=CUMULATIVE (WEIGHT*FLIGTH LENGTH): TRACK-LENGTH ESTIMAT.
C          IN ENERGY GROUP IG IN REGION ITALR(ITALY) IN TIME T
C      WIRLS()=TEMPORARY SECOND MOMENT TALLY FOR WIRL
C      WIRLV()=VARIANCE ESTIMATOR FOR WIRL
C      WIR(IT,ITALY,IG)=CUMULATIVE WEIGHT OF PARTICLES COLLIDING IN TIME BOX IT
C          IN ENERGY GROUP IG IN REGION ITALR(ITALY)
C      WISN(IT,ITALY,IG)=CUMULATIVE WEIGHT OF PARTICLES CROSSING SURFACE
C           SEGMENT ITALSS(ITALY) IN TIME BOX IT IN ENERGY GROUP IG FROM REGION
C           WITH HIGHER ID NUMBER TO REGION WITH LOWER ID NUMBER
C      WISNS()-TEMPORARY SECOND MOMENT TALLY FOR WISN
C      WISNV()-VARIANCE ESTIMATOR FOR WISN
C      WISP(IT,ITALY,IG)=CUMULATIVE WEIGHT OF PARTICLES CROSSING SURFACE
C           SEGMENT ITALSS(ITALY) IN TIME BOX IT IN ENERGY GROUP IG FROM REGION
C           WITH LOWER ID NUMBER TO REGION WITH HIGHER ID NUMBER
C      WISPS()=TEMPORARY SECOND MOMENT TALLY FOR WISP
C      WISPV()=VARIANCE ESTIMATOR FOR WISP
C      WIT(IT,IW)=IW-TH INTEGRAL TALLY IN TIME BOX IT
```

```
C      WSPL(ISPL)=WEIGHT OF ISPL'TH BANKED PARTICLE
C      WSPLT=PARTICLE WEIGHT MINIMUM FOR SPLITTING
C      X,Y,Z,=RECTANGULAR COORDINATES OF PARTICLE
C      XSTR(ISTR),YSTR(ISTR),ZSTR(ISTR),...=TEMPORARIES FOR STORAGE
C      OF NEXT GENERATION PARTICLES FOR CRITICALITY CALC.
C      XST(IST),YST(IST),ZST(IST),...=STORAGE FOR PRESENT GENERATION
C      PARTICLES IN CRITICALITY CALC.
C      X(ISPL),Y(ISPL),Z(ISPL)=RECTANGULAR COORDINATES OF ISPL'TH BANKED PARTICL
C      XU,YU,XYU,R2U ARE TEMPORARIES IN DIRECTION FINDER
C      A1,B1,C1,...,ETC=TEMPORARIES IN GEOMETRY ROUTINE.  OTHER TEMPORARIES
C           ARE FORMED BY ADDING SUFFIX T
C
C TIME BOXES
C      AN EVENT AT TIME T IS TALLIED IN TIME BOX IT IF TB(IT-1).LE.T.LT.TB(I),
C      WHERE TB(IT) IS THE UPPER LIMIT OF TIME BOX IT.  TIME BOX IT=1 COVERS THE
C      INTERVAL (0.,OFFSET). TIME BOXES IT=2,ITB1 ARE OF WIDTH DELT1, AND TIME
C      BOXES IT=ITB1+1,NT ARE OF WIDTH DELT2
C
C SURFACE DESCRIPTIONS
C      PLANE (1), A VECTOR (AS,BS,CS) IS NORMAL TO PLANE AND IS DIRECTED GENER-
C      ALLY OUT FROM ORIGIN.  LEAST DISTANCE FROM ORIGIN TO PLANE IS
C      DS/SQRT(AS**2+BS**2+CS**2).
C      SPHERE (2), RADIUS DS CENTERED AT (AS,BS,CS)
C      CIRCULAR CYLINDER (3), RADIUS GS WITH AXIS PASSING THRU (AS,BS,CS) IN
C      DIRECTION (DS,ES,FS)
C      ELLIPSOID (4), CENTERED AT (AS,BS,CS) WITH AXES PARALLEL TO X,Y,Z COOR-
C      DINATE AXES AND WITH RADII DS,ES,FS, RESPECTIVELY.
C      CONE(5), APEX AT (AS,BS,CS) WITH AXIS PARALLEL TO (DS,ES,FS) AND OPENING
C           ANGLE 2.*GS WHERE GS IS IN UNITS OF RADIANS
C
C SENSE CONVENTIONS
C      A POINT IN SPACE HAS POSITIVE SENSE WITH RESPECT FO A PLANE IF THE SPACE
C           POINT IS ON THE SIDE OF THE PLANE TOWARD WHICH THE NORMAL (AS,BS,CS)
C           POINTS, WITH RESPECT TO A SPHERE, CYLINDER, OR ELLIPSOID IF THE SPAC
C           POINT IS OUTSIDE THE SURFACE, WITH RESPECT TO A CONE
C
C MULTIGROUP CROSS SECTION LIBRARY
C      NEGATIVE SCATTERING CROSS SECTIONS AND LEGENDRE COMPONENTS ARE OK
C
C COLLISION PROCESSES
C      WHEN A COLLISION OCCURS IT IS TALLIED IN WIR, DELAYED PARTICLE TALLIES AR
C      INCREMENTED,AND THE CONTINUING PARTICLE WEIGHT IS MULTIPLIED BY THE PROMP
C      SECONDARIES PER COLLISION YIELD CM(1,IG,IM).  THE CONTINUING PARTICLE
C      EMERGES PROMPTLY AND ISOTROPICALLY AND IS CHOSEN TO BE A FISSION PARTICLE
C      (WITH PROBABILITY CM(2,IG,IM)) OR A SCATTERED PARTICLE.  IF FROM FISSION
C      ITS ENERGY SPECTRUM IS CHOSEN FROM CHIP.  IF FROM SCATTERING THE
C      SECTION AS A FUNCTION OF SCATTERING ANGLE.  IF THIS FACTOR IS NEGATIVE TH
C      PARTICLE IS TERMINATED BY WCO AND WCOCF IS INCREMENTED NEGATIVELY.
C
C CRITICALITY CALCULATION
C
C      FISSION WEIGHT IS COLLECTED IN TWFIS AND WFIS. TWFIS IS THE
C      ACCUMULATED FISSION WEIGHT OF ALL COLLISIONS IN A HISTORY
C      AND ALL HISTORIES IN A GENERATION. WFIS IS USED FOR THE
C      SELECTION OF FISSION SITES. FISSION WEIGHT IS ACCUMULATED
C      IN WFIS AT EACH COLLISION UNTIL IT EXCEEDS A PRESCRIBED
C      AMOUNT OF FISSION WEIGHT-AKBAR-AT WHICH TIME A FISSION
C      SITE IS RECORDED. AKBAR IS SET TO THE RUNNING AVERAGE
C      OF KEFF. AFTER FISSION SITE IS RECORDED WFIS IS REDUCED
C      BY AKBAR AND HISTORY CONTINUES. IF AT THE END OF EACH
```

```
C     HISTORY ANY WFIS IS LEFT OVER, AN UNBAISED GAME IS PLAYED
C     TO SEE IF THE LAST COLLISION SIT SHOULD BE A FISSION SITE.
C
C STORAGE
      DOUBLE PRECISION NKRN
      COMMON IA(116000),A(29000)
C     SOME ARRAYS ARE IN LABELED COMMON TO REDUCE LENGTH OF CALLS
      COMMON/OTHER/TITLE(18),LIBRY(10),NLIBS(3)
     1,IGMIN(40),IGMAX(40),V(40),CHIP(40)
     2,IDS(425),NSEN(425)
     3,NAS(135),IMIX(135),RIM(135)
     4,WDEL( 1),TD( 1)
     5,ITALR(135),ITALSS(425),NMAT( 20)
     1,ITP(40),AS(40),BS(40),CS(40),DS(40),ES(40),FS(40),GS(40),HS(40)
     7,D1( 40),D2( 40),IDEC( 40)
     8,IRSPL( 50),IGSPL( 50),XSPL( 50),YSPL( 50),ZSPL( 50),UXSPL( 50)
     9,UYSPL( 50),UZSPL( 50),TSPL( 50),WSPL( 50)
     1,TB(  1),SUM(  1)
     2,IRORS(10),ISUMTY(10)
C     ARRAYS WITH DIMENSION NG
C     ARRAYS WITH DIMENSION NSEG
C     ARRAYS WITH DIMENSION NREG
C     ARRAYS WITH DIMENSION NTPDEL
C     ARRAYS WITH LENGTHS NTALR,NTALSS,NMIX
C     ARRAYS WITH LENGTHS NSUR
C     ARRAYS WITH LENGTHS NBANK
C     ARRAYS WITH LENGTHS NT
C     ARRAYS WITH LENGTHS NSUM
      COMMON/PASS/   NKRN,MORE,NPUNCH,DELT1,DELT1I,DELT2,DELT2I,OFFSET
     1,TSPLT,WSPLT,WCO,WCOCF,WDELF,NLIBSC ,MATLIB,NING,ITB1,NBANK,NOR
     2,ISKIP,KTRA,IST1,IST2,KIMP,RIMU,RIML,MAR',NGMI,NGMA,NSTAD,KAN,NGMM
     3,NSTA,IPUNCH
      LENGIA=116000
      LENGA=29000
C
C     READ FORMATS
   10 FORMAT(18A4)
   12 FORMAT (12I6)
   13 FORMAT(10A4,2X,6I6)
   14 FORMAT(I6,2E12.6)
   16 FORMAT(I6,F6.0,10I6)
   17 FORMAT(1H ,I6,F6.0,10I6)
C     PRINT FORMATS
   20 FORMAT(1H ,18A4)
   22 FORMAT (1H ,12I9)
   23 FORMAT(1H ,10A4,2X,6I6)
   24 FORMAT(1H ,I6,2E12.6)
  100 FORMAT (/5H DATA)
  101 FORMAT(/10X,50H PLEASE MAKE LENGIA EXCEED LOCINI                    )
  102 FORMAT(/10X,50H NT    ITB1   NTALR   NTALSS   NIT    NMATMA    NSUM )
  103 FORMAT(/10X,50H PLEASE MAKE LENGA EXCEED LOCINA                     )
  104 FORMAT(/10X,50H PLEASE MAKE NSCAT .LE.NLIBSC                        )
  105 FORMAT(/10X,50H NREG   NSUR   NSEG   NMIX   NSCAT   NSENMA          )
  106 FORMAT(/10X,50H LOCINI    LENGIA   LOCINA   LENGA                   )
  107 FORMAT(/10X,50H NS   NKRN   MORE   NPUNCH   NOR    ISKIP            )
  151 FORMAT(/10X,50H LIBRY   MATLIB   NG   NP   NING   NTPDEL   KMUL     )
  152 FORMAT(/10X,50H NLIBSC    NLIBS(ISCAT),ISCAT=1,NLIBSC   NLIBSM      )
  111 FORMAT(/10X,50HKTRA IST1 IST2 NGMI NGMA MARI NSTAD KAN NSTA IPUNC)
  112 FORMAT(/10X,50H KIMP   RIMU   RIML                                  )
C
```

```
C     READ LIBRARY CARDS
      READ 13,LIBRY,MATLIB,NG,NP,NING,NTPDEL,KMUL
      PRINT 151
      PRINT23,LIBRY,MATLIB,NG,NP,NING,NTPDEL,KMUL
      READ 12,NLIBSC ,(NLIBS(ISCAT),ISCAT=1,NLIBSC ),NLIBSM
      PRINT 152
      PRINT22,NLIBSC ,(NLIBS(ISCAT),ISCAT=1,NLIBSC ),NLIBSM
C     READ TITLE AND DATA TO SET DIMENSIONS
   30 READ  10,TITLE
      PRINT  20,TITLE
      PRINT 100
      READ  12,NREG,NSUR,NSEG,NMIX,NSCAT,NSENMA
      PRINT 105
      PRINT 22,NREG,NSUR,NSEG,NMIX,NSCAT,NSENMA
      READ  12,NT,ITB1,NTALR ,NTALSS,NIT,NMATMA,NSUM
      PRINT 102
      PRINT 22,NT,ITB1,NTALR ,NTALSS,NIT,NMATMA,NSUM
      READ  16,NS,NKRN,MORE,NPUNCH,NOR,ISKIP
      PRINT 107
      PRINT 17,NS,NKRN,MORE,NPUNCH,NOR,ISKIP
      READ  12,KTRA,IST1,IST2,NGMI,NGMA,MARI,NSTAD,KAN,NSTA,IPUNCH
      PRINT 111
      PRINT 22,KTRA,IST1,IST2,NGMI,NGMA,MARI,NSTAD,KAN,NSTA,IPUNCH
      READ  14,KIMP,RIMU,RIML
      PRINT 112
      PRINT 24,KIMP,RIMU,RIML
      NBANK=100
C
C     SET STORAGE LOCATIONS IN IA. NSENMAX AND NMATMAX ARE REQUIRED AND
C          WASTEFUL BECAUSE WE DON'T YET KNOW  PARTICULAR VALUES
      NGMM=NGMA-NGMI+1
      LIDEN=1
      LISEN=LIDEN+NSEG*NSENMA +1
      LIAS=LISEN+NSEG*NSENMA +1
      LIAR=LIAS+NREG*NSEG+1
      LIMAT=LIAR+NREG*NSEG+1
      LIRST=LIMAT+NMIX*NMATMA+1
      LIRSTR=LIRST+KMUL*NS+1
      LOCINI=LIRSTR+NS*KMUL
C     SET STORAGE LOCATIONS IN A
      LCHID=1
      LDENS=LCHID+NTPDEL*NG+1
      LCL=LDENS+NMATMA *NMIX+1
      LCM=LCL+NP*NG+1
      LWIR=LCM+NP*NG*NMIX+1
      LWISN=LWIR+NT*NTALR*NGMM+1
      LWISP=LWISN+NT*NTALSS*NGMM+1
      LWIRL=LWISP+NT*NTALSS*NGMM+1
      LDENSM=LWIRL+NT*NTALR*NGMM+1
      LCSUM=LDENSM+NLIBSM*NSUM+1
      LDELPC=LCSUM+NSUM*NG+1
      LWIT =LDELPC+NTPDEL*NG*NMIX+1
      LCM1=LWIT+NT*NIT+1
      NP1=1
      NP2=1
      NP3=1
      IF (NSCAT.LT.1) GO TO 50
      NP1=NP-3
      LCM2=LCM1+(NP-3)*NG*NMIX
      IF (NSCAT.LT.2) GO TO 51
```

```
      NP2=NP-3
      LCM3=LCM2+(NP-3)*NG*NMIX
      IF (NSCAT.LT.3) GO TO 52
      NP3=NP-3
      LWIRS =LCM3+(NP-3)*NG*NMIX
      GO TO 53
   50 LCM2=LCM1+1
   51 LCM3=LCM2+1
   52 LWIRS=LCM3+1
   53 LWIRV=LWIRS+NT*NTALR*NGMM+1
      LWISNS=LWIRV+NT*NTALR*NGMM+1
      LWISNV=LWISNS+NT*NTALSS*NGMM+1
      LWISPS=LWISNV+NT*NTALSS*NGMM+1
      LWISPV=LWISPS+NT*NTALSS*NGMM+1
      LWIRLS=LWISPV+NT*NTALSS*NGMM+1
      LWIRLV=LWIRLS+NT*NTALR*NGMM+1
      LWITS=LWIRLV+NT*NTALR*NGMM+1
      LWITV=LWITS+NT*NIT+1
      LXST=LWITV+NT*NIT+1
      LXSTR=LXST+NS*KMUL+1
      LYST=LXSTR+NS*KMUL+1
      LYSTR=LYST+NS*KMUL+1
      LZST=LYSTR+NS*KMUL+1
      LZSTR=LZST+NS*KMUL+1
      LWST=LZSTR+NS*KMUL+1
      LWSTR=LWST+NS*KMUL+1
      LOCINA=LWSTR+NS*KMUL
      NE=NS*KMUL+1*(1-KMUL)
      NTPDE1=NTPDEL
      IF(NTPDEL.EQ.0)NTPDE1=1
      NI1=NIT
      IF(NIT.EQ.0)NI1=1
      NLIBS1=NLIBSM
      IF(NLIBSM.EQ.0)NLIBS1=1
      NSU1=NSUM
      IF(NSUM.EQ.0)NSU1=1
C      COMPUTE AND PRINT IA AND A ARRAY LENGT
      PRINT 106
      PRINT 22,LOCINI ,LENGIA,LOCINA,LE
      IF (LENGIA.GE.LOCINI ) GO TO 10
      PRINT 101
      GO TO 153
  108 IF (LENGA.GE.LOCINA) GO TO 109
      PRINT 103
      GO TO 153
  109 IF (NLIBSC .GE.NSCAT) GO TO 110
      PRINT 104
      GO TO 153
  110 CONTINUE
C
      CALL       PREP(NSUR,NSEG,NSENMA ,NREG,NMIX,NMATMA,NT,NTALR,NTALSS
     1,NIT,NSCAT,NG,NP,NTPDEL,NP1,NP2,NP3,NLIBSM,NSUM,KMUL,NS,NE
     2,NTPDE1,NI1,NLIBS1,NSU1
     2,          IA(LIDEN),IA(LISEN),IA(LIAS),IA(LIAR),IA(LIMAT)
     2,IA(LIRST),IA(LIRSTR)
     3,A(LCHID),A(LDENS),A(LCL),A(LCM),A(LWIR),A(LWISN),A(LWISP)
     3,A(LWIRL)
     4,A(LDENSM ),A(LCSUM)
     5,A(LDELPC),A(LWIT),A(LCM1),A(LCM2),A(LCM3)
     6,A(LWIRS),A(LWIRV),A(LWISNS),A(LWISNV) A(LWISPS),A(LWISPV)
```

```
     6,A(LWIRLS),A(LWIRLV)
     7,A(LWITS),A(LWITV),A(LXST),A(LXSTR),A(LYST),A(LYSTR)
     8,A(LZST),A(LZSTR),A(LWST),A(LWSTR))
C
      CALL       BUSY(NSUR,NSEG,NSENMA ,NREG,NMIX,NMATMA,NT,NTALR,NTALSS
     1,NIT,NSCAT,NG,NP,NTPDEL,NP1,NP2,NP3,NLIBSM,NSUM,KMUL,NS,NE
     2,NTPDE1,NI1,NLIBS1,NSU1
     2,         IA(LIDEN),IA(LISEN),IA(LIAS),IA(LIAR),IA(LIMAT)
     2,IA(LIRST),IA(LIRSTR)
     3,A(LCHID),A(LDENS),A(LCL),A(LCM),A(LWIR),A(LWISN),A(LWISP)
     3,A(LWIRL)
     4,A(LDENSM ),A(LCSUM)
     5,A(LDELPC),A(LWIT),A(LCM1),A(LCM2),A(LCM3)
     6,A(LWIRS),A(LWIRV),A(LWISNS),A(LWISNV),A(LWISPS),A(LWISPV)
     6,A(LWIRLS),A(LWIRLV)
     7,A(LWITS),A(LWITV),A(LXST),A(LXSTR),A(LYST),A(LYSTR)
     8,A(LZST),A(LZSTR),A(LWST),A(LWSTR) )
  153 STOP
      END
C
C
      SUBROUTINE PREP(NSUR,NSEG,NSENMA ,NREG,NMIX,NMATMA,NT,NTALR,NTALSS
     1,NIT,NSCAT,NG,NP,NTPDEL,NP1,NP2,NP3,NLIBSM,NSUM,KMUL,NS,NE
     2,NTPDE1,NI1,NLIBS1,NSU1
     2,IDEN,ISEN,IAS,IAR,IMAT
     2,IRST,IRSTR
     3,CHID,DENS,CL,CM,WIR,WISN,WISP,WIRL,DENSM,CSUM
     4,DELPC,WIT,CM1,CM2,CM3
     5,WIRS,WIRV,WISNS,WISNV,WISPS,WISPV,WIRLS,WIRLV,WITS,WITV
     6,XST,XSTR,YST,YSTR,ZST,ZSTR,WST,WSTR                          )
C
C       PREP STORAGE
C       SOME ARRAYS ARE IN LABELED COMMON TO REDUCE LENGTH OF CALLS
      DOUBLE PRECISION NKRN
      COMMON/OTHER/TITLE(18),LIBRY(10),NLIBS(3)
     1,IGMIN(40),IGMAX(40),V(40),CHIP(40)
     2,IDS(425),NSEN(425)
     3,NAS(135),IMIX(135),RIM(135)
     4,WDEL( 1),TD( 1)
     5,ITALR(135),ITALSS(425),NMAT( 20)
     1,ITP(40),AS(40),BS(40),CS(40),DS(40),ES(40),FS(40),GS(40),HS(40)
     7,D1( 40),D2( 40),IDEC( 40)
     8,IRSPL( 50),IGSPL( 50),XSPL( 50),YSPL( 50),ZSPL( 50),UXSPL( 50)
     9,UYSPL( 50),UZSPL( 50),TSPL( 50),WSPL( 50)
     1,TB(  1),SUM( 1)
     2,IRORS(10),ISUMTY(10)
C       ARRAYS WITH DIMENSION NG
C       ARRAYS WITH DIMENSION NSEG
C       ARRAYS WITH DIMENSION NREG
C       ARRAYS WITH DIMENSION NTPDEL
C       ARRAYS WITH LENGTHS NTALR,NTALSS,NMIX
C       ARRAYS WITH LENGTHS NSUR
C       ARRAYS WITH LENGTHS NBANK
C       ARRAYS WITH LENGTHS NT
C       ARRAYS WITH LENGTHS NSUM
      COMMON/PASS/   NKRN,MORE,NPUNCH,DELT1,DELT1I,DELT2,DELT2I,OFFSET
     1,TSPLT,WSPLT,WCO,WCOCF,WDELF,NLIBSC ,MATLIB,NING,ITB1,NBANK,NOR
     2,ISKIP,KTRA,IST1,IST2,KIMP,RIMU,RIML,MARI,NGMI,NGMA,NSTAD,KAN,NGMM
     3,NSTA,IPUNCH
      DIMENSION IDEN(NSEG,NSENMA),ISEN(NSEG,NSENMA),IAS(NREG,NSEG)
```

```
     1,IAR(NREG,NSEG),IMAT(NMATMA,NMIX)
     1,IRST(NE),IRSTR(NE)
     2,CHID(NTPDE1,NG),DENS(NMATMA,NMIX),CL(NP,NG),CM(NP,NG,NMIX)
     3,WIR(NT,NTALR,NGMM),WISN(NT,NTALSS,NGMM),WISP(NT,NTALSS,NGMM)
     3,WIRL(NT,NTALR,NGMM)
     3,WIRS(NT,NTALR,NGMM),WISNS(NT,NTALSS,NGMM),WISPS(NT,NTALSS,NGMM)
     3,WIRLS(NT,NTALR,NGMM)
     3,WIRV(NT,NTALR,NGMM),WISNV(NT,NTALSS,NGMM),WISPV(NT,NTALSS,NGMM)
     3,WIRLV(NT,NTALR,NGMM)
     4,DENSM(NLIBS1,NSU1),CSUM(NSU1,NG)
     5,DELPC(NTPDE1,NG,NMIX),WIT(NT,NI1)
     5,WITS(NT,NI1),WITV(NT,NI1)
     6,CM1(NP1,NG,NMIX),CM2(NP2,NG,NMIX),CM3(NP3,NG,NMIX)
     7,XST(NE),XSTR(NE),YST(NE),YSTR(NE),ZST(NE),ZSTR(NE)
     8,WST(NE),WSTR(NE)
C
C      READ FORMATS
   10 FORMAT(18A4)
   11 FORMAT (6E12.6)
   12 FORMAT (12I6)
   13 FORMAT(10A4,2X,6I6)
   14 FORMAT(2I6,2X,E12.6)
C      PRINT FORMATS
   20 FORMAT (1H1,16A5)
   21 FORMAT (1H ,6E16.6)
   22 FORMAT (1H ,12I9)
   23 FORMAT (1H ,10A4,2X,6I6)
   24 FORMAT (1H ,2I9,2X,E12.6)
   37 FORMAT (/10X,38H  DENSM(I,ISUM),I=1,NLIBSM  FOR ISUM= ,I6)
   38 FORMAT(/10X,50H  IRORS(ISUM)  ISUMTY(ISUM)                       )
  103 FORMAT(/10X,50H DELT1   DELT2   OFFSET   TSPLT                   )
  104 FORMAT(/10X,50H WSPLT   WCO   WCOCF   WDELF                      )
  106 FORMAT(/10X,50H ITP(IS)                                          )
  107 FORMAT(/10X,50H AS(IS),BS(IS),...                                )
  108 FORMAT (/10X,29H SURFACE SEGMENT NUMBER ISS= ,I6)
  109 FORMAT(/10X,50H IDS(ISS),NSEN(ISS)                               )
  110 FORMAT(/10X,50H IDEN(ISS,IS1),IS1=1,NSEN(ISS)                    )
  111 FORMAT(/10X,50H ISEN(ISS,IS1),IS1=1,NSEN(ISS)                    )
  112 FORMAT(/10X,19H REGION NUMBER IR= ,I6)
  113 FORMAT(/10X,50H NAS(IR)  IMIX(IR)  RIM(IR)                       )
  114 FORMAT(/10X,50H IAS(IR,ISS),ISS=1,NAS(IR)                        )
  115 FORMAT(/10X,50H IAR(IR,ISS),ISS=1,NAS(IR)                        )
  117 FORMAT(/10X,50H IMAT(I,IM),I=1,NMAT(IM)                          )
  116 FORMAT (/10X, 16H MIX NUMBER IM= ,I6,13H   NMAT(IM)= ,I6)
  118 FORMAT(/10X,50H DENS((I,IM),U=1,NMAT(IM)                         )
  119 FORMAT(/10X,50H TB(IT),IT=1,NT                                   )
  130 FORMAT (/10X,20H SURFACE NUMBER IS= ,I6)
  135 FORMAT (/10X,33H CSUM(ISUM,IG),IG=1,NG FOR ISUM= ,I6)
  144 FORMAT(/10X,50H ITALR(I),I=1,NTALR                               )
  145 FORMAT(/10X,50H ITALSS(I),I=1,NTALSS                             )
  146 FORMAT(/10X,50H V(IG),IG=1,NG                                    )
  147 FORMAT(/10X,50H CHIP(IG),IG=1,NG                                 )
  148 FORMAT(/10X,57H EMISSION SPECTRUM FOR DELAYED PARTICLES OF TYPE IT
     1PDEL=  ,I6)
  149 FORMAT(/10X,50H CHID(ITPDEL,IG),IG=1,NG                          )
  152 FORMAT(/10X,40H DELPC(ITPDEL,IG,1),IG=1,NG FOR ITPDEL= ,I6)
  312 FORMAT (/5X,34H COLLISION PARAMETERS FOR MIX IM= ,I6)
  313 FORMAT (/10X,43H CM(IP,IG,IM),IP=1,NP FOR ENERGY GROUP IG= ,I6,12H
     1   SUMSCA=  ,E12.6)
  314 FORMAT (/10X,29H PARTICLES FROM ENERGY GROUP ,I6,40H  ARE SCATTERE
```

```
   1D INTO ENERGY GROUPS FROM ,I6, 5H  TO ,I6)
 321 FORMAT (/10X,45H CM1(IP,IG,IM),IP=1,NP1 FOR ENERGY GROUP IG= ,I6)
 345 FORMAT (/10X,45H CM2(IP,IG,IM),IP=1,NP2 FOR ENERGY GROUP IG= ,I6)
 346 FORMAT (/10X,45H CM3(IP,IG,IM),IP=1,NP3 FOR ENERGY GROUP IG= ,I6)
C
C     READ REMAINING DATA
      READ  11,DELT1,DELT2,OFFSET,TSPLT
      PRINT 103
      PRINT 21,DELT1,DELT2,OFFSET,TSPLT
      READ  11,WSPLT,WCO,WCOCF,WDELF
      PRINT 104
      PRINT 21,WSPLT,WCO,WCOCF,WDELF
      DO 31 IS=1,NSUR
      IF (MARI.EQ.1) GO TO 1001
      PRINT 130,IS
 1001 READ  12,ITP(IS)
      IF (MARI.EQ.1) GO TO 1002
      PRINT 106
      PRINT 22,ITP(IS)
 1002 READ  11,AS(IS),BS(IS),CS(IS),DS(IS),ES(IS),FS(IS)
      IF (MARI.EQ.1) GO TO 1003
      PRINT 107
      PRINT 21,AS(IS),BS(IS),CS(IS),DS(IS),ES(IS),FS(IS)
 1003 READ  11,GS(IS),HS(IS)
      IF (MARI.EQ.1) GO TO 31
      PRINT 21,GS(IS),HS(IS)
   31 CONTINUE
      DO 32 ISS=1,NSEG
      IF (MARI.EQ.1) GO TO 1004
      PRINT 108,ISS
 1004 READ  12,IDS(ISS),NSEN(ISS)
      IF (MARI.EQ.1) GO TO 1005
      PRINT 109
      PRINT 22,IDS(ISS),NSEN(ISS)
 1005 NSENT=NSEN(ISS)
      IF (NSENT.EQ.0) GO TO 32
      READ  12,(IDEN(ISS,IS1),IS1=1,NSENT)
      IF (MARI.EQ.1) GO TO 1006
      PRINT 110
      PRINT 22,(IDEN(ISS,IS1),IS1=1,NSENT)
 1006 READ  12,(ISEN(ISS,IS1),IS1=1,NSENT)
      IF (MARI.EQ.1) GO TO 32
      PRINT 111
      PRINT 22,(ISEN(ISS,IS1),IS1=1,NSENT)
   32 CONTINUE
      DO 33 IR=1,NREG
      IF (MARI.EQ.1) GO TO 1007
      PRINT 112,IR
 1007 READ  14,NAS(IR),IMIX(IR),RIM(IR)
      IF (MARI.EQ.1) GO TO 1008
      PRINT 113
      PRINT 24,NAS(IR),IMIX(IR),RIM(IR)
 1008 NAST=NAS(IR)
      READ  12,(IAS(IR,ISS),ISS=1,NAST)
      IF (MARI.EQ.1) GO TO 1009
      PRINT 114
      PRINT 22,(IAS(IR,ISS),ISS=1,NAST)
 1009 READ  12,(IAR(IR,ISS),ISS=1,NAST)
      IF (MARI.EQ.1) GO TO 33
      PRINT 115
```

```
      PRINT 22,(IAR(IR,ISS),ISS=1,NAST)
   33 CONTINUE
      READ  12,(ITALR(I),I=1,NTALR)
      IF (MARI.EQ.1) GO TO 1010
      PRINT 144
      PRINT 22,(ITALR(I),I=1,NTALR)
 1010 IF (NTALSS.EQ.0) GO TO 1011
      READ  12,(ITALSS(I),I=1,NTALSS)
      IF (MARI.EQ.1) GO TO 1011
      PRINT 145
      PRINT 22,(ITALSS(I),I=1,NTALSS)
 1011 DO 34 IM=1,NMIX
      READ 12,NMAT(IM)
      PRINT 116,IM,NMAT(IM)
      NMATT=NMAT(IM)
      READ 12,(IMAT(I,IM),I=1,NMATT)
      PRINT 117
      PRINT22,(IMAT(I,IM),I=1,NMATT)
      READ 11,(DENS(I,IM),I=1,NMATT)
      PRINT 118
      PRINT21,(DENS(I,IM),I=1,NMATT)
   34 CONTINUE
      IF (NSUM.EQ.0) GO TO 39
      DO 35 ISUM=1,NSUM
      READ 11,(DENSM(I,ISUM),I=1,NLIBSM)
      PRINT 37,ISUM
      PRINT21,(DENSM(I,ISUM),I=1,NLIBSM)
      READ 12,IRORS(ISUM),ISUMTY(ISUM)
      PRINT 38
      PRINT22,IRORS(ISUM),ISUMTY(ISUM)
   35 CONTINUE
   39 CONTINUE
C
C      GENERATE TIME BOXES
      TB(1)=OFFSET
      IF(ITB1.EQ.1)GO TO 60
      DO 50 IT=2,ITB1
      TB(IT)=TB(IT-1)+DELT1
   50 CONTINUE
      ITB1P=ITB1+1
      DO 151 IT=ITB1P,NT
      TB(IT)=TB(IT-1)+DELT2
  151 CONTINUE
   60 CONTINUE
      PRINT 119
      PRINT 21,(TB(I),I=1,NT)
C
C      READ LIBRARY AND PREPARE MACROSCOPIC CROSS SECTIONS
      READ 11,(V(IG),IG=1,NG)
      IF (MARI.EQ.1) GO TO 1014
      PRINT 146
      PRINT21,(V(IG),IG=1,NG)
 1014 READ 11,(CHIP(IG),IG=1,NG)
      IF (MARI.EQ.1) GO TO 1015
      PRINT 147
      PRINT21,(CHIP(IG),IG=1,NG)
 1015 CONTINUE
      IF (NTPDEL.EQ.0) GO TO 307
      READ 11,((CHID(ITPDEL,IG),IG=1,NG),ITPDEL=1,NTPDEL)
      DO 308 ITPDEL=1,NTPDEL
```

```
      PRINT 148,ITPDEL
      PRINT 149
      PRINT21,(CHID(ITPDEL,IG),IG=1,NG)
  308 CONTINUE
      READ 11,((DELPC(ITPDEL,IG,1),IG=1,NG),ITPDEL=1,NTPDEL)
      DO 153 ITPDEL=1,NTPDEL
      PRINT 152,ITPDEL
      PRINT 21,(DELPC(ITPDEL,IG,1),IG=1,NG)
  153 CONTINUE
  307 CONTINUE
C
C      COMPUTE AND PRINT SUMMING CROSS SECTIONS
      IF (NSUM.EQ.0) GO TO 133
      DO 132 ISUM=1,NSUM
      DO 132 IG=1,NG
      CSUM(ISUM,IG)=0.
  132 CONTINUE
      DO 134 I=1,NLIBSM
      READ 13,LIBRY
      PRINT23,LIBRY
      READ 11,(CL(1,IG),IG=1,NG)
      PRINT21,(CL(1,IG),IG=1,NG)
      DO 134 ISUM=1,NSUM
      DO 134 IG=1,NG
      CSUM(ISUM,IG)=CSUM(ISUM,IG)+DENSM(I,ISUM)*CL(1,IG)
  134 CONTINUE
      DO 136 ISUM=1,NSUM
      PRINT 135 ,ISUM
      PRINT 21,(CSUM(ISUM,IG),IG=1,NG)
  136 CONTINUE
  133 CONTINUE
C
      IF(IPUNCH.EQ.2) GO TO 250
C
C    IPUNCH=0, READ MICRO. X-SECT AND PROCESS THEM
C    IPUNCH=1, READ MICRO. X-SECT, PROCESS THEM AND STORED IN FILE 6
C    IPUNCH=2, READ MACRO. X-SECTIONS DIRECTLY FROM FILE 6
C
C      COMPUTE MACROSCOPIC CROSS SECTIONS
      DO 300 IP=1,NP
      DO 300 IG=1,NG
      DO 300 IM=1,NMIX
      CM(IP,IG,IM)=0.
  300 CONTINUE
      DO 301 IMATLI =1,MATLIB
      READ (7,13) LIBRY,IDMAT
      DO 3000 IG=1,NG
 3000 READ (7,11)(CL(IP,IG),IP=1,NP)
C
C      IF THE SCATTERING MATRIX PART OF CL(IP,IG) IS IN THE LASL FORM THEN WE
C           MUST ALTER IT FROM CL( TO IG) TO CL( FROM IG)
      DO 302 IP=4,NP
      DO 302 IG=1,NG
      IF (IG+IP-NING.GT.NG) GO TO 303
      IF (IG+IP-NING.LT.1 ) GO TO 303
      CL(IP,IG)=CL(IP,IG+IP-NING)
      GO TO 302
  303 CL(IP,IG)=0.
  302 CONTINUE
C DEBUG PRINT 800 GOES HERE IF YOU WANT TO SEE MICROSCOPIC X-SECTION
```

```
C
      IF (MARI.EQ.1) GO TO 800
C      DEBUG PRINT 800
      PRINT 802,IDMAT
  802 FORMAT (/5X,41H MICROSCOPIC CROSS SECTIONS FOR MATERIAL ,I6)
      PRINT23,LIBRY,IDMAT
      DO 800 IG=1,NG
      PRINT 21,(CL(IP,IG),IP=1,NP)
  800 CONTINUE
C
      DO 301 IM=1,NMIX
      NMATT=NMAT(IM)
      DO 316 I=1,NMATT
      IF (IMAT(I,IM).NE.IDMAT) GO TO 316
      DO 306 IG=1,NG
      DO 306 IP=1,NP
      CM(IP,IG,IM)=CM(IP,IG,IM)+DENS(I,IM)*CL(IP,IG)
  306 CONTINUE
  316 CONTINUE
  301 CONTINUE
C
      IF (NSCAT.LT.1) GO TO 3325
C
C      HERE ANISOTROPIC MACROSCOPIC CROSS SECTIONS ARE PREPARED
      DO 324 IG=1,NG
      DO 324 IM=1,NMIX
      DO 322 IP=1,NP1
      CM1(IP,IG,IM)=0.
  322 CONTINUE
      IF (NSCAT.LT.2) GO TO 324
      DO 323 IP=1,NP2
      CM2(IP,IG,IM)=0.
  323 CONTINUE
      IF (NSCAT.LT.3) GO TO 324
      DO 326 IP=1,NP3
      CM3(IP,IG,IM)=0.
  326 CONTINUE
  324 CONTINUE
      DO 327 ISCAT=1,NSCAT
      NLIBST=NLIBS(ISCAT)
      DO 327 IMATLI =1,NLIBST
      READ (7,13)LIBRY,IDMAT
      DO 3001 IG=1,NG
 3001 READ (7,11)(CL(IP,IG),IP=1,NP)
C
C     IN CASK THE FACTOR 2L+1 IS NOT INCLUDED DO WE MUST DIVIDE BY IT
C
      FACT=2.*ISCAT+1.
      DO 3002 IG=1,NG
      DO 3002 IP=1,NP
      CL(IP,IG)=CL(IP,IG)/FACT
 3002 CONTINUE
C
C      IF THE SCATTERING MATRIX PART OF CL(IP,IG) IS IN THE LASL FORM THEN WE
C           MUST ALTER IT FROM CL( TO IG) TO CL( FROM IG)
      DO 332 IP=4,NP
      DO 332 IG=1,NG
      IF (IG+IP-NING.GT.NG) GO TO 333
      IF (IG+IP-NING.LT.1 ) GO TO 333
      CL(IP,IG)=CL(IP,IG+IP-NING)
```

```
      GO TO 332
 333 CL(IP,IG)=0.
 332 CONTINUE
C
C      DEBUG PRINT 801 GOES HERE IF YOU WANT TO SEE MICROSCOPIC CROSS SECTIONS
      IF (MARI.EQ.1) GO TO 801
C      DEBUG PRINT 801
      PRINT 803,IDMAT,ISCAT
 803 FORMAT (/5X,41H MICROSCOPIC CROSS SECTIONS FOR MATERIAL ,I6,13H  F
     1OR ISCAT= ,I6)
      PRINT23,LIBRY,IDMAT
      DO 801 IG=1,NG
      PRINT 21,(CL(IP,IG),IP=1,NP)
 801 CONTINUE
C
      DO 327 IM=1,NMIX
      NMATT=NMAT(IM)
      DO 328 I=1,NMATT
      IF (IMAT(I,IM).NE.IDMAT) GO TO 328
      DO 329 IG=1,NG
      GO TO (334,336,338),ISCAT
 334 DO 335 IP=1,NP1
      CM1(IP,IG,IM)=CM1(IP,IG,IM)+DENS(I,IM)*CL(IP+3,IG)
 335 CONTINUE
      GO TO 329
 336 DO 337 IP=1,NP2
      CM2(IP,IG,IM)=CM2(IP,IG,IM)+DENS(I,IM)*CL(IP+3,IG)
 337 CONTINUE
      GO TO 329
 338 DO 339 IP=1,NP3
      CM3(IP,IG,IM)=CM3(IP,IG,IM)+DENS(I,IM)*CL(IP+3,IG)
 339 CONTINUE
 329 CONTINUE
 328 CONTINUE
 327 CONTINUE
C
C DEBUG PRINT MACROSCOPIC CROSS SECTIONS
3325 IF (MARI.EQ.1) GO TO 318
C
C       PRINT MACROSCOPIC CROSS SECTIONS
 325 DO 318 IM=1,NMIX
      PRINT 309,IM
 309 FORMAT (/5X,40H MACROSCOPIC CROSS SECTIONS FOR MIX IM= ,I6)
      DO 318 IG=1,NG
      PRINT 310,IG
 310 FORMAT (/10X,43H CM(IP,IG,IM),IP=1,NP FOR ENERGY GROUP IG= ,I6)
      PRINT 21,(CM(IP,IG,IM),IP=1,NP)
      IF (NSCAT.LT.1) GO TO 318
      PRINT 317,IG
 317 FORMAT (/10X,45H CM1(IP,IG,IM),IP=1,NP1 FOR ENERGY GROUP IG= ,I6)
      PRINT 21,(CM1(IP,IG,IM),IP=1,NP1)
      IF (NSCAT.LT.2) GO TO 318
      PRINT 319,IG
 319 FORMAT (/10X,45H CM2(IP,IG,IM),IP=1,NP2 FOR ENERGY GROUP IG= ,I6)
      PRINT 21,(CM2(IP,IG,IM),IP=1,NP2)
      IF (NSCAT.LT.3) GO TO 318
      PRINT 320,IG
 320 FORMAT (/10X,45H CM3(IP,IG,IM),IP=1,NP3 FOR ENERGY GROUP IG= ,I6)
      PRINT 21,(CM3(IP,IG,IM),IP=1,NP3)
 318 CONTINUE
```

```
C
C     PROCESS MACROSCOPIC CROSS SECTIONS
      DO 305 IG=1,NG
      DO 305 IM=1,NMIX
      IF (NSCAT.LT.1) GO TO 330
      GO TO (331,341,343),NSCAT
  331 DO 340 IP=1,NP1
      IF (CM(IP+3,IG,IM).EQ.0.) GO TO 340
      CM1(IP,IG,IM)=3.*CM1(IP,IG,IM)/CM(IP+3,IG,IM)
  340 CONTINUE
      GO TO 330
  341 DO 342 IP=1,NP1
      IF (CM(IP+3,IG,IM).EQ.0.) GO TO 342
      CM1(IP,IG,IM)=3.*CM1(IP,IG,IM)/CM(IP+3,IG,IM)
      CM2(IP,IG,IM)=7.5*CM2(IP,IG,IM)/CM(IP+3,IG,IM)
  342 CONTINUE
      GO TO 330
  343 DO 344 IP=1,NP1
      IF (CM(IP+3,IG,IM).EQ.0.) GO TO 344
      CMO=1.-2.5*CM2(IP,IG,IM)/CM(IP+3,IG,IM)
      CM1(IP,IG,IM)=(3.*CM1(IP,IG,IM)-10.5*CM3(IP,IG,IM))/CM(IP+3,IG,IM)
      CM2(IP,IG,IM)=7.5*CM2(IP,IG,IM)/CM(IP+3,IG,IM)
      CM3(IP,IG,IM)=17.5*CM3(IP,IG,IM)/CM(IP+3,IG,IM)
      IF(KAN.EQ.0) GO TO 420
C
C  EQUIPROBABLE ANGLE SCATTERING METHOD
C
      NA=200
      DA=2./NA
      CPT=0.
      DO 430 IA=1,NA
      RA=-1.+IA*DA
      CPA=CMO*(RA+1.)/2.+CM1(IP,IG,IM)*(RA**2-1.)/4.
     *+CM2(IP,IG,IM)*(RA**3+1.)/6.+CM3(IP,IG,IM)*(RA**4-1.)/8.
      IF(.25.GE.CPT.AND..25.LT.CPA) RA1=RA
      IF(.50.GE.CPT.AND..50.LT.CPA) RA2=RA
      IF(.75.GE.CPT.AND..75.LT.CPA) RA3=RA
  430 CPT=CPA
      CM1(IP,IG,IM)=RA1
      CM2(IP,IG,IM)=RA2
      CM3(IP,IG,IM)=RA3
  420 CONTINUE
  344 CONTINUE
  330 SUMSCA =0.
      DO 304 IP=4,NP
      SUMSCA =SUMSCA +ABS(CM(IP,IG,IM))
  304 CONTINUE
      CM(1,IG,IM)=(CM(2,IG,IM)+SUMSCA )/CM(3,IG,IM)
      CM(2,IG,IM)=CM(2,IG,IM)/(CM(2,IG,IM)+SUMSCA )
      CM(3,IG,IM)=1./CM(3,IG,IM)
      CM(4,IG,IM)=CM(4,IG,IM)/SUMSCA
      DO 305 IP=5,NP
      CMTEMP=ABS(CM(IP-1,IG,IM))+ABS(CM(IP,IG,IM))/SUMSCA
      CM(IP,IG,IM)=SIGN(CMTEMP,CM(IP,IG,IM))
  305 CONTINUE
      DO 315 IG=1,NG
      IGMIN(IG)=IG+4-NING
      IGMAX(IG)=IG+NP-NING
      IF (IGMIN(IG).LT.1) IGMIN(IG)=1
      IF (IGMAX(IG).GT.NG) IGMAX(IG)=NG
```

```
 315 CONTINUE
C
C     DEBUG PRINT COLLISIONS PARAMETERS
      IF (MARI.EQ.1) GO TO 311
C
C      PRINT PROCESSED COLLISION PARAMETERS
      DO 311 IM=1,NMIX
      PRINT 312,IM
      DO 311 IG=1,NG
      PRINT 313,IG,SUMSCA
      PRINT 21,(CM(IP,IG,IM),IP=1,NP)
      IF (NSCAT.LT.1) GO TO 347
      PRINT 321,IG
      PRINT 21,(CM1(IP,IG,IM),IP=1,NP1)
      IF (NSCAT.LT.2) GO TO 347
      PRINT 345,IG
      PRINT 21,(CM2(IP,IG,IM),IP=1,NP2)
      IF (NSCAT.LT.3) GO TO 347
      PRINT 346,IG
      PRINT 21,(CM3(IP,IG,IM),IP=1,NP3)
 347  PRINT 314,IG,IGMIN(IG),IGMAX(IG)
 311  CONTINUE
C
 250  IF(IPUNCH.EQ.0) GO TO 220
      IF(IPUNCH.EQ.1) GO TO 252
      DO 254 IG=1,NG
      IGMIN(IG)=IG+4-NING
      IGMAX(IG)=IG+NP-NING
      IF(IGMIN(IG).LT.1) IGMIN(IG)=1
      IF(IGMAX(IG).GT.NG) IGMAX(IG)=NG
 254  CONTINUE
      DO 251 IM=1,NMIX
      DO 251 IG=1,NG
      READ (6,21)(CM(IP,IG,IM),IP=1,NP)
      READ (6,21)(CM1(IP,IG,IM),IP=1,NP1)
      READ (6,21)(CM2(IP,IG,IM),IP=1,NP2)
      READ (6,21)(CM3(IP,IG,IM),IP=1,NP3)
 251  CONTINUE
      GO TO 220
 252  DO 253 IM=1,NMIX
      DO 253 IG=1,NG
      WRITE(6,21)(CM(IP,IG,IM),IP=1,NP)
      WRITE(6,21)(CM1(IP,IG,IM),IP=1,NP1)
      WRITE(6,21)(CM2(IP,IG,IM),IP=1,NP2)
      WRITE(6,21)(CM3(IP,IG,IM),IP=1,NP3)
 253  CONTINUE
      DO 255 IG=1,NG
      IGMIN(IG)=IG+4-NING
      IGMAX(IG)=IG+NP-NING
      IF(IGMIN(IG).LT.1) IGMIN(IG)=1
      IF(IGMAX(IG).GT.NG) IGMAX(IG)=NG
 255  CONTINUE
 220  CONTINUE
C
C      PRECOMPUTE BEFORE EXPENSIVE DO LOOP
      DO 48 IG=1,NG
      V(IG)=1./V(IG)
   48 CONTINUE
      DELT1I=1./DELT1
      DELT2I=1./DELT2
```

```
      DO 140 IS=1,NSUR
      ITPT=ITP(IS)
      GO TO (140,140,141,142,141                     ),ITPT
  141 V1=DS(IS)**2+ES(IS)**2+FS(IS)**2
      DS(IS)=DS(IS)/V1
      ES(IS)=ES(IS)/V1
      FS(IS)=FS(IS)/V1
C       IF (ITPT.EQ.5) GO TO 143
      GO TO 140
  142 DS(IS)=1./DS(IS)**2
      ES(IS)=1./ES(IS)**2
      FS(IS)=1./FS(IS)**2
      GO TO 140
C 143 GS(IS)=(COS(GS(IS)))**2
  140 CONTINUE
      RETURN
      END
C
      SUBROUTINE BUSY(NSUR,NSEG,NSENMA ,NREG,NMIX,NMATMA,NT,NTALR,NTALSS
     1,NIT,NSCAT,NG,NP,NTPDEL,NP1,NP2,NP3,NLIBSM,NSUM,KMUL,NS,NE
     2,NTPDE1,NI1,NLIBS1,NSU1
     2,IDEN,ISEN,IAS,IAR,IMAT
     2,IRST,IRSTR
     3,CHID,DENS,CL,CM,WIR,WISN,WISP,WIRL,DENSM,CSUM
     4,DELPC,WIT,CM1,CM2,CM3
     5,WIRS,WIRV,WISNS,WISNV,WISPS,WISPV,WIRLS,WIRLV,WITS,WITV
     6,XST,XSTR,YST,YSTR,ZST,ZSTR,WST,WSTR                          )
C
C       BUSY STORAGE
C       SOME ARRAYS ARE IN LABELED COMMON TO REDUCE LENGTH OF CALLS
      DOUBLE PRECISION NKRN,NKRNT
      COMMON/OTHER/TITLE(18),LIBRY(10),NLIBS(3)
     1,IGMIN(40),IGMAX(40),V(40),CHIP(40)
     2,IDS(425),NSEN(425)
     3,NAS(135),IMIX(135),RIM(135)
     4,WDEL( 1),TD( 1)
     5,ITALR(135),ITALSS(425),NMAT( 20)
     1,ITP(40),AS(40),BS(40),CS(40),DS(40),ES(40),FS(40),GS(40),HS(40)
     7,D1( 40),D2( 40),IDEC( 40)
     8,IRSPL( 50),IGSPL( 50),XSPL( 50),YSPL( 50),ZSPL( 50),UXSPL( 50)
     9,UYSPL( 50),UZSPL( 50),TSPL( 50),WSPL( 50)
     1,TB(  1),SUM( 1)
     2,IRORS(10),ISUMTY(10)
C       ARRAYS WITH DIMENSION NG
C       ARRAYS WITH DIMENSION NSEG
C       ARRAYS WITH DIMENSION NREG
C       ARRAYS WITH DIMENSION NTPDEL
C       ARRAYS WITH LENGTHS NTALR,NTALSS,NMIX
C       ARRAYS WITH LENGTHS NSUR
C       ARRAYS WITH LENGTHS NBANK
C       ARRAYS WITH LENGTHS NT
C       ARRAYS WITH LENGTHS NSUM
C
      COMMON/PASS/    NKRN,MORE,NPUNCH,DELT1,DELT1I,DELT2,DELT2I,OFFSET
     1,TSPLT,WSPLT,WCO,WCOCF,WDELF,NLIBSC ,MATLIB,NING,ITB1,NBANK,NOR
     2,ISKIP,KTRA,IST1,IST2,KIMP,RIMU,RIML,MARI,NGMI,NGMA,NSTAD,KAN,NGMM
     3,NSTA,IPUNCH
      DIMENSION IDEN(NSEG,NSENMA),ISEN(NSEG,NSENMA),IAS(NREG,NSEG)
     1,IRST(NE),IRSTR(NE)
     1,IAR(NREG,NSEG),IMAT(NMATMA,NMIX)
```

```
     2,CHID(NTPDE1,NG),DENS(NMATMA,NMIX),CL(NP,NG),CM(NP,NG,NMIX)
     3,WIR(NT,NTALR,NGMM),WISN(NT,NTALSS,NGMM),WISP(NT,NTALSS,NGMM)
     3,WIRL(NT,NTALR,NGMM)
     3,WIRS(NT,NTALR,NGMM),WISNS(NT,NTALSS,NGMM),WISPS(NT,NTALSS,NGMM)
     3,WIRLS(NT,NTALR,NGMM)
     3,WIRV(NT,NTALR,NGMM),WISNV(NT,NTALSS,NGMM),WISPV(NT,NTALSS,NGMM)
     3,WIRLV(NT,NTALR,NGMM)
     4,DENSM(NLIBS1,NSU1),CSUM(NSU1,NG)
     5,DELPC(NTPDE1,NG,NMIX),WIT(NT,NI1)
     5,WITS(NT,NI1),WITV(NT,NI1)
     6,CM1(NP1,NG,NMIX),CM2(NP2,NG,NMIX),CM3(NP3,NG,NMIX)
     7,XST(NE),XSTR(NE),YST(NE),YSTR(NE),ZST(NE),ZSTR(NE)
     8,WST(NE),WSTR(NE)
C
C      READ FORMATS
   10 FORMAT(18A4)
   11 FORMAT (6E12.6)
   12 FORMAT (12I6)
   13 FORMAT(10A4,2X,6I6)
C      PRINT FORMATS
   20 FORMAT (1H1,18A4)
   21 FORMAT (1H ,6E16.6)
   22 FORMAT (1H ,12I9)
   23 FORMAT(1H ,10A4,2X,6I6)
   25 FORMAT (1H ,2I5,9I10)
   26 FORMAT (1H ,2I5,9E12.6)
   27 FORMAT (1H ,'GENERATION',2X,'KEFF',10X,'STANDARD DEV.'
     1,2X,'IFIST',4X,23HAKEFF*----*STANDARD DEV )
   28 FORMAT (1H ,I4,2X,2E12.5)
   29 FORMAT(1H ,4E12.5,I6)
  122 FORMAT(/10X,'WIR(IT,ITALY,IG),STAN. DEV.    WIRL(IT,ITALY,IG)',
     *'STAN.DEV.   , IG=1,NGMA FOR REGION    ',I6)
  123 FORMAT (/10X,35H WARNING ..BANK DIMENSION EXCEEDED ,I9,7H  TIMES )
  124 FORMAT(/10X,'WISP(IT,ITALY,IG),STANDARD DEV.IG=1,NG FOR SURF'
     1,'ACE SEGMENT ',I6)
  125 FORMAT(/10X
     1 ,'WISN(IT,ITALY,IG),STANDARD DEV.IG=1,NG FOR SURF'
     1 ,'ACE SEGMENT ',I6)
  126 FORMAT ('1'/10X,29H RESULTS FOR CASE WITH NKRN= ,I6/)
  127 FORMAT(/10X,50H WIT(IT,IW),STANDARD DEV.,IW=1,NT                  )
  128 FORMAT(/10X,50H  NS  ISPLC  ISPLO  NHS  NCOL  NDEL  NDOPE  NESCA )
  130 FORMAT(/10X,50H   WDEL(ITPDEL),ITPDEL=1,NTPDEL                    )
  144 FORMAT(/10X,18H REGION SUM ISUM= ,I6,18H FOR TALLY ITALY= ,I6,16H
     1FOR REGION IR= ,I6)
  145 FORMAT(/10X,50H WIR SUM(IT),IT=1,NT                               )
  147 FORMAT(/10X,27H SURFACE SEGMENT SUM ISUM= ,I6,18H  FOR TALLY ITALY
     1=,I6,27H  FOR SURFACE SEGMENT ISS= ,I6)
  148 FORMAT(/10X,50H WISP SUM(IT),IT=1,NT                              )
  150 FORMAT(/10X,50H WISN SUM(IT),IT=1,NT                              )
 1080 FORMAT(1H ,8H G NCOL=,I6,8H  NCOLH=,I6,13H IR,IG,IMIXT=,3I3)
 1090 FORMAT(1H ,7H X,Y,Z=,3E12.5,10H UX,UY,UZ=,3E12.5,3H W=,E12.5)
  650 FORMAT(1H ,2X,I4,6X,E12.5,2X,E12.5,2X,I4,2X,E12.5,2X,E12.5)
 1030 FORMAT(1H ,7H E IST=,I3,6H IHIT=,I3,4H IR=,I3,5H IRT=,I3,6H IDST=,
     1I3,6H ITPT=,I3,5H ISS=,I3,6H IAST=,I3)
 1040 FORMAT(1H ,10H A1,B1,C1=,3E12.5,21H D1(1DST),D2(IDST),D=,3E12.5)
 1050 FORMAT(1H ,34H F IDENT,ITPT,JSEN,ISEN(IAST,IS1),4I3)
 1060 FORMAT(1H ,12H F X1,Y1,Z1=,3E12.5,14H DTRY,D,SENSE=,3E12.5)
C
 4000 FORMAT(1H ,5X,37H PARTICLE KILLED BY GOING BELOW GROUP,I6)
 4001 FORMAT(1H ,5X,32H NO. PARTICLES WENT BELOW GROUP ,I6,6H WAS ,I6)
```

```
4002 FORMAT(1H ,I4,2X,2(I4,2X,4E12.5))
2888 FORMAT(1H,I4,2X,2E12.5,9X,2E12.5)
C
C      START BATCHES
      NKRNT=NKRN
      IF(KMUL.EQ.1)PRINT20,TITLE
      IF(KMUL.EQ.1)PRINT27
      TE=0.
      TES=0.
      AKBAR=.968
      AEIGEN=AKBAR
      VEIGEN=0.
      IDBG=0
      DO 43 IB=1,MORE
      NKRN=NKRNT
C
C      INITIALIZE  TALLIES
      IF(KMUL.EQ.1.AND.IB.GT.1)GO TO 52
      DO 40 IT=1,NT
      DO 40 IG=1,NGMM
      DO 41 ITALY=1,NTALR
      WIR(IT,ITALY,IG)=0.
      WIRL(IT,ITALY,IG)=0.
      WIRLV(IT,ITALY,IG)=0.
   41 WIRV(IT,ITALY,IG)=0.
      IF (NTALSS.EQ.0) GO TO 4400
      DO 42 ITALY=1,NTALSS
      WISP(IT,ITALY,IG)=0.
      WISPV(IT,ITALY,IG)=0.
      WISN(IT,ITALY,IG)=0.
   42 WISNV(IT,ITALY,IG)=0.
 4400 CONTINUE
      IF (NIT.EQ.0) GO TO 40
      DO 47 IW=1,NIT
      WIT(IT,IW)=0.
   47 WITV(IT,IW)=0.
   40 CONTINUE
      IF (NTPDEL.EQ.0) GO TO 50
      DO 49 ITPDEL=1,NTPDEL
   49 WDEL(ITPDEL)=0.
   50 CONTINUE
      NCOLH=0
      NESCA=0
      NCOL=0
      ISPL=0
      ISPLC=0
      ISPLO=0
   52 WCOC=0.
      NDEL=0.
      ISTR=1
      IFIST=0
      IBK=0
      WFIST=0.
      TWFIS=0.
      TWFISV=0.
      IF(IB.GT.ISKIP)AKBAR=AEIGEN
C
      NDOPE=0
C
C      START SOURCE PARTICLES
```

```
      DO 44 IST=1,NS
C
      IF(NCOLH.EQ.0) NESCA=NESCA+1
C
C      TRACKING PRINT B
      IF(KTRA.NE.1) GO TO 1001
      IF(IST.LT.IST1.OR.IST.GT.IST2) GO TO 1001
      PRINT 1000,IST
 1000 FORMAT(1H ,7H B IST=,I4)
 1001 CONTINUE
      T=0.
      IRT=0
      WFIS=0.
C
C      RESET SECOND MOMENT TALLIES FOR THIS STARTER
      TWFISS=0.
      DO 94 IT=1,NT
      DO 94 IG=1,NGMM
      IF(NTALR.EQ.0)GO TO 90
      DO 91 ITALY=1,NTALR
      WIRLS(IT,ITALY,IG)=0.
   91 WIRS(IT,ITALY,IG)=0.
   90 CONTINUE
      IF(NTALSS.EQ.0)GO TO 92
      DO 93 ITALY=1,NTALSS
      WISNS(IT,ITALY,IG)=0.
   93 WISPS(IT,ITALY,IG)=0.
   92 CONTINUE
      IF(NIT.EQ.0)GO TO 94
      DO 95 IW=1,NIT
   95 WITS(IT,IW)=0.
   94 CONTINUE
      NCOLH=0
C
C      ORIGINATE SOURCE PARTICLES
      IF(IB.EQ.1.AND.KMUL.EQ.1) GO TO 53
C      USE EIGENSOURCE DISTRIBUTION AFTER FIRST GENERATION GUESS
C      FOR EIGENVALUE CALCULATION
      IF(KMUL.EQ.0) GO TO 53
      X=XST(IST)
      Y=YST(IST)
      Z=ZST(IST)
      W=WST(IST)
      IR=IRST(IST)
      CALL ISODIR(UX,UY,UZ,NKRN)
      CALL GGUBS(NKRN,1,FRN)
      DO 96 IG1=1,NG
      IF(FRN.LT.CHIP(IG1))GO TO 97
   96 CONTINUE
   97 IG=IG1
      GO TO 499
C
   53 CALL SOURCE(X,Y,Z,UX,UY,UZ,IG,IR,W,CHIP,NKRN,NG)
  499 CONTINUE
      IMIXT=0
      IF(KTRA.NE.1)GO TO 1007
      IF(IST.LT.IST1.OR.IST.GT.IST2)GO TO 1007
      PRINT 1090,X,Y,Z,UX,UY,UZ,W
      PRINT 1080,NCOL,NCOLH,IR,IG,IMIXT
 1007 CONTINUE
```

```
C
C
C     CHOOSE TRIAL DISTANCE TO COLLISION
 507 CALL GGUBS(NKRN,1,FRN)
     IMIXT=IMIX(IR)
     D= -ALOG(FRN)*CM(3,IG,IMIXT)
     IHIT=0
     IREF=0
     ISSF=0
C
     IF (KTRA.NE.1) GO TO 1021
     IF (IST.LT.IST1.OR.IST.GT.IST2) GO TO 1021
     PRINT 1020,D
1020 FORMAT(1H ,3H D=,E12.5)
1021 CONTINUE
C
C     GEOMETRY SECTION
 505 NAST=NAS(IR)
     DO 599 IDS1=1,NSUR
     IDEC(IDS1)=0
 599 CONTINUE
     DO 500 ISS=1,NAST
C     NERT IS A PARAMETER FOR PRINTING THE HISTOY
     NERT=0
C     IAST IS THE ID NO. OF THE SURFACE SEGMENT WITH ORDER NO. ISS ADJACENT TO
C     REGION IR
     IAST=IAS(IR,ISS)
C     IDST IS THE ID NO. OF THE SURFACE CONTAINING SURF SEG WITH ID NO. IAST
     IDST=IDS(IAST)
C     ITPT IS THE TYPE NO. OF SURFACE WITH ID NO. IDST
     ITPT=ITP(IDST)
     IF (IRT.EQ.0) GO TO 511
     IF(IREF.EQ.1.AND.ISSF.NE.ISS)GO TO 511
     NASTT=NAS(IRT)
     DO 512 ISS1=1,NASTT
     IAST2=IAS(IRT,ISS1)
     IF (IDST.NE.IDS(IAST2)) GO TO 512
     IF(IDEC(IDST).EQ.1)GO TO 513
     D1(IDST)=D1(IDST)-DT
     D2(IDST)=D2(IDST)-DT
     IDEC(IDST)=1
     IF(KTRA.NE.1) GO TO 3334
     IF(IST.LT.IST1.OR.IST.GT.IST2) GO TO 3334
     PRINT 3333,IAST2
3333 FORMAT(1H ,' GO TO 513 FROM DO 512 LOOP FOR SS IAST2=',I6)
3334 CONTINUE
     GO TO 513
 512 CONTINUE
 511 D1(IDST)=0.
     D2(IDST)=0.
     GO TO (501,502,503,504,506                          ),ITPT
C     PLANE SURFACE WITH NORMAL (AS,BS,CS) AND WITH CLOSEST DISTANCE TO
C     ORIGIN DS/SQRT(AS**2+BS**2+CS**2)
 501 A1=AS(IDST)*UX+BS(IDST)*UY+CS(IDST)*UZ
     IF (ABS(A1).LT.1.E-20) GO TO 598
     B1=DS(IDST)-AS(IDST)*X-BS(IDST)*Y-CS(IDST)*Z
     C1=0.
     D1(IDST)=B1/A1
     IF (D1(IDST).LE.0.0) GO TO 598
     DTRY=D1(IDST)
```

```
      NPRT=1
      GO TO 520
C     SPHERE OF RADIUS DS CENTERED AT (AS,BS,CS)
 502 A1=1.
      B1=(X-AS(IDST))*UX+(Y-BS(IDST))*UY+(Z-CS(IDST))*UZ
      C1=(X-AS(IDST))**2+(Y-BS(IDST))**2+(Z-CS(IDST))**2-DS(IDST)**2
      GO TO 510
C     CIRCULAR CYLINDER OF RADIUS GS WITH AXIS PASSING THRU (AS,BS,CS) IN
C          DIRECTION (DS,ES,FS).  NOTE (DS,ES,FS) WAS NORMALIZED IN INITIALIZE
 503 V2=UX*DS(IDST)+UY*ES(IDST)+UZ*FS(IDST)
      V3=(X-AS(IDST))*UX+(Y-BS(IDST))*UY+(Z-CS(IDST))*UZ
      V4=(X-AS(IDST))**2+(Y-BS(IDST))**2+(Z-CS(IDST))**2
      V5=(X-AS(IDST))*DS(IDST)+(Y-BS(IDST))*ES(IDST)+(Z-CS(IDST))*
     1FS(IDST)
      A1=1.-V2**2
      B1=V3-V5*V2
      C1=V4-V5**2-GS(IDST)**2
      GO TO 510
C     ELLIPSOID CENTERED AT (AS,BS,CS) WITH AXES PARALLEL TO X,Y,Z AXES WITH
C          RADII DS,ES,FS, RESPECTIVELY.  THEN IN INITIALIZE DS,ES,FS ARE
C          REPLACED BY THEIR RECIPROCALS SQUARED
 504 A1=UX**2*DS(IDST)+UY**2*ES(IDST)+UZ**2*FS(IDST)
      B1=UX*(X-AS(IDST))*DS(IDST)+UY*(Y-BS(IDST))*ES(IDST)
     1+UZ*(Z-CS(IDST))*FS(IDST)
      C1=(X-AS(IDST))**2*DS(IDST)+(Y-BS(IDST))**2*ES(IDST)
     1+(Z-CS(IDST))**2*FS(IDST)-1.
      GO TO 510
C     CONE WITH APEX AT (AS,BS,CS) AND AXIS PARALLEL TO (DS,ES,FS) WITH
C          OPENING ANGLE 2.*GS.  NOTE (DS,ES,FS) WAS NORMALIZED AND (COSGS)**2
C          WAS STORED IN GS IN INITIALIZE
 506 V2=UX*DS(IDST)+UY*ES(IDST)+UZ*FS(IDST)
      V3=(X-AS(IDST))*UX+(Y-BS(IDST))*UY+(Z-CS(IDST))*UZ
      V4=(X-AS(IDST))**2+(Y-BS(IDST))**2+(Z-CS(IDST))**2
      V5=(X-AS(IDST))*DS(IDST)+(Y-BS(IDST))*ES(IDST)+(Z-CS(IDST))*
     1FS(IDST)
      A1=V2**2-GS(IDST)
      B1=V2*V5-GS(IDST)*V3
      C1=V5**2-GS(IDST)*V4
 510 B2=B1**2-A1*C1
C     ARE THE DISTANCE ROOTS COMPLEX
      IF (B2.LT.0.0) GO TO 598
      B3=SQRT(B2)
      IF (ABS(A1).LT.1.E-20) GO TO 598
      A1I=1./A1
      D1(IDST)=(-B1+B3)*A1I
      D2(IDST)=(-B1-B3)*A1I
 513 CONTINUE
C
C     ARE THE DISTANCE ROOTS BOTH NEGATIVE
      IF (D1(IDST).LE.0.0) GO TO 598
      DTRY=D2(IDST)
      NPRT=2
      IF (DTRY.LE.0.0) GO TO 519
      GO TO 520
 519 DTRY=D1(IDST)
      NPRT=1
 520 IF (DTRY.GT.D) GO TO 598
      NERT=1
 598 CONTINUE
C
```

```
C     TRACKING PRINT E
      IF(KTRA.NE.1) GO TO 1041
      IF(IST.LT.IST1.OR.IST.GT.IST2) GO TO 1041
      PRINT1030,IST,IHIT,IR,IRT,IDST,ITPT,ISS,IAST
      PRINT1040,A1,B1,C1,D1(IDST),D2(IDST),D
 1041 CONTINUE
      IF (NERT.EQ.1) GO TO 597
      GO TO 500
  597 CONTINUE
C
C      IF THIS POINT IS REACHED THEN WE HAVE A CANTIDATE DTRY FOR THE SHORTEST
C      FLIGHT TO A SURFACE SEGMENT ADJACENT TO REGION IR. NOW TEST SENSES TO
C      FIND IF R+DTRY*U IS ACTUALLY IN THE SURFACE SEGMENT WITH ID IAST.
      IF (NSEN(IAST).EQ.0) GO TO 550
      X1=X+DTRY*UX
      Y1=Y+DTRY*UY
      Z1=Z+DTRY*UZ
      NSENT=NSEN(IAST)
      DO 530 IS1=1,NSENT
      IDENT=IDEN(IAST,IS1)
      ITPT=ITP(IDENT)
      GO TO (531,532,533,534,535                          ),ITPT
  531 SENSE=AS(IDENT)*X1+BS(IDENT)*Y1+CS(IDENT)*Z1-DS(IDENT)
      GO TO 540
  532 SENSE=(X1-AS(IDENT))**2+(Y1-BS(IDENT))**2+(Z1-CS(IDENT))**2
     1-DS(IDENT)**2
      GO TO 540
  533 V4=(X1-AS(IDENT))**2+(Y1-BS(IDENT))**2+(Z1-CS(IDENT))**2
      V5=(X1-AS(IDENT))*DS(IDENT)+(Y1-BS(IDENT))*ES(IDENT)
     1+(Z1-CS(IDENT))*FS(IDENT)
      SENSE=V4-V5**2-GS(IDENT)**2
      GO TO 540
  534 SENSE=(X1-AS(IDENT))**2*DS(IDENT)    +(Y1-BS(IDENT))**2*
     1ES(IDENT)    +(Z1-CS(IDENT))**2*FS(IDENT)    -1.
      GO TO 540
  535 V4=(X1-AS(IDENT))**2+(Y1-BS(IDENT))**2+(Z1-CS(IDENT))**2
      V5=(X1-AS(IDENT))*DS(IDENT)+(Y1-BS(IDENT))*ES(IDENT)
     1+(Z1-CS(IDENT))*FS(IDENT)
      SENSE=V5**2-GS(IDENT)**2*V4
  540 JSEN=1
      IF (SENSE.LT.0.0) JSEN=-1
C
C     TRACKING PRINT F
      IF (KTRA.NE.1) GO TO 1061
      IF (IST.LT.IST1.OR.IST.GT.IST2) GO TO 1061
      PRINT 1060,X1,Y1,Z1,DTRY,D,SENSE
      PRINT 1050,IDENT,ITPT,JSEN,ISEN(IAST,IS1)
 1061 CONTINUE
C
      IF (ISEN(IAST,IS1)+JSEN.EQ.0) GO TO 541
C     THIS SENSE TEST HAS BEEN PASSED
      GO TO 530
C     THIS SENSE TEST HAS BEEN FAILED
  541 IF (NPRT.EQ.1) GO TO 500
      DTRY=D1(IDST)
      NPRT=1
      NERT=0
      GO TO 520
  530 CONTINUE
C     ALL TESTS HAVE BEEN PASSED SO IHIT IS THE ID NUMBER OF THE CLOSEST STRUCK
```

```
C     SURFACE SEGMENT OF THOSE YET TESTED
 550 IHIT=IAST
     ISST=ISS
     DTT=D-DTRY
     D=DTRY
 500 CONTINUE
C
C     IS COLLISION IN IR OR IS SURFACE SEGMENT IHIT HIT
     IF (IHIT.GT.0) GO TO 700
C
C     COLLISION STILL IN REGION IR
     NCOL=NCOL+1
     NCOLH=NCOLH+1
     IRT=0
     T=T+D*V(IG)
     IT=2.+(T-OFFSET)*DELT1I
     IF (IT.GT.ITB1) IT=ITB1+1.+(T-OFFSET-DELT1*(ITB1-1))*DELT2I
     IF(T.LT.OFFSET)IT=1
     IF (IT.GT.NT   ) GO TO 209
     X=X+D*UX
     Y=Y+D*UY
     Z=Z+D*UZ
     IF(KMUL.EQ.1.AND.IB.LE.ISKIP)GO TO 65
     IGM=IG-NGMI+1
     DO 64 ITALY=1,NTALR
     IF (IR.NE.ITALR(ITALY)) GO TO 64
     WIR(IT,ITALY,IGM)=WIR(IT,ITALY,IGM)+W
     WIRS(IT,ITALY,IGM)=WIRS(IT,ITALY,IGM)+W
     WIRL(IT,ITALY,IGM)=WIRL(IT,ITALY,IGM)+W*D
     WIRLS(IT,ITALY,IGM)=WIRLS(IT,ITALY,IGM)+W*D
  64 CONTINUE
  65 IF(NTPDEL.EQ.0) GO TO 67
     DO 66 ITPDEL=1,NTPDEL
     WDEL(ITPDEL)=WDEL(ITPDEL)+W*DELPC(ITPDEL,IG,IMIXT)
  66 CONTINUE
  67 W=W*CM(1,IG,IMIXT)
     UXT=UX
     UYT=UY
     UZT=UZ
     IGT=IG
C
C     THIS SECTION IS FOR THE SELECTION OF AN EIGEN-SOURCE DISTRIBUTION
C     AND IS PASSED IF A SOURCE SPECIFIED TRANSPORT PROBLEM IS DONE
C
 600 IF(KMUL.EQ.0) GO TO 61
     IF(CM(2,IG,IMIXT).EQ.0.)GO TO 630
     WFIS=W*CM(2,IG,IMIXT)
     TWFIS=TWFIS+W*CM(2,IG,IMIXT)
     TWFISS=TWFISS+W*CM(2,IG,IMIXT)
     IF(WFIS.GT.AKBAR)GO TO 617
 614 CALL GGUBS(NKRN,1,FRN)
     WFT=WFIS/AKBAR
     IF(FRN.GT.WFT)GO TO 630
 617 IFIST=IFIST+1
     IF(IBK.EQ.0)GO TO 620
C     IF BANK IS FILLED REPLACE FISSION SITES RANDOMLY
     CALL GGUBS(NKRN,1,FRN)
     FST=NS*FRN+1
     ISTR=IFIX(FST)
     WFIST=WFIST-WSTR(ISTR)
```

```
 620 XSTR(ISTR)=X
     YSTR(ISTR)=Y
     ZSTR(ISTR)=Z
     IRSTR(ISTR)=IR
     WSTR(ISTR)=AKBAR
     WFIST=WFIST+WSTR(ISTR)
     IF(ISTR.EQ.NS)IBK=1
     IF(IBK.EQ.0)ISTR=ISTR+1
     IF(WFIS.LT.AKBAR)WFIS=0.
     IF(WFIS.GT.AKBAR)WFIS=WFIS-AKBAR
     IF(WFIS.GT.AKBAR)GO TO 617
     IF(WFIS.GT.0.)GO TO 614
 630 W=W*(1.-CM(2,IG,IMIXT))
     GO TO 640
C      SELECT SCATTERING OR FISSION BRANCH FOR SOURCE SPECIFIED PROBLEM
C
  61 CALL GGUBS(NKRN,1,FRN)
     IF (FRN.LT.CM(2,IG,IMIXT)) GO TO 68
C
C      THE EMERGENT PARTICLE IS PROMPT AND SCATTERED
 640 CONTINUE
     CALL GGUBS(NKRN,1,FRN)
     DO 59 IP=4,NP
     IF (FRN.LT.ABS(CM(IP,IG,IMIXT))) GO TO 75
  59 CONTINUE
     IP=NP
  75 IG=IGMIN(IG)+IP-4
C
     IF (IG.GT.NGMA) GO TO 3044
C
     C=1.
     IP=IP-3
C
     IF(KAN.EQ.0) GO TO 646
C
C  EQUIPROBABLE ANGLE SCATTERING METHOD
C
 641 CALL GGUBS(NKRN,1,FRN)
     IF(FRN.LT..25) GO TO 642
     IF(FRN.LT..50) GO TO 643
     IF(FRN.LT..75) GO TO 644
     CSA=CM3(IP,IGT,IMIXT)+(FRN-.75)*4.*(1.-CM3(IP,IGT,IMIXT))
     GO TO 645
 642 CSA=-1.+FRN*4.*(CM1(IP,IGT,IMIXT)+1.)
     GO TO 645
 643 CSA=CM1(IP,IGT,IMIXT)+(FRN-.25)*4.*(CM2(IP,IGT,IMIXT)-
    *CM1(IP,IGT,IMIXT))
     GO TO 645
 644 CSA=CM2(IP,IGT,IMIXT)+(FRN-.50)*4.*(CM3(IP,IGT,IMIXT)-
    *CM2(IP,IGT,IMIXT))
 645 CONTINUE
     IF (KTRA.NE.1) GO TO 3399
     IF (IST.LT.IST1.OR.IST.GT.IST2) GO TO 3399
     PRINT 3388,IG,FRN,CSA
3388 FORMAT(1H ,' COLLI. TO GROUP IG=',I6,'  FRN FOR EASM= ',E12.5,
    *'  CSA=  ',E12.5)
3399 CONTINUE
     CALL ACHG(UX,UY,UZ,CSA,NKRN)
     GO TO 63
 646 CONTINUE
```

```
      CALL ISODIR(UX,UY,UZ,NKRN)
      COSCAT=UX*UXT+UY*UYT+UZ*UZT
      IF (NSCAT.LT.1) GO TO 63
      GO TO (76,77,78),NSCAT
   76 C=1.+COSCAT*CM1(IP,IGT,IMIXT)
      GO TO 63
   77 C=1.+COSCAT*CM1(IP,IGT,IMIXT)+(COSCAT**2-.3333333)
     1*CM2(IP,IGT,IMIXT)
      GO TO 63
   78 C=1.+COSCAT*CM1(IP,IGT,IMIXT)+(COSCAT**2-.3333333)
     1*CM2(IP,IGT,IMIXT)+COSCAT**3*CM3(IP,IGT,IMIXT)
      W=W*SIGN(1.,CM(IP+3,IGT,IMIXT))
      W=W*C
      GO TO 63
C
C     THE EMERGENT PARTICLE IS PROMPT AND ISOTROPIC FROM FISSION
   68 CALL GGUBS(NKRN,1,FRN)
      DO 69 IG1=1,NG
      IF (FRN.LT.CHIP(IG1)) GO TO 70
   69 CONTINUE
   70 IG=IG1
      C=1.
      CALL ISODIR(UX,UY,UZ,NKRN)
   63 CONTINUE
C
C     TRACKING PRINT G
      IF (KTRA.NE.1) GO TO 1091
      IF (IST.LT.IST1.OR.IST.GT.IST2) GO TO 1091
      PRINT1080,NCOL,NCOLH,IR,IG,IMIXT
      PRINT1090,X,Y,Z,UX,UY,UZ,W
 1091 CONTINUE
C
C     DELAYED PARTICLE TREATMENT
      IF (NTPDEL.EQ.0) GO TO 213
      DO 214 ITPDEL=1,NTPDEL
      IF (WDEL(ITPDEL).LT.WDELF) GO TO 214
  212 IF (ISPL.GT.199) GO TO 120
      NDEL=NDEL+1
      ISPL=ISPL+1
      ISPLC=ISPLC+1
      CALL GGUBS(NKRN,1,FRN)
      T=T-TD(ITPDEL)*ALOG(FRN)
      TSPL(ISPL)=T
      WSPL(ISPL)=WDEL(ITPDEL)
      WDEL(ITPDEL)=0.
      CALL GGUBS(NKRN,1,FRN)
      DO 215 IG1=1,NG
      IF (FRN.LT.CHID(ITPDEL,IG1)) GO TO 216
  215 CONTINUE
  216 IGSPL(ISPL)=IG1
      XSPL(ISPL)=X
      YSPL(ISPL)=Y
      ZSPL(ISPL)=Z
      UXSPL(ISPL)=UX
      UYSPL(ISPL)=UY
      UZSPL(ISPL)=UZ
      IRSPL(ISPL)=IR
  214 CONTINUE
C
  213 IF (ABS(W).GT.WCO) GO TO 211
```

```
      IF(NOR.EQ.1)GO TO 72
C
C      SUM OF KILLED WEIGHTS OPTION
C      KILL PARTICLE IF ITS WEIGHT W IS LESS THAN WCO AND IF THE CUMULATIVE
C      WEIGHT WCOC OF PREVIOSLY KILLED PARTICLES IS LESS THAN WCOCF.  NOTE
C      THAT WCOCF      MAY BE GREATER OR LESS THAN WSPLT.
      WCOC=WCOC+W
      IF (ABS(WCOC).LT.WCOCF) GO TO 209
      W=WCOC
      WCOC=0.
      GO TO 211
   72 CONTINUE
C
C      RUSSIAN ROULLETE OPTION TO KILL PARTICLE
      CALL GGUBS(NKRN,1,FRN)
      WTT=W/WCOCF
      IF(FRN.GT.WTT)GO TO 209
      W=WCOCF
C
C      SPLITTING GOES HERE OF FORM  IF(      )GO TO 210
C      SPLIT PARTICLE IF ITS WEIGHT W EXCEEDS WSPLT
  211 IF (ABS(W).LT.WSPLT) GO TO 507
  210 IF  (ISPL .GT.  49)  GO TO 120
      ISPL=ISPL+1
      ISPLC=ISPLC+1
      XSPL(ISPL)=X
      YSPL(ISPL)=Y
      ZSPL(ISPL)=Z
      UXSPL(ISPL)=UX
      UYSPL(ISPL)=UY
      UZSPL(ISPL)=UZ
      TSPL(ISPL)=T
      IRSPL(ISPL)=IR
      IGSPL(ISPL)=IG
      WSPL(ISPL)=W*.5
      W=W*.5
      GO TO 507
  120 ISPLO=ISPLO+1
      GO TO 507
C
C      HIT SURFACE SEGMENT WITH ID NUMBER IHIT AND ORDER NUMBER ISST OF THOSE
C      BOUNDING REGION IR
  700 T=T+D*V(IG)
      IT=2.+(T-OFFSET)*DELT1I
      IF (IT.GT.ITB1) IT=ITB1+1.+(T-OFFSET-DELT1*(ITB1-1))*DELT2I
      IF (IT.GT.NT   ) GO TO 209
      XT=X
      YT=Y
      ZT=Z
      IRT=IR
      DT=D
C      MOVE INTO NEW REGION
      IR=IAR(IR,ISST)
      X=X+D*UX
      Y=Y+D*UY
      Z=Z+D*UZ
C
C      TRACKING PRINT H
      IF (KTRA.NE.1) GO TO 1121
      IF (IST.LT.IST1.OR.IST.GT.IST2) GO TO 1121
```

```
      PRINT1110,IR,IRT,IG,IHIT,ISST
1110 FORMAT(1H ,10H H IR,IRT=,2I3,4H IG=,I3,6H IHIT=,I3,6H ISST=,I3)
      PRINT1120,X,Y,Z,UX,UY,UZ,D,W
1120 FORMAT(1H ,7H X,Y,Z=,3E12.5,10H UX,UY,UZ=,3E12.5,3H D=,E12.5,3H W=
    1,E12.5)
1121 CONTINUE
C     TALLY PATH LENGTH
      DO 7300 ITALY=1,NTALR
      IGM=IG-NGMI+1
      IF (IRT.NE.ITALR(ITALY)) GO TO 7301
      WIRL(IT,ITALY,IGM)=WIRL(IT,ITALY,IGM)+W*D
      WIRLS(IT,ITALY,IGM)=WIRLS(IT,ITALY,IGM)+W*D
7301 CONTINUE
7300 CONTINUE
      IF (NTALSS.EQ.0) GO TO 7400
C     TALLY A SURFACE CROSSING
      IF(KMUL.EQ.1.AND.IB.LE.ISKIP)GO TO 740
      DO 730 ITALY=1,NTALSS
      IF (IHIT.NE.ITALSS(ITALY)) GO TO 730
      IF (IR.GE.IRT) GO TO 710
      WISN(IT,ITALY,IGM)=WISN(IT,ITALY,IGM) +W
      WISNS(IT,ITALY,IGM)=WISNS(IT,ITALY,IGM)+W
      GO TO 730
 710 WISP(IT,ITALY,IGM)=WISP(IT,ITALY,IGM) +W
      WISPS(IT,ITALY,IGM)=WISPS(IT,ITALY,IGM)+W
      IF (IR.GT.NREG)GO TO 209
 730 CONTINUE
7400 CONTINUE
 740 IF (IR.GT.NREG)GO TO 209
C
C     SPLIT OR RUSSIAN ROULETTE ON IMPORTANCE OF REGIONS
C
      IF(KIMP.EQ.0)GO TO 507
      RIMT=RIM(IR)/RIM(IRT)
      IF(RIMT.GT.RIMU)GO TO 750
      IF(RIMT.GT.RIML)GO TO 507
      CALL GGUBS(NKRN,1,FRN)
      IF(FRN.GT.RIMT)GO TO 209
      W=W/RIMT
      GO TO 507
 750 IF  (ISPL .GT.  49)  GO TO 120
      ISPL=ISPL+1
      ISPLC=ISPLC+1
      XSPL(ISPL)=X
      YSPL(ISPL)=Y
      ZSPL(ISPL)=Z
      UXSPL(ISPL)=UX
      UYSPL(ISPL)=UY
      UZSPL(ISPL)=UZ
      TSPL(ISPL)=T
      IRSPL(ISPL)=IR
      IGSPL(ISPL)=IG
      WSPL(ISPL)=W*.5
      W=W*.5
      GO TO 507
C
3044 NDOPE=NDOPE+1
      IF (KTRA.NE.1) GO TO 4044
      IF (IST.LT.IST1.OR.IST.GT.IST2) GO TO 4044
      PRINT 4000,NGMA
```

```
4044 CONTINUE
C
C     DEPLETE BANK
 209 IF(ISPL.LT.1)GO TO 99
     X=XSPL(ISPL)
     Y=YSPL(ISPL)
     Z=ZSPL(ISPL)
     UX=UXSPL(ISPL)
     UY=UYSPL(ISPL)
     UZ=UZSPL(ISPL)
     T=TSPL(ISPL)
     W=WSPL(ISPL)
     IR=IRSPL(ISPL)
     IG=IGSPL(ISPL)
     ISPL=ISPL-1
     IRT=0
     GO TO 507
  99 CONTINUE
     IF(KMUL.EQ.1.AND.IB.LE.ISKIP)GO TO 106
C
C     INCREMENT VARIANCE ESTIMATORS
     DO 104 IT=1,NT
     DO 104 IG=1,NGMM
     IF(NTALR.EQ.0) GO TO 100
     DO 101 ITALY=1,NTALR
     WIRV(IT,ITALY,IG)=WIRV(IT,ITALY,IG)+WIRS(IT,ITALY,IG)**2
     WIRLV(IT,ITALY,IG)=WIRLV(IT,ITALY,IG)+WIRLS(IT,ITALY,IG)**2
 101 CONTINUE
 100 CONTINUE
     IF(NTALSS.EQ.0)GO TO 102
     DO 103 ITALY=1,NTALSS
     WISNV(IT,ITALY,IG)=WISNV(IT,ITALY,IG)+WISNS(IT,ITALY,IG)**2
     WISPV(IT,ITALY,IG)=WISPV(IT,ITALY,IG)+WISPS(IT,ITALY,IG)**2
 103 CONTINUE
 102 CONTINUE
     IF(NIT.EQ.0) GO TO 104
     DO 105 IW=1,NIT
     WITV(IT,IW)=WITV(IT,IW)+WITS(IT,IW)**2
 105 CONTINUE
 104 CONTINUE
 106 CONTINUE
     IF(KMUL.EQ.0)GO TO 44
     TWFISV=TWFISV+TWFISS**2
  44 CONTINUE
C
C     PRINT RESULTS
C
     IF(NSTAD.NE.0) GO TO 8110
     IF(ISPLO.GT.0)PRINT 123,ISPLO
     IF(KMUL.EQ.0)PRINT 126,NKRNT
C
     PRINT 4001,NGMA,NDOPE
C
C     CALCULATION OF EIGENVALUE, KEFF, THIS SECTION IS PASSED IF SOURCE
C     SPECIFIED TRANSPORT PROBLEM IS DONE
C
8110 CONTINUE
     IF(KMUL.EQ.0)GO TO 695
     EIGEN=TWFIS/NS
     TWFISV=(TWFISV/NS-EIGEN**2)/(NS-1)
```

```
      TWFISV=SQRT(TWFISV)
      IF(IB.LE.ISKIP)GO TO 654
      TE=TE+EIGEN
      TES=TES+EIGEN**2
      AEIGEN=TE/(IB-ISKIP)
      ISKIP1=ISKIP+1
      IF(IB.LE.ISKIP1)GO TO 654
      VEIGEN=(TES/(IB-ISKIP)-AEIGEN**2)/(IB-ISKIP-1)
      VEIGEN=SQRT(VEIGEN)
  654 CONTINUE
      PRINT650,IB,EIGEN,TWFISV,IFIST,AEIGEN,VEIGEN
C
C       STORE FISSION SITES FOR NEXT GENERATION INSOURCE STORAGE AND
C       NORMALIZE TOTAL FISSION WEIGHT TO NS
C
      NSTR=ISTR-1
      IF(IBK.EQ.1)NSTR=NS
      DO 655 ISTR=1,NSTR
      XST(ISTR)=XSTR(ISTR)
      YST(ISTR)=YSTR(ISTR)
      ZST(ISTR)=ZSTR(ISTR)
      IRST(ISTR)=IRSTR(ISTR)
  655 WST(ISTR)=WSTR(ISTR)*NS/WFIST
C
C       IF BANK IS NOT FILLED SPLIT PARTICLES RANDOMLY
C
      IF(IBK.EQ.1)GO TO 680
      NSTR1=NSTR+1
      DO 675 III=NSTR1,NS
      CALL GGUBS(NKRN,1,FRN)
      FST=NSTR*FRN
      IST=IFIX(FST)
      IF(IST.EQ.0)IST=1
      WST(IST)=WST(IST)/2.
      XST(III)=XST(IST)
      YST(III)=YST(IST)
      ZST(III)=ZST(IST)
      IRST(III)=IRST(IST)
  675 WST(III)=WST(IST)
  680 CONTINUE
  695 CONTINUE
      IF(KMUL.EQ.1.AND.IB.LT.MORE)GO TO 86
      DO 85 IT=1,NT
      IF(NSTAD.NE.0) GO TO 8111
      IF(KMUL.EQ.0)PRINT121,IT,TB(IT)
  121 FORMAT (/10X,27H RESULTS FOR TIME INTERVAL ,I6,13H  TO TB(IT)= ,
     1E12.6)
 8111 CONTINUE
      IF(KMUL.EQ.0)RNSI=NS
      IF(KMUL.EQ.1)RNSI=NS*(MORE-ISKIP)
C
      DO 83 ITALY=1,NTALR
      IM=IMIX(ITALR(ITALY))
      DO 151 IG=1,NGMM
      WIR(IT,ITALY,IG)=WIR(IT,ITALY,IG)/RNSI
      WIRV(IT,ITALY,IG)=WIRV(IT,ITALY,IG)/RNSI
      WIRV(IT,ITALY,IG)=(WIRV(IT,ITALY,IG)-WIR(IT,ITALY,IG)**2)/(RNSI-1)
      WIRV(IT,ITALY,IG)=ABS(SQRT(WIRV(IT,ITALY,IG)))
      WIRL(IT,ITALY,IG)=WIRL(IT,ITALY,IG)/RNSI
      WIRLV(IT,ITALY,IG)=WIRLV(IT,ITALY,IG)/RNSI
```

```
      WIRLV(IT,ITALY,IG)=(WIRLV(IT,ITALY,IG)-WIRL(IT,ITALY,IG)**2)/
     *(RNSI-1)
      WIRLV(IT,ITALY,IG)=ABS(SQRT(WIRLV(IT,ITALY,IG)))
      IGM=IG+NGMI-1
      WIRL(IT,ITALY,IG)=WIRL(IT,ITALY,IG)/CM(3,IGM,IM)
      WIRLV(IT,ITALY,IG)=WIRLV(IT,ITALY,IG)/CM(3,IGM,IM)
  151 CONTINUE
      IF(NSTAD.NE.0) GO TO 833
      PRINT122,ITALR(ITALY)
      PRINT 2888,(IG,WIR(IT,ITALY,IG),WIRV(IT,ITALY,IG),WIRL(IT,ITALY,
     *IG),WIRLV(IT,ITALY,IG),IG=1,NGMM)
  833 IF (NSTAD.EQ.0) GO TO 83
      WRITE(8,4002) ITALR(ITALY),(IG,WIR(IT,ITALY,IG),WIRV(IT,ITALY,IG),
     *WIRL(IT,ITALY,IG),WIRLV(IT,ITALY,IG),IG=1,NGMM)
   83 CONTINUE
      IF (NTALSS.EQ.0) GO TO 8100
      DO 81 ITALY=1,NTALSS
      DO 152 IG=1,NGMM
      WISP(IT,ITALY,IG)=WISP(IT,ITALY,IG)/RNSI
      WISPV(IT,ITALY,IG)=WISPV(IT,ITALY,IG)/RNSI
      WISPV(IT,ITALY,IG)=(WISPV(IT,ITALY,IG)-WISP(IT,ITALY,IG)**2)
     1/(RNSI-1)
      WISPV(IT,ITALY,IG)=ABS(SQRT(WISPV(IT,ITALY,IG)))
      WISN(IT,ITALY,IG)=WISN(IT,ITALY,IG)/RNSI
      WISNV(IT,ITALY,IG)=WISNV(IT,ITALY,IG)/RNSI
      WISNV(IT,ITALY,IG)=(WISNV(IT,ITALY,IG)-WISN(IT,ITALY,IG)**2)
     1/(RNSI-1)
      WISNV(IT,ITALY,IG)=ABS(SQRT(WISNV(IT,ITALY,IG)))
  152 CONTINUE
      IF(NSTAD.NE.0) GO TO 811
      PRINT 124,ITALSS(ITALY)
      PRINT 28,(IG,WISP(IT,ITALY,IG),WISPV(IT,ITALY,IG),IG=1,NGMM)
      PRINT 125, ITALSS(ITALY)
      PRINT 28,(IG,WISN(IT,ITALY,IG),WISNV(IT,ITALY,IG),IG=1,NGMM)
  811 IF(NSTAD.EQ.0.) GO TO 81
      WRITE(8,4002) ITALSS(ITALY),(IG,WISP(IT,ITALY,IG),WISPV(IT,ITALY,I
     *G),WISN(IT,ITALY,IG),WISNV(IT,ITALY,IG),IG=1,NGMM)
   81 CONTINUE
 8100 CONTINUE
      IF (NIT.EQ.0) GO TO 85
      DO 153 IW=1,NIT
      WIT(IT,IW)=WIT(IT,IW)/RNSI
      WITV(IT,IW)=WITV(IT,IW)/RNSI
      WITV(IT,IW)=(WITV(IT,IW)-WIT(IT,IW)**2)/(RNSI-1)
      WITV(IT,IW)=ABS(SQRT(WITV(IT,IW)))
  153 CONTINUE
      PRINT 127
      PRINT 21,(WIT(IT,IW),WITV(IT,IW),IW=1,NIT)
   85 CONTINUE
      NHS=NS+ISPLC
      IF(NSTAD.NE.0) GO TO 822
      PRINT 128
      PRINT 22,NS ,ISPLC,ISPLO,NHS,NCOL,NDEL,NDOPE,NESCA
  822 IF (NSTAD.EQ.1) WRITE(8,22) NS,ISPLC,ISPLO,NHS,NCOL,NDEL,NDOPE,
     *NESCA
      IF(NTPDEL.EQ.0)GO TO 139
      PRINT 130
      PRINT 21,(WDEL(ITPDEL),ITPDEL=1,NTPDEL)
   86 CONTINUE
C
```

```
C      COMPUTE AND PRINT SUMS
C
  139 IF (NSUM.EQ.0) GO TO 140
      DO 141 ISUM=1,NSUM
      IF (IRORS(ISUM).EQ.0) GO TO 142
      ITALYT=ISUMTY(ISUM)
      ITALRT=ITALR(ITALYT)
      IMIXT=IMIX(ITALRT)
      DO 143 IT=1,NT
      SUM(IT)=0.
      DO 143 IG=1,NG
      SUM(IT)=SUM(IT)+WIR (IT,ITALYT,IG)*CM(3,IG,IMIXT )*CSUM(ISUM,IG)
  143 CONTINUE
      PRINT 144,ISUM,ITALYT,ITALRT
      PRINT 145
      PRINT 21,(SUM(IT),IT=1,NT)
      GO TO 141
  142 ITALYT=ISUMTY(ISUM)
      ITALST=ITALSS(ITALYT)
      DO 146 IT=1,NT
      SUM(IT)=0.
      DO 146 IG=1,NG
      SUM(IT)=SUM(IT)+WISP(IT,ITALYT,IG)*CSUM(ISUM,IG)
  146 CONTINUE
      PRINT 147,ISUM,ITALYT,ITALST
      PRINT 148
      PRINT 21,(SUM(IT),IT=1,NT)
      DO 149 IT=1,NT
      SUM(IT)=0.
      DO 149 IG=1,NG
      SUM(IT)=SUM(IT)+WISN(IT,ITALYT,IG)*CSUM(ISUM,IG)
  149 CONTINUE
      PRINT 150
      PRINT 21,(SUM(IT),IT=1,NT)
  141 CONTINUE
  140 CONTINUE
C
C      BALANCE IN REGIONS TO CHECK THE GEOMETRY
      IF (NSTA.NE.1) GO TO 4399
      IT=1
      DO 4398 IG=1,NGMM
      DO 7890 IJ=1,NTALR
      II=ITALR(IJ)
      NAST=NAS(II)
      GOUT=0.
      GIN=0.
      DO 7891 JJ=1,NAST
      NIAS=IAS(II,JJ)
      NIAR=IAR(II,JJ)
      IF (NIAR.LT.II) GO TO 7892
      GIN=GIN+WISN(IT,NIAS,IG)
      GOUT=GOUT+WISP(IT,NIAS,IG)
      GO TO 7895
 7892 GIN=GIN+WISP(IT,NIAS,IG)
      GOUT=GOUT+WISN(IT,NIAS,IG)
 7895 CONTINUE
 7891 CONTINUE
      STORA=GIN-GOUT
      PRINT 7893,II,IG,GIN,GOUT,STORA
 7893 FORMAT(1H ,'  BALANCE IN REGION  ',I6, 'FOR GROUP',I4,' IN  OUT  S
     *TORA = ',3E12.5)
```

```
7890 CONTINUE
4398 CONTINUE
4399 CONTINUE
C
      NKRNT=NKRNT+2
   43 CONTINUE
      RETURN
      END
C
      SUBROUTINE ISODIR(UX,UY,UZ,NKRN)
      DOUBLE PRECISION NKRN
      CALL GGUBS(NKRN,1,FRN)
      UZ=2.*FRN-1.
   10 CALL GGUBS(NKRN,1,FRN)
      XU=FRN-.5
      CALL GGUBS(NKRN,1,FRN)
      YU=FRN-.5
      R2U=XU**2+YU**2
      IF(R2U.GT..25)GO TO 10
      XYU=SQRT((1.-UZ**2)/R2U)
      UX=XU*XYU
      UY=YU*XYU
      RETURN
      END
C
      SUBROUTINE ACHG(UX,UY,UZ,CSA,NKRN)
      DOUBLE PRECISION NKRN
      SSA=SQRT(1.-CSA*CSA)
  100 CALL GGUBS(NKRN,1,FRN)
      XA=2.*FRN-1.
      CALL GGUBS(NKRN,1,FRN)
      YA=2.*FRN-1.
      XY2=XA*XA+YA*YA
      IF(XY2.GE.1.) GO TO 100
      XY2=SQRT(XY2)
      CCA=XA/XY2
      SCA=YA/XY2
      SUZ=SQRT(1.-UZ*UZ)
      IF(SUZ.EQ.0.) GO TO 110
      CCH=UX/SUZ
      SCH=UY/SUZ
      GO TO 120
  110 CCH=0.
      SCH=1.
  120 UXT=CSA*UX+SSA*SCA*SCH-SSA*CCA*UZ*CCH
      UYT=CSA*UY-SSA*SCA*CCH-SSA*CCA*UZ*SCH
      UZT=CSA*UZ+SSA*CCA*SUZ
      UX=UXT
      UY=UYT
      UZ=UZT
      RETURN
      END
C
      FUNCTION SIGN(X,Y)
      IF (Y.GT.0.) GO TO 10
      IF (Y.LT.0.) GO TO 20
   10 SIGN =X
      GO TO 30
   20 SIGN =-X
   30 CONTINUE
      RETURN
      END
```

```
C
C ********* SUBROUTINE SOURCE ***********
C
C
C  THIS IS THE SOURCE SUBROUTINE USED FOR N-16 TAGGING OF SINGLE-
C  PHASE FLOW. THE OTHER SOURCES USED FOR N-16 TAGGING OF
C  1/2-STRATIFIED FLOW ARE AN IMAGE OR ROTATION OF THIS ONE.
C  THIS SOURCE SIMUTATES THE D-T SOURCES AT LOFT, BUT IT IS
C  ISOTROPIC AND SAMPLED TO  AVOID AS MUCH NEUTRON LEAKAGE
C  AS POSSIBLE FROM THE SYSTEM. (THEN, THE RESULTS FROM ANDYRPI ARE
C  CORRECTED FOR THE REAL SOURCE).
C  IT IS THEN, A SMALL DISK SOURCE OF 1.4 IN. DIA. LOCATED 2-IN FROM
C  THE PIPE WALL AND EMITTING NEUTRONS ISOTROPICALLY AT 84.2 DEGREES
C  (THE ORIGIN OF THE TOTAL TAGGING GEOMETRY WAS AT THE BASE AND ON
C  THE CENTRAL AXIS OF THE PIPE CYLINDER).
C
C
      SUBROUTINE SOURCE (X,Y,Z,UX,UY,UZ,IG,IR,W,CHIP,NKRN,NG)
      DIMENSION CHIP(40)
      DOUBLE PRECISION NKRN
C
C POSITION OF THE CENTER OF THE DISK
      R3=1.778
      ZS=50.
      R2=22.86
C  CHOOSE POSITION IN THE DISK SOURCE
      CALL GGUB (NKRN,1,FRN)
   10 X=R3-2.*R3*FRN
      CALL GGUB (NKRN,1,FRN)
C      Z=(ZS+R3)-2.*R3*FRN
C  SATISFY TO BE IN THE CIRCLE
      CIR=X*X+(Z-ZS)*(Z-ZS)
      IF (CIR.GT.(R3*R3)) GO TO 10
C  SATISFY TO BE AT THE ESTABLISH DISTANCE
      Y=R2
C  CHOOSE DIRECTION COSINES
   30 CALL GGUB (NKRN,1,FRN)
      UZ=2.*FRN-1.
   20 CALL GGUB (NKRN,1,FRN)
      XU=2.*FRN-1.
      CALL GGUB (NKRN,1,FRN)
      YU=-(1.-FRN*0.9)
      R2U=XU*XU+YU*YU
      IF (R2U.GT.1.) GO TO 20
      XYU=SQRT((1.-(UZ*UZ))/R2U)
      UX=XU*XYU
      UY=YU*XYU
C  SAMPLE TO SEE IF THE DIRECTION PROYECTS OUTSIDE THE INTERCEPTION
C  BETWEEN THE PLANE X-Z AND THE PIPE CYLINDER
      DI=-R2/UY
      XP=X+DI*UX
      ZP=Z+DI*UZ
      ZPP=ZP-50.
      ABX=ABS(XP)
      ABZ=ABS(ZPP)
      IF (ABX.GT.17.78.OR.ABZ.GT.50.) GO TO 30
C  FIRST ENERGY GROUP
      IG=1
C  FIRST REGION
      IR=1
C  WEIGTH ASSIGNED
      W=1.
      RETURN
      END
```

```
C
C          ******** PROGRAM: STATISTICS ********
C
C
C  THIS PROGRAM HANDLES THE STATISTICAL ANALYSIS OF THE MONTE CARLO
C  NEUTRON CALCULATION AT THE TAGGING POSITION FOR THE SPECIFIC
C  GEOMETRY USED
C  IT TAKES THE STORED RESULTS FROM THE BATCHES OF THE ANDYRPI RUN,
C  FINDS THE AVERAGED MEAN AND STANDARD DEVIATIONS FOR THE COLLISION
C  AND TRACK-LENGT ESTIMATORS FOR EACH REGION, THEN COUPLES BOTH
C  NEUTRON GROUP VALUES AND TRANSFORM THEM INTO SPECIFIC ACTIVITY
C  AT EACH TAGGED REGION, I.E. N-16/CM**3, PER PULSE.
C
C
C  VARIABLES
C
C   THE VARIABLES ARE NAMED THE SAME AS IN ANDYRPI, AND THE NEW ARE:
C
C  RNPP= SOURCE INTENSITY RNPP
C  CF=SOURCE CORRECTION FACTOR (COMBINATION OF BEING NON-ISOTROPIC
C     AND SAMPLED IN SUCH A WAY TO AVOID TOO MUCH LEAKAGE)
C  V1,V2 AND V3 ARE THE VOLUME REGIONS FOR THE AXIAL REGIONS
C  TVOL= TOTAL VOLUME OF THE PIPE
C  G(IG)=RATIO OF X-SECTION FOR (N,P) REACTION TO TOTAL X-SECTION
C        FOR ENERGY GROUP IG
C
C
C
      DIMENSION WIR(120,2,50),WIRV(120,2,50),WIRS(120,2),WIRVS(120,2),
     *WIRL(120,2,50),WIRLV(120,2,50),WILS(120,2),WILVS(120,2),
     *ISPLC(50),NHS(50),NCOL(50),WIRSS(120),WIRVV(120),G(2),
     *WILSS(120),WILVV(120),NDOPE(50),NESCA(50)
C     FORMATS
C
   12 FORMAT (13X,4E12.5,6X,4E12.5)
   13 FORMAT (10X,I9,9X,2I9,9X,2I9)
   14 FORMAT (10X,'WIR(IT,ITALY,IG),STAN. DEV.   ,WIRL(IT,ITALY,IG)',
     *'STAN.DEV. , IG=1,NGMA FOR REGION  ',I6)
   15 FORMAT (1H ,I4,2X,2E12.5,6X,2E12.5)
   16 FORMAT (1H ,6X,2E12.5,6X,2E12.5)
   18 FORMAT (12X,'ISPLC      NHS      NCOL      NDOPE      NESCA')
   19 FORMAT (7X,5F10.2)
   26 FORMAT ('COLL. ESTIMATOR',I5,2(I4,2X,2E12.5,2X),5X,2E12.5)
  260 FORMAT ('T.LEN.ESTIMATOR',I5,2(I4,2X,2E12.5,2X),5X,2E12.5)
   27 FORMAT (I4,2X,2E12.5,10X,2E12.5)
   28 FORMAT (14X,'REGION,GOUP, N-16/NEUTRON FOR EACH GROUP, TOTAL N',
     *'-16/NEUTRON')
   29 FORMAT ('TOTAL N-16/NEUTRON PRODUCTION FROM COLLISION &TRACK',
     *' LENGTH ESTIMATORS')
   31 FORMAT ('REGION, N-16/(CM**3)*PULSE AND  STANDARD DEVIATION',
     *' FROM COLLISION &TRACK LENGTH ESTIMATORS')
   32 FORMAT ('TOTAL N-16/(CM**3)*PULSE PRODUCTION FROM COLLISION',
     8'&TRACK LENGTH ESTIMATORS')
  130 FORMAT (1H ,'BATCH',I4,2X,5I9)
  330 FORMAT (1H )
  140 FORMAT (1H ,'BATCH,     IG: WIR, ST.D., WIRL, ST.D.,      IG: WIR, S
     *T.D., WIRL, ST.D. FOR REGION',I6)
  270 FORMAT (I4,2X,I4,2X,4E12.5,I4,2X,4E12.5)
C
      MORE=50
```

```
      NGMA=2
      NREG=119
      FMORE=FLOAT(MORE)
      SQMOR=SQRT(FMORE)
      CF=0.354*0.582
      RNPP=1.3*(10.**(10.))
      V1=792.8156
      V2=594.6117
      V3= 396.4078
      F1=CF*RNPP/V1
      F2=CF*RNPP/V2
      F3=CF*RNPP/V3
      G(1)=0.03775/3.052
      G(2)=0.023/3.17
      TVOL=32.*V1+32.*V2+48.*V3
C
C    INITIATE
       RCOL=0.
       RHS=0.
       RISPL=0.
       DOPE=0.
       ESCA=0.
       DO 200 K1=1,NREG
       DO 201 K2=1,NGMA
       WIRS(K1,K2)=0.
       WIRVS(K1,K2)=0.
       WILS(K1,K2)=0.
       WILVS(K1,K2)=0.
  201  CONTINUE
       WIRSS(K1)=0.
       WIRVV(K1)=0.
       WILSS(K1)=0.
       WILVV(K1)=0.
  200  CONTINUE
       WI=0.
       WIV=0.
       WIL=0.
       WILV=0.
C
C   READ THE RESULTS FROM ANDYRPI
C
       DO 10 I=1,MORE
       DO 20 J=1,NREG
       READ (8,12)(WIR(J,K,I),WIRV(J,K,I),WIRL(J,K,I),WIRLV(J,K,I),
     *K=1,NGMA)
   20  CONTINUE
       READ (8,13) ISPLC(I),NHS(I),NCOL(I),NDOPE(I),NESCA(I)
   10  CONTINUE
       WRITE(9,330)
       DO 1000 KM=1,NREG
       WRITE(9,140) KM
       DO 1001 MK=1,MORE

       WRITE(9,270) MK,(IG,WIR(KM,IG,MK),WIRV(KM,IG,MK),WIRL(KM,IG,MK),
     *WIRLV(KM,IG,MK),IG=1,NGMA)
 1001  CONTINUE
       WRITE(9,330)
 1000  CONTINUE
       WRITE(9,18)
       DO 2000 KK=1,MORE
```

```
      WRITE(9,130) KK,ISPLC(KK),NHS(KK),NCOL(KK),NDOPE(KK),NESCA(KK)
 2000 CONTINUE
      WRITE(9,330)
C
C CALCULATES THE AVERAGED VALUES
C
      DO 40 IJ=1,MORE
      RHS=RHS+NHS(IJ)
      RCOL=RCOL+NCOL(IJ)
      RISPL=RISPL+ISPLC(IJ)
      DOPE=DOPE+NDOPE(IJ)
      ESCA=ESCA+NESCA(IJ)
      DO 50 KL=1,NREG
      DO 60 LK=1,NGMA
      WIRS(KL,LK)=WIRS(KL,LK)+WIR(KL,LK,IJ)
      WIRVS(KL,LK)=WIRVS(KL,LK)+WIRV(KL,LK,IJ)*WIRV(KL,LK,IJ)
      WILS(KL,LK)=WILS(KL,LK)+WIRL(KL,LK,IJ)
      WILVS(KL,LK)=WILVS(KL,LK)+WIRLV(KL,LK,IJ)*WIRLV(KL,LK,IJ)
   60 CONTINUE
   50 CONTINUE
   40 CONTINUE
      RCOL=RCOL/MORE
      RHS=RHS/MORE
      RISPL=RISPL/MORE
      DOPE=DOPE/MORE
      ESCA=ESCA/MORE
      DO 90 I1=1,NREG
      WRITE(9,330)
      WRITE (9,14) I1
      DO 90 IG=1,NGMA
      WIRS(I1,IG)=WIRS(I1,IG)/MORE
      WIRVS(I1,IG)=WIRVS(I1,IG)/MORE
      WIRVS(I1,IG)=ABS(SQRT(WIRVS(I1,IG)))/SQMOR
      WILS(I1,IG)=WILS(I1,IG)/MORE
      WILVS(I1,IG)=WILVS(I1,IG)/MORE
      WILVS(I1,IG)=ABS(SQRT(WILVS(I1,IG)))/SQMOR
      WRITE(9,27) IG,WIRS(I1,IG),WIRVS(I1,IG),WILS(I1,IG),WILVS(I1,IG)
   90 CONTINUE
      WRITE (9,330)
      WRITE (9,18)
      WRITE (9,19) RISPL,RHS,RCOL,DOPE,ESCA
      WRITE (9,330)
      WRITE (9,28)
C
C  COUPLES BOTH GROUPS FOR LIQUID REGIONS
C
      DO 400 J1=3,114
      DO 500 J2=1,NGMA
      WIRS(J1,J2)=WIRS(J1,J2)*G(J2)
      WIRVS(J1,J2)=WIRVS(J1,J2)*G(J2)
      WIRSS(J1)=WIRSS(J1)+WIRS(J1,J2)
      WIRVV(J1)=WIRVV(J1)+WIRVS(J1,J2)*WIRVS(J1,J2)
      WILS(J1,J2)=WILS(J1,J2)*G(J2)
      WILVS(J1,J2)=WILVS(J1,J2)*G(J2)
      WILSS(J1)=WILSS(J1)+WILS(J1,J2)
      WILVV(J1)=WILVV(J1)+WILVS(J1,J2)*WILVS(J1,J2)
  500 CONTINUE
      WIRVV(J1)=ABS(SQRT(WIRVV(J1)))
      WILVV(J1)=ABS(SQRT(WILVV(J1)))
      WRITE(9,330)
```

```
      WRITE(9,26)J1,(J2,WIRS(J1,J2),WIRVS(J1,J2),J2=1,NGMA),WIRSS(J1),WI
     *RVV(J1)
      WRITE(9,260)J1,(J2,WILS(J1,J2),WILVS(J1,J2),J2=1,NGMA),WILSS(J1),
     *WILVV(J1)
      WI=WI+WIRSS(J1)
      WIV=WIV+WIRVV(J1)*WIRVV(J1)
      WIL=WIL+WILSS(J1)
      WILV=WILV+WILVV(J1)*WILVV(J1)
  400 CONTINUE
      WIV=ABS(SQRT(WIV))
      WILV=ABS(SQRT(WILV))
      WRITE (9,330)
      WRITE (9,29)
      WRITE (9,16) WI,WIV,WIL,WILV
C
C  FINDS N-16 SPECIFIC ACTIVITIES
C
      DO 510 L1=3,10
      WIRSS(L1)=WIRSS(L1)*F1
      WIRVV(L1)=WIRVV(L1)*F1
      WILSS(L1)=WILSS(L1)*F1
      WILVV(L1)=WILVV(L1)*F1
  510 CONTINUE
      DO 501 L1=11,18
      WIRSS(L1)=WIRSS(L1)*F2
      WIRVV(L1)=WIRVV(L1)*F2
      WILSS(L1)=WILSS(L1)*F2
      WILVV(L1)=WILVV(L1)*F2
  501 CONTINUE
      DO 502 L1=19,42
      WIRSS(L1)=WIRSS(L1)*F3
      WIRVV(L1)=WIRVV(L1)*F3
      WILSS(L1)=WILSS(L1)*F3
      WILVV(L1)=WILVV(L1)*F3
  502 CONTINUE
      DO 503 L1=43,50
      WIRSS(L1)=WIRSS(L1)*F2
      WIRVV(L1)=WIRVV(L1)*F2
      WILSS(L1)=WILSS(L1)*F2
      WILVV(L1)=WILVV(L1)*F2
  503 CONTINUE
      DO 504 L1=51,66
      WIRSS(L1)=WIRSS(L1)*F1
      WIRVV(L1)=WIRVV(L1)*F1
      WILSS(L1)=WILSS(L1)*F1
      WILVV(L1)=WILVV(L1)*F1
  504 CONTINUE
      DO 505 L1=67,74
      WIRSS(L1)=WIRSS(L1)*F2
      WIRVV(L1)=WIRVV(L1)*F2
      WILSS(L1)=WILSS(L1)*F2
      WILVV(L1)=WILVV(L1)*F2
  505 CONTINUE
      DO 506 L1=75,98
      WIRSS(L1)=WIRSS(L1)*F3
      WIRVV(L1)=WIRVV(L1)*F3
      WILSS(L1)=WILSS(L1)*F3
      WILVV(L1)=WILVV(L1)*F3
  506 CONTINUE
      DO 507 L1=99,106
```

```
      WIRSS(L1)=WIRSS(L1)*F2
      WIRVV(L1)=WIRVV(L1)*F2
      WILSS(L1)=WILSS(L1)*F2
      WILVV(L1)=WILVV(L1)*F2
  507 CONTINUE
      DO 508 L1=107,114
      WIRSS(L1)=WIRSS(L1)*F1
      WIRVV(L1)=WIRVV(L1)*F1
      WILSS(L1)=WILSS(L1)*F1
      WILVV(L1)=WILVV(L1)*F1
  508 CONTINUE
      WRITE (9,330)
      WRITE (9,31)
      DO 600 JJ=3,114
      WRITE (9,330)
      WRITE (9,15) JJ,WIRSS(JJ),WIRVV(JJ),WILSS(JJ),WILVV(JJ)
  600 CONTINUE
      WI=WI*RNPP*CF/TVOL
      WIV=WIV*RNPP*CF/TVOL
      WIL=WIL*RNPP*CF/TVOL
      WILV=WILV*RNPP*CF/TVOL
      WRITE (9,330)
      WRITE (9,32)
      WRITE (9,16) WI,WIV,WIL,WILV
      STOP
      END
```

ANDYRPI Input Description

Line or Order	Format	Contents*	
1	7A6,5I6	LIBRY,MATLIB,NG,NP,NING,NTPDEL,KMUL	
2	12I6	NLIBSC,(NLIBS(ISCAT),ISCAT=1,NLIBSC),NLIBSM	
3	16A5	TITLE	
4	12I6	NREG,NSUR,NSEG,NMIX,NSCAT,NSENMA	
5	12I6	NT,ITB1,NTALR,NTALSS,NIT,NMATMA,NSUM	
6	12I6	NS,NKRN,MORE,NPUNCH,NOR,ISKIP	
7	12I6	KTRA,IST1,IST2,NGMI,NGMA,MARI,NSTAD,KAN,NSTA	
8	12I6	KIMP,RIMU,RIML	
9	6E12.6	DELT1,DELT2,OFFSET,TSPLT	
10	6E12.6	WSPLT,WCO,WCOCF,WDELF	
11	12I6	ITP(IS)	A card triple for each Surface IS=1,NSUR
12	6E12.6	AS(IS),BS(IS).......	
13	6E12.6	GS(IS),HS(IS)	
14+...	12I6	IDS(ISS),NSEN(ISS)	A card triple for each Surface Segment ISS=1,NSEG
15+...	12I6	(IDEN(ISS,IS1),IS1=1,NSEN(ISS))	
16+...	12I6	(ISEN(ISS,IS1),IS1=1,NSEN(ISS))	
17+...	12I6	NAS(IR),IMIX(IR),RIM(IR)	A card triple for each Region IR=1,NREG
18+...	12I6	(IAS(IR,ISS),ISS=1,NAS(IR))	
19+...	12I6	(IAR(IR,ISS),ISS=1,NAS(IR))	
20+...	12I6	(ITALR(I),I=1,NTALR)	
21+...	12I6	(ITALSS(I),I=1,NTALSS)	

* Variables are defined on comment cards at the beginning of ANDYRPI

22+...	12I6	NMAT(IM)	A card triple
23+...	12I6	(IMAT(I,IM),I=1,NMAT(IM))	for each
24+...	6E12.6	(DENS(I,IM),I=1,NMAT(IM))	Mix IM=1,NMIX
25+...	6E12.6	(DENSM(I,ISUM),I=1,NLIBSM)	A card pair for
26+...	12I6	IRORS(ISUM),ISUMTY(ISUM)	each Sum ISUM=1,NSUM
27+...	6E12.6	(V(IG),IG=1,NG)	
28+...	6E12.6	(CHIP(IG),IG=1,NG)	

On the other hand, the cross-sections are read from other file with the following format, and for P_o to P_3 components:

7A6,5I6	ALPHANUMERIC TITLE,IDMAT	Multiple cards
6E12.6	(CL(IP,IG),IP=1,NP), for IG=1,NG	for each IMATLI=1,MATLIB

The following pages show characteristic parts of the imput which was used for ^{16}N tagging of single-phase flow.

Line or
Order

```
1        CASKDATA FOR H  O  AND  FE                       3   40    43     4     0
2          3       3      3      3      0
3       NON-UNIFORM N-16 TAGGING FOR WATER AT 1000PSIA,500DEG.F. 14IN,160 PIPE
4          119    16    375     3      3     5
5            1     1    119     0      0     2     0
6         1000     1     50     0      1
7            0     0      0     2      1     1     1
8           00.         0.
9       1.       E 071.      E 071.      E 071.      E 07
10      2.          0.1          0.5         0.
11           1
12
13      0.          0.           1.          0.
.            1
.       0.          0.           1.          2.      E 01
.
             1
        0.          0.           1.          3.5     E 01

             1
        0.          0.           1.          4.5     E 01

             1
        0.          0.           1.          5.5     E 01

             1
        0.          0.           1.          6.5     E 01

             1
        0.          0.           1.          8.0     E 01

             1
        0.          0.           1.          1.0     E 02

             1
        1.          0.           0.          0.

             1
        0.          1.           0.          0.

             1
        0.70711     0.70711      0.          0.

             1
       -0.70711     0.70711    0.          0.

             3
        0.          0.           0.          0.          0.          1.
        2.3      E 01
             3
        0.          0.           0.          0.          0.          1.
        1.778    E 01
             3
        0.          0.           0.          0.          0.          1.
        1.420876E 01
             3
        0.          0.           0.          0.          0.          1.
        1.004711E 01
14+..        1     2
15+..       13    14
```

Line or Order				
16+..	-1	+1		
.	8	2		
.	13	14		
.	-1	+1		
	13	2		
	1	8		
	+1	-1		
	8	3		
	10	14	15	
	+1	-1	+1	
	8	3		
	10	14	15	
	-1	-1	+1	
	1	3		
	10	14	15	
	-1	-1	+1	
	15	4		
	7	8	9	11
	+1	-1	-1	+1
	15	4		
	7	8	10	11
	+1	-1	+1	-1
	15	4		
	7	8	10	12
	+1	-1	-1	+1
	15	4		
	7	8	9	12
	+1	-1	-1	-1
	15	4		
	7	8	9	11
	+1	-1	+1	-1
	15	4		
	7	8	10	11
	+1	-1	-1	+1
	15	4		
	7	8	10	12
	+1	-1	+1	-1
	15	4		
	7	8	9	12
	+1	-1	+1	+1
	15	4		
	6	7	9	11
	+1	-1	-1	+1
	15	4		
	6	7	10	11
	+1	-1	+1	-1
	15	4		
	6	7	10	12
	+1	-1	-1	+1
	15	4		
	6	7	9	12
	+1	-1	-1	-1
	15	4		
	6	7	9	11
	+1	-1	+1	-1
	15	4		
	6	7	10	11
	+1	-1	-1	+1
	15	4		
	6	7	10	12

Line or Order												
	+1	-1	+1									
	14	3										
	3	6	10									
	+1	-1	-1									
	14	3										
	1	3	10									
	+1	-1	+1									
	14	3										
	1	3	10									
	+1	-1	-1									
	10	5										
	6	8	9	14	15							
	+1	-1	-1	-1	+1							
	10	5										
	6	8	9	14	15							
	+1	-1	+1	-1	+1							
	10	5										
	3	6	9	14	15							
	+1	-1	-1	-1	+1							
	10	5										
	3	6	9	14	15							
	+1	-1	+1	-1	+1							
	10	5										
	1	3	9	14	15							
	+1	-1	-1	-1	+1							
	10	5										
	1	3	9	14	15							
	+1	-1	+1	-1	+1							
	6	3										
	10	14	15									
	+1	-1	+1									
	6	3										
	10	14	15									
	-1	-1	+1									
	3	3										
	10	14	15									
	+1	-1	+1									
	3	3										
	10	14	15									
	-1	-1	+1									
	1	3										
	10	14	15									
	+1	-1	+1									
17+..	9	1										
18+..	1	2	3	359	360	361	362	363	364			
19+..	120	120	120	2	115	116	117	118	119			
.	13	2										
.	4	7	8	13	14	15	16	21	22	359	365	366
	371											
.	120	3	4	9	10	11	12	17	18	1	115	115
	116											
	6	3										
	7	63	119	120	231	239						
	2	59	10	4	120	11						
	6	3										
	8	64	120	121	232	240						
	2	60	3	5	120	12						
	6	3										

Line or Order

	5	3										
	110	222	215	342	350							
	50	105	99	98	114							
	5	3										
	111	223	224	343	351							
	51	114	108	99	120							
	5	3										
	112	224	225	344	352							
	52	107	109	100	120							
	5	3										
	113	225	226	345	353							
	53	108	110	101	120							
	5	3										
	114	226	227	346	354							
	54	109	111	102	120							
	5	3										
	115	227	228	347	355							
	55	110	112	103	120							
	5	3										
	116	228	229	348	356							
	56	111	113	104	120							
	5	3										
	117	229	230	349	357							
	57	112	114	105	120							
	5	3										
	118	230	223	350	358							
	58	113	107	106	120							
	13	2										
	5	9	10	11	12	17	18	19	20	360	365	366
	372											
	120	5	6	7	8	13	14	15	16	1	2	2
	117											
	17	2										
	23	24	29	30	31	32	37	38	39	40	45	46
	361	367	368	371	373							
	19	20	25	26	27	28	33	34	35	36	41	42
	1	117	117	2	118							
	17	2										
	25	26	27	28	33	34	35	36	41	42	43	44
	362	367	368	372	374							
	21	22	23	24	29	30	31	32	37	38	39	40
	1	116	116	115	119							
	13	2										
	47	48	53	54	55	56	61	62	363	369	370	373
	375											
	43	44	49	50	51	52	57	58	1	119	119	116
	120											
	13	2										
	6	49	50	51	52	57	58	59	60	364	369	370
	374											
	120	45	46	47	48	53	54	55	56	1	118	118
	117											
20+..	1	2	3	4	5	6	7	8	9	10	11	12
	13	14	15	16	17	18	19	20	21	22	23	24
	25	26	27	28	29	30	31	32	33	34	35	36
	37	38	39	40	41	42	43	44	45	46	47	48

```
Line or
Order

              49      50      51      52      53      54      55      56      57      58      59      60
              61      62      63      64      65      66      67      68      69      70      71      72
              73      74      75      76      77      78      79      80      81      82      83      84
              85      86      87      88      89      90      91      92      93      94      95      96
              97      98      99     100     101     102     103     104     105     106     107     108
             109     110     111     112     113     114     115     116     117     118     119
  22+..        1
  23+..        2
  24+..   4.523   E-06
    .          1
    .          3
    .     0.08419  E 00
               2
               1       2
          5.2632  E-022.6316  E-02
  27+..   5.3392  E 094.828   E 094.3711  E 093.9534  E 093.4859  E 093.0784  E 09
          2.7852  E 092.3981  E 092.1680  E 092.119   E 091.87    E 091.4563  E 09
          1.0251  E 094.6052  E 088.0     E 073.3375  E 071.3892  E 077.4437  E 06
          2.418   E 061.4628  E 068.8939  E 051.3823  E 053.0     E 103.0     E 10
          3.0     E 103.0     E 103.0     E 103.0     E 103.0     E 103.0     E 10
          3.0     E 103.0     E 103.0     E 103.0     E 103.0     E 103.0     E 10
          3.0     E 103.0     E 103.0     E 103.0     E 10
  28+..   1.          1.          1.          1.          1.          1.
          1.          1.          1.          1.          1.          1.
          1.          1.          1.          1.          1.          1.
          1.          1.          1.          1.          1.          1.
          1.          1.          1.          1.          1.          1.
          1.          1.          1.          1.          1.          1.
          1.          1.          1.          1.
```

Sample Output for ^{16}N Tagging of Single-Phase Flow

The following pages contain characteristic parts of the output obtained for ^{16}N tagging of single-phase flow. The results from ANDYRPI were coupled to obtain statistical mean and variance for the 50 batches of 1,000 neutrons each. The resultant values are converted into ^{16}N specific activities for the fluid regions. The program STATISTICS handles all these values. The output has five major parts described as follows:

Part	Description
A	The collision an track-length estimators for each batch and region are printed.
B	The resultant statistical mean and variance for both estimators are shown for each region.
C	The ^{16}N production per neutron, for each neutron group and total, and from both estimators are shown for each fluid region.
D	The ^{16}N specific activities per source pulse are shown for each fluid region.
E	Finally, the total specific activity in the pipe volume is evaluated per source pulse.

Part A

******* N-16 TAGGING OF SINGLE-PHASE FLOW *******

SAMPLE OUTPUT FROM COUPLING THE ANDYRPI RESULTS BY STATISTICS FOR THE 50 BATCHES OF 1000 NEUTRONS EACH.

BATCH, IG: WIR, ST.D., WIRL, ST.D., IG: WIR, ST.D., WIRL, ST.D. FOR REGION 1

BATCH	IG	WIR	ST.D.	WIRL	ST.D.	IG	WIR	ST.D.	WIRL	ST.D.
1	1	0.0	0.0	0.57566E-04	0.10989E-05	2	0.0	0.0	0.19311E-05	0.47585E-06
2	1	0.0	0.0	0.58576E-04	0.13851E-05	2	0.0	0.0	0.12075E-05	0.32555E-06
3	1	0.0	0.0	0.57858E-04	0.10335E-05	2	0.0	0.0	0.16895E-05	0.43369E-06
4	1	0.0	0.0	0.56932E-04	0.10541E-05	2	0.0	0.0	0.14130E-05	0.40982E-06
5	1	0.0	0.0	0.57160E-04	0.12538E-05	2	0.0	0.0	0.18084E-05	0.72954E-06
6	1	0.0	0.0	0.56776E-04	0.11596E-05	2	0.0	0.0	0.11666E-05	0.28679E-06
7	1	0.0	0.0	0.58585E-04	0.11597E-05	2	0.0	0.0	0.16628E-05	0.48383E-06
8	1	0.0	0.0	0.57860E-04	0.11360E-05	2	0.0	0.0	0.18492E-05	0.45752E-06
9	1	0.0	0.0	0.57529E-04	0.99745E-06	2	0.0	0.0	0.22420E-05	0.65985E-06
10	1	0.0	0.0	0.60520E-04	0.15073E-05	2	0.0	0.0	0.21450E-05	0.53144E-06
11	1	0.0	0.0	0.58227E-04	0.10892E-05	2	0.0	0.0	0.24123E-05	0.62198E-06
12	1	0.0	0.0	0.57347E-04	0.10222E-05	2	0.0	0.0	0.13776E-05	0.43647E-06
13	1	0.0	0.0	0.57267E-04	0.10891E-05	2	0.0	0.0	0.15560E-05	0.36112E-06
14	1	0.0	0.0	0.57053E-04	0.10466E-05	2	0.0	0.0	0.28307E-05	0.90184E-06
15	1	0.10000E-02	0.10000E-02	0.57401E-04	0.94661E-06	2	0.0	0.0	0.20127E-05	0.62597E-06
16	1	0.0	0.0	0.56504E-04	0.89820E-06	2	0.0	0.0	0.14402E-05	0.44883E-06
17	1	0.0	0.0	0.56445E-04	0.11839E-05	2	0.0	0.0	0.19753E-05	0.47716E-06
18	1	0.0	0.0	0.58633E-04	0.14417E-05	2	0.0	0.0	0.12991E-05	0.40298E-06
19	1	0.0	0.0	0.57230E-04	0.10736E-05	2	0.0	0.0	0.16388E-05	0.34877E-06
20	1	0.0	0.0	0.56137E-04	0.78554E-06	2	0.0	0.0	0.17165E-05	0.38465E-06
21	1	0.10000E-02	0.10000E-02	0.55887E-04	0.86227E-06	2	0.0	0.0	0.17104E-05	0.43868E-06
22	1	0.0	0.0	0.56276E-04	0.93798E-06	2	0.0	0.0	0.22667E-05	0.56048E-06
23	1	0.15141E-02	0.15141E-02	0.58777E-04	0.12550E-05	2	0.0	0.0	0.15231E-05	0.41415E-06
24	1	0.0	0.0	0.57007E-04	0.94236E-06	2	0.0	0.0	0.15864E-05	0.48450E-06
25	1	0.0	0.0	0.57437E-04	0.94917E-06	2	0.0	0.0	0.15075E-05	0.48840E-06
26	1	0.0	0.0	0.57107E-04	0.10100E-05	2	0.0	0.0	0.15379E-05	0.36297E-06
27	1	0.0	0.0	0.56233E-04	0.94593E-06	2	0.0	0.0	0.25108E-05	0.57068E-06
28	1	0.0	0.0	0.56556E-04	0.87171E-06	2	0.0	0.0	0.16160E-05	0.44728E-06
29	1	0.0	0.0	0.55715E-04	0.80230E-06	2	0.0	0.0	0.17057E-05	0.44228E-06
30	1	0.0	0.0	0.59987E-04	0.12635E-05	2	0.0	0.0	0.11807E-05	0.34003E-06
31	1	0.0	0.0	0.58447E-04	0.10483E-05	2	0.0	0.0	0.19988E-05	0.52767E-06
32	1	0.10000E-02	0.10000E-02	0.58022E-04	0.10958E-05	2	0.0	0.0	0.19404E-05	0.67930E-06
33	1	0.0	0.0	0.58601E-04	0.12903E-05	2	0.0	0.0	0.13725E-05	0.35532E-06
34	1	0.10000E-02	0.10000E-02	0.57439E-04	0.10490E-05	2	0.0	0.0	0.15243E-05	0.40598E-06
35	1	0.0	0.0	0.59983E-04	0.12274E-05	2	0.0	0.0	0.10201E-05	0.43263E-06
36	1	0.0	0.0	0.57898E-04	0.96016E-06	2	0.0	0.0	0.21686E-05	0.76619E-06
37	1	0.0	0.0	0.57434E-04	0.10454E-05	2	0.0	0.0	0.16406E-05	0.42707E-06
38	1	0.0	0.0	0.58498E-04	0.13212E-05	2	0.0	0.0	0.14540E-05	0.37200E-06
39	1	0.0	0.0	0.56608E-04	0.98398E-06	2	0.0	0.0	0.21504E-05	0.51269E-06
40	1	0.0	0.0	0.57848E-04	0.93364E-06	2	0.0	0.0	0.19086E-05	0.46306E-06
41	1	0.0	0.0	0.57811E-04	0.98073E-06	2	0.0	0.0	0.16121E-05	0.43029E-06
42	1	0.0	0.0	0.56896E-04	0.99215E-06	2	0.0	0.0	0.37527E-05	0.90376E-06
43	1	0.0	0.0	0.56926E-04	0.10357E-05	2	0.0	0.0	0.13087E-05	0.32738E-06
44	1	0.0	0.0	0.58893E-04	0.11382E-05	2	0.0	0.0	0.14643E-05	0.34171E-06
45	1	0.0	0.0	0.58075E-04	0.10235E-05	2	0.0	0.0	0.12820E-05	0.32495E-06
46	1	0.0	0.0	0.54628E-04	0.90913E-06	2	0.0	0.0	0.16712E-05	0.44812E-06
47	1	0.0	0.0	0.59117E-04	0.12876E-05	2	0.0	0.0	0.67462E-06	0.20129E-06
48	1	0.0	0.0	0.56524E-04	0.10578E-05	2	0.0	0.0	0.17368E-05	0.41203E-06
49	1	0.0	0.0	0.57718E-04	0.13020E-05	2	0.0	0.0	0.20277E-05	0.41240E-06
50	1	0.0	0.0	0.57173E-04	0.10944E-05	2	0.0	0.0	0.25364E-05	0.58427E-06

BATCH, IG: WIR, ST.D., WIRL, ST.D., IG: WIR, ST.D., WIRL, ST.D. FOR REGION 2

BATCH	IG	WIR	ST.D.	WIRL	ST.D.	IG	WIR	ST.D.	WIRL	ST.D.
1	1	0.16730E-01	0.65337E-02	0.13434E-01	0.41828E-02	2	0.28114E-02	0.20424E-02	0.56416E-02	0.34040E-02

Part B

```
        WIR(IT,ITALY,IG),STAN. DEV.  ,WIRL(IT,ITALY,IG)STAN.DEV. , IG=1,NCMA FOR REGION      1
1   0.11028E-03 0.50170E-04             0.57542E-04 0.15430E-06
2   0.0         0.0                     0.17553E-05 0.69901E-07

        WIR(IT,ITALY,IG),STAN. DEV.  ,WIRL(IT,ITALY,IG)STAN.DEV. , IG=1,NGMA FOR REGION      2
1   0.21013E-01 0.12693E-02             0.20037E-01 0.11656E-02
2   0.51616E-02 0.71078E-03             0.52558E-02 0.66833E-03

        WIR(IT,ITALY,IG),STAN. DEV.  ,WIRL(IT,ITALY,IG)STAN.DEV. , IG=1,NGMA FOR REGION      3
1   0.15007E-03 0.70719E-04             0.17889E-03 0.51827E-04
2   0.70190E-04 0.51140E-04             0.99681E-04 0.27551E-04

        WIR(IT,ITALY,IG),STAN. DEV.  ,WIRL(IT,ITALY,IG)STAN.DEV. , IG=1,NGMA FOR REGION      4
1   0.34681E-03 0.87378E-04             0.43115E-03 0.72877E-04
2   0.42876E-04 0.30318E-04             0.59365E-04 0.23144E-04

        WIR(IT,ITALY,IG),STAN. DEV.  ,WIRL(IT,ITALY,IG)STAN.DEV. , IG=1,NGMA FOR REGION      5
1   0.62576E-03 0.12326E-03             0.57745E-03 0.70918E-04
2   0.58836E-04 0.41825E-04             0.96804E-04 0.30506E-04

        WIR(IT,ITALY,IG),STAN. DEV.  ,WIRL(IT,ITALY,IG)STAN.DEV. , IG=1,NGMA FOR REGION      6
1   0.85181E-03 0.15957E-03             0.57665E-03 0.67635E-04
2   0.12863E-03 0.52512E-04             0.21772E-03 0.56380E-04

        WIR(IT,ITALY,IG),STAN. DEV.  ,WIRL(IT,ITALY,IG)STAN.DEV. , IG=1,NGMA FOR REGION      7
1   0.38419E-03 0.90866E-04             0.52913E-03 0.65584E-04
2   0.13050E-03 0.61635E-04             0.98957E-04 0.24376E-04

        WIR(IT,ITALY,IG),STAN. DEV.  ,WIRL(IT,ITALY,IG)STAN.DEV. , IG=1,NGMA FOR REGION      8
1   0.64325E-03 0.14026E-03             0.68856E-03 0.88690E-04
2   0.12130E-03 0.66479E-04             0.17536E-03 0.37170E-04

        WIR(IT,ITALY,IG),STAN. DEV.  ,WIRL(IT,ITALY,IG)STAN.DEV. , IG=1,NGMA FOR REGION      9
1   0.62246E-03 0.13369E-03             0.49305E-03 0.83157E-04
2   0.11686E-03 0.52437E-04             0.13716E-03 0.44870E-04

        WIR(IT,ITALY,IG),STAN. DEV.  ,WIRL(IT,ITALY,IG)STAN.DEV. , IG=1,NGMA FOR REGION     10
1   0.21740E-03 0.10701E-03             0.18516E-03 0.51414E-04
2   0.49772E-04 0.35530E-04             0.88800E-04 0.28485E-04

        WIR(IT,ITALY,IG),STAN. DEV.  ,WIRL(IT,ITALY,IG)STAN.DEV. , IG=1,NGMA FOR REGION     11
1   0.39621E-02 0.33098E-03             0.41718E-02 0.23157E-03
2   0.40364E-03 0.11127E-03             0.40433E-03 0.61041E-04

        WIR(IT,ITALY,IG),STAN. DEV.  ,WIRL(IT,ITALY,IG)STAN.DEV. , IG=1,NGMA FOR REGION     12
1   0.26120E-02 0.26124E-03             0.25047E-02 0.17662E-03
2   0.34730E-03 0.10008E-03             0.30240E-03 0.52566E-04

        WIR(IT,ITALY,IG),STAN. DEV.  ,WIRL(IT,ITALY,IG)STAN.DEV. , IG=1,NGMA FOR REGION     13
1   0.14525E-02 0.19080E-03             0.15924E-02 0.10413E-03
2   0.42009E-03 0.11515E-03             0.40610E-03 0.62138E-04

        WIR(IT,ITALY,IG),STAN. DEV.  ,WIRL(IT,ITALY,IG)STAN.DEV. , IG=1,NGMA FOR REGION     14
1   0.16050E-02 0.19756E-03             0.14570E-02 0.10040E-03
2   0.38401E-03 0.11180E-03             0.43625E-03 0.66648E-04
```

Part C

REGION,GOUP, N-16/NEUTRON FOR EACH GROUP, TOTAL N-16/NEUTRON

COLL. ESTIMATOR	3	1	0.15562E-05	0.87472E-06	2	0.50926E-06	0.37105E-06	0.23654E-05	0.95017E-06
T.LEN.ESTIMATOR	3	1	0.22127E-05	0.64104E-06	2	0.72324E-06	0.19990E-06	0.29359E-05	0.67149E-06
COLL. ESTIMATOR	4	1	0.42897E-05	0.10808E-05	2	0.31109E-06	0.21997E-06	0.46008E-05	0.11029E-05
T.LEN.ESTIMATOR	4	1	0.53329E-05	0.90142E-06	2	0.43072E-06	0.16792E-06	0.57636E-05	0.91692E-06
COLL. ESTIMATOR	5	1	0.77400E-05	0.15245E-05	2	0.42689E-06	0.30346E-06	0.81669E-05	0.15545E-05
T.LEN.ESTIMATOR	5	1	0.71424E-05	0.87718E-06	2	0.70236E-06	0.22134E-06	0.78448E-05	0.90467E-06
COLL. ESTIMATOR	6	1	0.10536E-04	0.19737E-05	2	0.93326E-06	0.38100E-06	0.11469E-04	0.20102E-05
T.LEN.ESTIMATOR	6	1	0.71325E-05	0.83657E-06	2	0.15797E-05	0.40907E-06	0.87122E-05	0.93123E-06
COLL. ESTIMATOR	7	1	0.47520E-05	0.11239E-05	2	0.94684E-06	0.44719E-06	0.56989E-05	0.12096E-05
T.LEN.ESTIMATOR	7	1	0.65448E-05	0.81120E-06	2	0.71799E-06	0.17686E-06	0.72627E-05	0.83026E-06
COLL. ESTIMATOR	8	1	0.79563E-05	0.17348E-05	2	0.88012E-06	0.48234E-06	0.88364E-05	0.18006E-05
T.LEN.ESTIMATOR	8	1	0.85167E-05	0.10970E-05	2	0.12723E-05	0.26969E-06	0.97891E-05	0.11297E-05
COLL. ESTIMATOR	9	1	0.76992E-05	0.16536E-05	2	0.84789E-06	0.38045E-06	0.85471E-05	0.16968E-05
T.LEN.ESTIMATOR	9	1	0.60985E-05	0.10286E-05	2	0.99518E-06	0.32555E-06	0.70937E-05	0.10788E-05
COLL. ESTIMATOR	10	1	0.26890E-05	0.13236E-05	2	0.36112E-06	0.25779E-06	0.30502E-05	0.13484E-05
T.LEN.ESTIMATOR	10	1	0.22903E-05	0.63593E-06	2	0.64429E-06	0.20667E-06	0.29346E-05	0.66867E-06
COLL. ESTIMATOR	11	1	0.49008E-04	0.40939E-05	2	0.29286E-05	0.80734E-06	0.51936E-04	0.41728E-05
T.LEN.ESTIMATOR	11	1	0.51601E-04	0.28643E-05	2	0.29336E-05	0.44288E-06	0.54535E-04	0.28983E-05
COLL. ESTIMATOR	12	1	0.32308E-04	0.32312E-05	2	0.25198E-05	0.72616E-06	0.34828E-04	0.33118E-05
T.LEN.ESTIMATOR	12	1	0.30981E-04	0.21846E-05	2	0.21941E-05	0.38139E-06	0.33175E-04	0.22177E-05
COLL. ESTIMATOR	13	1	0.17966E-04	0.23599E-05	2	0.30480E-05	0.83545E-06	0.21014E-04	0.25034E-05
T.LEN.ESTIMATOR	13	1	0.19696E-04	0.12879E-05	2	0.29465E-05	0.45084E-06	0.22643E-04	0.13646E-05
COLL. ESTIMATOR	14	1	0.19853E-04	0.24436E-05	2	0.27862E-05	0.81119E-06	0.22639E-04	0.25747E-05
T.LEN.ESTIMATOR	14	1	0.18021E-04	0.12419E-05	2	0.31652E-05	0.48357E-06	0.21186E-04	0.13327E-05
COLL. ESTIMATOR	15	1	0.13582E-04	0.19441E-05	2	0.11020E-05	0.45628E-06	0.14684E-04	0.19969E-05
T.LEN.ESTIMATOR	15	1	0.17662E-04	0.12104E-05	2	0.23904E-05	0.42141E-06	0.20052E-04	0.12817E-05
COLL. ESTIMATOR	16	1	0.20313E-04	0.25838E-05	2	0.19226E-05	0.58760E-06	0.22236E-04	0.26497E-05
T.LEN.ESTIMATOR	16	1	0.20355E-04	0.15167E-05	2	0.24591E-05	0.40281E-06	0.22814E-04	0.15692E-05
COLL. ESTIMATOR	17	1	0.34008E-04	0.34040E-05	2	0.47761E-05	0.11795E-05	0.38784E-04	0.36025E-05
T.LEN.ESTIMATOR	17	1	0.30079E-04	0.22223E-05	2	0.39619E-05	0.59557E-06	0.34041E-04	0.23008E-05
COLL. ESTIMATOR	18	1	0.47644E-04	0.40583E-05	2	0.23796E-05	0.67476E-06	0.50024E-04	0.41140E-05
T.LEN.ESTIMATOR	18	1	0.53403E-04	0.29355E-05	2	0.27738E-05	0.45091E-06	0.56177E-04	0.29699E-05
COLL. ESTIMATOR	19	1	0.19700E-03	0.79880E-05	2	0.98225E-05	0.14351E-05	0.20682E-03	0.81159E-05
T.LEN.ESTIMATOR	19	1	0.18563E-03	0.43531E-05	2	0.97134E-05	0.84827E-06	0.19535E-03	0.44350E-05
COLL. ESTIMATOR	20	1	0.52693E-04	0.41987E-05	2	0.24278E-05	0.65838E-06	0.55121E-04	0.42500E-05
T.LEN.ESTIMATOR	20	1	0.55411E-04	0.27277E-05	2	0.47078E-05	0.55781E-06	0.60118E-04	0.27842E-05
COLL. ESTIMATOR	21	1	0.28043E-04	0.29482E-05	2	0.20397E-05	0.63633E-06	0.30083E-04	0.30161E-05
T.LEN.ESTIMATOR	21	1	0.26812E-04	0.15483E-05	2	0.28976E-05	0.40854E-06	0.29710E-04	0.16013E-05

COLL. ESTIMATOR	102	1	0.26988E-04	0.29483E-05	2	0.31099E-05	0.77781E-06	0.30098E-04 0.30492E-05
T.LEN.ESTIMATOR	102	1	0.24380E-04	0.16854E-05	2	0.36517E-05	0.53053E-06	0.28032E-04 0.17669E-05
COLL. ESTIMATOR	103	1	0.20340E-04	0.25361E-05	2	0.22051E-05	0.69992E-06	0.22545E-04 0.26309E-05
T.LEN.ESTIMATOR	103	1	0.23786E-04	0.16207E-05	2	0.24485E-05	0.36396E-06	0.26234E-04 0.16611E-05
COLL. ESTIMATOR	104	1	0.30230E-04	0.30802E-05	2	0.36040E-05	0.89091E-06	0.33834E-04 0.32064E-05
T.LEN.ESTIMATOR	104	1	0.29592E-04	0.16670E-05	2	0.35385E-05	0.44211E-06	0.33130E-04 0.17247E-05
COLL. ESTIMATOR	105	1	0.46083E-04	0.39334E-05	2	0.46857E-05	0.99453E-06	0.50768E-04 0.40572E-05
T.LEN.ESTIMATOR	105	1	0.40563E-04	0.20071E-05	2	0.44299E-05	0.52965E-06	0.44992E-04 0.20758E-05
COLL. ESTIMATOR	106	1	0.59192E-04	0.43727E-05	2	0.52140E-05	0.10767E-05	0.64406E-04 0.45033E-05
T.LEN.ESTIMATOR	106	1	0.58211E-04	0.27370E-05	2	0.49574E-05	0.61774E-06	0.63168E-04 0.28058E-05
COLL. ESTIMATOR	107	1	0.45079E-05	0.11379E-05	2	0.16239E-05	0.54862E-06	0.61317E-05 0.12633E-05
T.LEN.ESTIMATOR	107	1	0.74448E-05	0.11008E-05	2	0.11105E-05	0.29995E-06	0.85553E-05 0.11410E-05
COLL. ESTIMATOR	108	1	0.84762E-05	0.16216E-05	2	0.78451E-06	0.35090E-06	0.92607E-05 0.16591E-05
T.LEN.ESTIMATOR	108	1	0.95177E-05	0.11161E-05	2	0.11046E-05	0.27913E-06	0.10622E-04 0.11505E-05
COLL. ESTIMATOR	109	1	0.11085E-04	0.19042E-05	2	0.99544E-06	0.40821E-06	0.12080E-04 0.19475E-05
T.LEN.ESTIMATOR	109	1	0.92903E-05	0.10624E-05	2	0.13164E-05	0.29319E-06	0.10607E-04 0.11021E-05
COLL. ESTIMATOR	110	1	0.10883E-04	0.17857E-05	2	0.14289E-05	0.56624E-06	0.12312E-04 0.18733E-05
T.LEN.ESTIMATOR	110	1	0.96932E-05	0.11292E-05	2	0.15749E-05	0.39889E-06	0.11268E-04 0.11976E-05
COLL. ESTIMATOR	111	1	0.11588E-04	0.18668E-05	2	0.19746E-05	0.67667E-06	0.13563E-04 0.19856E-05
T.LEN.ESTIMATOR	111	1	0.93136E-05	0.11061E-05	2	0.14358E-05	0.33669E-06	0.10749E-04 0.11562E-05
COLL. ESTIMATOR	112	1	0.69981E-05	0.13836E-05	2	0.90041E-06	0.40461E-06	0.78985E-05 0.14415E-05
T.LEN.ESTIMATOR	112	1	0.95938E-05	0.10328E-05	2	0.17434E-05	0.35208E-06	0.11337E-04 0.10912E-05
COLL. ESTIMATOR	113	1	0.85497E-05	0.16086E-05	2	0.14643E-05	0.52127E-06	0.10014E-04 0.16909E-05
T.LEN.ESTIMATOR	113	1	0.97109E-05	0.11122E-05	2	0.19803E-05	0.45242E-06	0.11691E-04 0.12007E-05
COLL. ESTIMATOR	114	1	0.99539E-05	0.17420E-05	2	0.50926E-06	0.29525E-06	0.10463E-04 0.17669E-05
T.LEN.ESTIMATOR	114	1	0.80064E-05	0.11565E-05	2	0.10600E-05	0.33757E-06	0.90665E-05 0.12047E-05

TOTAL N-16/NEUTRON PRODUCTION FROM COLLISION &TRACK LENGTH ESTIMATORS
0.55214E-02 0.41036E-04 0.55229E-02 0.23702E-04

Part D REGION, N-16/(CM**3)*PULSE AND STANDARD DEVIATION FROM COLLISION &TRACK LENGTH ESTIMATORS

3	0.79910E+01	0.32099E+01	0.99183E+01	0.22684E+01
4	0.15543E+02	0.37260E+01	0.19471E+02	0.30976E+01
5	0.27590E+02	0.52513E+01	0.26501E+02	0.30562E+01
6	0.38746E+02	0.67908E+01	0.29432E+02	0.31459E+01
7	0.19252E+02	0.40863E+01	0.24535E+02	0.28048E+01
8	0.29851E+02	0.60829E+01	0.33070E+02	0.38162E+01
9	0.28874E+02	0.57323E+01	0.23964E+02	0.36446E+01
10	0.10304E+02	0.45553E+01	0.99136E+01	0.22589E+01

86	0.28861E+03	0.24106E+02	0.29196E+03	0.14356E+02
87	0.28211E+03	0.23115E+02	0.27389E+03	0.13521E+02
88	0.36006E+03	0.26634E+02	0.34367E+03	0.12698E+02
89	0.58719E+03	0.32961E+02	0.60065E+03	0.17544E+02
90	0.12515E+04	0.50111E+02	0.12299E+04	0.28266E+02
91	0.84774E+03	0.42280E+02	0.86957E+03	0.24716E+02
92	0.52856E+03	0.31908E+02	0.51201E+03	0.16679E+02
93	0.29531E+03	0.23580E+02	0.31257E+03	0.12664E+02
94	0.21442E+03	0.20085E+02	0.26490E+03	0.13682E+02
95	0.25303E+03	0.22335E+02	0.23685E+03	0.12930E+02
96	0.31362E+03	0.24412E+02	0.29418E+03	0.12123E+02
97	0.46103E+03	0.29774E+02	0.48416E+03	0.16674E+02
98	0.73857E+03	0.38675E+02	0.83212E+03	0.24599E+02
99	0.28104E+03	0.20110E+02	0.27340E+03	0.12889E+02
100	0.23560E+03	0.17811E+02	0.20859E+03	0.98087E+01
101	0.16867E+03	0.14925E+02	0.15053E+03	0.77122E+01
102	0.13557E+03	0.13734E+02	0.12626E+03	0.[illegible]9586E+01
103	0.10155E+03	0.11850E+02	0.11817E+03	0.74822E+01
104	0.15240E+03	0.14443E+02	0.14923E+03	0.77684E+01
105	0.22868E+03	0.18275E+02	0.20266E+03	0.93500E+01
106	0.29011E+03	0.20284E+02	0.28453E+03	0.12638E+02
107	0.20714E+02	0.42676E+01	0.28902E+02	0.38544E+01
108	0.31285E+02	0.56048E+01	0.35885E+02	0.38865E+01
109	0.40810E+02	0.65789E+01	0.35832E+02	0.37231E+01
110	0.41592E+02	0.63285E+01	0.38066E+02	0.40457E+01
111	0.45819E+02	0.67079E+01	0.36314E+02	0.39059E+01
112	0.26683E+02	0.48699E+01	0.38300E+02	0.36863E+01
113	0.33830E+02	0.57123E+01	0.39496E+02	0.40562E+01
114	0.35347E+02	0.59688E+01	0.30629E+02	0.40698E+01

Part E

TOTAL N-16/(CM**3)*PULSE PRODUCTION FROM COLLISION&TRACK LENGTH ESTIMATORS

0.23316E+03	0.17329E+01	0.23322E+03	0.10009E+01

APPENDIX D

TRANSPORT CODE BY FINITE DIFFERENCE METHODS

The following pages contain a listing of the program used to couple the Monte Carlo results at the tagging and detector positions with a transport by finite difference methods. There is also included numerical sample input and output of the code for the single-phase flow.

```
C
C  THIS PROGRAM COUPLES THE MONTE CARLO CALCULATIONS AT THE SOURCE
C  AND DETECTOR LOCATIONS WITH A TRANSPORT BASED ON FINITE
C  DIFFERENCE METHOS
C
C
C  THE DESCRIPTION OF THE TIME-EXPLICIT FINITE DIFFERENCE SCHEME
C  IS DESCRIBED IN SECTION 2.3.3. THE 1/7-POWER LAW TURBULENT
C  VELOCITY PROFILE IS ASSUMED.
C  ALL THE VARIABLES ARE PROPERLY UNDIMENSIONED THROUGH THE PROGRAM
C  THE COUPLING OF THE MONTE CARLO IS IMPLICITELY IN THE FINITE
C  DIFFERENCE SCHEME, I.E. THE AXIAL AND RADIAL SOURCE AND DETECTOR
C  REGIONS CORRESPONDED TO A DEFINED AXIAL AND RADIAL MESH POINTS
C  DEPENDING ON THE AXIAL AND RADIAL MESH INCREMENTS.
C  THE N-16 SPECIFIC ACTIVITIES FOR EACH FLUID REGION ARE NORMALIZED
C  TO THE TOTAL N-16 SPECIFIC ACTIVITY. THEREFORE, THE IMPUT
C  CONCENTRATIONS ARE UNDIMENSIONED.
C  THE DETECTOR EFFICIENCIES FOR EACH REGION ARE INSERTED IN THIS
C  PROGRAM AS: EFFICIENCY PER UNIT OF N-16 CONCENTRATION.
C  THE UNITS OF THE INSERTED DIMENSIONED VARIABLES ARE IN CGS SYSTEM.
C
C*VARIABLE DESCRIPTION: AS THEY ARE READ OR DEFINED THROUGH PROGRAM*
C
C
C  NTI=NO. OF TIME DIVISIONS
C  NR= NO. OF RADIAL DIVISIONS
C  NL= NO. OF AXIAL DIVISIONS
C  LI= AXIAL SOURCE POSITION (INITIAL)
C  NDI=AXIAL DETECTOR POSITION (INITIAL)
C  NT= NO. OF TIME MESH=NTI+1
C  NJ= NO. OF RADIAL MESH=NR+1
C  NK= NO. OF AXIAL MESH=NL+1
C  R=  I.D. OF PIPE
C  RL= TOTAL LENGTH OF THE PIPE
C  DELT=TIME INCREMENT (WITH DIMENSION)
C  VE= MEAN VELOCITY OF THE FLOW
C  FEO=SQRT(1/2*FRICTION FACTOR)
C  VIS=VISCOSITY
C  R1= RADIUS OF THE INNER CYLINDER IN MONTE CARLO GEOMETRY
C  RL1=LENGTH OF THE 1 AND 7 AXIAL MONTE CARLO GEOMETRY REGIONS
C  RL2=LENGTH OF THE 2 AND 6 AXIAL MONTE CARLO GEOMETRY REGIONS
C  RL3=LENGTH OF THE 3,4 AND 5 AXIAL MONTE CARLO GEOMETRY REGIONS
C  RLAN=DECAY CONSTANT FOR N-16
C  DER=RADIAL INCREMENT (WITH DIMENSION)
C  DEX=AXIAL INCREMENT (WITH DIMENSION)
C  NR1=UP RADIAL MESH NUMBER FOR THE OUTER RADIAL REGIONS
C  NR2=UP RADIAL MESH NUMBER FOR THE INNER RADIAL REGIONS
C  L1 TO L7=UP AXIAL MESH NUMBER FOR THE 1 TO 7 AXIAL SOURCE REGIONS
C  ND1 TO ND7=UP AXIAL MESH NUMBER FOR THE 1 TO 7 AXIAL DETECTOR REGIONS
C  DETT=TIME MESH INCREMENT (NO DIMENSION)
C  DEXX=AXIAL MESH INCREMENT (NO DIMENSION)
C  DERR=RADIAL MESH INCREMENT (NO DIMENSION)
C  PE = PECLET NUMBER
C  VISD=VISCOSITY (NO DIMENSION)
C  TA(1,J)=CONCENTRATION FOR OUTER RADIAL REGION AT AXIAL POSITION J
C  TA(2,J)=CONCENTRATION FOR INNER RADIAL REGION AT AXIAL POSITION J
C  DR(1,I)=DETECTOR EFF. FOR OUTER RADIAL REGION AT AXIAL POSITION I
C  DR(2,I)=DETECTOR EFF. FOR INNER RADIAL REGION AT AXIAL POSITION I
C  ARLOF=EXPERIMENTAL LOFT AREA
C  CI=TOTAL N-16 CONCENTRATION IN THE PIPE
```

```
C
C  DEFINITION OF COEFFICIENTS SECTION: THEY ARE UNDIMENSIONED
C
C  THE VELOCITIES FOR EACH RADIAL REGION HAVE BEEN AVERAGED OVER THE
C  AREA OF THAT RADIAL REGION ASSUMING 1/7-POWER LAW.
C  F1,F1I,F2,F2I ARE THE EXPONENTS  FROM INTEGRATING THE VELOCITIES
C  Z= RADIUS OF RADIAL JJ
C  ZH=Z+1/2
C  ZHH=Z-1/2
C  ARE(JJ)=AREA OF RADIAL REGION JJ
C  U(JJ)=AVERAGED VELOCITY OVER ARE(JJ) FOR THE RADIAL REGION JJ
C  E= DISPERSION COEFFICIENT OF RADIAL JJ
C  EH=E+1/2
C  EHH=E-1/2
C  A(JJ),B(JJ),C(JJ),D(JJ),F(JJ)=COEFFICIENTS FOR FINITE DIFFERENCE
C                               EQUATIONS
C
C  CVE=CORRECTED AVERAGED VELOCITY. THIS IS EVALUATED TO MAKE SURE
C      THAT THE INTEGRATION OVER EACH RADIAL REGION WAS CORRECT
C
C  INITIAL CONDITIONS
C
C  THE INITIAL CONDITIONS DEPEND ON THE DEFINITION OF THE AXIAL AND
C  RADIAL MESH NUMBERS THAT DEFINE THE N-16 TAGGED REGIONS
C
C  EXPLICIT METHOD
C
C  Y(N+1,J,K)=SOLUTION AT THE NEXT TIME STEP FOR RADIAL J AXIAL K
C
C  NOTICE THAT THE SOLUTIONS DEPEND ON THE BOUNDARY CONDITIONS
C  AT THE CENTER PIPE LINE AND PIPE WALLS.
C  THE SOLUTION FOR EACH RADIAL AND AXIAL REGION AT THE DETECTOR
C  POSITION ARE NORMALIZED TO THE NO. OF N-16.
C  THE NORMALIZED CONCENTRATIONS AT DETECTOR POSITIONS ARE COUPLED
C  WITH THE DETECTOR EFFICIENCIES TO OBTAIN COUNTING RATE
C
C  X(JJ)=TIME FOR JJ TIME STEP
C  YY(L,M)=NORMALIZED CONCENTRATIONS AT DETECTOR REGIONS
C  YX(JJ)=COUNTING RATE AT TIME X(JJ)
C  EF=TEMPORAL VARIABE WHICH EVALUATES THE N-16 DECAY
C  AREA=TOTAL AREA UNDER THE ANALITICAL TIME PROFILE
C  FE=NORMALIZATION FACTOR BETWEEN EXPERIMENTAL AND CALCULATED AREAS
C
C  THE NEXT PART OF THE PROGRAM REFERS TO PLOTTING THE FINAL PROFILE
C  XDUM AND YDUM ARE THE VARIABLES FOR THE PLOT SUBROUTINE
C
C
      INTEGER TITLE(20),XLABEL(10),YLABEL(10),SIZE,NPOINT(1),
     *POINTS(1,4)
      LOGICAL OPTION(10)
      REAL X(1000),YX(1000),XDUM(1000),YDUM(1000)
      DIMENSION A(21),B(21),C(21),D(21),F(21),Y(2,21,606),
     *YY(2,7),DR(2,7),ARE(21),U(21),TA(2,7)
C
C VARIABLES
C
C FORMATS
   12 FORMAT(10E12.5)
   13 FORMAT(20I6)
   14 FORMAT(1H )
```

```
   20 FORMAT(' TIME STEPS,RADIAL DIVISIONS,AXIAL DIVISIONS')
   21 FORMAT('RADIUS,LENGTH,TIME INCR.,MEAN VELOCITY,FEO,VISCOSITY')
   22 FORMAT('**** VALUES FOR RADIAL NO.  ',I6,' ****')
   23 FORMAT(' VALUES OF DER,DEX,DETT,DEXX,DERR,PE  ')
   24 FORMAT(' INITIAL AXIAL POSITIONS AT TAGGING AND DETECTION')
   26 FORMAT(' TIME(SEC)  AND  FINAL COUNTS/ TIME CHANNEL')
   28 FORMAT( 'DETECTOR RESPONSE FOR OUTER AND INNER REGIONS ')
   29 FORMAT('EXPERIMENTAL LOFT AREA',E12.5,'TOTAL CONCENTRATION',E12.5)
   30 FORMAT('VALUES OF R1,RL1,RL2,RL3')
   31 FORMAT('VALUES OF L1,L2,L3,L4,L5,L6,L7')
   38 FORMAT(' N-16 CONCENTRATIONS FOR OUTER AND INNER REGIONS')
   41 FORMAT('VALUES OF ND1,ND2,ND3,ND4,ND5,ND6,ND7')
   37 FORMAT(' CORRECTED MEAN VELOCITY =  ',E12.5)
   27 FORMAT('VALUES OF Z, ZH, ZHH, E, EH, EHH, ARE, U')
   39 FORMAT('VALUES OF COEFFICIENTS A, B, C, D, E, AND F')
C
C  READ IMPUT
C
      READ(5,13) NTI,NR,NL,LI,NDI
      WRITE(6,14)
      WRITE(6,20)
      WRITE(6,14)
      WRITE(6,13) NTI,NR,NL
      WRITE(6,14)
      WRITE(6,24)
      WRITE(6,14)
      WRITE(6,13) LI,NDI
      NT=NTI+1
      NJ=NR+1
      NK=NL+1
      READ(5,12) R,RL,DELT,VE,FEO,VIS
      WRITE(6,14)
      WRITE(6,21)
      WRITE(6,14)
      WRITE(6,12) R,RL,DELT,VE,FEO,VIS
      READ(5,12) R1,RL1,RL2,RL3
      WRITE(6,14)
      WRITE(6,30)
      WRITE(6,14)
      WRITE(6,12) R1,RL1,RL2,RL3
      RLAN=0.0975
C
C  DEFINE RADIAL INCREMENT AND AXIAL INCREMENT(DIMENSION)
      DER=R/NR
      DEX=RL/NL
C  DEFINE LIMITS FOR AXIAL AND RADIAL REGIONS AT TAGGING
      NR2=R1/DER+1
      NR1=NJ-NR2
      NR2=NR1+1
      L1=LI+RL1/DEX
      L2=L1+RL2/DEX
      L3=L2+RL3/DEX
      L4=L3+RL3/DEX
      L5=L4+RL3/DEX
      L6=L5+RL2/DEX
      L7=L6+RL1/DEX
      WRITE(6,14)
      WRITE(6,31)
      WRITE(6,14)
      WRITE(6,13) L1,L2,L3,L4,L5,L6,L7
```

```
C  DEFINE LIMITS FOR AXIAL AND RADIAL REGIONS AT DETECTOR
      ND1=NDI+RL1/DEX
      ND2=ND1+RL2/DEX
      ND3=ND2+RL3/DEX
      ND4=ND3+RL3/DEX
      ND5=ND4+RL3/DEX
      ND6=ND5+RL2/DEX
      ND7=ND6+RL1/DEX
      WRITE(6,14)
      WRITE(6,41)
      WRITE(6,14)
      WRITE(6,13) ND1,ND2,ND3,ND4,ND5,ND6,ND7
C  DEFINE TIME,AXIAL AND RADIAL INCREMENTS(NO DIMENSION)
      DETT=(FEO/R)*VE*DELT
      DEXX=(FEO/R)*0.61667*DEX
      DERR=-DER/R
      PE=1./(FEO*0.81667)
      VISD=VIS/(FEO*VE*R)
      WRITE(6,14)
      WRITE(6,23)
      WRITE(6,14)
      WRITE(6,12) DER,DEX,DETT,DEXX,DERR,PE
      WRITE(6,14)
C
C  READ INITIAL CONCENTRATIONS AND DETECTOR EFFICIENCIES
C
      READ(5,12) (TA(1,MS),MS=1,7)
      WRITE(6,14)
      WRITE(6,38)
      WRITE(6,14)
      WRITE(6,12) (TA(1,MT),MT=1,7)
      READ(5,12) (TA(2,MB),MB=1,7)
      WRITE(6,14)
      WRITE(6,14)
      WRITE(6,12) (TA(2,MT),MT=1,7)
C
      READ(5,12) (DR(1,MS),MS=1,7)
      WRITE(6,14)
      WRITE(6,28)
      WRITE(6,14)
      WRITE(6,12) (DR(1,MT),MT=1,7)
      READ(5,12) (DR(2,MB),MB=1,7)
      WRITE(6,14)
      WRITE(6,14)
      WRITE(6,12) (DR(2,MT),MT=1,7)
      READ(5,12) ARLOF,CI
      WRITE(6,14)
      WRITE(6,29) ARLOF,CI
      WRITE(6,14)
C
C  DEFINE COEFFICIENTS
C
      F1=8./7.
      F1I=1./F1
      F2=15./7.
      F2I=1./F2
      DO 50 JJ=1,NJ
      Z=(JJ-1)*DER/R
      ZH=(JJ-0.5)*DER/R
      ZHH=(JJ-1.5)*DER/R
```

```
      IF(JJ.EQ.1) ZHH=ZH
      IF(JJ.EQ.NJ) ZH=ZHH
      ARE(JJ)=ZHH*ZHH-ZH*ZH+2.*(ZH-ZHH)
      IF(JJ.EQ.1) ARE(JJ)=-(1.-ZH)*(1.-ZH)+(1.-Z)*(1.-Z)
      IF(JJ.EQ.NJ) ARE(JJ)=(1.-ZH)*(1.-ZH)+(1.-Z)*(1.-Z)
      U(JJ)=(2./ARE(JJ))*(F1I*(ZH**F1-ZHH**F1)-F2I*(ZH**F2-ZHH**F2))
      IF(JJ.EQ.1) U(JJ)=(2./ARE(JJ))*(F1I*(ZH**F1-Z**F1)-F2I*(ZH**F2
     *-Z**F2))
      IF(JJ.EQ.NJ) U(JJ)=(2./ARE(JJ))*(F1I*(Z**F1-ZHH**F1)-F2I*(Z**F2
     *-ZHH**F2))
      E=7.*FEO*0.81667*(1.-Z)*(Z**(6./7.))+VISD
      EH=7.*FEO*0.81667*(1.-ZH)*(ZH**(6./7.))+VIS
      EHH=7.*FEO*Q.81667*(1.-ZHH)*(ZHH**(6./7.))+VIS
      ONE=U(JJ)*DETT/DEXX
      TWO=(E*DETT)/(PE*PE*DEXX*DEXX)
      C(JJ)=TWO
      B(JJ)=ONE+TWO
      IF(JJ.EQ.NJ) GO TO 51
      THR=DETT/(DERR*DERR*(1.-Z))
      D(JJ)=THR*EHH*(1.-ZHH)
      F(JJ)=THR*EH*(1.-ZH)
      A(JJ)=1.-ONE-2.*TWO-D(JJ)-F(JJ)
      GO TO 52
   51 D(JJ)=4.*E*DETT/(DERR*DERR)
      A(JJ)=1.-ONE-2.*TWO-D(JJ)
      F(JJ)=0.
   52 CONTINUE
      WRITE(6,22) JJ
      WRITE(6,14)
      WRITE(6,27)
      WRITE(6,14)
      WRITE(6,12) Z,ZH,ZHH,E,EH,EHH,ARE(JJ),U(JJ)
      WRITE(6,14)
      WRITE(6,39)
      WRITE(6,14)
      WRITE(6,12) A(JJ),B(JJ),C(JJ),D(JJ),F(JJ)
      WRITE(6,14)
   50 CONTINUE
C
C  EVALUATE CORRECTED MEAN VELOCITY
C
      CVE=0.
      DO 731 JS=1,NJ
      CVE=CVE+U(JS)*ARE(JS)
  731 CONTINUE
      CVE=VE*0.81667/CVE
      WRITE(6,14)
      WRITE(6,37) CVE
      WRITE(6,14)
C
C  INITAL CONDITIONS
C
      DO 550 JI=1,NJ
      IF(JI.LE.NR1) L=1
      IF(JI.GE.NR2) L=2
      DO 560 KI=1,NK
      IF(KI.LT.LI) Y(1,JI,KI)=0.
      IF(KI.GT.L7) GO TO 561
      IF(KI.GE.LI.AND.KI.LE.L1) Y(1,JI,KI)=TA(L,1)
      IF(KI.GE.L1.AND.KI.LE.L2) Y(1,JI,KI)=TA(L,2)
```

```
      IF(KI.GE.L2.AND.KI.LE.L3) Y(1,JI,KI)=TA(L,3)
      IF(KI.GE.L3.AND.KI LE.L4) Y(1,JI,KI)=TA(L,4)
      IF(KI.GE.L4.AND.KI.LE.L5) Y(1,JI,KI)=TA(L,5)
      IF(KI.GE.L5.AND.KI.LE.L6) Y(1,JI,KI)=TA(L,6)
      IF(KI.GE.L6.AND.KI.LE.L7) Y(1,JI,KI)=TA(L,7)
      GO TO 562
  561 Y(1,JI,KI)=0.
  562 CONTINUE
  560 CONTINUE
  550 CONTINUE
      WRITE(6,14)
C
C EXPLICIT METHOD
C
      AREA=0.
      DO 100 NN=1,NTI
      N=1
      DO 200 J1=1,NJ
      Y(N+1,J1,1)=0.
  200 CONTINUE
      DO 300 K1=2,NK
      IF(K1.EQ.NK) GO TO 301
      Y(N+1,1,K1)=A(1)*Y(N,1,K1)+B(1)*Y(N,1,K1-1)+C(1)*Y(N,1,K1+1)+
     *(-D(1)+F(1))*Y(N,2,K1)
      GO TO 302
  301 Y(N+1,1,NK)=0.
  302 CONTINUE
  300 CONTINUE
      DO 400 KJ=2,NK
      IF(KJ.EQ.NK) GO TO 401
      Y(N+1,NJ,KJ)=A(NJ)*Y(N,NJ,KJ)+B(NJ)*Y(N,NJ,KJ-1)+C(NJ)*Y(N,NJ,KJ+1
     *)+D(NJ)*Y(N,NJ-1,KJ)
      GO TO 402
  401 Y(N+1,NJ,NK)=0.
  402 CONTINUE
  400 CONTINUE
      DO 500 K=2,NK
      DO 600 J=2,NR
      IF(K.EQ.NK) GO TO 601
      Y(N+1,J,K)=A(J)*Y(N,J,K)+B(J)*Y(N,J,K-1)+C(J)*Y(N,J,K+1)+
     *D(J)*Y(N,J-1,K)+F(J)*Y(N,J+1,K)
      GO TO 602
  601 Y(N+1,J,K)=0.
  602 CONTINUE
  600 CONTINUE
  500 CONTINUE
C
      DO 557 KW=1,NK
      DO 558 JW=1,NJ
      Y(N,JW,KW)=Y(N+1,JW,KW)
  558 CONTINUE
  557 CONTINUE
C
      DO 805 JM=1,2
      DO 805 KM=1,7
      YY(JM,KM)=0.
  805 CONTINUE
      DO 860 JJ=1,NJ
      IF(JJ.LE.NR1) L=1
      IF(JJ.GE.NR2) L=2
```

```
      DO 870 KK=NDI,ND7
      IF(KK.GE.NDI.AND.KK.LE.ND1) YY(L,1)=YY(L,1)+Y(N,JJ,KK)*ARE(JJ)*DEX
     */RL1
      IF(KK.GE.ND1.AND.KK.LE.ND2) YY(L,2)=YY(L,2)+Y(N,JJ,KK)*ARE(JJ)*DEX
     */RL2
      IF(KK.GE.ND2.AND.KK.LE.ND3) YY(L,3)=YY(L,3)+Y(N,JJ,KK)*ARE(JJ)*DEX
     */RL3
      IF(KK.GE.ND3.AND.KK.LE.ND4) YY(L,4)=YY(L,4)+Y(N,JJ,KK)*ARE(JJ)*DEX
     */RL3
      IF(KK.GE.ND4.AND.KK.LE.ND5) YY(L,5)=YY(L,5)+Y(N,JJ,KK)*ARE(JJ)*DEX
     */RL3
      IF(KK.GE.ND5.AND.KK.LE.ND6) YY(L,6)=YY(L,6)+Y(N,JJ,KK)*ARE(JJ)*DEX
     */RL2
      IF(KK.GE.ND6.AND.KK.LE.ND7) YY(L,7)=YY(L,7)+Y(N,JJ,KK)*ARE(JJ)*DEX
     */RL1
  870 CONTINUE
  860 CONTINUE
C
      YX(NN)=0.
      X(NN)=NN*DELT
      EF=EXP(-RLAN*X(NN))
      DO 660 LL=1,2
      DO 670 MM=1,7
      YY(LL,MM)=YY(LL,MM)*EF*CI
      YX(NN)=YX(NN)+YY(LL,MM)*DR(LL,MM)
  670 CONTINUE
  660 CONTINUE
      AREA=AREA+YX(NN)
C
  100 CONTINUE
      WRITE(7,12) (X(LH),YX(LH),LH=1,NTI)
      AREA=AREA*DELT
      FE=ARLOF/AREA
      DO 98 LT=1,NTI
      YX(LT)=YX(LT)*FE
   98 CONTINUE
      WRITE(6,14)
      WRITE(6,26)
      WRITE(6,14)
      WRITE(6,12)(X(NI),YX(NI),NI=1,NTI)
C
C
 1200 FORMAT (20A4)
 1300 FORMAT (40A4)
 1400 FORMAT (10L1)
 1500 FORMAT (4A4)
 1600 FORMAT (I1)
      READ (4,1200) (TITLE(I),I=1,20)
      READ (4,1300) (XLABEL(I),I=1,10)
      READ (4,1300) (YLABEL(I),I=1,10)
      READ (4,1400) (OPTION(I),I=1,10)
      READ (4,1500) ((POINTS(I,J),J=1,4),I=1,1)
      READ (4,1600) SIZE
      CALL PLOT(TITLE,XLABEL,YLABEL,OPTION,SIZE,X,YX,NTI,
     *1300,NTI,1,1,1,XDUM,YDUM,POINTS)
      STOP
      END
```

Sample Input for Transport Code

```
   500    14   605     6   160
14.20876E+00 6.05    E+02 0.02    E+00 3.5     E+01 0.05    E+00 1.062   E-03
10.04711E+0020.          15.          10.
 0.096   E+00 0.6426 E+00 2.202   E+00 3.616   E+00 2.202   E+00 0.6426 E+00 0.096   E+00
 0.1494  E+00 0.7698 E+00 2.013   E+00 2.660   E+00 2.013   E+00 0.7698 E+00 0.1494  E+00
 0.3664  E+00 0.9676 E+00 1.5317  E+00 2.1516  E+00 1.5317  E+00 0.9676 E+00 0.3664  E+00
 0.77145E+00 1.9445  E+00 2.6212  E+00 3.1662  E+00 2.6212  E+00 1.9445 E+00 0.77145E+00
 2.3826  E+02 9.3144 E+02
```

Sample Output for Transport Code

```
**** FINITE DIFFERENCE METHOD FOR L3-7 PNA DATA BLOCK 26 ****
TIME STEPS,RADIAL DIVISIONS,AXIAL DIVISIONS
  500    14   605
INITIAL AXIAL POSITIONS AT TAGGING AND DETECTION
    6   160
RADIUS,LENGTH,TIME INCR.,MEAN VELOCITY,FEO,VISCOSITY
0.14209E+02 0.60500E+03 0.20000E-01 0.35000E+02 0.50000E-01 0.10620E-02
VALUES OF R1,RL1,RL2,RL3
0.10047E+02 0.20000E+02 0.15000E+02 0.10000E+02
VALUES OF L1,L2,L3,L4,L5,L6,L7
   26    41    51    61    71    86   106
VALUES OF ND1,ND2,ND3,ND4,ND5,ND6,ND7
  180   195   205   215   225   240   260
VALUES OF DER,DEX,DETT,DEXX,DERR,PE
0.10149E+01 0.10000E+01 0.24633E-02 0.28738E-02-0.71428E-01 0.24490E+02

N-16 CONCENTRATIONS FOR OUTER AND INNER REGIONS
0.96000E-01 0.64260E+00 0.22020E+01 0.36160E+01 0.22020E+01 0.64260E+00 0.96000E-01

0.14940E+00 0.76980E+00 0.20130E+01 0.26600E+01 0.20130E+01 0.76980E+00 0.14940E+00
DETECTOR RESPONSE FOR OUTER AND INNER REGIONS
0.36640E+00 0.96760E+00 0.15317E+01 0.21516E+01 0.15317E+01 0.96760E+00 0.36640E+00

0.77145E+00 0.19445E+01 0.26212E+01 0.31662E+01 0.26212E+01 0.19445E+01 0.77145E+00
EXPERIMENTAL LOFT AREA 0.23826E+03TOTAL CONCENTRATION 0.93144E+03
**** VALUES FOR RADIAL NO.        1 ****
VALUES OF Z, ZH, ZHH, E, EH, EHH, ARE, U
0.0          0.35714E-01 0.35714E-01 0.42710E-04 0.16907E-01 0.16907E-01 0.70153E-01 0.54293E+00
VALUES OF COEFFICIENTS A, B, C, D, E, AND F
0.51885E+00 0.46539E+00 0.21240E-04 0.78713E-02 0.78713E-02
**** VALUES FOR RADIAL NO.        2 ****
```

```
VALUES OF Z, ZH, ZHH, E, EH, EHH, ARE, U
0.71428E-01 0.10714E+00 0.35714E-01 0.27682E-01 0.38683E-01 0.16907E-01 0.13265E+00 0.68749E+00
VALUES OF COEFFICIENTS A, B, C, D, E, AND F
0.36190E+00 0.59790E+00 0.13767E-01 0.84768E-02 0.17958E-01
**** VALUES FOR RADIAL NO.       3 ****
VALUES OF Z, ZH, ZHH, E, EH, EHH, ARE, U
0.14286E+00 0.17857E+00 0.10714E+00 0.46259E-01 0.54689E-01 0.38683E-01 0.12245E+00 0.75594E+00
VALUES OF COEFFICIENTS A, B, C, D, E, AND F
0.26128E+00 0.67095E+00 0.23005E-01 0.19455E-01 0.25304E-01
**** VALUES FOR RADIAL NO.       4 ****
VALUES OF Z, ZH, ZHH, E, EH, EHH, ARE, U
0.21429E+00 0.25000E+00 0.17857E+00 0.60014E-01 0.66394E-01 0.54689E-01 0.11224E+00 0.80172E+00
VALUES OF COEFFICIENTS A, B, C, D, E, AND F
0.19492E+00 0.71703E+00 0.29845E-01 0.27604E-01 0.30598E-01
**** VALUES FOR RADIAL NO.       5 ****
VALUES OF Z, ZH, ZHH, E, EH, EHH, ARE, U
0.28571E+00 0.32143E+00 0.25000E+00 0.69808E-01 0.74380E-01 0.66394E-01 0.10204E+00 0.83562E+00
VALUES OF COEFFICIENTS A, B, C, D, E, AND F
0.14655E+00 0.75096E+00 0.34716E-01 0.33658E-01 0.34115E-01
**** VALUES FOR RADIAL NO.       6 ****
VALUES OF Z, ZH, ZHH, E, EH, EHH, ARE, U
0.35714E+00 0.39286E+00 0.32143E+00 0.76067E-01 0.78974E-01 0.74380E-01 0.91837E-01 0.86281E+00
VALUES OF COEFFICIENTS A, B, C, D, E, AND F
0.11088E+00 0.77738E+00 0.37828E-01 0.37906E-01 0.36011E-01
**** VALUES FOR RADIAL NO.       7 ****
VALUES OF Z, ZH, ZHH, E, EH, EHH, ARE, U
0.42857E+00 0.46429E+00 0.39286E+00 0.79050E-01 0.80392E-01 0.78974E-01 0.81633E-01 0.88565E+00
VALUES OF COEFFICIENTS A, B, C, D, E, AND F
0.85354E-01 0.79843E+00 0.39312E-01 0.40512E-01 0.36387E-01
**** VALUES FOR RADIAL NO.       8 ****
```

```
VALUES OF Z, ZH, ZHH, E, EH, EHH, ARE, U
0.50000E+00 0.53571E+00 0.46429E+00 0.78939E-01 0.78786E-01 0.80392E-01 0.71429E-01 0.90541E+00
VALUES OF COEFFICIENTS A, B, C, D, E, AND F
0.68517E-01 0.81532E+00 0.39257E-01 0.41586E-01 0.35321E-01
**** VALUES FOR RADIAL NO.        9 ****
VALUES OF Z, ZH, ZHH, E, EH, EHH, ARE, U
0.57143E+00 0.60714E+00 0.53571E+00 0.75869E-01 0.74277E-01 0.78786E-01 0.61224E-01 0.92286E+00
VALUES OF COEFFICIENTS A, B, C, D, E, AND F
0.59437E-01 0.82875E+00 0.37730E-01 0.41208E-01 0.32873E-01
**** VALUES FOR RADIAL NO.       10 ****
VALUES OF Z, ZH, ZHH, E, EH, EHH, ARE, U
0.64286E+00 0.67857E+00 0.60714E+00 0.69944E-01 0.66957E-01 0.74277E-01 0.51020E-01 0.93853E+00
VALUES OF COEFFICIENTS A, B, C, D, E, AND F
0.57445E-01 0.83923E+00 0.34783E-01 0.39447E-01 0.29094E-01
**** VALUES FOR RADIAL NO.       11 ****
VALUES OF Z, ZH, ZHH, E, EH, EHH, ARE, U
0.71429E+00 0.75000E+00 0.67857E+00 0.61249E-01 0.56904E-01 0.66957E-01 0.40816E-01 0.95274E+00
VALUES OF COEFFICIENTS A, B, C, D, E, AND F
0.62047E-01 0.84709E+00 0.30459E-01 0.36368E-01 0.24039E-01
**** VALUES FOR RADIAL NO.       12 ****
VALUES OF Z, ZH, ZHH, E, EH, EHH, ARE, U
0.78571E+00 0.82143E+00 0.75000E+00 0.49855E-01 0.44184E-01 0.56904E-01 0.30612E-01 0.96574E+00
VALUES OF COEFFICIENTS A, B, C, D, E, AND F
0.72809E-01 0.85257E+00 0.24793E-01 0.32053E-01 0.17777E-01
**** VALUES FOR RADIAL NO.       13 ****
VALUES OF Z, ZH, ZHH, E, EH, EHH, ARE, U
0.85714E+00 0.89286E+00 0.82143E+00 0.35822E-01 0.28852E-01 0.44184E-01 0.20408E-01 0.97770E+00
VALUES OF COEFFICIENTS A, B, C, D, E, AND F
0.89233E-01 0.85584E+00 0.17815E-01 0.26665E-01 0.10447E-01
**** VALUES FOR RADIAL NO.       14 ****
```

VALUES OF Z, ZH, ZHH, E, EH, EHH, ARE, U

0.92857E+00 0.96428E+00 0.89286E+00 0.19203E-01 0.10957E-01 0.28852E-01 0.10204E-01 0.98853E+00

VALUES OF COEFFICIENTS A, B, C, D, E, AND F

0.11005E+00 0.85686E+00 0.95498E-02 0.20895E-01 0.26451E-02

**** VALUES FOR RADIAL NO. 15 ****

VALUES OF Z, ZH, ZHH, E, EH, EHH, ARE, U

0.10000E+01 0.96428E+00 0.96428E+00 0.42932E-04 0.10957E-01 0.10957E-01 0.12756E-02 0.99656E+00

VALUES OF COEFFICIENTS A, B, C, D, E, AND F

0.14569E+00 0.85421E+00 0.21350E-04 0.82910E-04 0.0

CORRECTED MEAN VELOCITY = 0.35000E+02

TIME(SEC) AND FINAL COUNTS/ TIME CHANNEL

0.20000E-01	0.0	0.40000E-01	0.0	0.60000E-01	0.0	0.80000E-01	0.0	0.10000E+00	0.0
0.12000E+00	0.0	0.14000E+00	0.0	0.16000E+00	0.0	0.18000E+00	0.0	0.20000E+00	0.0
0.22000E+00	0.0	0.24000E+00	0.0	0.26000E+00	0.0	0.28000E+00	0.0	0.30000E+00	0.0
0.32000E+00	0.0	0.34000E+00	0.0	0.36000E+00	0.0	0.38000E+00	0.0	0.40000E+00	0.0
0.42000E+00	0.0	0.44000E+00	0.0	0.46000E+00	0.0	0.48000E+00	0.0	0.50000E+00	0.0
0.52000E+00	0.0	0.54000E+00	0.0	0.56000E+00	0.0	0.58000E+00	0.0	0.60000E+00	0.0
0.62000E+00	0.0	0.64000E+00	0.0	0.66000E+00	0.0	0.68000E+00	0.0	0.70000E+00	0.0
0.72000E+00	0.0	0.74000E+00	0.0	0.76000E+00	0.0	0.78000E+00	0.0	0.80000E+00	0.0
0.82000E+00	0.0	0.84000E+00	0.0	0.85000E+00	0.0	0.88000E+00	0.0	0.90000E+00	0.0
0.92000E+00	0.0	0.94000E+00	0.0	0.96000E+00	0.0	0.98000E+00	0.0	0.10000E+01	0.0
0.10200E+01	0.0	0.10400E+01	0.0	0.10600E+01	0.0	0.10800E+01	0.18485E-05	0.11000E+01	0.15953E-04
0.11200E+01	0.73935E-04	0.11400E+01	0.24400E-03	0.11600E+01	0.64268E-03	0.11800E+01	0.14372E-02	0.12000E+01	0.28363E-02
0.12200E+01	0.50718E-02	0.12400E+01	0.83757E-02	0.12600E+01	0.12959E-01	0.12800E+01	0.18992E-01	0.13000E+01	0.26600E-01
0.13200E+01	0.35853E-01	0.13400E+01	0.46770E-01	0.13600E+01	0.59330E-01	0.13800E+01	0.73470E-01	0.14000E+01	0.89105E-01
0.14200E+01	0.10613E+00	0.14400E+01	0.12441E+00	0.14600E+01	0.14385E+00	0.14800E+01	0.16430E+00	0.15000E+01	0.18567E+00
0.15200E+01	0.20783E+00	0.15400E+01	0.23072E+00	0.15600E+01	0.25431E+00	0.15800E+01	0.27866E+00	0.16000E+01	0.30394E+00
0.16200E+01	0.33045E+00	0.16400E+01	0.35867E+00	0.16600E+01	0.38921E+00	0.16800E+01	0.42282E+00	0.17000E+01	0.46032E+00
0.17200E+01	0.50256E+00	0.17400E+01	0.55036E+00	0.17600E+01	0.60448E+00	0.17800E+01	0.66554E+00	0.18000E+01	0.73403E+00
0.18200E+01	0.81030E+00	0.18400E+01	0.89456E+00	0.18600E+01	0.98690E+00	0.18800E+01	0.10873E+01	0.19000E+01	0.11956E+01
0.19200E+01	0.13119E+01	0.19400E+01	0.14360E+01	0.19600E+01	0.15681E+01	0.19800E+01	0.17084E+01	0.20000E+01	0.18573E+01
0.20200E+01	0.20154E+01	0.20400E+01	0.21835E+01	0.20600E+01	0.23625E+01	0.20800E+01	0.25536E+01	0.21000E+01	0.27580E+01
0.21200E+01	0.29770E+01	0.21400E+01	0.32122E+01	0.21600E+01	0.34648E+01	0.21800E+01	0.37364E+01	0.22000E+01	0.40283E+01
0.22200E+01	0.43418E+01	0.22400E+01	0.46780E+01	0.22600E+01	0.50379E+01	0.22800E+01	0.54224E+01	0.23000E+01	0.58319E+01
0.23200E+01	0.62670E+01	0.23400E+01	0.67279E+01	0.23600E+01	0.72149E+01	0.23800E+01	0.77281E+01	0.24000E+01	0.82677E+01
0.24200E+01	0.88341E+01	0.24400E+01	0.94276E+01	0.24600E+01	0.10049E+02	0.24800E+01	0.10699E+02	0.25000E+01	0.11378E+02
0.25200E+01	0.12088E+02	0.25400E+01	0.12829E+02	0.25600E+01	0.13603E+02	0.25800E+01	0.14411E+02	0.26000E+01	0.15253E+02
0.26200E+01	0.16130E+02	0.26400E+01	0.17044E+02	0.26600E+01	0.17993E+02	0.26800E+01	0.18980E+02	0.27000E+01	0.20005E+02
0.27200E+01	0.21066E+02	0.27400E+01	0.22166E+02	0.27600E+01	0.23304E+02	0.27800E+01	0.24480E+02	0.28000E+01	0.25694E+02
0.28200E+01	0.26947E+02	0.28400E+01	0.28239E+02	0.28600E+01	0.29570E+02	0.28800E+01	0.30940E+02	0.29000E+01	0.32350E+02
0.29200E+01	0.33800E+02	0.29400E+01	0.35290E+02	0.29600E+01	0.36819E+02	0.29800E+01	0.38388E+02	0.30000E+01	0.39997E+02
0.30200E+01	0.41644E+02	0.30400E+01	0.43331E+02	0.30600E+01	0.45057E+02	0.30800E+01	0.46820E+02	0.31000E+01	0.48621E+02
0.31200E+01	0.50458E+02	0.31400E+01	0.52330E+02	0.31600E+01	0.54236E+02	0.31800E+01	0.56174E+02	0.32000E+01	0.58143E+02
0.32200E+01	0.60140E+02	0.32400E+01	0.62163E+02	0.32600E+01	0.64210E+02	0.32800E+01	0.66278E+02	0.33000E+01	0.68363E+02
0.33200E+01	0.70464E+02	0.33400E+01	0.72577E+02	0.33600E+01	0.74700E+02	0.33800E+01	0.76828E+02	0.34000E+01	0.78959E+02
0.34200E+01	0.81089E+02	0.34400E+01	0.83214E+02	0.34600E+01	0.85332E+02	0.34800E+01	0.87439E+02	0.35000E+01	0.89530E+02

0.35200E+01	0.91601E+02	0.35400E+01	0.93649E+02	0.35600E+01	0.95669E+02	0.35800E+01	0.97656E+02	0.36000E+01	0.99607E+02
0.36200E+01	0.10152E+03	0.36400E+01	0.10338E+03	0.36600E+01	0.10519E+03	0.36800E+01	0.10695E+03	0.37000E+01	0.10865E+03
0.37200E+01	0.11029E+03	0.37400E+01	0.11186E+03	0.37600E+01	0.11336E+03	0.37800E+01	0.11479E+03	0.38000E+01	0.11614E+03
0.38200E+01	0.11741E+03	0.38400E+01	0.11860E+03	0.38600E+01	0.11970E+03	0.38800E+01	0.12071E+03	0.39000E+01	0.12164E+03
0.39200E+01	0.12247E+03	0.39400E+01	0.12322E+03	0.39600E+01	0.12386E+03	0.39800E+01	0.12442E+03	0.40000E+01	0.12487E+03
0.40200E+01	0.12523E+03	0.40400E+01	0.12549E+03	0.40600E+01	0.12566E+03	0.40800E+01	0.12573E+03	0.41000E+01	0.12570E+03
0.41200E+01	0.12558E+03	0.41400E+01	0.12536E+03	0.41600E+01	0.12505E+03	0.41800E+01	0.12465E+03	0.42000E+01	0.12416E+03
0.42200E+01	0.12358E+03	0.42400E+01	0.12291E+03	0.42600E+01	0.12216E+03	0.42800E+01	0.12133E+03	0.43000E+01	0.12041E+03
0.43200E+01	0.11943E+03	0.43400E+01	0.11836E+03	0.43600E+01	0.11723E+03	0.43800E+01	0.11603E+03	0.44000E+01	0.11477E+03
0.44200E+01	0.11344E+03	0.44400E+01	0.11206E+03	0.44600E+01	0.11062E+03	0.44800E+01	0.10913E+03	0.45000E+01	0.10759E+03
0.45200E+01	0.10601E+03	0.45400E+01	0.10438E+03	0.45600E+01	0.10272E+03	0.45800E+01	0.10102E+03	0.46000E+01	0.99285E+02
0.46200E+01	0.97525E+02	0.46400E+01	0.95739E+02	0.46600E+01	0.93930E+02	0.46800E+01	0.92103E+02	0.47000E+01	0.90258E+02
0.47200E+01	0.88400E+02	0.47400E+01	0.86532E+02	0.47600E+01	0.84655E+02	0.47800E+01	0.82774E+02	0.48000E+01	0.80890E+02
0.48200E+01	0.79006E+02	0.48400E+01	0.77124E+02	0.48600E+01	0.75247E+02	0.48800E+01	0.73377E+02	0.49000E+01	0.71516E+02
0.49200E+01	0.69666E+02	0.49400E+01	0.67828E+02	0.49600E+01	0.66006E+02	0.49800E+01	0.64200E+02	0.50000E+01	0.62413E+02
0.50200E+01	0.60645E+02	0.50400E+01	0.58898E+02	0.50600E+01	0.57173E+02	0.50800E+01	0.55473E+02	0.51000E+01	0.53797E+02
0.51200E+01	0.52147E+02	0.51400E+01	0.50524E+02	0.51600E+01	0.48929E+02	0.51800E+01	0.47363E+02	0.52000E+01	0.45826E+02
0.52200E+01	0.44319E+02	0.52400E+01	0.42843E+02	0.52600E+01	0.41398E+02	0.52800E+01	0.39984E+02	0.53000E+01	0.38603E+02
0.53200E+01	0.37253E+02	0.53400E+01	0.35935E+02	0.53600E+01	0.34650E+02	0.53800E+01	0.33397E+02	0.54000E+01	0.32177E+02
0.54200E+01	0.30988E+02	0.54400E+01	0.29832E+02	0.54600E+01	0.28708E+02	0.54800E+01	0.27616E+02	0.55000E+01	0.26555E+02
0.55200E+01	0.25525E+02	0.55400E+01	0.24526E+02	0.55600E+01	0.23558E+02	0.55800E+01	0.22619E+02	0.56000E+01	0.21710E+02
0.56200E+01	0.20831E+02	0.56400E+01	0.19980E+02	0.56600E+01	0.19157E+02	0.56800E+01	0.18362E+02	0.57000E+01	0.17594E+02
0.57200E+01	0.16852E+02	0.57400E+01	0.16137E+02	0.57600E+01	0.15447E+02	0.57800E+01	0.14781E+02	0.58000E+01	0.14140E+02
0.58200E+01	0.13522E+02	0.58400E+01	0.12927E+02	0.58600E+01	0.12355E+02	0.58800E+01	0.11804E+02	0.59000E+01	0.11275E+02
0.59200E+01	0.10766E+02	0.59400E+01	0.10276E+02	0.59600E+01	0.98066E+01	0.59800E+01	0.93556E+01	0.60000E+01	0.89227E+01
0.60200E+01	0.85074E+01	0.60400E+01	0.81091E+01	0.60600E+01	0.77273E+01	0.60800E+01	0.73614E+01	0.61000E+01	0.70108E+01
0.61200E+01	0.66751E+01	0.61400E+01	0.63537E+01	0.61600E+01	0.60461E+01	0.61800E+01	0.57519E+01	0.62000E+01	0.54705E+01
0.62200E+01	0.52015E+01	0.62400E+01	0.49444E+01	0.62600E+01	0.46988E+01	0.62800E+01	0.44642E+01	0.63000E+01	0.42403E+01
0.63200E+01	0.40265E+01	0.63400E+01	0.38226E+01	0.63600E+01	0.36280E+01	0.63800E+01	0.34426E+01	0.64000E+01	0.32657E+01
0.64200E+01	0.30973E+01	0.64400E+01	0.29368E+01	0.64600E+01	0.27839E+01	0.64800E+01	0.26384E+01	0.65000E+01	0.25000E+01
0.65200E+01	0.23682E+01	0.65400E+01	0.22429E+01	0.65600E+01	0.21238E+01	0.65800E+01	0.20105E+01	0.66000E+01	0.19029E+01
0.66200E+01	0.18006E+01	0.66400E+01	0.17035E+01	0.66600E+01	0.16113E+01	0.66800E+01	0.15238E+01	0.67000E+01	0.14408E+01
0.67200E+01	0.13620E+01	0.67400E+01	0.12873E+01	0.67600E+01	0.12165E+01	0.67800E+01	0.11493E+01	0.68000E+01	0.10857E+01
0.68200E+01	0.10254E+01	0.68400E+01	0.96837E+00	0.68600E+01	0.91432E+00	0.68800E+01	0.86316E+00	0.69000E+01	0.81473E+00
0.69200E+01	0.76892E+00	0.69400E+01	0.72558E+00	0.69600E+01	0.68458E+00	0.69800E+01	0.64582E+00	0.70000E+01	0.60918E+00
0.70200E+01	0.57455E+00	0.70400E+01	0.54183E+00	0.70600E+01	0.51091E+00	0.70800E+01	0.48170E+00	0.71000E+01	0.45412E+00
0.71200E+01	0.42807E+00	0.71400E+01	0.40348E+00	0.71600E+01	0.38027E+00	0.71800E+01	0.35837E+00	0.72000E+01	0.33769E+00
0.72200E+01	0.31819E+00	0.72400E+01	0.29979E+00	0.72600E+01	0.28243E+00	0.72800E+01	0.26607E+00	0.73000E+01	0.25063E+00
0.73200E+01	0.23607E+00	0.73400E+01	0.22235E+00	0.73600E+01	0.20942E+00	0.73800E+01	0.19722E+00	0.74000E+01	0.18573E+00
0.74200E+01	0.17490E+00	0.74400E+01	0.16469E+00	0.74600E+01	0.15507E+00	0.74800E+01	0.14601E+00	0.75000E+01	0.13748E+00
0.75200E+01	0.12943E+00	0.75400E+01	0.12186E+00	0.75600E+01	0.11472E+00	0.75800E+01	0.10800E+00	0.76000E+01	0.10167E+00
0.76200E+01	0.95707E-01	0.76400E+01	0.90092E-01	0.76600E+01	0.84805E-01	0.76800E+01	0.79826E-01	0.77000E+01	0.75137E-01
0.77200E+01	0.70723E-01	0.77400E+01	0.66566E-01	0.77600E+01	0.62653E-01	0.77800E+01	0.58968E-01	0.78000E+01	0.55499E-01
0.78200E+01	0.52233E-01	0.78400E+01	0.49158E-01	0.78600E+01	0.46264E-01	0.78800E+01	0.43539E-01	0.79000E+01	0.40974E-01
0.79200E+01	0.38559E-01	0.79400E+01	0.36286E-01	0.79600E+01	0.34146E-01	0.79800E+01	0.32132E-01	0.80000E+01	0.30236E-01
0.80200E+01	0.28451E-01	0.80400E+01	0.26771E-01	0.80600E+01	0.25190E-01	0.80800E+01	0.23702E-01	0.81000E+01	0.22300E-01
0.81200E+01	0.20982E-01	0.81400E+01	0.19740E-01	0.81600E+01	0.18572E-01	0.81800E+01	0.17472E-01	0.82000E+01	0.16437E-01
0.82200E+01	0.15463E-01	0.82400E+01	0.14545E-01	0.82600E+01	0.13682E-01	0.82800E+01	0.12870E-01	0.83000E+01	0.12105E-01
0.83200E+01	0.11385E-01	0.83400E+01	0.10707E-01	0.83600E+01	0.10070E-01	0.83800E+01	0.94692E-02	0.84000E+01	0.89042E-02
0.84200E+01	0.83725E-02	0.84400E+01	0.78720E-02	0.84600E+01	0.74009E-02	0.84800E+01	0.69575E-02	0.85000E+01	0.65402E-02
0.85200E+01	0.61475E-02	0.85400E+01	0.57779E-02	0.85600E+01	0.54300E-02	0.85800E+01	0.51027E-02	0.86000E+01	0.47946E-02
0.86200E+01	0.45047E-02	0.86400E+01	0.42319E-02	0.86600E+01	0.39752E-02	0.86800E+01	0.37336E-02	0.87000E+01	0.35064E-02
0.87200E+01	0.32926E-02	0.87400E+01	0.30914E-02	0.87600E+01	0.29022E-02	0.87800E+01	0.27242E-02	0.88000E+01	0.25567E-02
0.88200E+01	0.23993E-02	0.88400E+01	0.22512E-02	0.88600E+01	0.21119E-02	0.88800E+01	0.19809E-02	0.89000E+01	0.18578E-02
0.89200E+01	0.17421E-02	0.89400E+01	0.16333E-02	0.89600E+01	0.15310E-02	0.89800E+01	0.14349E-02	0.90000E+01	0.13446E-02
0.90200E+01	0.12598E-02	0.90400E+01	0.11801E-02	0.90600E+01	0.11052E-02	0.90800E+01	0.10349E-02	0.91000E+01	0.96893E-03
0.91200E+01	0.90697E-03	0.91400E+01	0.84880E-03	0.91600E+01	0.79421E-03	0.91800E+01	0.74299E-03	0.92000E+01	0.69493E-03
0.92200E+01	0.64985E-03	0.92400E+01	0.60758E-03	0.92600E+01	0.56794E-03	0.92800E+01	0.53078E-03	0.93000E+01	0.49595E-03
0.93200E+01	0.46331E-03	0.93400E+01	0.43273E-03	0.93600E+01	0.40408E-03	0.93800E+01	0.37725E-03	0.94000E+01	0.35214E-03
0.94200E+01	0.32862E-03	0.94400E+01	0.30661E-03	0.94600E+01	0.28601E-03	0.94800E+01	0.26675E-03	0.95000E+01	0.24872E-03
0.95200E+01	0.23187E-03	0.95400E+01	0.21611E-03	0.95600E+01	0.20139E-03	0.95800E+01	0.18762E-03	0.96000E+01	0.17476E-03
0.96200E+01	0.16274E-03	0.96400E+01	0.15152E-03	0.96600E+01	0.14105E-03	0.96800E+01	0.13126E-03	0.97000E+01	0.12214E-03
0.97200E+01	0.11362E-03	0.97400E+01	0.10567E-03	0.97600E+01	0.98257E-04	0.97800E+01	0.91344E-04	0.98000E+01	0.84899E-04
0.98200E+01	0.78891E-04	0.98400E+01	0.73293E-04	0.98600E+01	0.68076E-04	0.98800E+01	0.63217E-04	0.99000E+01	0.58692E-04
0.99200E+01	0.54478E-04	0.99400E+01	0.50556E-04	0.99600E+01	0.46905E-04	0.99800E+01	0.43508E-04	0.10000E+02	0.40348E-04

DISTRIBUTION

Contracts Officer (USNRC) - (2)
Dr. S. Fabic (USNRC)
A. L. M. Hon (USNRC)
Dr. Y. Y. Hsu (USNRC)
Dr. N. Kondic (USNRC)
A. W. Savolainen (USNRC)
Dr. L. S. Tong (USNRC)
Dr. N. Zuber (USNRC)
Dr. P. Bailey (EPRI)
Prof. S. Banerjee (UC/Santa Barbara)
Prof. S. G. Bankoff (Northwestern)
Prof. J. Bataille (Lyon)
Prof. G. Birkoff (Harvard)
Prof. G. CArrier (Harvard)
Dr. S. H. Chan (U of Wisconsin/Milwaukee)
Dr. J. Chen (Lehigh)
Dr. S. C. Cheng (U of Ottawa)
Mr. K. Condie (INEL)
Dr. J. M. Delhaye (CEA)
Dr. G. E. Dix (GE)
Dean A. Dukler (U of Houston)
Dr. T. Fernandez (EPRI)
Dr. M. H. Fontana (ORNL)
Prof. J. M. Gonzalez-Santalo (Mexico)
Prof. P. Griffith (MIT)
Dr. D. Groeneveld (AECL)
Dr. M. Ishii (ANL)
Dr. P. Kehler (ANL)
Dr. P. A. Lottes (ANL)
Dr. W. T. Sha (ANL)
Dr. G. Kosaly (Washington U)
Prof. P. Lax (NYU)
Dr. P. Lee (SUNY/Stonybrook)
Prof. F. Marble (Cal Tech)
Prof. K. Miller (UC-Berkeley)
Prof. V. E. Schrock (UC-Berkeley)
G. L. Shires (AEE/Winfrith)
Prof. C. Truesdell (Johns Hopkins)
Dr. G. B. Wallis/Dr. H. Richter (Dartmouth)
Dr. E. Feldman (EG&G)
Dr. G. Lassahn (EG&G)
Dr. L. Leach (EG&G)
Dr. C. Solbrig (EG&G)
L. L. Wheat (EG&G)
Dr. L. Ybarrondo (EG&G)
Folsom Library (C. O'Connell) (RPI)
Departmental Library (RPI)
Dr. R. C. Block (RPI)
Dr. H. E. Breed (RPI)
M. Barasch (RPI)
L-Y Cheng (RPI)
W. Conlon (RPI)

DISTRIBUTION (continued)

Dr. D. A. Drew (RPI)
M. Fakory (RPI)
Dr. J. E. Flaherty (RPI)
Dr. R. R. Gay (NUS)
Dr. R. T. Lahey, Jr. (RPI) - (15)
Dr. H. Littman (RPI)
K. Ohkawa (RPI)
N. Saba (RPI)
S. Sim (RPI)
Dr. O. C. Jones (RPI)

120555078877 2 ANR7
US NRC
ADM DIV OF TIDC
POLICY & PUBLICATIONS MGT BR
PDR NUREG COPY
LA 212
WASHINGTON DC 20555

EG&G Idaho, Inc.
P.O. Box 1625
Idaho Falls, Idaho 83415